THE INFLUENCE OF TWO-DIMENSIONAL HILLS ON SIMULATED ATMOSPHERIC BOUNDARY LAYERS

A thesis presented for the Degree

of

Doctor of Philosophy in Mechanical Engineering

at the

University of Canterbury

Christchurch

New Zealand.

by

J. R. Pearse B.E. (Hons)

University of Canterbury August, 1979

VOLUME I

ACKNOWLEDGEMENTS

I wish to express my thanks to Dr D. Lindley and Professor D.C. Stevenson for their conscientious and enthusiastic supervision of this project. Their interest and encouragement is gratefully acknowledged.

I would also like to thank Mr J. S. Smaill and Dr A. J. Bowen for their advice and assistance.

My sincere thanks are also due to the technical staff of the Department of Mechanical Engineering who have provided assistance during the execution of this project; in particular, to the workshop staff led by Mr E. D. Retallick, to Mr H. J. Anink for the maintenance of all the electronic equipment, and to Mr L. M. Cheeseman.

The assistance of Miss J. M. Shelton and Mr T. Bird for skilfully tracing the figures for this thesis is appreciated. My thanks also to Miss B.V. Nottingham and Mrs P. M. Dowell for diligently typing this thesis.

The author was supported by a University Grants Committee Postgraduate Scholarship and an Edward and Isabel Kidson Scholarship awarded by the University Grants Committee, and their assistance is gratefully acknowledged. The author also wishes to thank the William Georgetti Scholarship Board for their financial support by means of the William Georgetti Scholarship.

Finally, I would like to thank my parents for their interest and support.

ABSTRACT

This thesis describes the development of a number of simulated atmospheric boundary layers and their application to the investigation of wind flow over hills.

A review is made of the current knowledge of the wind flow over hills. The atmospheric boundary layer wind tunnel in the Department of Mechanical Engineering was recommissioned and a model 1:300 rural boundary layer established. Measurements of the mean and fluctuating velocities, energy spectra and autocorrelation functions were made in the flow over model two-dimensional triangular hills of slope 3^{o}, 9^{o}, 14^{o} and 27^{o}. Once a certain slope was reached large scale separated flow occurred after the hill crest. The largest increase in velocity occurred for the hill with a slope of 14^{o}. Measurements were also made over round crested hills with the same aspect ratio. Comparison of the flow fields showed that the crest shape had little effect on the flow over the hills.

A rural atmospheric boundary layer of 1:3000 scale was established and measurements were made over a selection of the model triangular hills. An increase in the hill height to boundary layer height ratio was found to decrease the amplification factors at the hill crests.

Measurements were also made over a number of model triangular hills in an urban model boundary layer of about 1:400 scale which was developed. The effect of the higher velocity gradient was to cause an increase in the amplification factors at the hill crests.

A digital data handling system capable of accepting the voltage output from a single hot wire anemometer was developed. Software was written to control the analog to digital converter and transmit the data samples to a minicomputer remote from the wind tunnel. The data samples are stored on disc. When data collection has finished the data is analysed. Software is described which calculates the mean, standard deviation, spectral density function, autocorrelation function and probability density function of the stored data.

CONTENTS

VOLUME I

CHAPTER Page

CHAPTER Page

CHAPTER Page

CHAPTER Page

VOLUME II

Page

SECTION Page

SECTION Page

SECTION Page

LIST OF FIGURES

VOLUME II (Appendix 2)

LIST OF TABLES

VOLUME II (Appendix 2)

LIST OF SYMBOLS

$a,b,c,$	arbitrary constants.
A_F	frontal area associated with one roughness element.
A_p	plan area associated with one roughness element.
A_z	amplification factor defined as the mean wind speed at a height z above level ground divided by the reference mean wind speed which is measured at the same height above local ground level but in the undisturbed flow over flat ground, upstream of the hill.
$A_{z_{max}}$	maximum amplification factor at a given longitudinal position over a hill.
b	arbitrary constant.
c	arbitrary constant
$C_{ii}(\tau)$	autocovariance function, $\overline{i(t).i(t+\tau)}$
$C_{ij}(r,r',\tau)$	general cross-covariance function, $\overline{i(r,t).j(r',t+\tau)}$
d	zero plane displacement.
d_a	characteristic dimension of prototype.
d_m	characteristic dimension of model.
$\frac{d_m}{d_a}$	linear scaling of an atmospheric boundary layer simulation.
D	diameter.
e	fluctuating component of anemometer output voltage.
E	linearised anemometer output voltage.
f, f_m	$\frac{nz}{\overline{U}}$, $\left(\frac{nz}{\overline{U}}\right)_p$ dimensionless spectral frequencies.
G	gain of the DISA dual summing unit.
H	model hill height ($\frac{H}{L}$ is model hill aspect ratio).
H_a	height of the atmospheric surface layer.
i(r,t)	general value of u, v or w gust component at point r and time t where i = u, v or w.
k	$\frac{n}{\overline{U}}$, spectrum wave number.
k_p	spectral peak wave number.
k_r	roughness element height.

k_{p_u} spectral peak wave number of the u velocity component.

k_{p_v} spectral peak wave number of the v velocity component.

k_{p_w} spectral peak wave number of the w velocity component.

k_v reduced frequency at which viscous cut off of the energy spectrum of the turbulence becomes noticeable.

k_z spectrum peak wave number at height z.

k_3 hot wire anemometer calibration constant, relating the linearised anemometer voltage to the air velocity.

k_{10} surface drag coefficient at a height of 10 m ,

i.e. $k_{10} = \left(\frac{u*}{\overline{U}_{10}} \right)^2$

k_∞ $\left(\frac{u*}{\overline{U}_\infty} \right)^2$ surface drag coefficient referred to boundary layer depth δ.

ℓ height of the inner region in the flow over the model hills after Jackson and Hunt (1975).

Lu_x integral length scale of turbulence of streamwise velocity component in the streamwise direction.

Lu_y integral length scale of turbulence of streamwise velocity component in the lateral direction.

Lv_x integral length scale of turbulence of the lateral velocity component in the streamwise direction.

Lw_x integral length scale of the turbulence of the vertical velocity component in the streamwise direction.

L scaling length in the model atmospheric spectra.

L distance from the hill crest to where the hill height is half its maximum value.

n frequency.

n_p spectral peak frequency.

N number of samples.

N prefix indicating lateral distance to the right of the wind tunnel centreline when facing downstream.

p subscript referring to a spectral peak value.

p(x) probability density function.

$P_{ij}(r,r',n)$ co-spectral function, in-phase component of $S_{ij}(r,r',n)$.

ΔP	local slope at the hill crest.
$Q_{ij}(r,r',n)$	quad-spectral function, out-of-phase component of $S_{ij}(r,r',n)$.
r,r'	position vectors denoting points (x,y,z) and(x',y',z') respectively.
R	eddy Reynolds number $\frac{u\ell}{\varepsilon}$ where u is a reference velocity, ℓ is a reference hill dimension and ε is the eddy viscosity, assumed constant.
s	sample standard deviation.
$S_{ii}(n)$	power spectral density function.
$S_{ij}(r,r',n)$	general cross-spectral density function.
S	model scale factor, $\frac{da}{dm}$.
S	prefix indicating lateral distance to the left of the wind tunnel centreline when facing downstream.
Δs	fractional speedup ratio, the increase in wind speed at a given height to the undisturbed wind speed at the same displacement above the surface.
t	time.
T	time interval over which a record was obtained.
T	averaging time used with the Bruel and Kjaer 2114 spectrometer (Appendix One).
T_E	Eulerian time scale of turbulence.
ΔT	time interval between samples.
$\overline{U},\overline{V},\overline{W}$	streamwise, lateral and vertical mean velocities respectively.
u,v,w,	fluctuating component of streamwise, lateral and vertical velocity respectively.
U,V,W,	instantaneous velocity in streamwise, lateral and vertical directions respectively.
u',v',w'	streamwise, lateral and vertical rms velocity fluctuations respectively.
$\overline{U}_\theta$	apparent cooling velocity incident on a hot wire.
$\overline{U}_{\theta_{eff}}$	effective cooling velocity incident on a hot wire.
$\overline{U}_\delta$	mean streamwise velocity at Z = δ.

$\overline{U}_{ref}$	mean flow velocity at a reference height in the wind tunnel.
$\overline{U}_{\infty}$	mean streamwise velocity at $z = \delta$.
$\overline{U}_{ref}(\delta)$	mean streamwise velocity at $z = \delta$ in the upstream reference approach flow incident on the model hills.
$\overline{U}_z$	mean velocity at a height z above the surface.
U_n	(n = 1,2,3...N) : values of a time series.
u(t) v(t) w(t)	fluctuating components of wind speed along the x, y and z axes respectively.
$\overline{U}$	sample mean.
u_*	friction velocity , $\sqrt{\frac{\tau o}{\rho}}$
W	width of Torro block roughness elements in Chapter nine (3.2 cm).
w	width of the class interval of the probability density function.
x,y,z	a system of rectangular cartesian coordinates with the x axis defined in the streamwise direction, the y axis in the lateral direction and the z axis in the vertical direction; over a model hill the z distance is always measured above the hill surface.
X	distance downstream of the bar grid.
x_1	$\frac{nL}{\overline{U}_{10}}$ as in Harris spectrum.
x(k)	represents samples of the time function.
X(j)	represents the frequency components.
w	width of the class interval of the probability density function.
Z_o	roughness length.
α	exponent of the mean velocity profile power law.
γ	inclination of the flow to the axis of a cross-wire probe.
$\gamma^2_{ij}(r,r',n)$	general coherence function.
δ	boundary layer thickness.
δ_u	velocity boundary layer depth following a change in surface roughness; height at which the new mean velocity is within 1% of the old mean velocity.
δ_e	equilibrium boundary layer depth following a change in surface roughness.

ε	eddy viscosity.
ε^2	mean square error of the probability density function.
λ_e	effective streamwise spacing of two dimensional bars.
κ	von Karman constant.
ν	kinematic viscosity.
ρ	mass of air.
$\rho_{ii}(\tau)$	autocorrelation function.
$\rho_{ij}(r,r',\tau)$	general cross-correlation function.
θ	inclination of mean flow to the horizontal.
ϕ	cross-wire probe wire angle.
σ_i	standard deviation of U, V or W velocity component.
ψ	stream function.
τ	shear stress.
τ	incremental time lag.
τ_o	surface shear stress.
ω	angular velocity.

Subscripts

a	full scale values from the atmosphere.
i,j	refers to u, v or w velocity component.
m	model values.
o	reference quantity.
p	spectral peak value.
ref.	reference quantity measured in the undisturbed flow over flat ground upstream of the hill.
U,V,W	streamwise, lateral and vertical velocity components.
z	height above ground.

Suffixes

A prime (') denotes a value at the point (x',y',z').

A bar ($\bar{}$) denotes a value averaged over time.

Two vertical bars ($|\ |$) denote the absolute value of a quantity.

CHAPTER 1

INTRODUCTION

1.1 Atmospheric wind research

In recent years there has been a growing interest in the nature of the wind. The direct economic loss resulting from windstorm damage to large structures, domestic homes and crops has helped to stimulate this interest. In addition architects, city planners and engineers who are concerned with human comfort have begun examining such things as wind generated noise, oscillations of buildings due to wind and wind buffeting of pedestrians. An awareness of environmental protection has aroused concern about pollutant dispersion which requires a knowledge of wind characteristics. More recently the need to develop new energy sources has lead to a great deal of interest in developing power from the wind.

The study of the interaction between the atmospheric wind and man and his works on the Earth's surface has developed into the field of wind engineering which embodies the fields of meteorology, structural mechanics and fluid mechanics.

In 1969 a programme of research into atmospheric boundary layer phenomena was initiated in the Department of Mechanical Engineering at the University of Canterbury. Wind damage to forests was investigated by Papesch (1971). An atmospheric boundary layer wind tunnel was designed and commissioned by Raine (1974) and subsequently used to test a variety of model windbreaks in a rigorously simulated 1:300 rural atmospheric boundary layer. A programme of wind tunnel and field tests aimed at investigating the wind flow over escarpments has been conducted by Bowen and Lindley (1974), (1977). Further work was performed by Meroney et. al. (1978) involving a 1:5000 scale wind tunnel investigation of the characteristics of the Rakaia Gorge, complemented by a field programme. Sophisticated field measuring equipment using fast response propellor anemometers has been developed by Flay (1978).

The purpose of the present project was to investigate the wind flow over simple hill shapes using a model atmospheric boundary layer flow.

1.2 Applications of the project

(a) Prediction of design wind loads

Many structures which are vulnerable to the wind are mounted on hill sites (e.g. television masts, transmission line pylons, radio antennae). It is necessary to know as accurately as possible the velocity of the wind at each part of the structure because the loads and pressures on the structure must be derived from appropriate design wind loads. This is especially important as the height of structures continues to increase and the safety factor is lowered by economic considerations. The design wind loads associated with escarpments and hills have in many cases been shown to be inadequate: Freeston (1974), Bowen and Lindley (1974). This is partly because many of the early building codes were derived from empirical formulae or laboratory tests in uniform flow boundary layers. This project was performed with the aim of investigating the effect of hills on the flow in the atmospheric boundary layer and it should assist the calculation of the effect of local terrain on structures.

(b) Environmental effects

Concern about the environment has lead to increased interest in the dispersion of pollutants. The prediction of minimum pollution concentrations are required to determine stack sizes and the proximity of the pollution source to population centres. This requires a detailed knowledge of the transportation characteristics of wind which often requires a knowledge of wind flow over topography.

Other environmental effects of wind are concerned with the interaction of wind on the growth of trees and vegetation, the prediction of the spread of forest fires and wind as an element of weather forecasting.

(c) Aviation

The large number of inadequately or unexplained aircraft accidents in mountainous terrain points to inadequate safety heights and a lack of knowledge of mountain airflows. Better understanding of wind flow over hills would assist with the operation of aircraft.

(d) Wind power plant siting

An investigation of the wind flow over hills also has applications in wind power plant siting. It is desirable to locate wind power plants on hills to take advantage of the faster moving airstreams that can occur over hills.

Because the available wind power increases as the cube of the wind speed the penalty for selecting a poor wind power site is severe. While mean velocities are of primary interest in wind power plant siting, turbulence quantities are also required for calculating the wind loading on the blades and supporting structure.

(e) Numerical modelling

There are two approaches to simulation of the natural wind : physical modelling and numerical modelling. A valuable part of numerical modelling is the verification of the model by comparing the numerically obtained results with those found in the laboratory. There is a shortage of laboratory data with which to compare numerical models as noted by Jackson and Hunt (1975).

1.3 Value of wind tunnels in the study of atmospheric winds

Agreement between the results obtained from wind tunnel and field tests have been confirmed by a number of investigators. For good correlation between wind tunnel tests and field tests it is essential that atmospheric flows are simulated. However all the requirements for similarity between wind tunnel flows and atmospheric motion cannot be met simultaneously, Teunissen (1972), so only those quantities of greatest significance may be simulated. In the present work the Ekman Spiral could not be simulated. Thermal effects could not be simulated either, but there are many instances when high winds occur and stratification does not occur.

The wind tunnel is an expedient way of conducting investigations into atmospheric flows as various flow parameters may be varied independently and their effect on the flow observed. Strictly this is only possible in a non-equilibrium boundary layer. Wind tunnels are also useful for investigating quantities which are very difficult to measure in the field such as the effect of a hill on the gradient height. Wind tunnel tests may be used to guide field programmes, which would lead to a reduction in the time and expense of a field programme.

The controlled conditions possible in a wind tunnel mean that for any given atmospheric flow situation it is cheaper, more reliable, less time consuming and easier to collect data than in a corresponding field test.

1.4 Objectives of the project

The specific objectives of the project were:-

(a) To review the numerical, laboratory and field work concerned with the wind flow over hills.

(b) To recommission the atmospheric boundary layer wind tunnel in the Department of Mechanical Engineering.

(c) To develop a digital data handling system capable of accepting the output from a hot wire anemometer and analysing the data collected.

(d) To simulate a neutrally stable rural atmospheric boundary layer of scale about 1:300.

(e) To measure the flow properties over a series of two-dimensional model hills in the 1:300 simulated rural atmospheric boundary layer with the aim of:

(i) investigating changes in the mean velocity and turbulence structure as the wind flows over the hills,

(ii) comparing results obtained with those predicted by numerical approaches,

(iii) conducting a limited investigation of the effect of the hill shape on the wind flow over the hills,

(iv) investigating the effect of using a smooth hill surface in a boundary layer developed over a rough surface,

(v) investigating the effect of hill slope on the wind flow over hills.

(f) To simulate a neutrally stable rural atmospheric boundary layer of scale about 1:3000 and to test a selection of the hills previously used to investigate the effect of the ratio of the hill height to the boundary layer height on the wind flow over the hills.

(g) To simulate a neutrally stable urban atmospheric boundary layer of scale about 1:300 and to test a selection of the hills previously used to investigate the effect of the approach flow mean velocity profile and turbulence intensity on the wind flow over the hills.

The thesis is divided into sections which closely follow the objectives listed above.

A review of the theoretical, laboratory and field studies involving the wind flow over hills is presented in Chapter 2. Chapter 3 describes the development and evaluation of a 1:300 rural atmospheric boundary layer simulation. Chapter 4 is concerned with investigating the effect of the hill slope on the wind flow over hills. This chapter includes a description of the experimental apparatus, the procedure and results of the investigation together with a discussion and comparison of the results with existing data.

Whereas Chapter 4 was concerned with an investigation of the hill slope, Chapter 5 is concerned with an examination of the effect of the hill shape on the flow of wind over hills.

Chapter 6 determines the effect of using smooth surfaced hills in simulated atmospheric boundary layers developed over rough surfaces.

Chapter 7 describes the development and evaluation of a 1:3000 rural atmospheric boundary layer simulation. Measurements made over a number of hills placed in the boundary layer described in Chapter 7 are discussed and compared with those made in the 1:300 rural atmospheric boundary layer simulation in Chapter 8. Conclusions can therefore be drawn as to the influence of the hill height on the wind flow over hills.

Chapter 9 describes the development and evaluation of a 1:400 urban boundary layer simulation. Chapter 10 discusses and compares measurements made over a number of hills in the urban boundary layer simulation with those made in the 1:300 rural atmospheric boundary layer.

Conclusions to the project are presented in Chapter 11, and references are listed in alphabetical order at the end of the thesis.

The operation, limitations and accuracy of the hot wire anemometer and the analog signal processing equipment is discussed in Appendix 1. Appendix 2 which is contained in Volume 2 contains a detailed description of the development of a digital data handling system used to process the signal from a hot wire anemometer.

CHAPTER 2

REVIEW OF WIND FLOW OVER HILLS

2.1 Review of theoretical studies

The aerodynamic action of an obstacle placed in a boundary layer is simple in principle. Streamlines are compressed as the flow moves over the crest of the obstacle and therefore the velocity of the flow increases. The increase in velocity reduces as the distance from the crest increases. The velocity increases as the hill slope increases and once a certain slope is reached large scale separated flow appears downstream of the crest of the obstacle.

Reviews of the literature on wind flow over hills have been given by Corby (1954), Queney et.al. (1960), Davidson (1964), Nichols (1973), Meroney et.al. (1976), Bowen (1977) and Bouwmeester et.al. (1978).

Corby, Queney et.al. and Nichols review the early theoretical work on wind flow over hills. Corby discusses the work of Queney (1947), Scorer (1949) and Long (1953). All the models described by these authors used perturbation theory for a laminar, frictionless, isentropic fluid. Queney and Long developed their theories for uniform airstreams. The results obtained are therefore unlikely to predict the wind flow over ridges in the aerodynamically rough flow in the atmosphere. Some of Scorer's work allows for the variation of wind shear in the vertical.

Much of the early work was concerned with upper level atmospheric flow, lee waves and the effects of stratification. Exceptions are the work of Bartkowski (1965), Rosenberg (Golding (1955)) and Prandtl (Putnam (1948)) who developed models for uniform potential flow over low hills. The results are of little value as they apply to uniform airstreams.

More recently numerical models have been developed which try to account for all possible influences on the wind field. These models employ three-dimensional time dependent calculations and have applications in weather forecasting, predicting pollution levels and in fire behaviour prediction. Examples of these models are those of Fosberg et.al. (1976) and Hadeen and Friend (1972). Some of these models rely on the interpolation of observed data together with continuity and terrain constraints to predict the wind field.

Only those theories concerned with the flow over a two-dimensional hill are reviewed. There are a number of such models. One type of model is concerned with the interaction of surface temperatures with a vertical temperature gradient to produce thermal slope winds. Such models are described by Mahrer and Pielke (1975), Raymond (1972). These models usually consider a fairly large horizontal scale. In the present work potential temperatures are assumed uniform. A second type of model neglects stratification effects and is concerned only with the effects of the pressure field induced by the flow over the hill. Theoretical models of this nature have been considered by Alexander and Coles (1971), Frost, Maus and Fichtl (1974), Taylor and Gent (1974), Jackson and Hunt (1975), Deaves (1975), Astley et.al. (1977), Lindley et.al. (1977), Taylor (1977), Derickson and Meroney (1977).

These theories attempt to solve the governing equations of fluid motion using numerical techniques or by obtaining analytic solutions to physical models. Most of the theories do not allow for flow separation but there are some semi-analytical models which attempt to account for flow separation effects and these have also been reviewed.

2.1.1 Theoretical studies of wind flow over two-dimensional hills

The relevant theories are reviewed chronologically except where similar work by the same author appears in different years.

Alexander and Coles (1971)

Alexander and Coles consider the changes in velocity as the flow in a boundary layer moves over a general surface obstruction. The velocity at any point over the obstruction may be found for a given hill shape and upwind velocity profile.

The method adopted consists of solving the two-dimensional Navier-Stokes equations together with the continuity equation by introducing the vorticity and stream function. The resulting partial differential equations are:

$$\nabla^2 \psi = - \omega \qquad (2.1)$$

$$\nabla^2\psi + R\left(\frac{\partial\psi}{\partial x}\frac{\partial\omega}{\partial z} - \frac{\partial\psi}{\partial z}\frac{\partial\omega}{\partial x}\right) = 0 \qquad (2.2)$$

These two equations are written in finite difference form and solved using an iterative technique with appropriate boundary conditions.

In deriving equations 2.1 and 2.2 the eddy viscosity ε was assumed constant with height, so no value for the surface roughness Z_o is used. It is therefore difficult to apply the method to any given flow situation. The assumption of a constant eddy viscosity also results in a forced linearisation of the velocity profile close to the ground. Hinze (1959) gives:

$$\frac{\tau}{\rho} = \varepsilon\left(\frac{\partial U}{\partial z} + \frac{\partial W}{\partial x}\right) \qquad (2.3)$$

so near the ground:

$$\frac{\tau}{\rho} = \varepsilon \frac{\partial U}{\partial z} \qquad (2.4)$$

In the layer adjacent to the surface the stress τ and density ρ are generally assumed to be constant. Thus if the eddy viscosity ε is also constant so is $\frac{\partial U}{\partial z}$ which therefore implies that $U = a\ z + b$ near $z = 0$. Hence the velocity profile is forced to become linear near the ground. Close to the ground it is well known that the velocity profile is described by a logarithmic law and the results of Alexander and Coles are therefore of no quantitative value.

The advantage of the approach used by Alexander and Coles over other numerical models is that the flow over any hill shape may be readily examined.

Frost, Maus and Fichtl (1974)

Frost, Maus and Fichtl consider atmospheric flow over semi-elliptic cylinders which have upstream and downstream separation regions. The geometry of these cylinders simulates buildings or hills and the elliptic shape allows parametric variation of the aspect ratio. The concepts of boundary layer theory are extended by introducing the idea of a disturbed boundary layer rather than considering the complete equations of motion for turbulent flow. However the boundary layer approximations are invalid in the upstream and downstream separation regions.

In the upstream separation region pressure gradients are iteratively introduced for streamlines farther and farther from the body. This method of handling the separation region relies on the assumption that the flow over the

ellipse is not appreciably influenced by the localised separation and will be driven by pressure gradients well away from the body; an assumption which is not entirely satisfactory.

In the downstream separation region the adverse pressure gradients are much more severe and the above method is no longer considered applicable.

Results are presented for a number of ellipses which show that the maximum value of the wind speed occurs at the crest of the ellipse. The value of the maximum wind speed decreases as the elliptical aspect ratio increases or the surface roughness decreases. Larger separation regions were found to occur with a decrease in the elliptical aspect ratio or an increase in the surface roughness.

Figure 2.1 compares the wind profile at the crest of a 2:1 ellipse for two different surface roughness lengths. The ratio of the heights of the maximum velocity $\frac{\ell_1}{\ell_2}$ from figure 2.1 is approximately $\frac{4}{3}$. Equation 2.7 derived by Jackson and Hunt (1975) gives $\frac{\ell_1}{\ell_2} = (\frac{z_{01}}{z_{02}})^{1/5} = 1.32$. This is good agreement despite many of the assumptions of Jackson and Hunt's theory not being met.

The effect of varying the aspect ratio of the ellipse while keeping the surface roughness length constant is illustrated in figure 2.2. The ratio of the height of maximum velocity $\frac{\ell_3}{\ell_4}$ is approximately $\frac{3}{6}$. Equation 2.7 derived by Jackson and Hunt gives $\frac{\ell_3}{\ell_4} = 0.57$.

Frost et.al. obtained a value for the fractional speedup Δs of 1.0 for the 2:1 ellipse and 0.4 for the 4:1 ellipse, for a surface roughness length of $\frac{z_0}{H} = 0.001$. Using equation 2.8 values of the fractional speedup of 1.0 and 0.5 respectively are obtained, which once again shows good agreement with the theory of Jackson and Hunt.

Theoretical models for the flow over bluff bodies which include flow separation effects have also been considered by Fraenkel (1961), Kiya and Arie (1972) and Bitte and Frost (1976). All of these models require a large amount of empirical information.

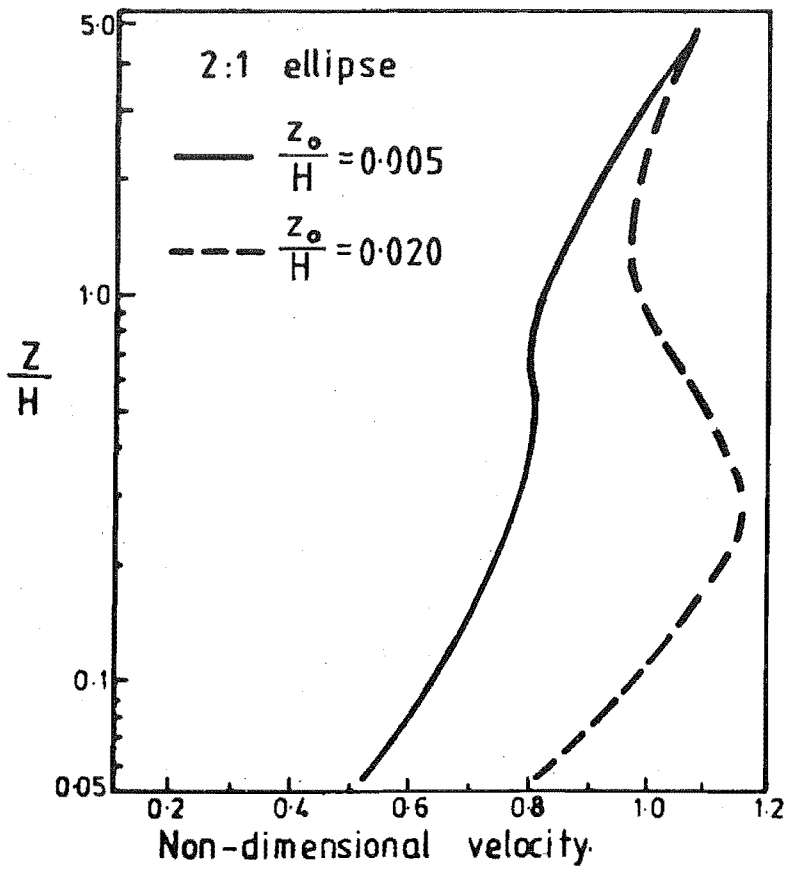

FIG. 2·1 WIND PROFILES AT THE CREST AFTER FROST ET. AL. (1974)

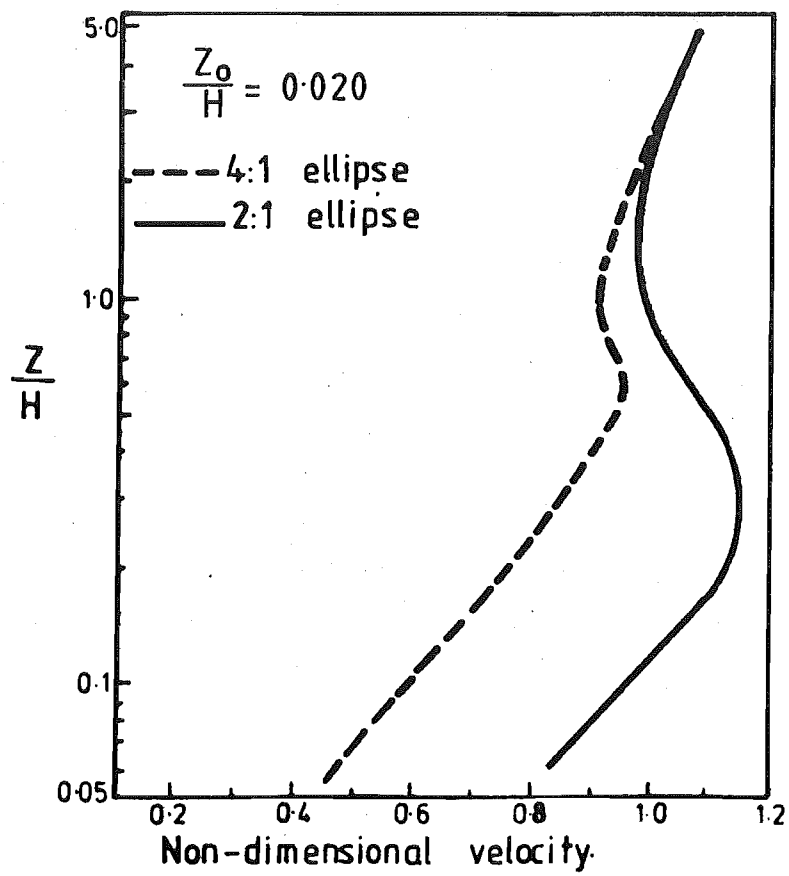

FIG 2·2 WIND PROFILES AT THE CREST AFTER FROST ET. AL. (1974)

Taylor and Gent (1974)

The method of Taylor and Gent consists of conformally mapping the region above a two-dimensional hill into a half plane. The limitation of the method is that it is difficult to predict the resulting surface shape.

Closure of the equations is obtained using two alternative models : a mixing length model and a turbulent energy equation model. After setting appropriate boundary conditions and domain dimensions the equations are solved using an iterative method and a finite difference scheme.

Results are presented for the flow over a specific hill shape. The results show very little difference between the surface pressure and surface shear stress obtained using the two closure methods. The surface shear stress and surface pressure increase with hill height and surface roughness. A rather crude extrapolation procedure suggests that separation will occur when the maximum slope of a bell-shaped hill exceeds about 19^{o}.

Taylor (1977a)

This is an extension of the work of Taylor and Gent (1974) which should prove more useful for dealing with flow over arbitrary topography than the conformal mapping technique used by Taylor and Gent. The model is based on a non-orthogonal coordinate mapping and is for non-separating, unstratified, two-dimensional flow over a constant surface roughness.

The form for the eddy viscosity described by Hinze (1959) is used. The equations of motion are transformed from a cartesian coordinate system and solved using a finite difference scheme. Results are presented for flow over Gaussian hills, valleys and sloping escarpments.

The small differences between results obtained using the method described and the method of Taylor and Gent (1974) is shown to be due to differences in the form chosen for the mixing length and closure hypotheses.

Taylor (1977b)

Taylor extended his surface layer model of Taylor (1977a) so hills of a much larger horizontal scale may be considered. Coriolis effects and a second horizontal component of wind velocity have been included.

The same closure assumption is made as in Taylor (1977a). Similarly, the turbulent energy equation and the equations for momentum and continuity are transformed into a non-orthogonal coordinate system and solved using a finite difference technique subject to appropriate boundary conditions.

A second horizontal wind velocity component is included in the model so the effect of the angle between the wind direction and the topographical features were able to be determined. The results show that the largest changes in the flow quantities occur when the flow is normal to the hill in which case the second horizontal wind component is unaffected by the hill.

Jackson and Hunt (1975)

Jackson and Hunt use an analytical theory rather than a numerical solution of various equations of motion to predict the wind flow over a low hill. The analytical approach is very useful. The flow over the hill is divided into an inner and outer region and the perturbation velocities and pressures in each region are considered. Arbitrary boundary conditions on the velocity and pressure are therefore avoided. The governing equations for the inner and outer region together with the boundary and matching conditions for the two regions are solved for the flow over a hill described by the equation:

$$f\left(\frac{x}{2L}\right) = \frac{1}{1 + \left(\frac{x}{2L}\right)^2} \qquad (2.5)$$

An important result of the analysis is that the thickness of the inner region, ℓ is given by:

$$\frac{\ell}{2L} \ln \frac{\ell}{z_o} = \text{constant of } O(1) \qquad (2.6)$$

which can be approximated by the expression:

$$\frac{\ell}{z_o} = c\left(\frac{2L}{z_o}\right)^{4/5}, \quad c = O(1) \qquad (2.7)$$

Another important result of the analysis of Jackson and Hunt is that they find that the fractional speedup, ΔS is given by:

$$\Delta S = 2\left(\frac{H}{2L}\right) \qquad (2.8)$$

The analysis is unfortunately limited to analytically well behaved hill shapes because the knowledge of an integral involving the shape of the lower boundary is required.

The fractional speedup is shown to be insensitive to the surface roughness and to be determined by the pressure gradient well above the hill where the perturbation pressure and velocity fields are shown to be irrotational and independent of the boundary layer thickness. Therefore the velocity and pressure changes over the hill can be calculated using simple potential theory. Reynolds stresses are shown to be important close to the wall, but negligible at large distances from the wall.

The analysis is limited to very low hills because of the assumptions associated with linearising the equations. For a rural boundary layer the theory is valid for hills with a maximum slope of about 0.05. The authors claim that reasonable results may be obtained for steeper hills. This claim is presumably made on the basis of a reasonable comparison with a small number of field and wind tunnel tests. The assumed logarithmic velocity profile does not describe atmospheric flow well outside a region close to the ground.

The method of Jackson and Hunt was modified and extended by Jackson (1975) to include flow over escarpments of a small size and slope.

Deaves (1975)

Deaves developed a numerical method for calculating the wind flow over two-dimensional hills. The method is closely based on that of Alexander and Coles (1971) but Deaves uses Prandtl's mixing length hypothesis to obtain the variation in the eddy viscosity with height instead of assuming the eddy viscosity is constant. This is a more realistic description of the variation of the eddy viscosity with height in the Earth's boundary layer.

The two-dimensional Navier-Stokes equations and the continuity equation are solved by writing the equations in a finite difference form and applying a relaxation technique with appropriate boundary conditions. The method is shown to be insensitive to realistic boundary conditions and closure assumptions. The results obtained agree well with other reported results.

Deaves fails to state what value of the roughness length was used in the results presented. The results also fail to predict the shear stress minima upwind and downwind of the hill as found by Taylor (1977a).

The advantage of the method of Deaves is that the slender obstruction may be of arbitrary shape. This is in contrast to the methods of Taylor and Gent (1974) and Jackson and Hunt (1975) where transformation of the lower boundary or a knowledge of an integral involving the shape of the boundary limits the method to analytically well behaved hill shapes.

Astley, Lindley, Bowen and Flay (1977)

Astley et.al. attempt to solve the full Navier-Stokes equations, the continuity equation and an arbitrary closure assumption using a finite element approach. A single matrix equation is derived which must be solved using an iterative scheme with appropriate boundary conditions.

The finite element approach appears to work well for the case of uniform flow, but for flow over irregular topography the set of equations will not converge. The convergence problem appears to be related to the introduction of the convective matrix which leads to instability in the iterative scheme.

Lindley, Astley, Flay and Bowen (1977)

In an effort to overcome the convergence problems of the method described by Astley et.al. (1977) a frozen vorticity approach is adopted. The method relies on the results obtained by Jackson and Hunt (1975) who showed that except for a small region close to the surface the flow is effectively inviscid.

The vorticity equation $\nabla^2\psi = -\omega$ is solved within a control surface with set boundary conditions which may be easily varied. The problem is formulated in terms of finite elements and the resulting matrix equation is solved iteratively for the stream function.

The method is shown to give good agreement with the wind tunnel results of Bowen and Lindley (1974) for an escarpment of slope $\tan^{-1}\frac{1}{2}$, although separation and the action of Reynolds stresses cause poor agreement downstream of the separation point. Further comparisons of the theory with field and wind tunnel measurements are reported by Astley (1977).

The advantage of the finite element approach over other numerical methods, especially the finite difference method is that the topography may be completely arbitrary. In addition, the grid size may be varied to accommodate different rates of change in the flow quantities in different areas. Any initial vorticity distribution corresponding to different incident velocity profiles may be used.

Derickson and Meroney (1977)

Derickson and Meroney describe an inviscid flow model which uses stream function vorticity and an equation for potential temperature. The solution of the equations involves a coordinate transformation. Horizontal and vertical grid expansions are used to give increased resolution at the hill crest.

Results are presented for the flow over two sinusoidal hills with $\frac{H}{L} = 0.5$ and 0.67. The numerically calculated flow compares well with wind tunnel measurements over the same hills made by Bouwmeester et.al. (1978). Small differences in the results are due to differences in the upstream approach conditions and the imposed conditions on the numerical model well above the hill. The good agreement suggests that speed up is primarily an inviscid mechanism, and that viscosity and turbulence are merely modifying effects.

2.1.2. Conclusions

It was considered worthwhile to review the relevant theories in detail because they are reported to accurately model wind tunnel and field measurements of wind flow over hills. Jackson and Hunt (1975), Deaves (1975) and Astley (1977) all present results which show good correspondence between their theoretical results and experimental results.

The theories reviewed are subject to the limitations described below.

(a) Hills of gentle slope

Most of the theories are limited to describing the wind flow over hills with a very gentle slope. This requirement arises because of three conditions: the inability of the theoretical models to handle separated flow, the requirements of a turbulence closure hypothesis and simplifications necessary to solve the equations.

(i) Linearisation of the equations. Generally the equations describing the flow must be simplified before they can be solved. Jackson and Hunt (1975) solve their equations for the flow over a hill described by $y = H\, f(\frac{x}{L})$. They require that:

$$f(\frac{x}{2L}) \to 0 \quad \text{as} \quad (\frac{x}{2L}) \to \pm \infty \tag{2.9}$$

$$\text{and } \frac{H}{2L} << \left(\frac{\ln \frac{\ell}{z_o}}{\ln \frac{L}{z_o}}\right)^2 \quad \text{and} \quad \frac{2L}{z_o} \to \infty \tag{2.10}$$

For rural terrain these conditions imply that $\frac{H}{L} < 0.025$. The method of Jackson and Hunt (1975) can therefore only be applied with confidence to very gentle hills.

The requirements necessary to simplify the equations are usually the most demanding constraints.

(ii) Turbulence closure. A number of the theoretical approaches reviewed use Prandtl's mixing length hypothesis to relate the Reynolds stresses to the mean flow. The use of the mixing length hypothesis is not strictly correct in such applications where the flow curvature is relatively large. Prandtl's mixing length hypothesis was developed for the case of uniform flow where it yields the well known logarithmic law describing the velocity profile. It has been applied to the non-uniform flow over hills, an assumption which is likely to limit the results obtained to hills of small slope.

(iii) Separation. Most of the theories require that the flow does not separate. This requirement is likely to limit the maximum value of $\frac{H}{L}$ to about 0.4. There are some theories which attempt to handle flow separation. Such theories apply only to very simple hill shapes and usually require a large amount of empirical information.

(b) Well-behaved hill shapes

Many of the theories are limited to analytically well-behaved hill shapes. Taylor and Gent (1974) require a transformation of the lower boundary. They report that it is easiest to select a given transformation and see what the

shape of the resulting surface is than to try and predict the shape of the surface. Similarly Jackson and Hunt (1975) describe a theoretical approach which requires the knowledge of an integral involving the shape of the lower boundary.

There are some theories that may be applied to arbitrary topography, notably those of Astley (1977) and Deaves (1975).

(c) General limitations of two-dimensional ridge flow

Flow perpendicular to simple two-dimensional ridges is a very simple approach to a complex atmospheric flow phenomena. In the atmosphere the shape of the hill or ridge is very irregular which may cause a wind direction dependency of the speed up factor. The roughness of the surface is also very important as an internal boundary layer could develop along the slope and over the summit. The effect of buoyancy forces may radically alter the speed up factor. The only theoretical model reviewed which allowed for the effects of stratification was that of Derickson and Meroney (1977). Most of the other authors claim that there are many instances when high winds occur and stratification has a small effect on the flow.

2.2 Review of laboratory studies

A review of the early laboratory work on wind flow over hills is given by Corby (1954), Petterssen (1961) and Lange (1961).

Petterssen (1961) discusses the poor correspondence between anemometer measurements in the field and wind tunnel measurements over the corresponding hills made as part of the Putnam wind power project in 1948. Lange (1961) also discusses these measurements and reasons that the poor agreement is due to the laminar airstreams used in the wind tunnels compared to the turbulent air found in the field. Also, there was difficulty in determining the undisturbed wind at the level concerned.

Corby (1954) in his review of laboratory work concludes that modelling has met with only little or partial success because of the absence of dynamical similarity. Qualitative agreement between wind tunnel and field results were found in the work of Field and Warren (1933) and Abe (1941). Field and Warren modelled the flow around the Rock of Gibraltar and even though stability

was not simulated reasonable agreement was shown with field observations. Abe modelled the flow around Mt. Fuji. It was the first attempt to simulate wind shear and stability in wind tunnel experiments.

It was not until the work of Jensen (1958) that a sound basis has developed for wind tunnel modelling. Since then there have been many contributions which have assisted the development of topographical modelling.

Only the work concerned with the flow over two-dimensional obstacles in shear layers is reviewed in this section. There is a large volume of work related to the flow over topographical models but this work is site specific and only the most general conclusions may be drawn from it.

2.2.1 Measurements of wind flow over hills in the laboratory

The relevant laboratory work is reviewed in chronological order - except where similar work by the same author appears in different years.

Plate and Lin (1965)

Plate and Lin tested two types of models in a wind tunnel : wedges, where the vertical face was placed towards the flow; and symmetrical sinusoidal hills. The models were placed in a number of turbulent boundary layers artificially thickened by means of a trip fence and surface roughness at the wind tunnel entrance. The effect of the boundary layer height, different vertical temperature gradients and mean velocities of 4.6 m/s to 18 m/s on the flow over the models were investigated.

One purpose of the study was to obtain model laws which permit the scaling of natural boundary layer flows with obstructions in a wind tunnel. The momentum equation was derived in a form such that the validity of the assumptions about pressure effects may be checked against measurements made. The investigation yielded very satisfactory agreement between assumptions and experimental results for the velocity distributions at large distances downstream from the models, but no conclusions could be drawn for the flow in the standing eddy region directly downstream of the hill.

Mean velocity and turbulence intensity profiles are presented at a number of longitudinal positions. There is ample evidence on the effect of the boundary layer thickness and mean velocity on the flow over the obstacles, but no consistent trends are obvious.

Plate and Lin divided the flow over the obstacle into three zones : a region of undisturbed flow upstream from the model, a region of highly disturbed flow near the model and a region where the boundary layer is being re-established. A boundary for each zone was found by plotting mean velocity profiles on a semi-logarithmic graph and observing the disturbed and undisturbed velocity profiles. Analytical expressions for the boundaries were determined.

The turbulence intensity profiles show that there is a steep increase in turbulence in the vicinity of the hill which decreases rapidly with downstream distance. The spectra of the fluctuating velocity component at the crest appears to be invariant with height which indicates that no new turbulence is generated. Downstream of the hill, the spectra show increased energy at low frequencies compared to the spectra at the crest.

Chang (1966)

Chang investigated the separation region between the free stream and the separation bubble downstream of a wedge shaped hill. Half-jet theories were applied to the separated flows considered and compared to the measured velocity distributions.

The experiments were performed in a closed circuit wind tunnel at free stream velocities of 9.2 m/s and 13.9 m/s. A small trip fence and some surface roughness were placed at the entrance to the tunnel. No pressure corrections to the wind tunnel roof were made after the installation of the models. Pitot tubes were used to measure the mean velocity and hot wire anemometers were used to measure the fluctuating components of the velocity. Static pressures were measured using the holes of a cylindrical pitot-static probe and it is therefore likely that the static pressure measurements suffered from probe misalignment as the flow was assumed to be parallel to the floor and walls of the wind tunnel. The flow reattachment point was measured using a specially developed dual hot wire probe.

The mean velocity profiles are given in the region behind the hills. The measured mean velocity profiles were found to give good agreement with half-jet theories after the effect of the initial boundary layer thickness and the normal pressure gradient across the mixing region had been allowed for.

de Bray (1973)

de Bray measured the mean velocity over a number of two-dimensional escarpments with source, sine wave and straight-line approach ramps placed normal to the flow. The tests were performed in two turbulent boundary layers with mean velocity profile power law exponents of $\frac{1}{7}$ and $\frac{1}{8.5}$ and local turbulence intensity values of 12% and 15% respectively close to the ground. Some tests were also made in a uniform flow.

The purpose of the tests was to check the "escarpment rule" in some codes of practice which is used for calculating the wind loads on buildings and structures.

Measurements were confined to mean velocities made with a pitot-static probe. The measurements must consequently be treated with caution in regions of high turbulence intensity. Also, no allowance appears to have been made for the effect of the flow angle on the pitot-static tube.

The measured mean velocity profiles show that greater speed up near the ground occurs for shear flows than for a uniform flow. Gentle slopes not qualifying for correction under the escarpment rule were found to yield increases in the dynamic pressure of up to 100% close to the ground.

Counihan (1973)

Counihan describes tests made over a series of two-dimensional sinusoidal hills and escarpments with various ramp angles in a simulated rural atmospheric boundary layer. Tests were performed using two different hill heights. The surfaces of the models were coated with sand to obtain the desired surface roughness.

The mean velocity profile at the crest of the sinusoidal hills was found to be more uniform as the hill slope decreased to the smallest value of $\frac{H}{L}$ used, which was 0.33. As the hill slope decreased the wake extent decreased. Separation was found to occur when the ratio of $\frac{H}{L}$ was greater than 0.43.

The five escarpments had similar mean velocity profiles at the crest which agrees with the measurements reported by Bowen and Lindley (1977). The steeper escarpment ramps caused the perturbations in the downstream flow to reduce more quickly.

A number of the hills and escarpments caused lee waves to occur in the wake flow, and the conditions for the occurrence of lee waves is presented.

Counihan (1974)

Counihan extends his previous work over single hills to the flow over concatenated sinusoidal hills in a simulated rural boundary layer. The mean velocity, velocity fluctuations and the Reynolds stress were measured at various positions over the hills.

At the crest of the first hill the mean velocity was increased and the turbulence intensity was reduced at all heights compared to the upstream reference values. At the crest of any subsequent hill the mean velocity was lower and the turbulence intensity was higher than the upstream reference values. The flow patterns were found to become repetitive downstream of the third hill, which is consistent with the flow moving over a rougher surface.

The trends in the Reynolds stress were similar to the trends in the turbulence intensity. The Reynolds stress was reduced at the crest of the first hill but was increased at the crest of any subsequent hill relative to the upstream reference values.

Freeston (1974)

Freeston continued the work of de Bray (1973) which investigated the escarpment rule in recent Codes of Practice. The Codes of Practice are largely empirical and modify the upwind profile using an artificial base which depends on the escarpment.

Three escarpments with approach ramp angles of 20°, 40° and 60°, a 1 in 4 sine ramp and a source ramp were placed in a simulated atmospheric boundary layer generated using a Cowdrey grid and some surface roughness. The wind tunnel static pressure gradient was set to zero by means of an adjustable roof after the escarpments were placed in the wind tunnel. Measurements were restricted to mean velocities measured using a pitot-static rake and surface static pressures.

The sine, source and 20° ramp escarpments showed no evidence of flow separation and had similar peak pressures at or near the crest. The 40° and 60° escarpments exhibited flow separation with reattachment distances of two

to four escarpment heights downstream of the crest. The escarpments exhibiting flow separation had a less permanent effect on the flow which was noticeable at large distances downstream of the crests. There was a reduction in wind speed up to four escarpment heights upstream of the crests.

The results obtained lead Freeston to conclude that the codes are inadequate both in the shape of the velocity profiles and in the extent of their downwind influence.

Bowen and Lindley (1974)

Bowen and Lindley present preliminary results for the flow over a cliff escarpment and an escarpment of slope ¼ placed in the 1:300 rural atmospheric boundary layer simulation described by Raine (1974).

In these tests the surface layer of the models were smooth compared to the upstream wind tunnel roughness elements which lead Bowen and Lindley to suggest that the mean velocity profiles would recover more slowly than for a rough hill surface.

Only mean wind speeds and mean dynamic pressures are presented.

Bowen and Lindley (1977)

Bowen and Lindley investigated the flow over four two-dimensional forward facing escarpments of slope 0, 1, ½ and ¼. The escarpments were placed in the same boundary layer used by Bowen and Lindley (1974), but in these tests the escarpments were covered with the upstream wind tunnel roughness elements. The mean wind speed, turbulence intensity and energy spectra over the escarpments were measured using a hot wire anemometer.

The mean velocity profiles over the escarpments were found to be insensitive to the escarpment slope angle. From the mean velocity profiles the amplification factors for the flow over the escarpments were calculated. The maximum amplification factor obtained was higher than that found by previous investigators. Bowen and Lindley suggest that this is caused by the displacement depth due to the roughness elements making the effective height above the surface less than the actual height measured above the surface.

The measured mean velocity profile in the approach flow reported by Raine (1974) does not indicate that a zero plane displacement depth is needed in the approach flow as a logarithmic velocity profile fits the data very well close to the ground. It is difficult to see how the relatively high values of the amplification factor obtained can be used as the sole criteria for a zero plane displacement.

Significant changes in the turbulence characteristics of the flow were shown to occur only in the wake region which grew after the crest in all cases. This was a region of high shear and low mean velocities where the energy in the flow shifted to higher frequencies. The size of the wake region was found to increase as the escarpment slope angle increased.

Rider and Sandborn (1977)

Rider and Sandborn investigated the effect of the hill shape on the approach flow by subjecting a single approach profile to six different hill shapes. Each hill was of the same length (42 cm) and the same height (2.5 cm), and the hill shapes tested were a full sine wave, half sine wave, triangular, trapezoidal, ramp and box.

Measurements were made in a 0.37 m x 0.37 m x 2.54 m open circuit wind tunnel at a zero pressure gradient. A turbulent boundary layer was grown by the use of five trip fences followed by 1.22 m of roughness. Profiles of the mean and fluctuating longitudinal velocity component were measured at the foot and at the crest of each hill. The upstream reference approach profile was measured in the same longitudinal position as the foot of the hills, but with no hill present. Therefore the true velocity profile incident on the hills was not obtained as it is likely that the upstream velocity profile was changing appreciably with streamwise distance.

The triangular and sinusoidal hills were found to have the greatest speed up. The local turbulence intensity was reduced as the flow moved over the hills as predicted by the theory of turbulence undergoing a contraction.

Comparison of the results with those from a much larger wind tunnel showed that small scale flow systems can be used to determine the gross features of the flow over hills. The flow characteristics over the hills therefore appeared to be independent of the Reynolds number.

Bouwmeester, Meroney and Sandborn (1978)

The wind tunnel programme described by Bouwmeester et.al. was commenced early in 1975 with the aim of assisting in locating suitable sites for wind energy conversion systems. The influence of turbulence, hill shape, surface roughness and thermal stratification over a range of triangular and sinusoidal hill shapes was investigated.

In phase 1 of the work the hill models were mounted on a false floor in the wind tunnel. Mean velocities were measured using a Kiehl probe and a pitot-static probe. Turbulence quantities were measured using a dual hot wire anemometer probe. In phase 2 and 3 of the work static pressures close to the hill surface were measured with a disc probe which is largely insensitive to the flow angle. In these cases coolant channels were placed upstream of the hills and tests were also made with some additional surface roughness.

The triangular and sinusoidal ridges used were found to have the same speed up if the average upstream and downstream slopes were the same. The separation region was very dependent on the upstream and downstream slopes. A large separation region lead to reduced velocities at the crest.

The effect of thermal stratification on the flow was also investigated. Stratification resulted in reduced turbulence over the ridge and a much larger downstream separation region. The speed up at the crest decreased with stable stratification and increased with unstable stratification.

A technique for predicting the mean velocity profile at the hill crests was developed. The technique involved approximating the velocity profile at the crest by a power law. Using the method developed it was possible to predict the wind tunnel results to better than 5%.

In the inner region close to the ground over the hill there was a strong interaction between the turbulence and the main flow. The longitudinal turbulence intensity and the shear stress increased towards the crest. Further out in the boundary layer the longitudinal turbulence intensity increased towards the base of the hills and decreased over the crest. The spectra and probability density functions along a streamline did not show much change.

The largest speed up was found to occur for symmetrically shaped hills which just avoid flow separation.

2.2.2 Conclusions

There are very few tests of model hills in carefully simulated atmospheric boundary layers.

From the laboratory experiments reviewed the following conclusions may be drawn:

(i) As the wind flows over a hill the mean velocity increases and the turbulence intensity decreases. The maximum velocity occurs at the crest and is greatest for symmetrical hills which just avoid flow separation. The changes in the mean velocity and turbulence compared to the upstream reference conditions are largest close to the ground and decrease rapidly with height above the ground.

(ii) If the hill is of sufficient slope a wake region may form downstream of the hill. This is a region of high shear and low mean velocities where significant changes in the turbulence characteristics occur. The size of the wake region decreases as the hill slope decreases and the downstream distance increases.

(iii) The mean wind speed and turbulence at the hill crest for given approach flow conditions depends on the hill slope, hill shape, surface roughness length of the approach flow and thermal stratification.

2.3 Review of field studies

Field investigations of the wind flow over hills are required to validate the results obtained by the numerical and laboratory studies. But rigorous field tests over hills which lead to the experimental verification of speed up factors in the atmosphere are very scarce due to the following factors:

(i) Hills in the field are rarely a perfect shape and irregular shaped hills lead to a directional dependency of the speed up factor.

(ii) The experiments required are complex and simultaneous measurements at a number of heights and longitudinal positions are required in the absence of thermal effects because the speed up depends on conditions such as stability and insolation.

(iii) Wind direction will vary with time which will cause the effective slope and roughness of the hill to change as well as the angle of the hill crest to the flow. These factors will cause the wind flow pattern over the hill to change.

(iv) Some field measurements over hills have been made at sites which have poor exposure. For example much of the data collected during the E.R.A. wind survey (Golding and Stodhart (1952), Wax (1954), Tagg (1957)) used 3.1 m high masts. At this height the local roughness will have a large influence on the results.

Frequently, conflicting reports are made on wind measurements over hills in the atmosphere. Juul (1949) made simultaneous measurements on flat ground and on a nearby exposed hilltop. The results shown in figure 2.3 suggest that the high wind speeds on the hilltop are caused by a lack of friction due to such obstacles as trees and buildings. Davidson (1964) in a review of wind power site selection procedure doubts if any speed up over hills exists: "... In general it may be concluded that it is almost impossible a priori to estimate the numerical value of the speed up if indeed such a factor exists for any particular locality".

In contrast Shellard (1963) has shown that unusually high winds do occur over hills and ridges.

A number of wind surveys have been made in hilly terrain in which it is difficult to deduce anything about the nature of the wind flow over hills. Archibald (1973) made measurements at a single height at two hilltop sites. While each site exhibits very high annual windspeeds, little can be deduced from the measurements about the effect of the hill on the wind flow over it. This is partly due to the absence of measurements of the upstream approach flow.

Some wind surveys do indicate that substantial speed up effects exist over hills. Measurements made by Hardy (1977) at a number of sites on a Hawaiian Island suggest that the mean hourly windspeed at a ridge site is about twice that at a nearby coastal location. Weidner and Stearns (1978) made measurements as part of a four station micrometeorological network which also showed that substantially higher wind speeds were recorded on hills and higher ground than on flat ground.

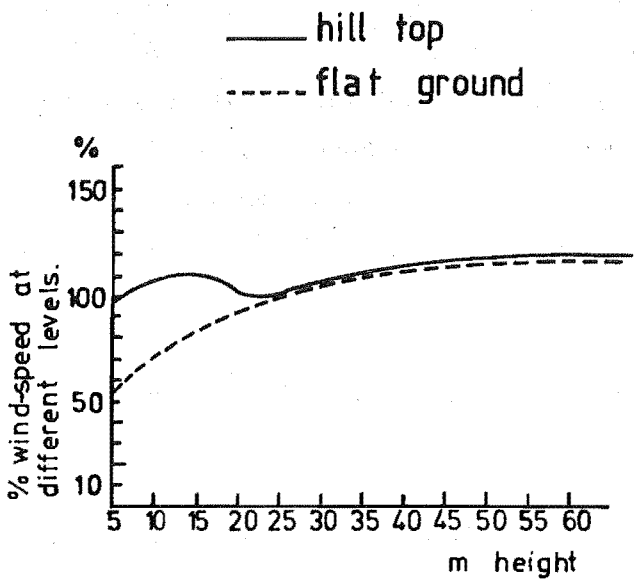

FIG 2·3 WIND-SPEED MEASUREMENTS AFTER JUUL (1949)

The E.R.A. made a wind survey over most of the United Kingdom in the 1950's, the purpose of which was to assess the potential of wind as a source of energy. Results of the survey have been presented by Golding and Stodhart (1952), Wax (1954) and Tagg (1957). Good wind power sites were found on hill-tops and the high wind speeds measured confirm that speed up over hills exists. Most of the measurements were made at a single height at the hill crest and no simultaneous measurements were made of the upwind undisturbed wind profile. It is therefore difficult to draw any conclusions about the effect of the hill. Tagg (1957) concludes: ..."Clearly little information can be extracted from the results about the effect of any particular slope on the flow of wind over a hill". The best sites were found to be "fairly steep, smoothly shaped hills" well exposed, free from screening by higher ground and with a maximum slope of less than 1/3 ($\frac{H}{L} < 0.67$).

2.3.1 Measurements of wind flow over hills in the atmosphere

The field work concerned with the wind flow over hills is reviewed below in chronological order except where similar work by the same author appears in different years.

Frenkiel (1962)

Frenkiel presents the results of a study of wind behaviour at two hill sites. One site was at the crest of a hill which was part of a mountain ridge; the other site was at the crest of an isolated conical hill. For more than one year continuous measurements of wind speed, wind direction and the vertical temperature gradient were made at the crest of each hill at heights of 10 m, 25 m and 40 m. The aim of the study was to correlate the topography of a site with the wind flow over it.

The mean velocity profiles were found to be determined by the upwind hill profile and the thermal stratification and to be unaffected by the wind speed. The crest velocity profiles obtained under neutrally stable conditions showed the importance of the hill profile near the measurement mast. A larger velocity gradient at the hill crest was found to occur for either a slight rise near the crest or an increase in the hill slope further upwind of the crest.

Frenkiel suggests that no vertical wind gradient will occur at the hill crest when the hill has a small hilltop area and a slope of about 16°.

Frenkiel (1963)

Frenkiel presents results for the gust variation over the two hills previously described. The gust variation with height and the gust amplitude are tabulated as 1 s or 2 s means.

The gust factors appear to be independent of wind direction and therefore hill slope.

Shellard (1963)

Shellard compares the mean wind speeds obtained by the British Meteorological Office at the summits of two hills, Lowther Hill and Drum with the windspeeds at two low-level stations 45 km away. Ratios of the mean windspeeds of 1.9 and 1.8 respectively were obtained indicating a substantial increase in windspeed at the hill crests. Reasonable estimates of the mean windspeeds at the hill crests were obtained assuming flat ground and using an 0.17 power law and a gradient height of 400 m. Based on these results the increased wind speed at the hill crests is due to the normal increase in wind speed with height.

Davidson (1964)

Davidson reviews the work of Golding and Stodhart (1952), Frenkiel (1962) and Shellard (1963).

Results are presented from measurements made at a coastal site in the Netherlands. An increase in wind speed of about 12% occurred at the hill crest, but this value was very dependent on wind direction and therefore hill slope.

Experimental results of mean wind speed and direction at two sites in the French Alps are also presented. By comparison with sites away from the Alps, speed up occurs when the wind direction is within 30° of the normal to the ridge and the air is stable.

Mitsuta (1971)

In this work measurements were made at sixteen anemometer sites in the Naruto Straits, Japan, for a period of five years to obtain design data prior to erecting powerlines. The Naruto Straits consists of a 5 km wide channel which narrows to 1.2 km for a short distance; the results obtained therefore apply to rather unusual topography.

Wind profiles obtained from two masts show that the effect of the topography was to produce a nearly uniform velocity profile with the maximum wind speeds occurring at low levels.

Measurements were also made on a ridge site using eight anemometers at a 10 m height spaced at 40 m intervals along the ridge. When the wind was incident on the ridge at right angles an average amplification factor of 1.8 was measured relative to a station on the upwind side of the ridge. There were large variations in the velocity readings along the ridge due to local topographic effects.

Hardman, Helliwell and Hopkins (1973)

This work updates British Meteorological Office data over the United Kingdom previously presented by Shellard (1963). Longer records now exist at the hill sites of Lowther Hill (8 yrs) and at Great Dun Fell (10 yrs). The wind speed data from these two isolated hills are compared to wind speed data from nearby sites on level terrain. As found by Shellard (1963) for Lowther Hill and Drum, the wind speeds on isolated hilltops are given to a good approximation by the air at the same height in the free air upstream of the hill assuming a 0.17 power law and a gradient height of 400 m.

Eliseev (1973)

This work discusses a stereophotogrammetric survey over an isolated hill whose profile is shown in figure 2.4. Ten minute windspeed averages were measured over the hill at heights up to 70 m. Measurements were made during the morning and evening, and the average speed of the approach flow was 3.0 m/s at a height of 5 m. This low speed combined with the time of the surveys suggests that the measurements are likely to be influenced by thermal effects.

The measured variation of the amplification factor with height is shown in figure 2.5 at a number of positions over the hill : at a distance x = -150 m from the hilltop (1); above the hilltop (2); on the leeward side of the hill at a distance x = 100 m (3). The reference velocity, $\bar{U}_o$ used was that measured 50 m upwind from the foot of the hill. The profiles in figure 2.5 show that the amplification factor decreases with height except behind the crest where very low wind speeds occur close to the ground due to flow separation at the crest.

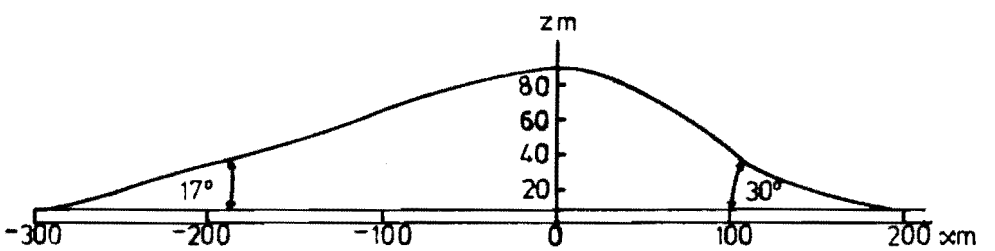

FIG 2·4 HILL PROFILE AFTER ELISEEV (1973)

1 = 150m upstream of hill top

2 = at the hill top

3 = 100m downstream of hill top

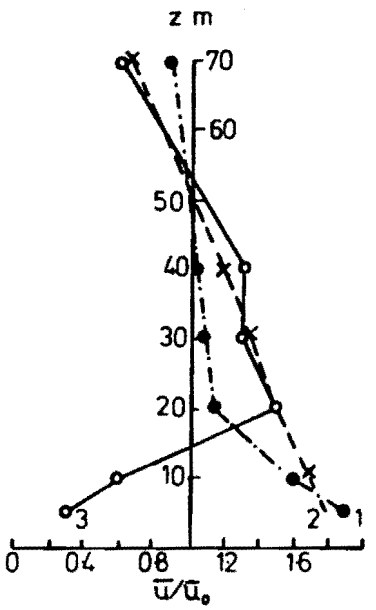

FIG. 2·5 AMPLIFICATION FACTORS AFTER ELISEEV (1973)

Bowen and Lindley (1974)

In this work, measurements of 20 min mean windspeeds were made over a 26^{o} sloping escarpment and a cliff escarpment up to a height of 10 m above the ground using cup anemometers. All the measurements were made when the wind was within 20^{o} of a line normal to the escarpments. Because of the inherent inaccuracies of cup anemometers in shear flows the mean velocity readings were judged accurate to within 7%.

Wind profiles were measured at a number of longitudinal positions over the escarpments. Each wind profile was compared to the undisturbed wind profile five escarpment heights upstream of the escarpment crest which had a power law exponent of 0.10 and 0.45 for the sloping and cliff escarpments respectively.

The wind profiles lay within 20% of those obtained in corresponding wind tunnel tests except very close to the ground. Bowen and Lindley suggest that this deviation was due to differences in the roughness and flow separation effects between the wind tunnel and the field.

The investigation revealed that the values of the amplification factor varied widely, but were usually within the range 1.1 to 1.4. Local peak values of up to 1.7 for the sloping escarpment and 2.1 for the cliff escarpment were measured close behind the crest and within the first escarpment height above the local ground level. The values of the amplification factor were consistently greater for the cliff than for the sloping escarpment.

The major modifications to the flow was confined to 2 or 2.5 escarpment heights above the ground and extended to 12 escarpment heights downstream of the escarpment edge.

Jensen and Peterson (1978)

This work discusses the measurements made by Panofsky and Petersen (1972), and Peterson, Kristensen and Su (1976). The aim of these measurements was to study the roughness change associated with the flow of air from water to land and so improve the theoretical models which apply to such a roughness change. The variation in the surface elevation of the site was found to affect the measurements more than the variation in the surface roughness. Careful re-

analysis of the results of Panofsky and Petersen (1972) showed that speed up was occurring over the small escarpment.

The theoretical treatment of two-dimensional flow over hills by Jackson and Hunt (1975); Frost, Maus and Fichtl (1974), and Taylor and Gent (1974) were reviewed and applied to the flow over the escarpment studied by Panofsky and Petersen (1972). The theories are all shown to predict the measured results well despite a noticeable roughness change and the application of the hill theories to an escarpment shape.

The fractional speed up was calculated for the 28 velocity profiles measured over a small rise by Peterson, Kristensen and Su (1976). There is some scatter, but no observed dependence on the Richardson Number or the wind-speed. The maximum fractional speed up was found to be closely predicted by the theory of Jackson and Hunt (1975).

Jensen and Peterson divide the wind profile over the escarpment into three sections: a region close to the ground where the flow is adjusting to the combined conditions of a changed surface roughness and an imposed pressure field; an intermediate region; and a region well above the ground where the flow is uninfluenced by the surface conditions.

Sacre (1978)

Sacre made measurements over a 50 m high hill with an average slope of 10° situated in open country. On the axis of greatest hill slope three 25 m masts were erected. One mast was placed 1900 m upwind of the hill crest, another mast was placed on the upwind hill slope and the third mast was placed near the hill crest. Arrays of Gill propellor anemometers were attached to the masts at heights of 10 m, 15 m, 20 m and 25 m.

Because the topography was irregular at each mast, the measured flow characteristics were divided according to the incident wind direction into twelve sectors each of 10°. Twenty minute means of the flow quantities were then studied sector by sector. For all the results presented the mean wind speed was always greater than 6 m/s to ensure neutrally stable conditions.

The turbulence intensity was found to decrease over the summit while the integral time scale in the longitudinal direction increased. Length scales were calculated using Taylor's hypothesis which is not valid as the flow is

changing appreciably with streamwise distance. The increase in kinetic energy and the Reynolds stress was found to be slightly less than the square of the fractional speed up. The ratio of the component variances over the hill was found to remain the same. This is in contrast to the results of Rider and Sandborn (1977a).

Relations were found to describe the variation in speedup with roughness, local topography and the overall effect of the hill. The overall fractional speedup was found to be approximately equal to three times the upwind slope, a conclusion that is supported by Jackson and Hunt (1975).

2.3.2 Conclusion

In the preceding review the field measurements of wind flow over hills have been summarised.

The following conclusions are made:

(i) The mean velocity profile at the hill crest depends on the overall hill slope, the local roughness, the hill gradient close to the mast, the thermal temperature gradient and the approach mean wind velocity profile, but is independent of the wind speed.

(ii) There is a lack of carefully controlled field tests aimed at systematically evaluating the influence of various parameters on the wind flow over hills. In a large number of investigations no measurements of the upstream approach wind structure were made, so it is difficult to correlate the wind flow at the crest with the upstream incident wind structure. In a number of reports no measurements of the thermal temperature gradient, or wind direction, was made so the effect of these parameters on the measurements is uncertain.

(iii) Some tests have been made in very unusual topographic conditions (e.g. Mitsuta (1971)) and it is impossible to deduce any more than very general trends from such measurements.

(iv) There is a lack of turbulence measurements over hills. This is undoubtedly due to the inability of such instruments as cup counter anemometers to record wind speed fluctuations.

CHAPTER 3

A 1:300 RURAL ATMOSPHERIC BOUNDARY LAYER SIMULATION

The atmospheric boundary layer wind tunnel in the Department of Mechanical Engineering was designed and constructed by Raine (1974). In the original design the two stage fan unit was at the entrance to the working section but in early 1976 the fan unit was relocated on the mezzanine floor downstream of the working section as suggested by Raine.

The advantages of relocating the fan assembly were:

(i) to reduce the noise level,

(ii) to improve the flow quality by overcoming the poor uniformity at the discharge side of the fans and making the flow at the entrance to the working section less turbulent.

The purpose of the work described in this section was to reestablish a simulated atmospheric rural boundary layer of linear scale about 1:300, similar to Raine's simulation. Such a boundary layer is characterised by a power law exponent of about 0.17 and a roughness length Z_o of about 5 cm.

3.1 Experimental apparatus

3.1.1 The wind tunnel

Despite the modifications described above, the description of the wind tunnel facility given by Raine (1974) is still relevant.

Figure 3.1 is a diagram of the wind tunnel. Air enters the working section of the wind tunnel through a coarse honeycomb consisting of cardboard tubes 6 cm in diameter and 25 cm in length. On each side of the coarse honeycomb there is a fine wire gauze screen which causes a reduction in the turbulence intensity and improves the flow uniformity. After passing through a 1.25 contraction which provides a more uniform and less turbulent flow the air enters a second honeycomb. This honeycomb was not present in the 1:300 simulation described in this chapter but was used in the simulations described in Chapters seven and nine. The cell length of the second honeycomb was 7.5 cm and with

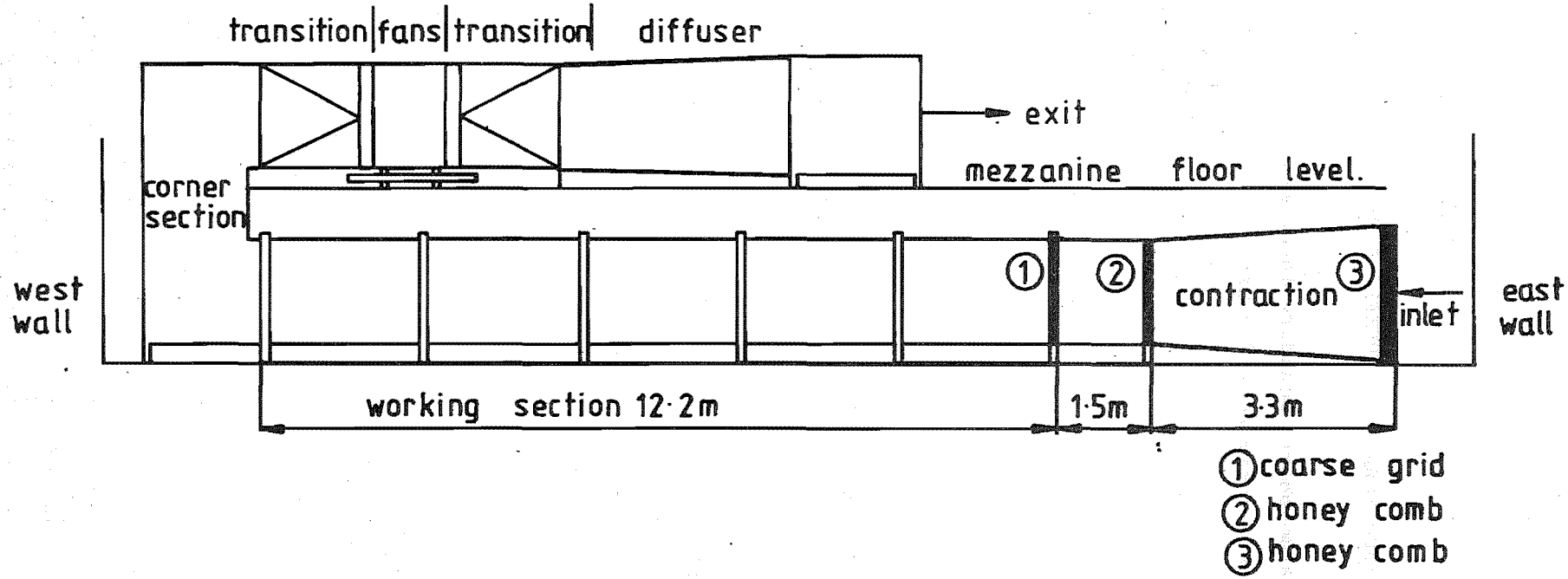

FIG. 3·1 ATMOSPHERIC BOUNDARY LAYER WIND TUNNEL.

0.95 cm across the flats of the hexagon cells the cell length to mesh ratio was 8. The purpose of this honeycomb was to provide flow straightening, remove lateral and vertical fluctuations in the flow and reduce the streamwise velocity fluctuations.

The working section of the wind tunnel is of square cross-section 1.22 m x 1.22 m with a 12.2 m long working section. The roof is suspended on threaded steel rods which permit adjustment of the longitudinal pressure gradient. The north wall consists of wood panelling and is fitted with flush surface static pressure taps at mid-tunnel height. Each static pressure tap in the wall is also connected to a static tap in the wind tunnel roof so the measured static pressure at any streamwise position is an average of the static pressure at the wall and at the roof.

The floor of the wind tunnel has an access slot running the length of the wind tunnel. Under the floor a motorised trolley runs on a track. On a vertical bar fixed to the trolley a horizontal bar is mounted and probes may be fixed to this bar. Air operated pistons on the horizontal bar ensure the bar provides a firm support. Streamwise and vertical traversing is therefore provided with a minimum of blockage.

After passing through the working section the flow moves through two corner sections incorporating guide vanes to a two stage Woods 48J½-2 contra-rotating fan unit. The pitch of the blades in this unit may be adjusted to avoid induced flow swirl in the working section.

The air is exhausted through a diffuser at the mezzanine floor level.

A view of the working section of the wind tunnel is shown in figure 3.2.

3.1.2 Flow measuring equipment

All mean and turbulence flow velocity measurements were made with two channels of DISA 55D00 series hot wire anemometer sets. These are shown in figure 3.3. The longitudinal component of the flow velocity was measured using a DISA 55F25 or 55F31 single wire probe. The single wire was orientated in a horizontal plane with the mean velocity perpendicular to the wire. A DISA 55A32 cross wire probe was used to measure the vertical and lateral velocity components v', w', the w component energy spectra and the Reynolds stress $-\overline{uw}$. The longitudinal component of the flow velocity could also be measured using

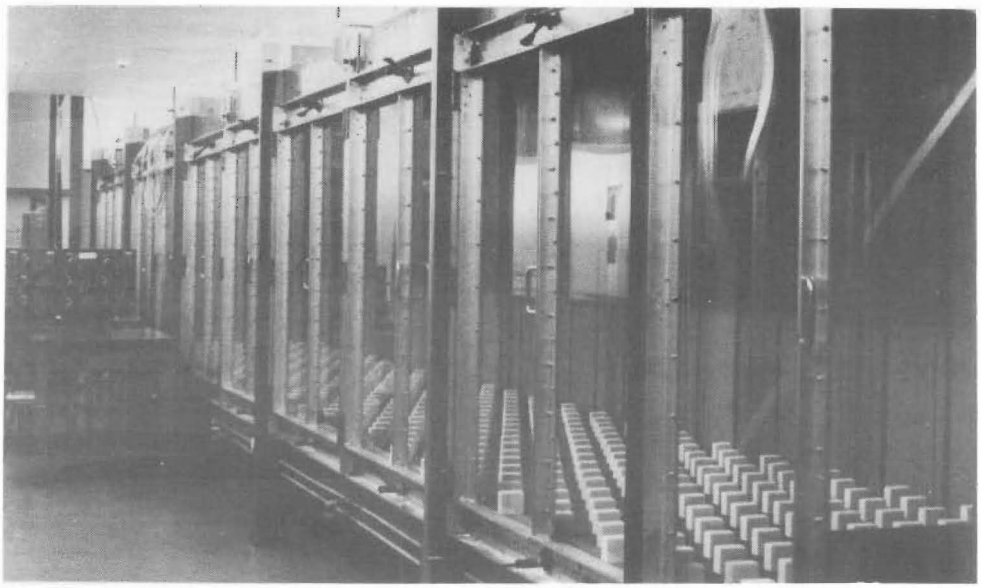

Fig. 3.2 The working section of the wind tunnel

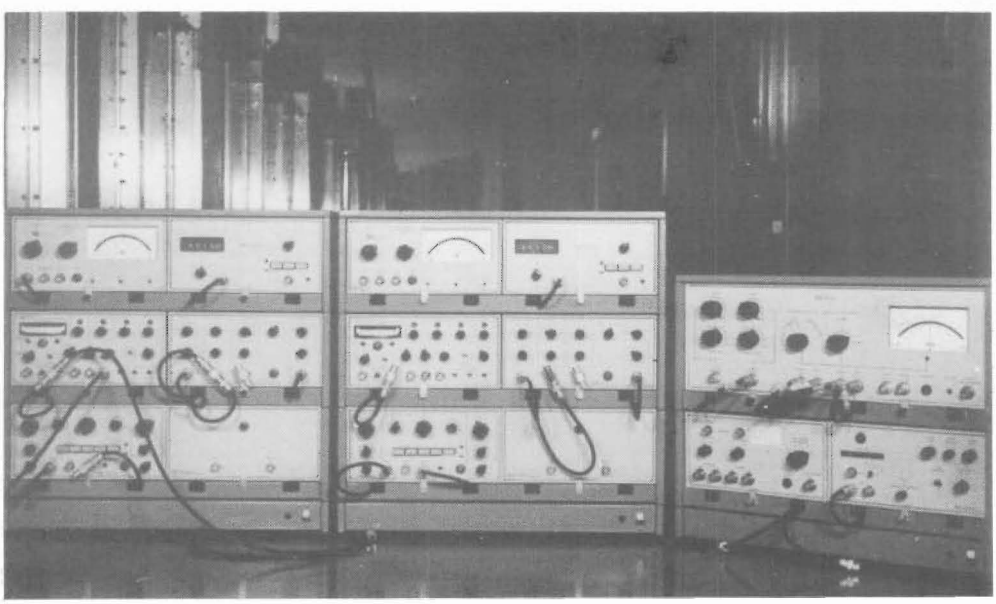

Fig. 3.3 The D.I.S.A. hot wire equipment

the cross wire probe and this provided a useful check on the operation of the equipment.

The two anemometer sets were connected as shown in figure 3.4 and operated according to the instructions in the DISA operating manuals.

The hot wire probes were calibrated daily using a Thermosystems (T.S.I.) Model 1125 calibrator unit. This unit provides a uniform, swirl free flow over the flow velocity range found in the wind tunnel.

Details of the operating procedure of the hot wire anemometers and estimates of the errors associated with their use are described in Appendix 1.

All measurements of absolute velocity were made using a Prandtl pitot-static probe and a Setra Model 237 low range pressure transducer which had been calibrated against a Schiltknecht 612A Precision Micromanometer. The output from the pressure transducer was read on a T.S.I. DC/RMS voltmeter, Model 1037 operated on a 10s time constant.

The output from the reference pitot-static probe fixed in the wind tunnel was read directly on a Schiltknecht 612A Precision Micromanometer.

For much of the later work a digital data acquisition system was developed as described in Appendix 2. This system was not available for the work described in this chapter, so all the measurements were made using analog equipment.

3.1.3 Flow traversing equipment

The probe traversing equipment is shown in figure 3.5. To avoid blockage of the wind tunnel flow the horizontal arm of the traversing trolley was kept about 35 cm above the wind tunnel floor and the DISA 55H01 traversing mechanism and DISA 52C01 stepper motor with a geared guide tube were mounted on the horizontal arm of the traversing trolley. The stepper motor was driven from the stepper motor drive in the DISA 52B01 sweep drive unit which was housed in the DISA TCA unit. A DISA 55F25 probe was mounted in a probe holder and attached by means of a guide tube and collet to the geared guide tube. The DISA 55F31 probes were mounted in a probe holder and attached by means of a collet to the horizontal arm of the traversing trolley.

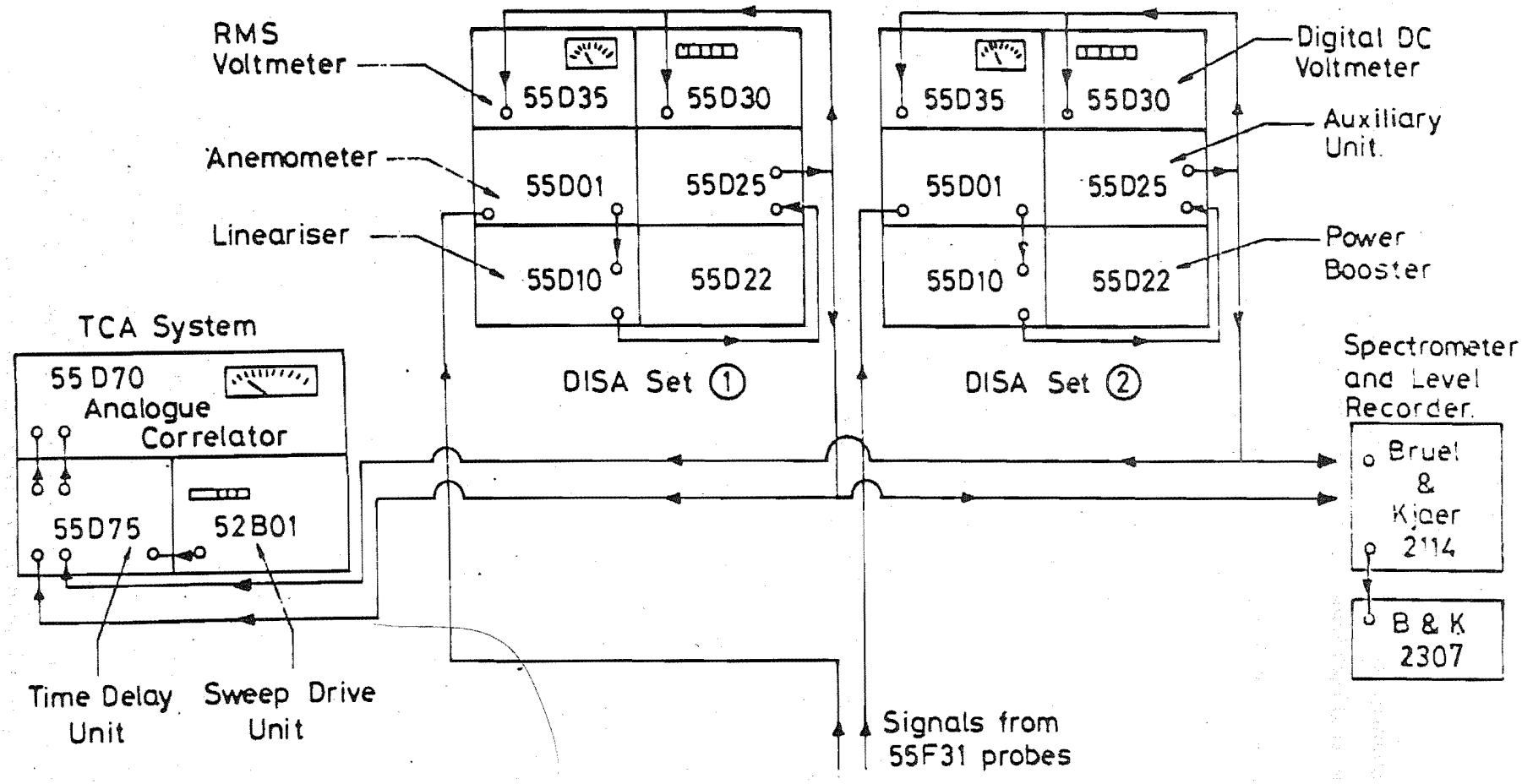

FIG 3·4 CONNECTION DIAGRAM FOR HOT-WIRE ANEMOMETERS AFTER RAINE (1974)

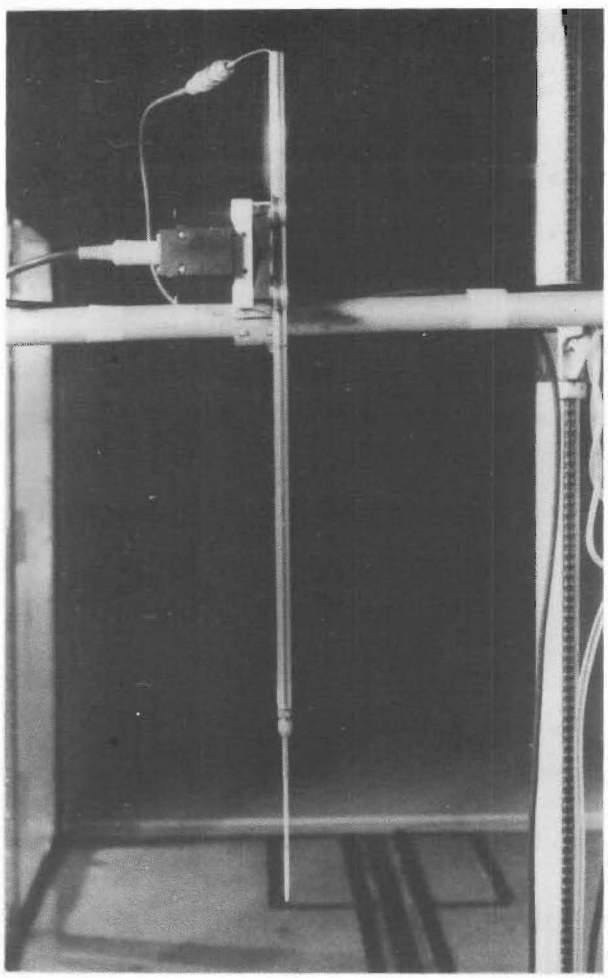

Fig. 3.5 The probe traversing equipment

The probes were traversed at lateral locations 25 cm north and south of the wind tunnel centre line. These were considered satisfactory positions to locate any non-uniformities in the flow. Wind tunnel centre line measurements were avoided because of the possible influence of the vertical bar of the traversing trolley on the flow.

Measurements in the bottom 25 cm of the boundary layer were made using the DISA 52C01 stepper motor. The remainder of the measurements were made using the probe attached to the horizontal arm of the traversing trolley. After a number of measurements had been made the probe was returned to a datum and the signal checked. If any drift had occurred linear interpolation was applied to the intermediate measurements.

When absolute velocity measurements were required the pitot-static tube was attached to the DISA geared guide tube by means of two clamps.

3.1.4 Signal processing

The linearised hot wire anemometer output was fed to a DISA 55D30 DC voltmeter and DISA 55D35 RMS voltmeter for the measurement of the mean and standard deviation of the signal.

For this part of the project, although the development of the digital data acquisition system was underway it was not yet available for signal processing. Spectral analysis was therefore performed using a Bruel and Kjaer Type 2114 $\frac{1}{3}$ octave bandwidth spectrometer and Type 2307 level recorder. The disadvantage of these instruments were the long processing times and lack of low frequency information due to the relatively high low frequency cut-off. These disadvantages were overcome with the development of the digital system described in Appendix 2.

Correlation measurements were made using a DISA TCA unit which consisted of a DISA 55D70 analog correlator, a DISA 55D75 time delay unit and a DISA 52B01 sweep drive unit. The output from the correlator unit was recorded on a Hewlett-Packard 7035B X-Y recorder.

The DISA 55D70 analog correlator was also used for measurement of the Reynolds stress.

3.2 Experimental procedure

Raine (1974) concluded that a simulated atmospheric rural boundary of linear scale as large as 1:300 was possible in the 12.2 m long working section only if a step change and boundary layer growth scheme was adopted. Since Raine completed his work a large number of similar schemes have been reported in the literature verifying Raine's conclusions : Gandemer (1973), Hunt and Fernholz (1975), Melbourne (1977).

It was therefore decided to work with the coarse grid, initial trip fence and Torro roughness elements but avoid the use of successive trip fences along the working section which were used in Raine's simulation. No other simulations make use of successive trip fences along the working section and a uniform downstream roughness should hasten the establishment of equilibrium conditions which is desirable.

3.2.1 The grid

The grid was placed at the entrance to the working section and was therefore located at X = 0 m. The purpose of the grid was to introduce large scale turbulence at all heights.

The wooden grid used by Raine (1974) was found to have warped and was replaced with a metal grid. The metal grid consisted of 1.9 cm square bars which move in a track in which the bars may be clamped. This infinitely adjustable grid was found to be satisfactory. In the work described in this chapter two 1.9 cm bars were placed together to form 3.8 cm bars both vertically and horizontally.

The initial grid arrangement used seven uniformly spaced horizontal bars and seven uniformly spaced vertical bars.

3.2.2 The trip fence

The purpose of the trip fence was to cause an initial thickening of the boundary layer and an increase in the turbulence level at all heights.

The trip fence was placed 0.61 m downstream of the grid and was made of 16G aluminium sheet 15 cm high as used by Raine (1974). Four bolts held a 0.3 cm hardboard sheet 10 cm high to the front edge of the aluminium fence. Slots

in the hardboard sheet allowed the height of the fence to be adjusted. This adjustment was found to be essential as small changes in the fence height caused marked changes in the turbulence levels downstream. The fence was held in position by 0.48 cm diameter fence posts glued to the rear face of the fence and fitted to holes drilled in the wind tunnel floor.

The initial trip fence height was set at 15 cm.

3.2.3 Surface roughness

The surface roughness consisted of 12.7 cm x 12.7 cm Torro baseboard squares glued to 1.2 m lengths of 0.3 cm thick hardboard, previously used by Raine (1974). The dimensions of the surface roughness elements are shown in figure 3.6.

The surface roughness extended from immediately behind the trip fence to 11.5 m downstream of the grid.

3.2.4 Wind tunnel conditions

All the tests described in this chapter were carried out at the maximum wind tunnel speed of 19 m/s at 90 cm above the floor at X = 9 m. A reference pitot-static probe was placed in the flow at X = 9 m, z = 1 m and 15 cm in from the north wall of the wind tunnel and was continuously monitored to ensure the wind tunnel speed was consistent.

The height of the wind tunnel roof at the grid was set at 1.23 m and a divergence of 0.6° was set for the remaining panels except for the last roof panel which was set horizontal.

3.2.5 Flow uniformity

Initial checks were made of the lateral uniformity at a number of streamwise locations. These measurements were made using a pitot-static rake shown in figure 3.7, and with the initial grid and trip fence arrangements described above.

The results presented in figure 3.8 show the variation in the dynamic pressure which is proportional to the square of the velocity. The variation in the mean velocity shown in figure 3.8 was considered satisfactory.

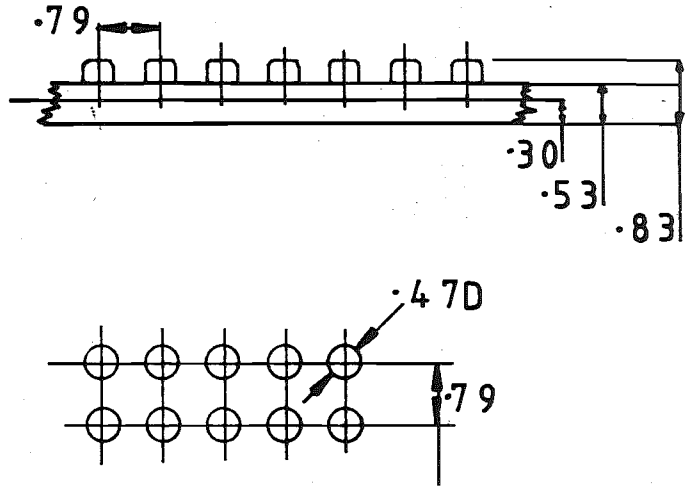

All dimensions in cm.

FIG 3·6 TORRO ROUGHNESS.

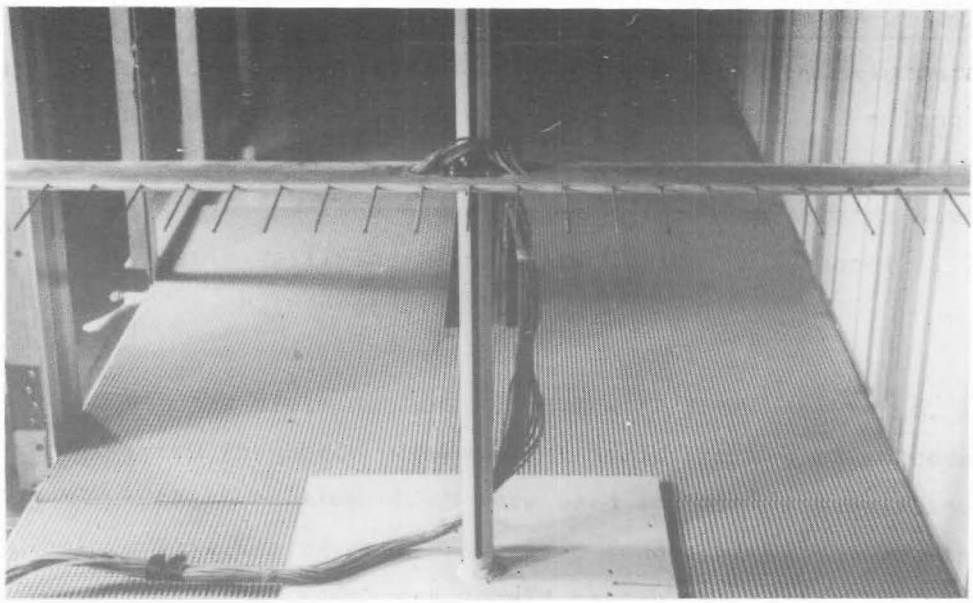

Fig. 3.7 Photograph of the pitot-static rake

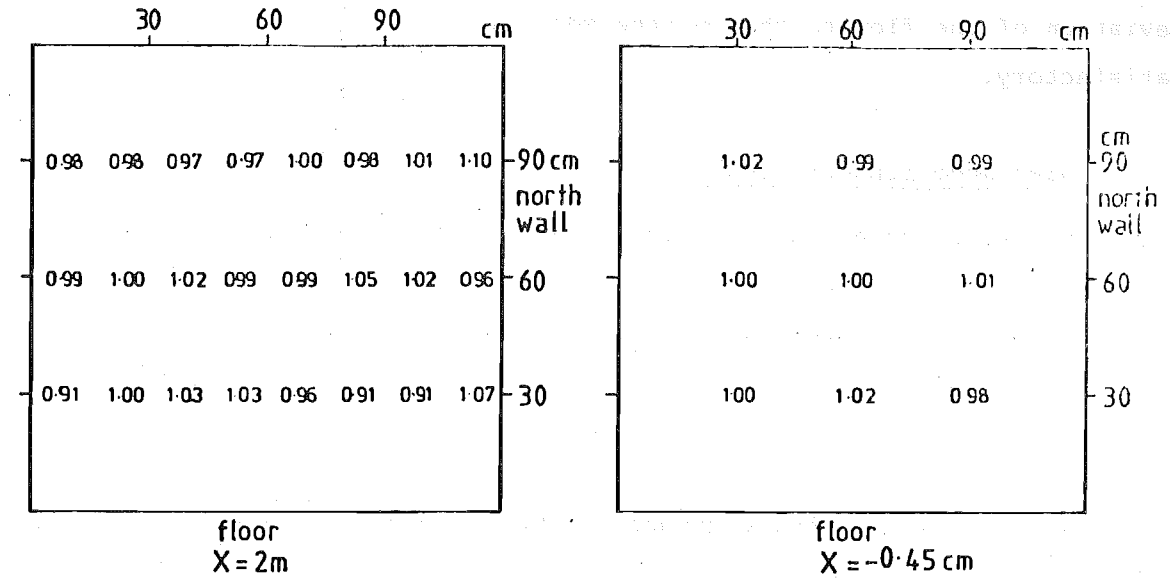

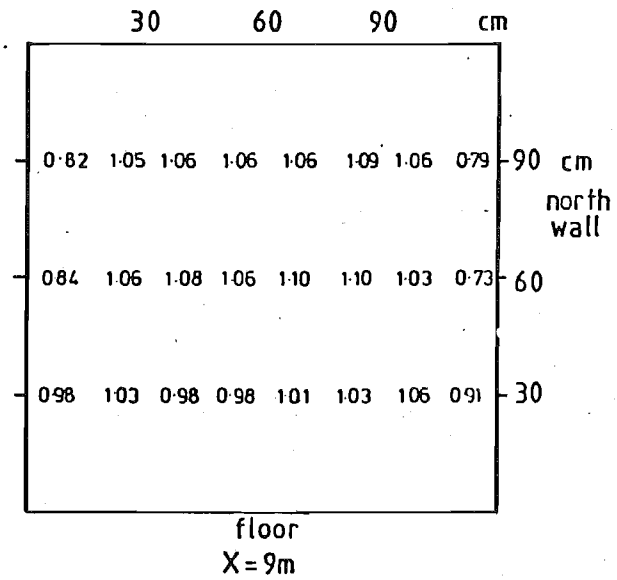

- flow away from reader
- X = distance downstream of working section entrance
- values graphed are :-

$$\frac{\text{dynamic pressure}}{\text{average dynamic pressure at each height.}}$$

FIG 3·8 FLOW UNIFORMITY MEASUREMENTS.

3.2.6 Swirl measurements

Raine (1976) recorded a number of problems associated with flow swirl in the working section of the wind tunnel. Preliminary measurements were therefore made with a five hole yaw probe at X = 9 m. The maximum measured deviation of the flow to that of the mean flow was 3^{o} and this was considered satisfactory.

3.2.7 Wind modelling procedure

The trip fence height and grid bar spacings were adjusted until the mean velocity and turbulence intensity profiles at X = 9 m were considered satisfactory for a rural atmospheric boundary layer simulation with a roughness length Z_o of about 5 cm. This was achieved with a trip fence height of 18 cm and the grid arrangement shown in table 3.1.

The rural atmospheric boundary layer simulation is evaluated in section 3.3.

3.3 Detailed evaluation of the final layout

In this section detailed measurements are presented for the final simulation.

The following measurements were made:

(i) mean velocity profile,
(ii) u, v and w component turbulence intensity,
(iii) Reynolds stress.
(iv) u and w component energy spectra,
(v) autocorrelation coefficients,
(vi) lateral and vertical cross-correlation coefficients of the u velocity component,
(vii) self preservation of the flow at X = 11 m,
(viii) static pressure gradient.

3.3.1 Mean velocity profiles

The mean velocity profile at X = 9 m is shown in figures 3.9 and 3.10. Figure 3.9 indicates that the worst lateral non-uniformity is ± 1.8% about the lateral mean at z = 25 cm. This was considered acceptable and compared favourably with the simulation described by Raine (1974).

Horizontal grid bars	
Bar number	Distance from the top of the iron clamping frame at the floor to the centre of the bar
1	11.7 cm
2	24.3
3	36.9
4	49.3
5	62.6
6	77.0
7	93.6
8	109.6

Vertical grid bars	
Bar number	Distance from the outer edge of the iron clamping frame on the north wall to the centre of the bar.
1	12.4 cm
2	29.1
3	45.9
4	62.4
5	79.0
6	95.4
7	111.9

Each bar is 1.9 cm x 3.8 cm with the largest face towards the flow.

TABLE 3.1. Final grid arrangement.

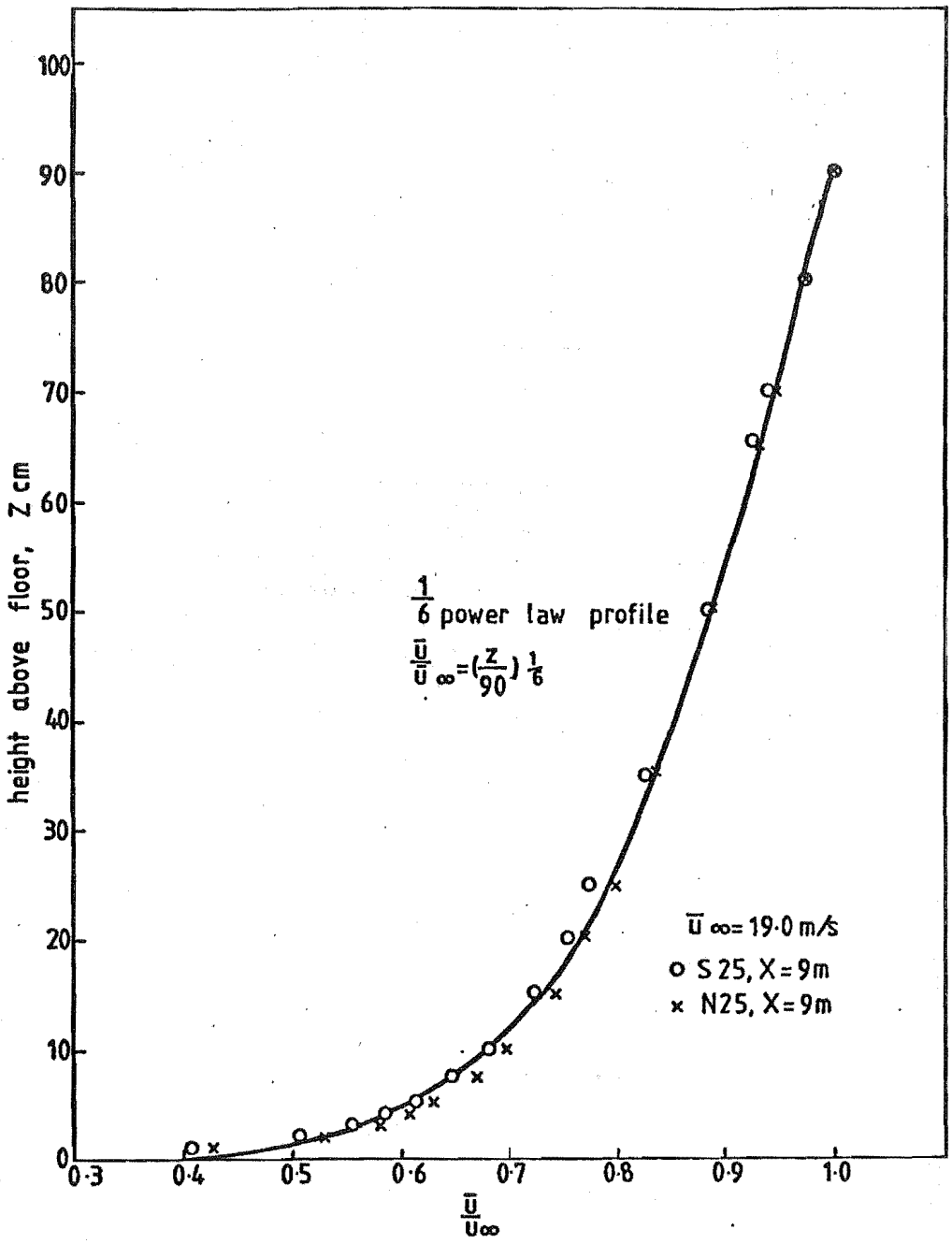

FIG 3·9 MEAN VELOCITY PROFILE.

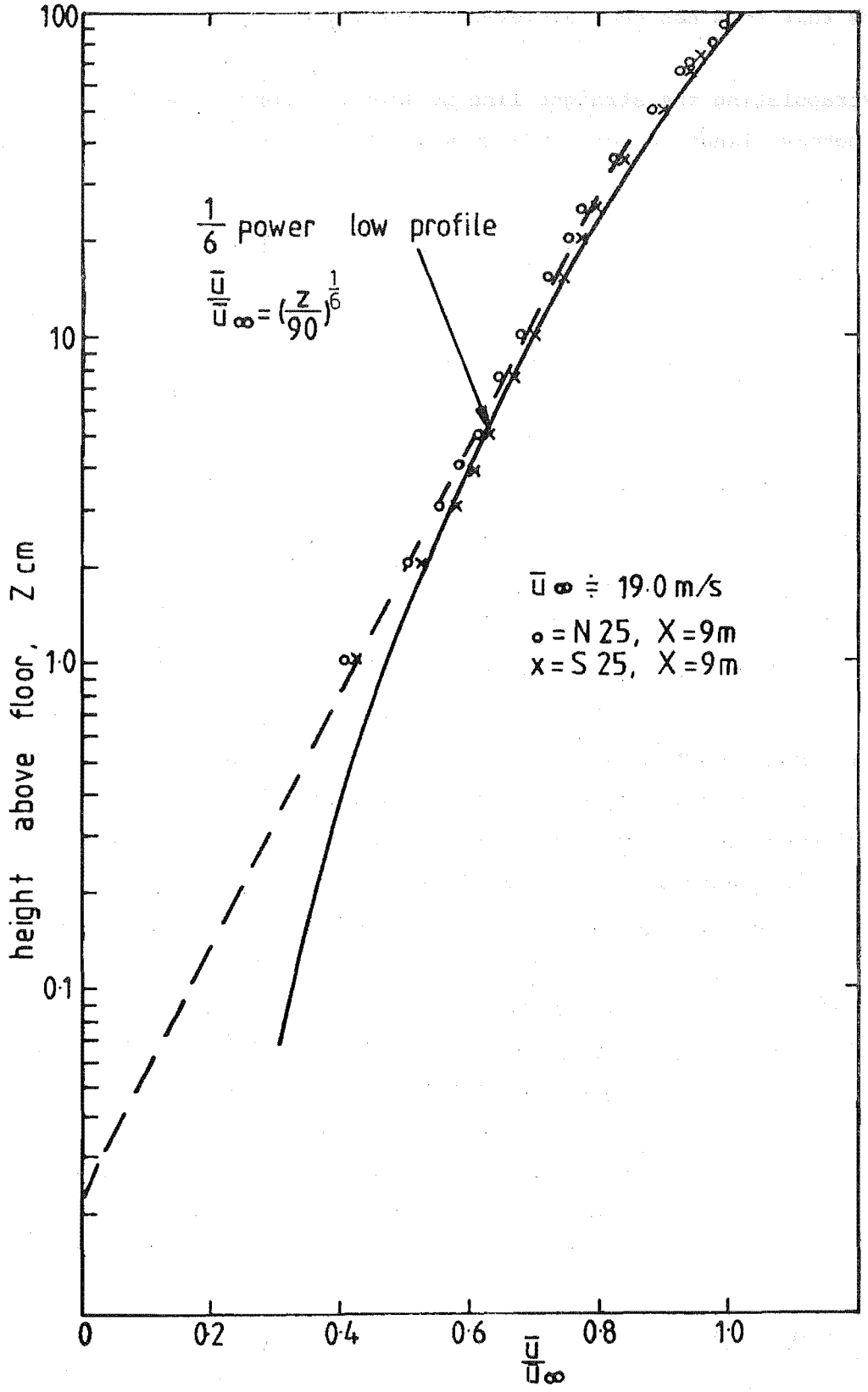

FIG 3·10 MEAN VELOCITY PROFILE

Figure 3.9 shows the close agreement with a 1/6 power law mean velocity profile which is representative of flow over rural terrain. The lower part of the atmospheric boundary layer is best represented by a log law and figure 3.10 shows that this has been achieved in the simulation.

Extrapolating the straight line portion of figure 3.10 yields a value of the roughness length Z_o of 0.023 cm which may be compared to Raine's value of 0.020 cm.

3.3.2 Turbulence intensity profiles

Figure 3.11 is a plot of the turbulence intensity profiles in the form $\frac{u'}{\bar{U}_\infty}$, $\frac{v'}{\bar{U}_\infty}$, and $\frac{w'}{\bar{U}_\infty}$. From this figure close to the floor

$$u' : v' : w' = 2.30 : 1.90 : 1.00$$

which compares favourable with the data of Teunissen (1970):

$$u' : v' : w' = 1.92 : 1.54 : 1.00.$$

Further out in the boundary layer

$$u' : v' : w' = 1.19 : 1.00 : 1.00$$

This indicates that w' is too high in the outer part of the boundary layer. Results obtained by Raine (1974) and Cook (1973) show a similar trend. Raine attributes the high w' values in the outer part of the boundary layer to the use of trip fences to thicken the boundary layer and the consequent high shear stress values that occur in the accelerated boundary layer growth process.

Figure 3.12 shows the variation in the local u component turbulence intensity with height. Lateral uniformity is shown to be good and reasonable agreement with Raine's results were obtained. The profile shape is shown to be satisfactory when compared with the design curve of E.S.D.U. (1972) plotted for Z_o = 5 cm which is a realistic roughness length for rural terrain. From figure 3.12 the turbulence intensity profile was considered to be scaled at about 1:300 between the simulation and the atmosphere.

3.3.3 Reynolds stress profile

The Reynolds stress profile 25 cm south of the wind tunnel centre line is shown in figure 3.13 where comparisons are made with the 1:300 simulation described by Raine (1974) and the data of E.S.D.U. (1974).

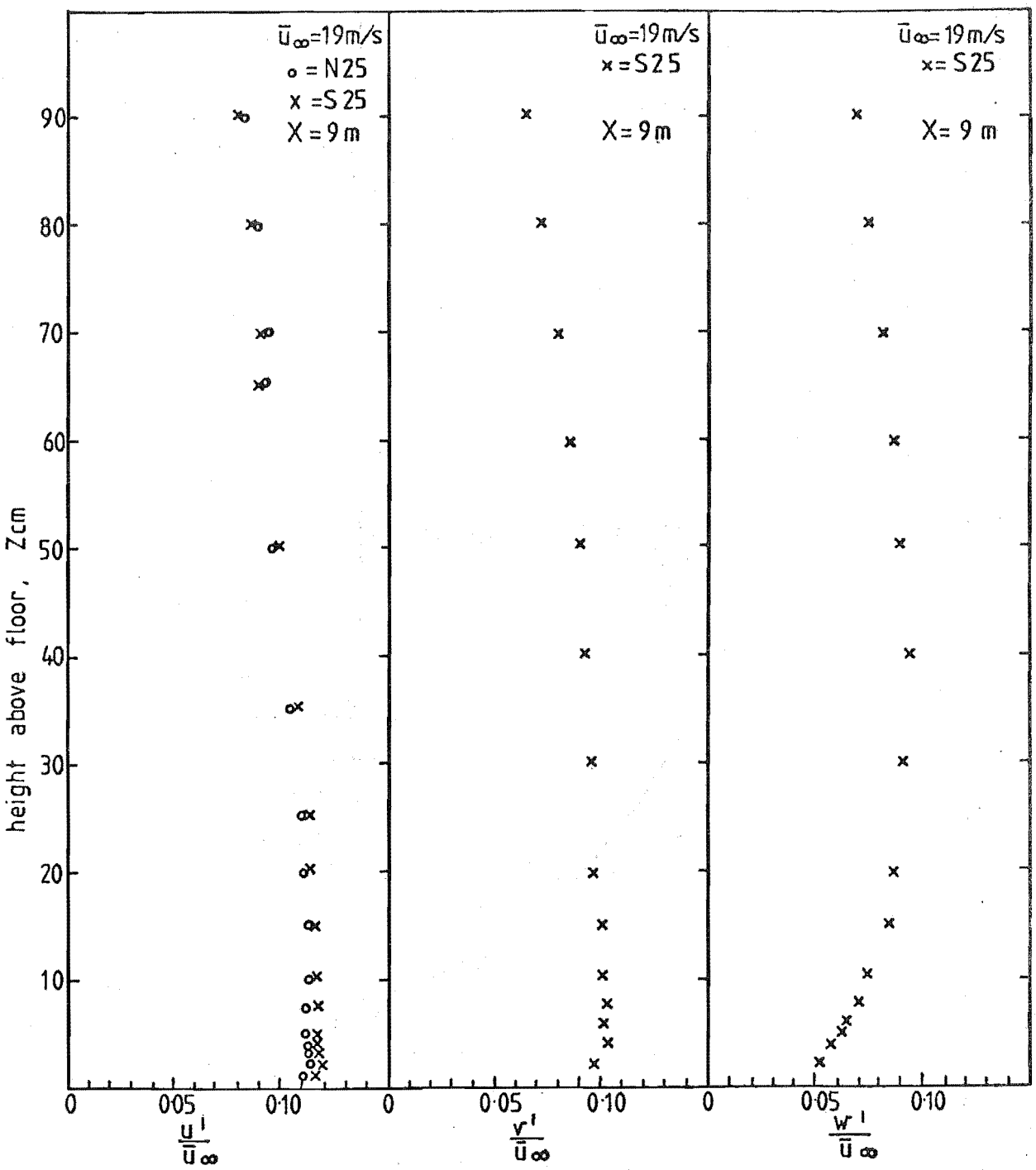

FIG 3·11 TURBULENCE INTENSITY PROFILES

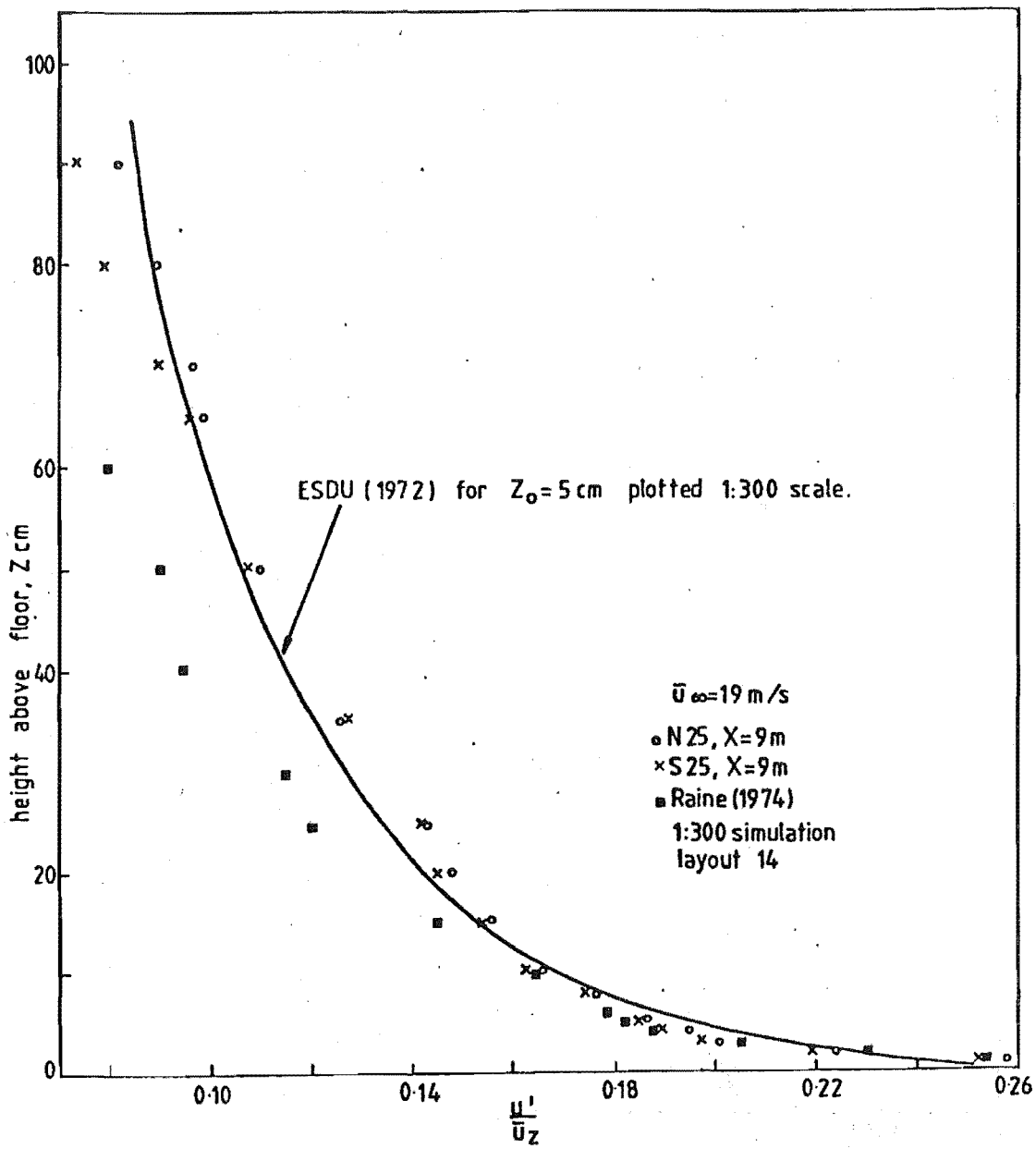

FIG 3·12 U COMPONENT TURBULENCE INTENSITY.

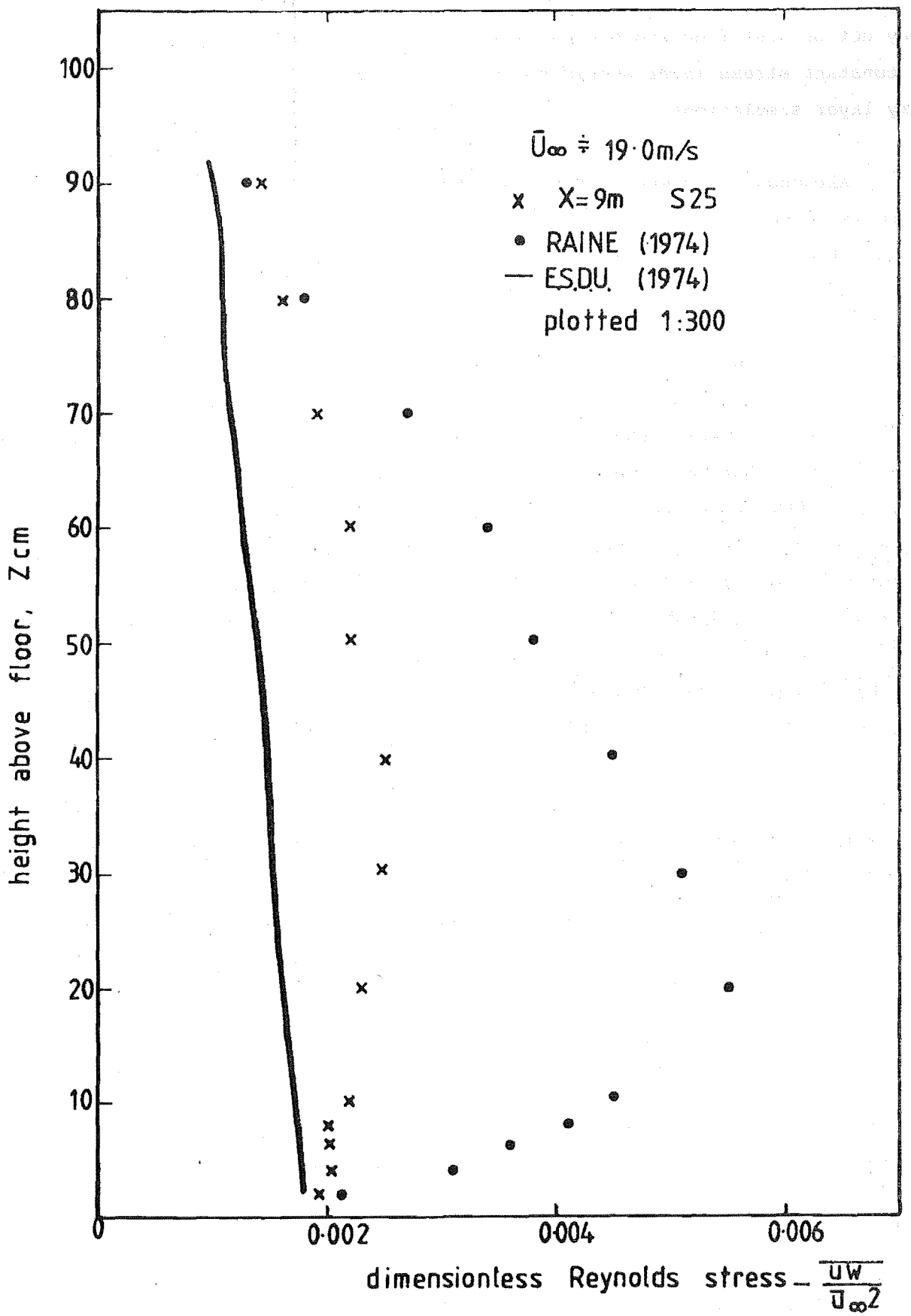

FIG 3·13 REYNOLDS STRESS PROFILE

It is current practice to attempt to create a depth of constant stress in atmospheric boundary layer simulations. Raine suggests that this practice may not be justified and quotes Plate (1971) who states that the achievement of a constant stress layer should not be considered critical in atmospheric boundary layer simulations.

Although the measured Reynolds stress profile shown in figure 3.13 is more representative of a rural atmospheric boundary layer than that obtained by Raine, the stress is still uncharacteristically high. Raine notes that this is a common feature of accelerated growth boundary layers and attributes the occurrence of the high stress levels to the use of high shear devices such as the grid and the trip fence used to achieve the simulation.

If it is assumed that $\tau_o = - \rho \overline{uw}_{max}$ then the Reynolds stress measurements made in the atmospheric boundary layer simulation may be compared to the measured values of the atmospheric surface drag coefficient k_{10}. Davenport (1963) quotes values for k_{10} in rural terrain of between 0.0035 and 0.0070. Raine found $k_{10} = 0.017$, a value which appeared too high for a rural boundary layer. In the present simulation the value for k_{10} based on the maximum shear stress $- \frac{\overline{uw}}{\overline{U}_\infty^2} = 0.0025$ is $k_{10} = 0.008$, assuming that the gradient wind speed is equal to the streamwise velocity at the outside of the boundary layer and that the linear scaling of the simulation is 1:300. This value is seen to be a little high but was considered acceptable.

The value of the friction velocity u_* calculated from the maximum shear stress $- \frac{\overline{uw}}{\overline{U}_{\infty max}^2}$ is $u_* = 0.90$ m/s. Close to the floor of the wind tunnel at $z = 2$ cm, $\frac{-\overline{uw}}{\overline{U}_\infty^2} = 0.0020$ and using the definition of the surface drag coefficient k_z:

$$k_z = \left(\frac{u_*}{\bar{U}_z} \right)^2 \qquad (3.1)$$

then $u_* = 0.85$ m/s close to the floor.

The value of the friction velocity may also be estimated from the slope of the logarithmic mean velocity profile derived by Schlichting (1960):

$$\frac{U}{u_*} = \frac{1}{\kappa} \log_e \frac{z}{Z_o} \qquad (3.2)$$

where κ = the von Karman constant 0.4

u_* = the friction velocity = $\sqrt{\frac{\tau_o}{\rho}}$

Z_o = the roughness length.

Equation (3.2) has been well verified in the atmospheric boundary layer. From figure 3.10 the friction velocity is 0.87 m/s. The three values of the friction velocity are all reasonably close.

Using a value for the friction velocity of $u_* = 0.87$ m/s, a single mean turbulence intensity value for each velocity component was expressed in terms of the friction velocity. These values show good agreement with the full scale values derived by Panofsky (1969) for adiabatic conditions as shown in the table below:

z = 2 cm:	Panofsky (1969)	Present work
$\frac{u'}{u_*}$	2.5	2.5
$\frac{v'}{u_*}$	2.0	2.1
$\frac{w'}{u_*}$	1.3	1.1

In conclusion, the uncharacteristically high Reynolds stress level in Raine's simulation appears to have been due in part to the high shear induced by the two stage fan unit upstream of the working section and the use of additional subsidiary trip fences along the working section.

The Reynolds stress level is still high for a rural boundary layer simulation.

3.3.4 u and w velocity component energy spectra

The shape of the u velocity component spectra in figure 3.14 appears reasonable when compared to the Harris' model atmospheric spectrum, Harris (1968). From the location of the spectral peak relative to that of the Harris' spectrum the turbulence appears to be scaled slightly smaller than 1:300. Length scale estimates were obtained from the measured spectra using the following equations derived by Teunissen (1970):

$$Lu_x = \frac{A}{k_{pu}} \quad A = 0.146 \text{ or } 0.212 \qquad (3.3)$$

$$Lw_x = \frac{0.106}{k_{pw}} \qquad (3.4)$$

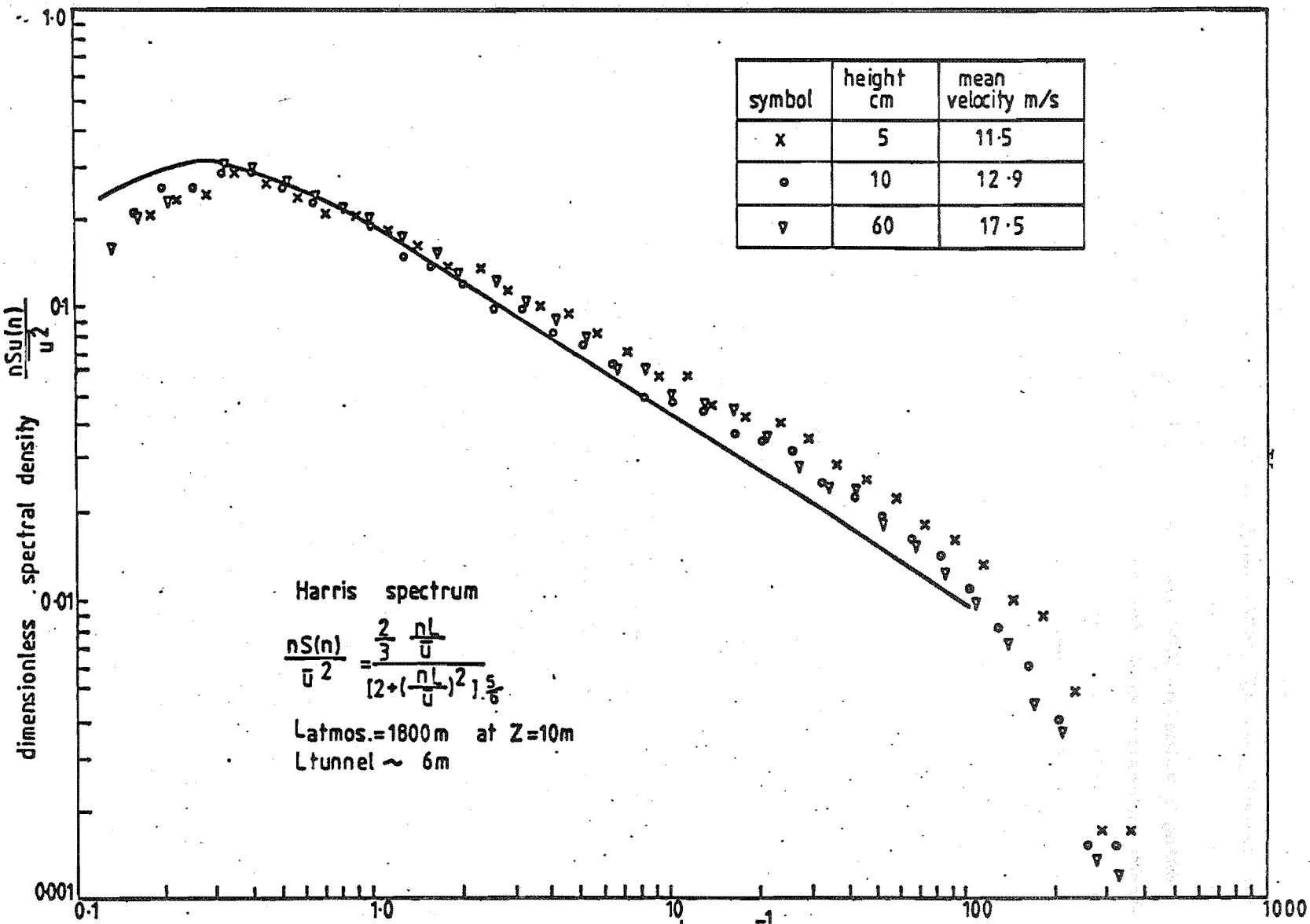

FIG 3·14 ENERGY SPECTRA FOR THE u VELOCITY COMPONENT.

The length scale estimates are summarised in table 3.2. The above equations are an estimate of the true integral scale only in so far as the actual measured spectrum has the same shape as the von Karman isotropic spectrum.

The spectra in figure 3.14 show the desired $-\frac{2}{3}$ slope in the region after the spectral peak which is characteristic of the von Karman isotropic spectrum. The spectra also show an inertial subrange of about two orders of magnitude on the k axis. Templin (1969) states that viscous effects are unlikely to be important if $\frac{k_v}{k_p} > 10$ or 100 where k_v is the reduced frequency at which viscous cut-off of the energy spectrum of the turbulence becomes noticeable and k_p is the location of the spectral peak. From figure 3.14 it may be seen that this criteria is satisfied so viscous effects are unlikely to be important.

The measured w component energy spectra are shown in figure 3.15 and display the expected variation with height as found in the atmosphere and as measured by Raine (1974). The measured w spectra are compared with the von Karman spectrum and the Busch-Panofsky spectrum.

The von Karman spectrum is given by:

$$\frac{n\, S_w(n)}{\overline{w^2}} = 2\, Lu_x\, k \left[\frac{1 + 188.4(Lu_x\, k)^2}{1 + 70.7(Lu_x\, k)^{2\ 11/6}} \right] \qquad (3.5)$$

The value of Lu_x was obtained from the autocorrelation curve at z = 10 cm in figure 3.16 which yields a value of Lu_x = 34.4 cm.

The Busch-Panofsky spectrum is given by:

$$\frac{n\, S_w(n)}{\overline{w^2}} = \frac{0.636\, \frac{f}{f_m}}{1 + 1.5(\frac{f}{f_m})^{5/3}} \qquad (3.6)$$

where $f = kz$

and $f_m = k_p z$

The value of k_p was taken as 4.2 m^{-1} from figure 3.15.

Length scales estimated from the peak of the w spectra are summarised in table 3.2 (page 69).

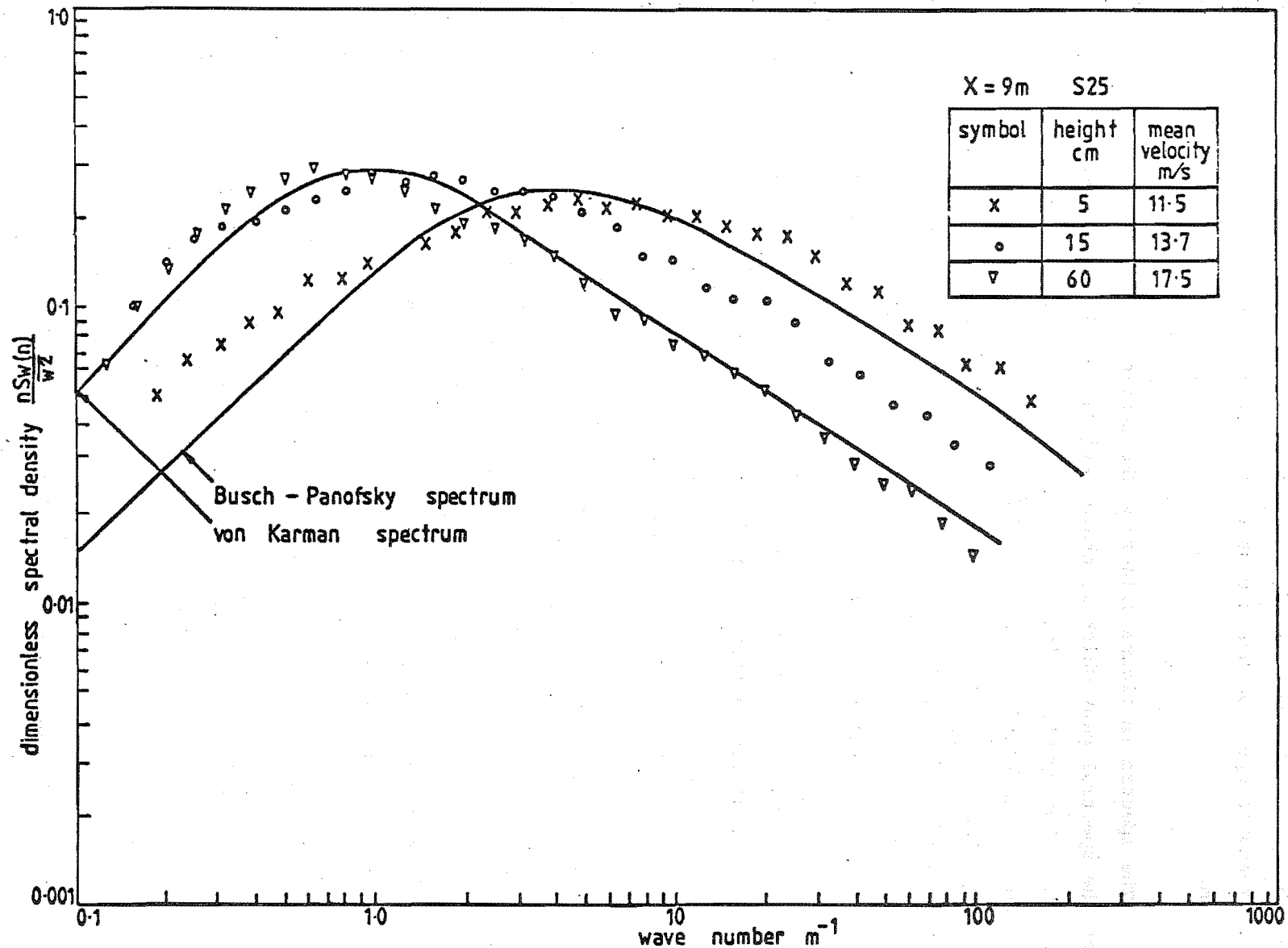

FIG 3·15 ENERGY SPECTRA FOR THE w VELOCITY COMPONENT.

3.3.5 Correlation coefficients

Figure 3.16 is a plot of the autocorrelation coefficient versus the delay time. For this work the digital data acquisition system was not available and the autocorrelation coefficients were measured using the DISA TCA system and a Hewlett-Packard 7035B X-Y recorder as described in Appendix 1. An example of the output from the X-Y recorder is shown in figure 3.17. From each recorder plot a mean curve was drawn and these are plotted in figure 3.16.

At 10 cm above the floor the autocorrelation coefficient has a much larger magnitude over much of the delay range compared to the correlation coefficients at z = 5 cm and z = 60 cm. This trend is undesirable since in the atmosphere the length scale increases monotonically with height. A similar trend is evident in the results of Raine (1974) where his autocorrelation coefficients at z = 15 cm were large compared to the autocorrelation coefficients at other heights above the floor.

Turbulent length scales derived from the autocorrelation curves are presented in table 3.2. These length scales were subject to a considerable error because of the fluctuations of the measured signal as illustrated in figure 3.17 and the long tails of the autocorrelation functions which sometimes lay outside the maximum delay range of 100 ms. Length scales were calculated using Taylor's hypothesis. Taylor's hypothesis is generally assumed to apply in the atmospheric boundary layer but the validity of applying Taylor's hypothesis to the whole velocity signal was considered uncertain. Hinze (1959) states that Taylor's hypothesis can only be applied where $\frac{u'}{\bar{U}} << 1$. This requirement is not satisfied in the atmospheric simulation near the ground where $\frac{u'}{\bar{U}} \simeq 0.25$. Teunissen (1970) concludes that Taylor's hypothesis becomes decreasingly accurate for low wave numbers, so part of the low-frequency end of the spectra may be excluded.

Figure 3.18 is a plot of the lateral correlation coefficient against the lateral separation for zero time lag at a number of heights above the ground. The general trend is for an increase in the length scale with height, however the length scale at z = 15 cm appears slightly high compared to that at z = 5 cm and z = 60 cm.

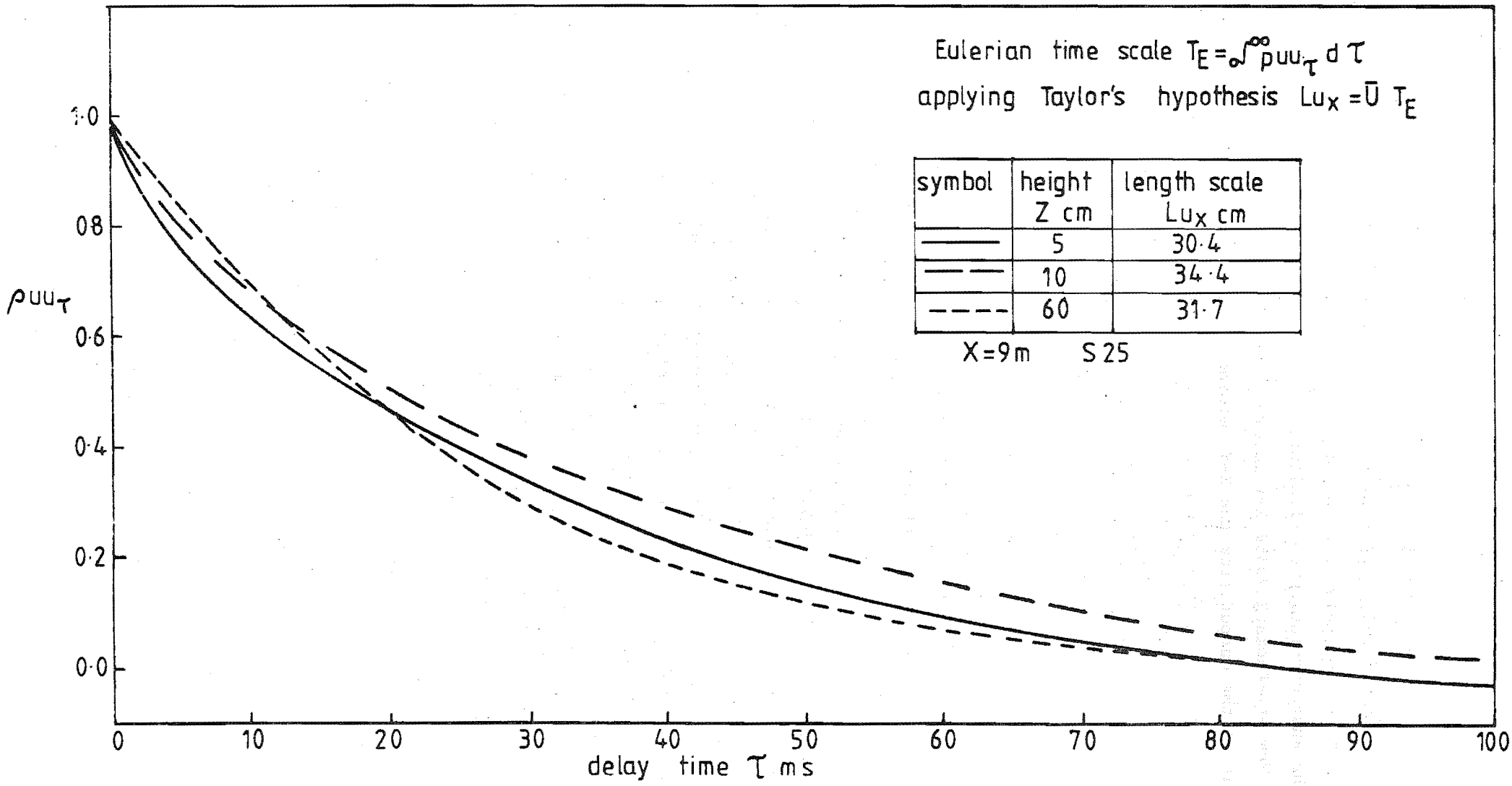

FIG 3·16 AUTOCORRELATION COEFFICIENTS.

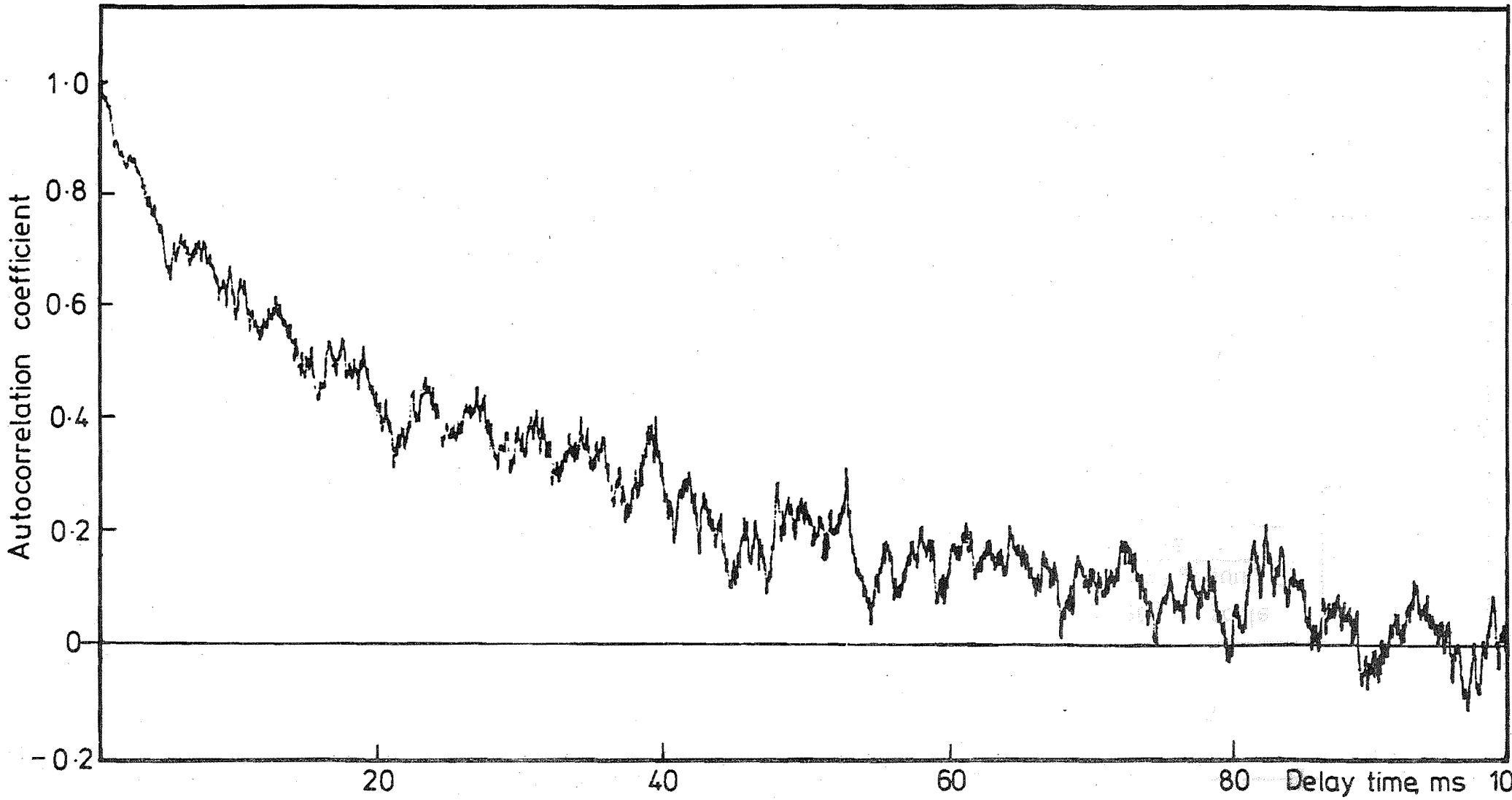

FIG. 3·17 AUTOCORRELATION OBTAINED USING THE ANALOG SYSTEM.

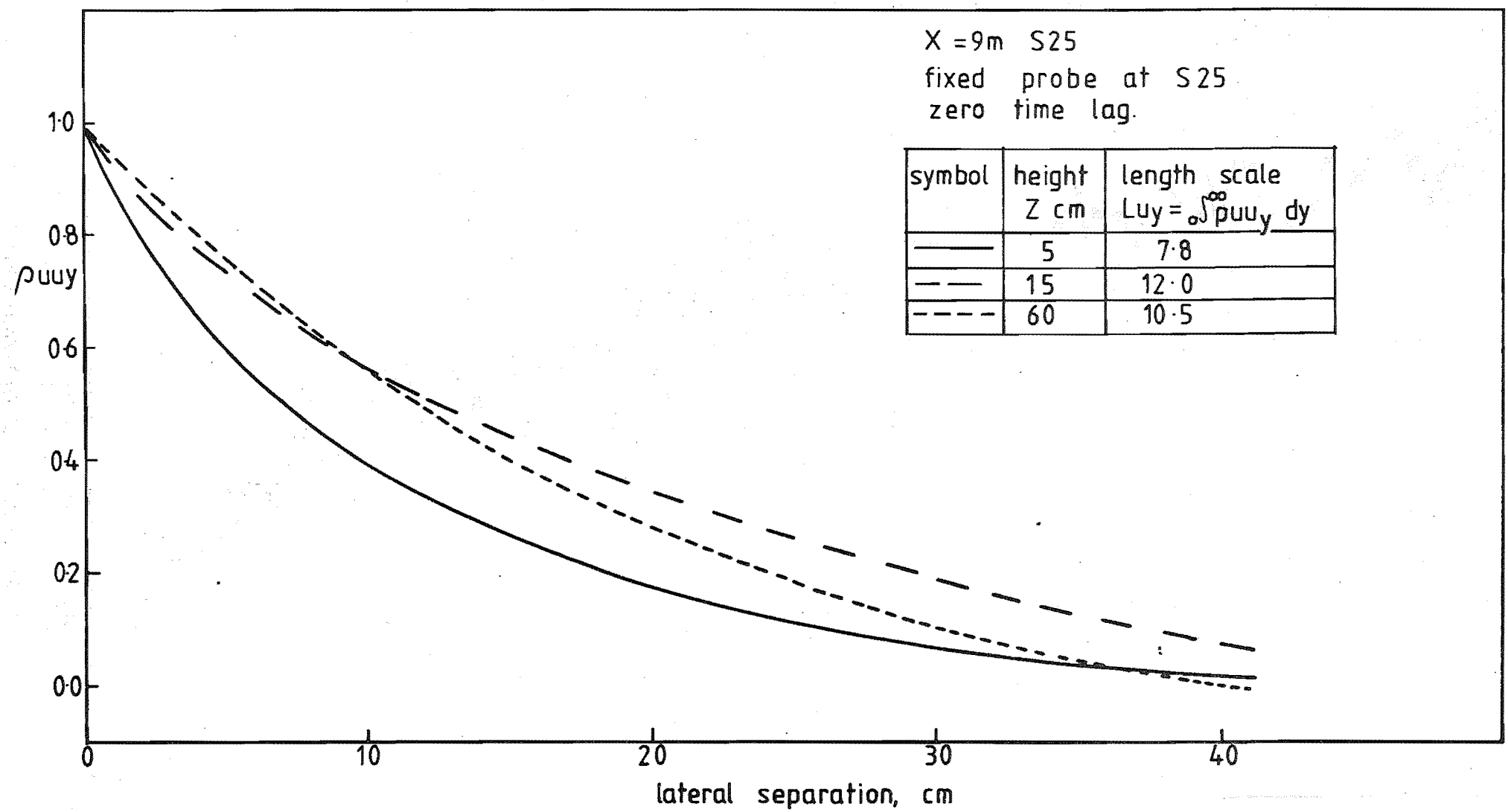

FIG 3-18 LATERAL CORRELATION COEFFICIENT OF THE U VELOCITY COMPONENT.

Correlation curves in the vertical direction are shown in figure 3.19. The vertical length scales derived from these curves show the desired increase with height.

Turbulent length scales derived from the correlation curves are summarised in table 3.2 for comparison with those derived from the energy spectra, and are discussed further in section 3.3.6.

3.3.6 Linear scaling of the simulation

Estimates of the linear scaling of the simulation were made using the methods described by Raine (1974) and Cook (1977). Both methods are based on the measured length scales of turbulence. When the length scale of turbulence was calculated from the spectral peak inaccuracies occurred due to uncertainties in the exact location of the spectral peak due to flat topped spectra and a lack of resolution in the spectral estimates. Length scales of turbulence calculated from the autocorrelation functions also involved inaccuracies due to large fluctuations in the measured function especially at large time lags.

Many previous simulations such as those of Counihan (1969), Davenport and Isyumov (1967), and Campbell and Standen (1969) all show length scales decreasing with height and little attention has usually been paid to obtaining the correct variation in length scale with height.

The estimates of the linear scaling of the simulation using the method of Raine (1974) and Cook (1977) are summarised in table 3.3 and are discussed below.

Raine (1974)

The estimates of the linear scaling of the simulation made using Raine's method are summarised in table 3.3 which may be compared to Raine's table 6.9.

Comparison of the boundary layer depth (assuming a gradient height in the atmosphere of 300 m) and the turbulence intensity profiles between the simulation and atmospheric data leads to a linear scaling of about 1:300. Comparison of the roughness lengths leads to a linear scaling of about 1:200. Raine suggests that roughness lengths only provide a realistic estimate of the linear scaling if there is a long enough fetch of roughness for equilibrium flow. Results presented in section 3.3.7 and the fact that the flow is slowly

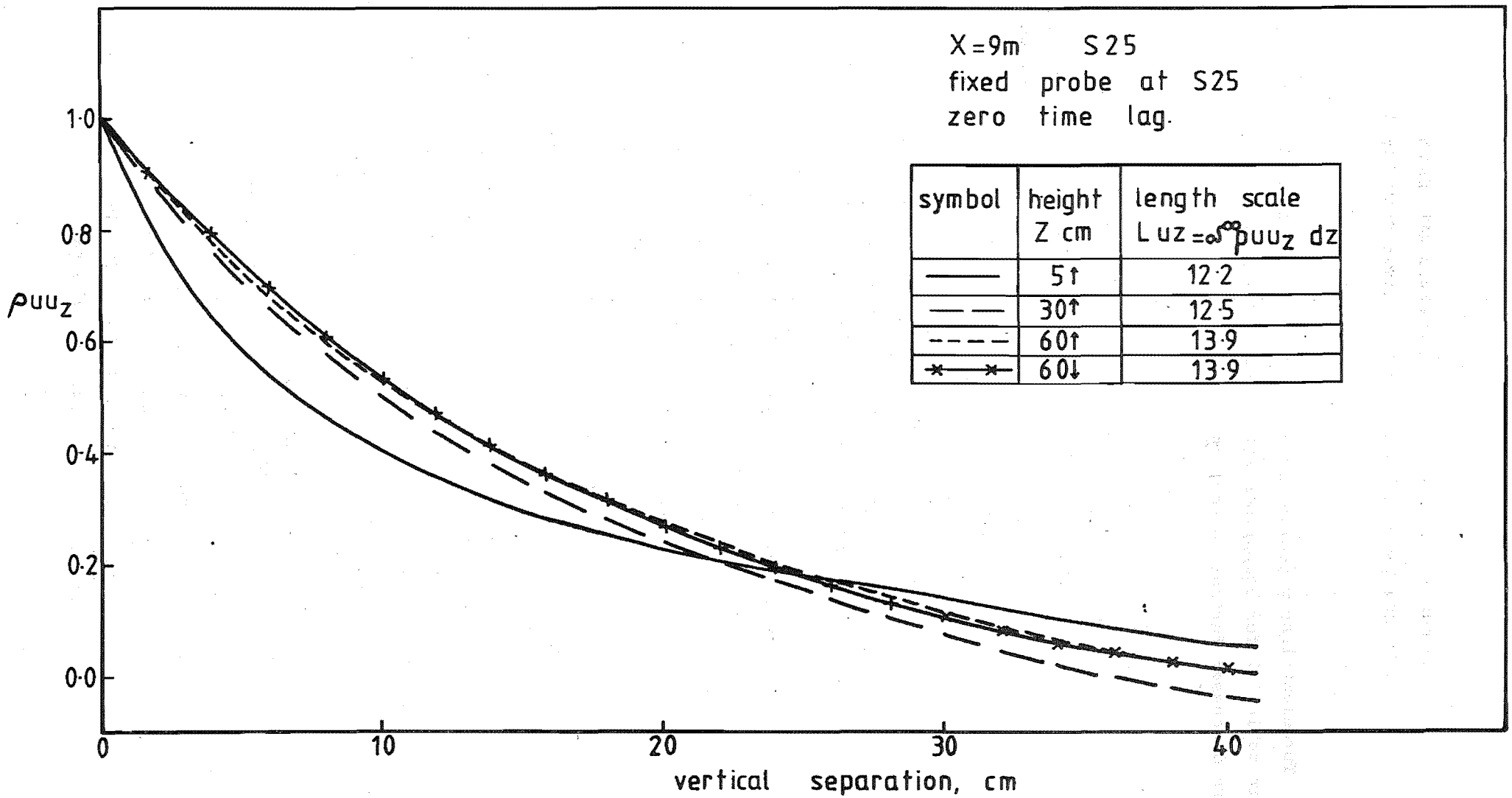

FIG 3-19 VERTICAL CORRELATION COEFFICIENT OF THE U VELOCITY COMPONENT.

Location		Spectral peak wave number u component	Spectral peak wave number w component	Integral length scales of turbulence, cm					
				Derived from spectra			Derived from correlation curves		
X m	z cm	kp_u m^{-1}	kp_w m^{-1}	$Lu_x = \frac{0.146}{kp_u}$	$Lu_x = \frac{0.212}{kp_w}$	$Lw_x = \frac{0.106}{kp_w}$	Lu_x	Lu_y	Lu_z
9	5	0.37	4.2	39	5	2.5	30	8	12
9	10	0.35		42			34		
9	15		1.4		15	8		12	
9	60	0.37	0.7	39	30	15	32	11	14

TABLE 3.2 Tabulated length scale data

Location		Linear scaling $\frac{dm}{da}$ based on			Turbulence length scale L_{ux} from spectra	Linear scaling $\frac{dm}{da}$ based on				Turbulence length scale L_{ux} from autocorr.	Linear scaling $\frac{dm}{da}$ based on		
x m	z cm	$\frac{\delta_m}{\delta_a}$	$\frac{z_{om}}{z_{oa}}$	Turb. intensity profile		eqtn 3.8	eqtn 3.9	eqtn 3.10	Cook(1977)		eqtn 3.8	eqtn 3.10	Cook(1977)
9	5	1:330	1:217	1:300	39 cm	1:280	1:475	1:40	1:110	30 cm	1:405	1:65	1:155
9	10	1:330	1:217	1:300	42 cm	1:285	1:480	1:70	1:139	34 cm	1:370	1:104	1:184
9	60	1:330	1:217	1:300	39 cm	1:453	1:775	1:480	1:371	32 cm	1:600	1:728	1:496

TABLE 3.3 Estimates of the linear scale of the simulation

changing with streamwise distance as discussed in section 3.3.9 suggests that the flow is not in equilibrium. Therefore the scaling estimate based on the roughness length may not be representative of the scaling of the simulation.

The remaining estimates of the scale of the simulation in table 3.3 are based on turbulent length scales. As in Raine's simulation the turbulence length scale Lu_x at z = 10 cm and z = 15 cm tends to be high in relation to Lu_x at z = 5 cm and z = 60 cm. The increase in Lu_x at z = 15 cm is not as high as in Raine's simulation and this can probably be attributed to the lower Reynolds stress values in the present work.

The equations used by Raine for calculating the variation in length scale with height in the atmosphere are:

$$Lu_x = 101 \left[\frac{\bar{U}_z}{\bar{U}_{10}}\right] m \qquad (3.7)$$

$$Lu_x = 151 \left[\frac{\bar{U}_z}{\bar{U}_{10}}\right] m \qquad (3.8)$$

$$Lu_x = 11.04\ z^{\frac{1}{2}}\ m \qquad (3.9)$$

Cook (1977)

The method described by Cook (1977) for determining a model scale factor was also used to determine the linear scale of the simulation described in this chapter. The method involves calculating the initial scale factor from the roughness length Z_o and the length scale Lu_x at various heights above the surface. Other flow properties are then checked against full scale data at this scale factor.

From the design curve given by E.S.D.U. (1972) the initial scale factor S can be determined from the equation:

$$S = \frac{91.3\ (z-d)_m^{0.491}}{Lu_{x_m}^{1.403}\ Zo_m^{0.088}} \qquad (3.10)$$

where the subscript m refers to model values.

The values of the scale factor S obtained from equation (3.10) assuming no zero plane displacement height are presented in table 3.3.

There is a large variation among the different estimates of the linear scaling. Considering the evidence of table 3.3, a reasonable estimate of the linear scale of the simulation is 1:300.

3.3.7 Comparison of the boundary layer characteristics with those predicted by the literature.

Gartshore and de Croos (1976) use a data correlation for the wall stress associated with rough boundaries and a semi-empirical calculation method to predict the shape of boundary layers in exact equilibrium with the roughness beneath them. The method therefore provides a relationship between roughness geometry and velocity profile shape which allows a choice of roughness to be made for any desired velocity profile in wind tunnel simulations of the atmospheric wind.

The relevant boundary layer characteristics of the simulation described in this chapter are:

nominal boundary layer thickness = $\delta = 90 \times 10^{-2}$ m

exponent of the power law velocity profile = $\alpha = 0.167$

roughness element height = $k_r = 3.0 \times 10^{-3}$ m

and $\frac{\lambda e}{k_r} = \frac{A_p}{A_F} = 4.43$

where:

λ_e = effective streamwise spacing of two-dimensional bars,

A_p = plan area associated with one roughness element,

A_F = frontal area associated with one roughness element.

From figure 3.6 which describes the roughness element geometry of the Torro baseboard used in the simulation described in this chapter:

$A_p = 0.79 \times 0.79$ cm^2

$A_F = 0.3 \times 0.47$ cm^2

For $\delta = 0.167$ and $\frac{\delta}{k_r} = 300$ from Gartshore and de Croos's figure 2 $\frac{\lambda_e}{k_r} = 50$ which does not compare well with the actual value of $\frac{\lambda_e}{k} = 4.43$.

It is therefore apparent that the boundary layer has not reached a state of equilibrium. A boundary layer established by Gartshore and de Croos was close to equilibrium after passing over a streamwise fetch equal to about 350 times the roughness element height. Counihan (1971) suggests that equilibrium would be reached after a fetch of about 1000 roughness element heights but states that the fetch will vary with the initial conditions imposed. In the simulation described in this chapter the flow had passed over a streamwise fetch equal to 2800 roughness element heights. It appears that the grid and trip fence effectively destroy any equilibrium the flow would have after passing over only the roughness.

3.3.8 Flow self preservation at X = 11 m

In the first 30 cm above the ground figure 3.20 shows that the flow has speeded up relative to the flow higher up in the boundary layer between X = 9 m and X = 11 m. The increase in velocity close to the ground is about 4%. There has been no deterioration in the lateral uniformity.

Figure 3.21 shows that the local turbulence intensity has decreased between X = 9 m and X = 11 m, especially in the lower to middle section of the boundary layer. Near the ground the decrease is partly due to the increase in the mean velocity $\bar{U}$, but it is also evident that u' is decreasing with streamwise fetch.

In figure 3.22 the u component energy spectra at X = 11 m is compared with the Harris spectrum which is plotted to the same scale as in figure 3.14. Comparing figures 3.14 and 3.22 the spectral peak wave numbers are lower at X = 11 m than at X = 9 m. At a height of 5 cm above the floor the spectral peak has moved from 0.37 m^{-1} to 0.34 m^{-1}, and at a height of 10 cm from 0.35 m^{-1} to 0.32 m^{-1}. The shift in the spectral peak wave number reflects an increase in the longitudinal length scale of the turbulence.

In evaluating his final 1:300 rural atmospheric boundary layer simulation Raine (1974) did not use Torro baseboard after X = 9 m, where the flow was allowed to move over the smooth wind tunnel floor. Between X = 9 m and X = 11 m Raine measured changes in the mean velocity of up to 20% and shifts in the spectral peak to frequencies below the cut-off frequency of the spectral analyser. The flow self preservation in the present work was therefore considerably better than that measured by Raine.

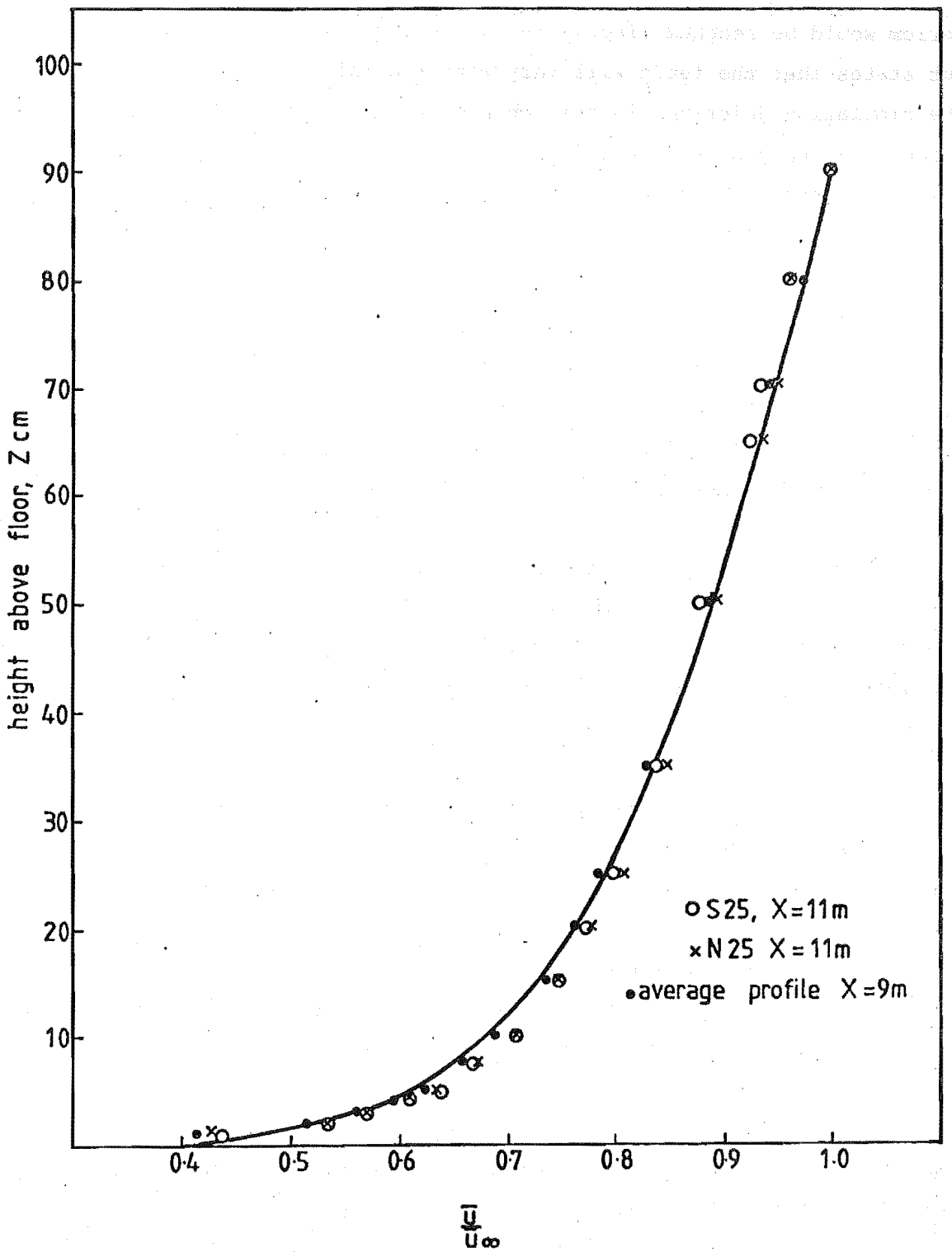

FIG 3·20 MEAN VELOCITY PROFILE AT X=11m

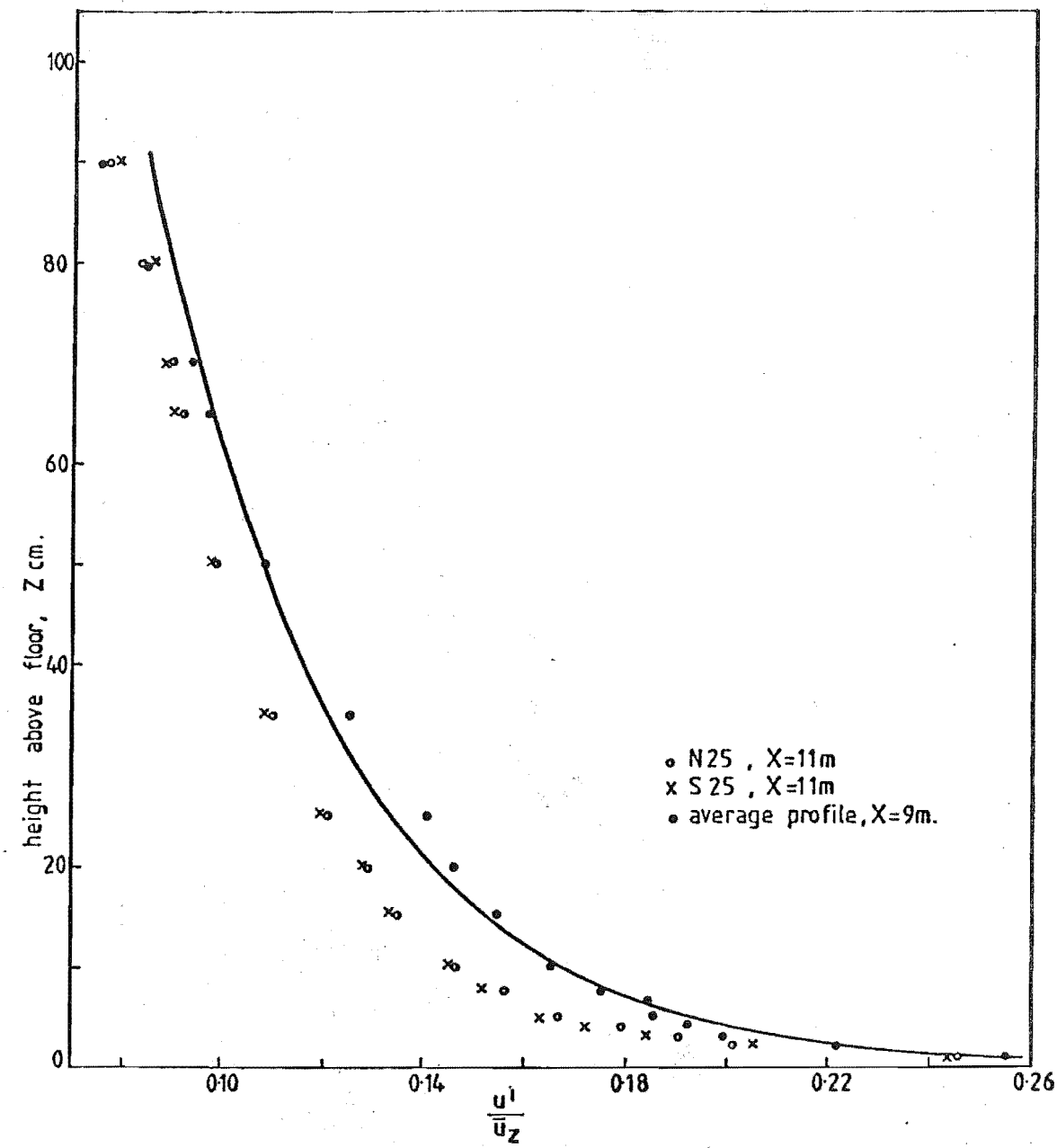

FIG 3·21 TURBULENCE INTENSITY PROFILE AT X=11m.

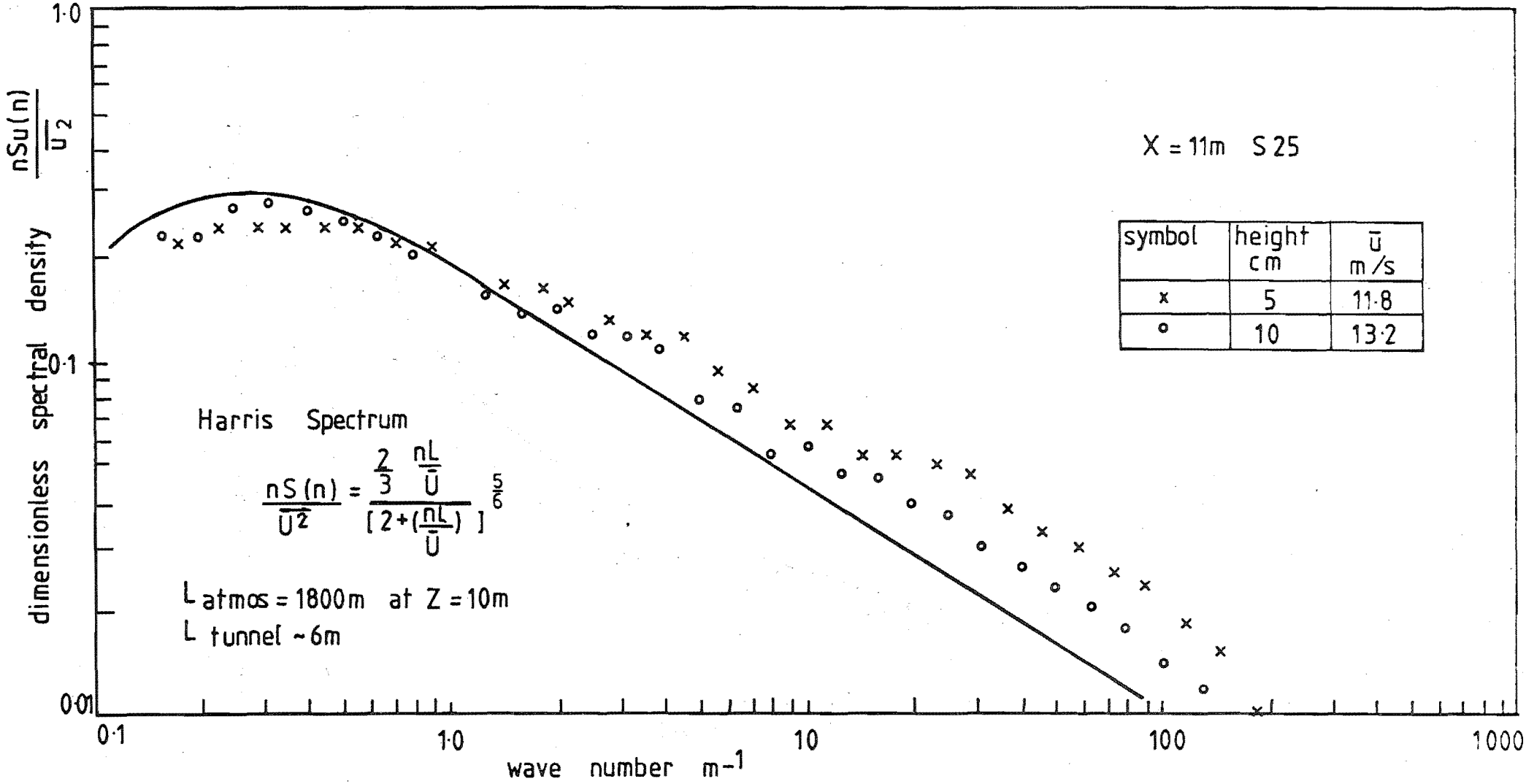

FIG 3·22 ENERGY SPECTRA FOR u VELOCITY COMPONENT.

3.3.9 Static pressure gradient

Across the working section at X = 9 m the variation in static pressure measured with the pitot-static rake illustrated in figure 3.7 was negligible.

Along the working section the static pressure measurements at the flush wall mounted static pressure taps showed that there was a variation of 0.15 cm H_2O about the mean static pressure. The variation in static pressure along the working section was considered acceptable and the roof setting was not adjusted.

3.4 Conclusions

As in the 1:300 rural atmospheric boundary layer simulation described by Raine (1974) the following requirements of the model flow have been satisfied:

(i) fully aerodynamically rough flow,
(ii) absence of static pressure gradients,
(iii) correctness of the mean velocity profile,
(iv) substantially correct turbulence intensity profiles,
(v) an approximate constant stress surface layer,
(vi) satisfactory scaling of u and w component energy spectra,
(vii) integral length scales of turbulence reasonably correct,
(viii) good lateral uniformity.

The flow characteristics in the boundary layer described in this chapter are very similar to those obtained by Raine, and the boundary layer was considered to be a good representation of a neutrally stable simulated rural atmospheric boundary layer of approximately 1:300 linear scale.

The same boundary layer generating apparatus of grid, trip fence and Torro roughness were used as in Raine's simulations. However the use of successive trip fences along the working section was avoided.

The Reynolds stress level, w' velocity fluctuations and turbulent length scales in the lower part of the boundary layer are not correct. This was also the case in the simulation described by Raine. The deviation of these quantities from the desired values appears to be less than in Raine's simulation and this was attributed to the better quality of flow at the entrance to the working section, the removal of the fans from upstream of the working section

and the absence of successive trip fences along the working section. The placement of the fans downstream of the working section resulted in less noise being generated, and more uniform flow at the entrance to the working section. This removed the need for upstream deflector vanes.

A honeycomb was not installed at the entrance to the working section as in the atmospheric boundary layer simulations described in Chapters seven and nine. In retrospect it was considered that fitting this extra honeycomb would have resulted in a better quality of flow at the entrance to the working section with the removal of any large lateral, vertical and streamwise velocity fluctuations.

CHAPTER 4

INFLUENCE OF THE HILL SLOPE ON THE WIND FLOW OVER HILLS

4.1 Introduction

The purpose of the tests described in this chapter was to investigate the effect of the hill slope on the wind flow over hills. The literature contains few reports of rigorous tests aimed at systematically evaluating the influence of the hill slope on the wind flow over hills in a carefully simulated atmospheric boundary layer.

Measurements were made in the upstream approach flow, the region over the hill and in the flow downstream of triangular hills of slope 2.9°, 8.5°, 14.0° and 26.6°. Mean velocity, longitudinal velocity fluctuations and u velocity component energy spectra and autocorrelation functions were measured.

Experimental results are discussed in section 4.5 in relation to the review of previous work given in Chapter Two.

4.2 Experimental apparatus

4.2.1 The model hills

Two-dimensional hill models were selected because many natural obstacles exhibit similar configurations and two dimensions provides a simplification to an otherwise complicated flow situation. Triangular hills have a simple, easily defined shape and an obvious separation point.

Hill slopes of 2.9°, 8.5°, 14.0° and 26.6° yielding $\frac{H}{L}$ values of 0.1, 0.3, 0.5 and 1.0 were selected on the basis of the review work in Chapter Two. This range of hill slopes encompasses the range of slopes commonly found in nature. It was expected that the slopes would range from those with the smooth flow characteristics of the more gentle hills found in nature to those with large scale eddying in the flow after the hill crest.

A hill height of 5 cm was chosen because this would cause a maximum blockage of only 4% of the wind tunnel cross-sectional area. Also, a 5 cm high hill requires a 2 m hill length for the most gentle hill slope which is able to be accommodated in the 3 m length of the available wind tunnel working section.

The model hills were made of acrylic sheet ($\frac{H}{L}$ = 0.3, 0.5, 1.0) or wood ($\frac{H}{L}$ = 0.1) and constructed in two halves so the traversing system could be moved between the hills to aid streamwise traversing. The two hill sections consisted of two rib sections covered with an 0.6 cm thickness of the construction material. Figure 4.1 shows the hill of $\frac{H}{L}$ = 1.0 mounted in the wind tunnel.

In all cases the surface roughness of the hills was smooth. Some previous investigators (e.g. Freeston (1974) had used smooth hill surfaces while others had used rough hill surfaces (e.g. Counihan (1973). The author is aware of no comparison of the effect of using smooth or rough hill surfaces in simulated atmospheric boundary layers developed over rough surfaces. It was proposed to investigate the effect of the hill surface roughness and the results of this investigation are presented in Chapter Six.

4.3 Experimental procedure

Preliminary measurements showed that the flow at ten hill heights upstream of the foot of the model hills was uninfluenced by the presence of the model hills. The hills were therefore placed in the simulated rural atmospheric boundary layer described in Chapter Three so that the upstream foot of each hill was at X = 9.5 m. In this way each hill was subjected to the same approach flow. The model hills were held by screws to the wind tunnel floor. The screws were flush with the hill surface.

No measurable changes in the static pressure gradient at mid-tunnel height were observed after the installation of the model hills and because of the small obstruction offered by the hill models no pressure correction by means of the wind tunnel roof was made.

The flow measuring and flow traversing equipment described in section 3.1 was used to measure the local mean velocity and longitudinal velocity fluctuations at the following vertical and streamwise locations:

vertical locations: $\frac{z}{H}$ = 0.2, 0.4, 0.6, 0.8, 1.0, 1.5, 2.0, 3.0, 4.0, 5.0, 7.0, 10.0, 13.0.

streamwise locations: $\frac{X}{L}$ = 0, ±0.5, ±1.0, ±1.5, ±2.0.

x = 10H upstream of the start of the hills (reference approach flow).

x = 10H downstream of the end of the hills.

x = 1H, 2H and 5H upstream and downstream of the hills as required.

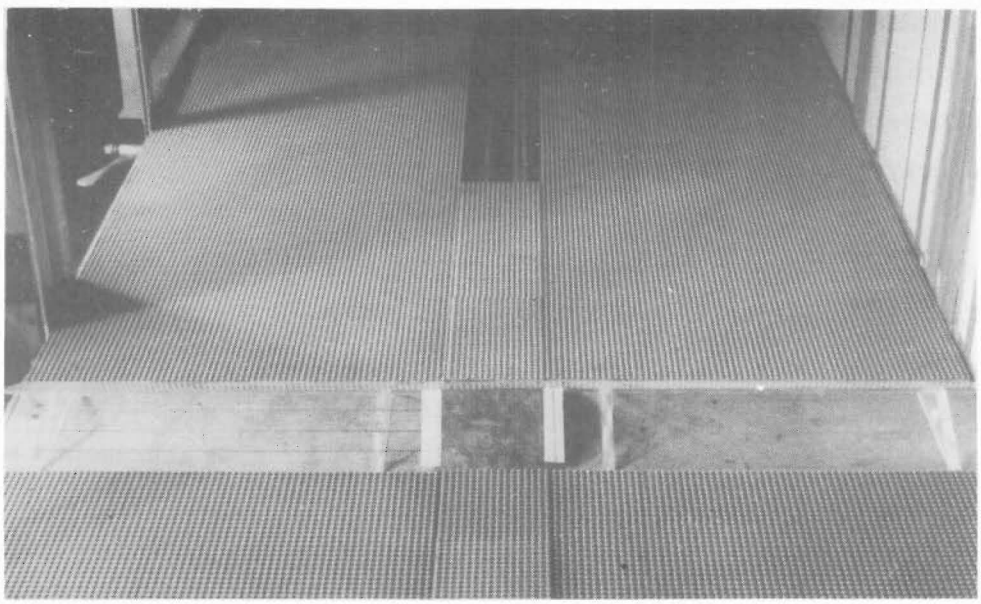

Fig. 4.1 Photograph of model hill mounted in the wind tunnel

Energy spectra and autocorrelation functions of the u velocity component were measured at a height of $\frac{z}{H}$ = 0.2, 1.0 and 2.0, 10H upstream of the start of the hill, at the hill crest and 10H downstream of the end of the hill.

The limitations of hot wire anemometers in the highly turbulent wake region downstream of the hill crests are well known and measurements in this region will only indicate trends.

Considering the excellent lateral uniformity of the flow, measurements were made in only one lateral position, 25 cm south of the wind tunnel centreline.

The procedure for making a vertical traverse was such that a return was always made to a reference point at a height of 25 cm. Measurements made between a return to the reference point were corrected by a proportion of the total error accumulated. Changes in the signal from the hot wire anemometer were always small and appeared to be proportional to the change in the air temperature.

So the velocity measurements at each streamwise location could be normalised with those in the approach flow a streamwise traverse at a height of $\frac{z}{H}$ = 13 was made over each hill.

4.4 Experimental results

4.4.1 Mean velocity profiles and amplification factors

The lines of equal amplification factor for the flow over the four triangular hills are presented in figure 4.2.

As the flow approaches the hills the velocity decreases. The maximum reduction occurs at the upstream foot of the hills ($\frac{x}{L}$ = -2) for all four hills, and the greater the slope of the hill the greater the reduction in velocity. At the upstream foot of the hills changes in the velocity of more than 10% compared to the upstream reference values at the same height occur within 1.5H of the ground.

From $\frac{x}{L}$ = -2 to the hill crest at $\frac{x}{L}$ = 0 the velocity increases for all the hills. The mean velocity profiles at the crest for the four hills are presented in figure 4.3 and shows that the hills with an aspect ratio of 0.3 and 0.5 have almost uniform velocity profiles at the crest.

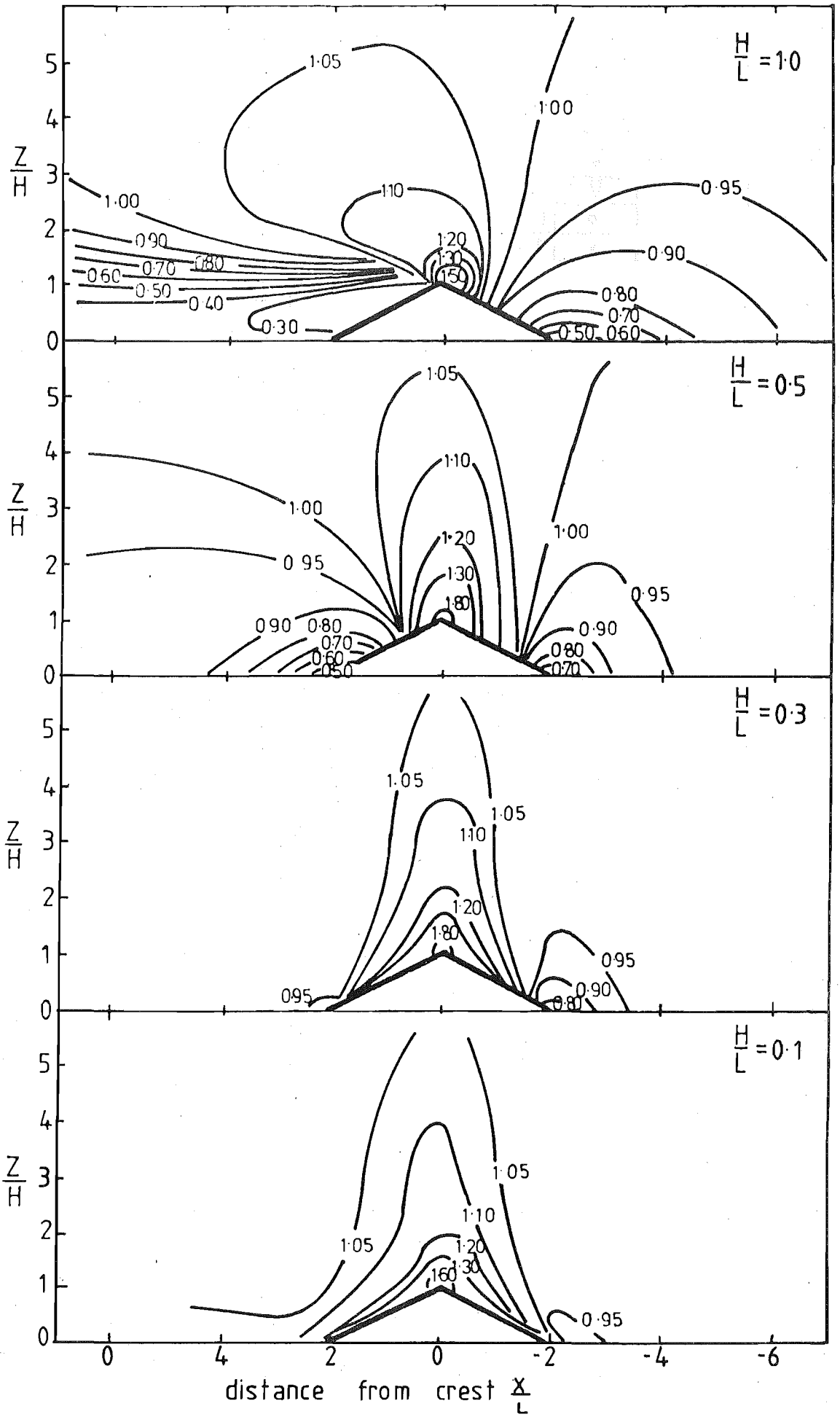

FIG 4·2 LINES OF EQUAL AMPLIFICATION FACTOR

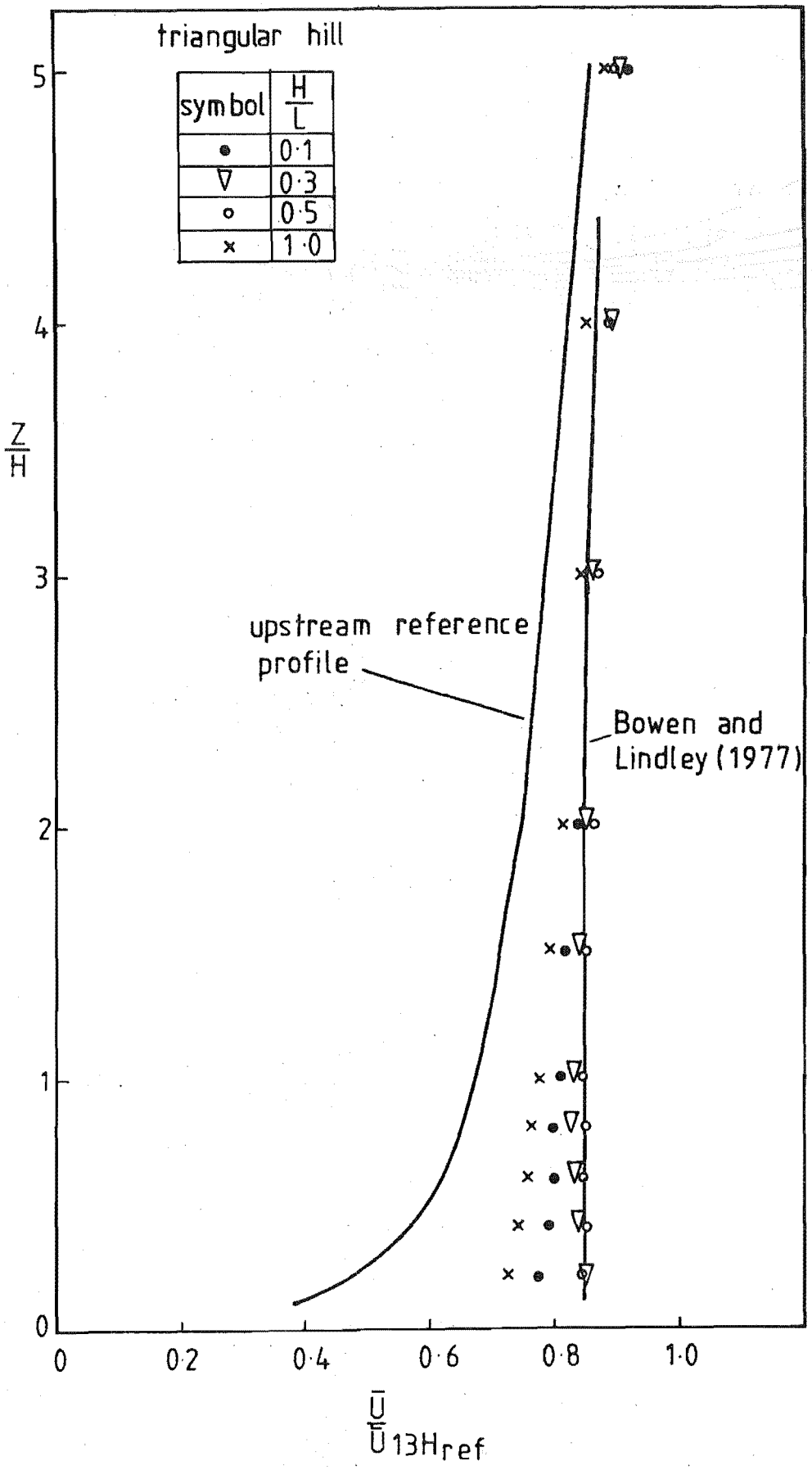

FIG 4·3 MEAN VELOCITY PROFILES AT $\frac{x}{L} = 0$

The variation of the amplification factor at the hill crest with height and hill aspect ratio is shown in figure 4.4. The amplification factor at any height is greatest for the hill with an aspect ratio of 0.5. The hill with $\frac{H}{L} = 1.0$ has the lowest amplification factor at all heights.

In the region after the crest the velocity is reduced for all the hills. Figure 4.5 shows that at the foot of the hills downstream of the hill crest the velocity profiles for the hills with an aspect ratio of 0.1 and 0.3 are almost identical to the upstream reference profile although some speedup is evident close to the ground.

Downstream of the hills, those hills with an aspect ratio of 0.5 and 1.0 have amplification factors very much less than 1.0, whereas for those hills with an aspect ratio of 0.3 and 0.1 the amplification factors are slightly greater than 1.0.

4.4.2 Turbulence intensity profiles

Lines of equal local turbulence intensity $\frac{u'}{\bar{U}}$ in the flow over the four triangular hills are shown in figure 4.6.

At the upwind foot of the hills there is an increase in the local turbulence intensity for all the hills. In the region before the hill crest the larger the aspect ratio of the hill, the greater the value of the local turbulence intensity.

In analysing the results changes in the velocity fluctuation u' were also examined. At the upwind foot of the hills the only change in the velocity fluctuations occurs for the steepest hill where u' decreases as can be seen from figure 4.7a.

At the crest of the hills the longitudinal velocity fluctuations decrease. As shown in figure 4.7b the maximum reduction occurs at a height of $\frac{z}{H} = 0.2$ where u' is only 80% of its upstream reference value for the hills with an aspect ratio of 0.1 and 1.0. The value of the local turbulence intensity has also decreased at the hill crests relative to the upstream reference values due to a decrease in the velocity fluctuations u' and an increase in the mean velocity $\bar{U}$. The largest decrease occurs for the hill with the smallest value of $\frac{H}{L}$ as can be seen by comparing the positions of the 0.13 isoturb in figure 4.6.

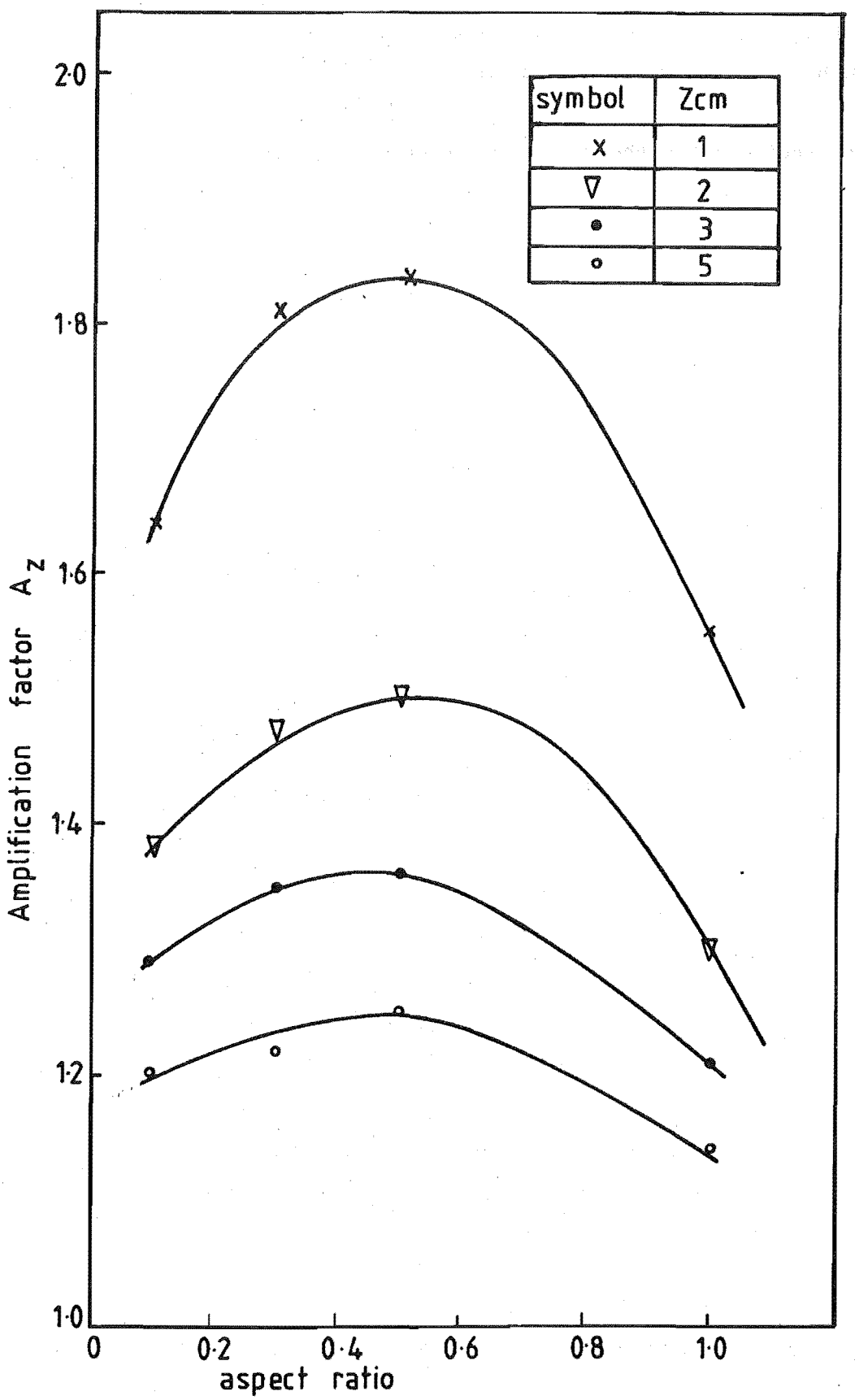

FIG 4·4 VARIATION OF AMPLIFICATION FACTOR AT THE CREST WITH ASPECT RATIO AND HEIGHT.

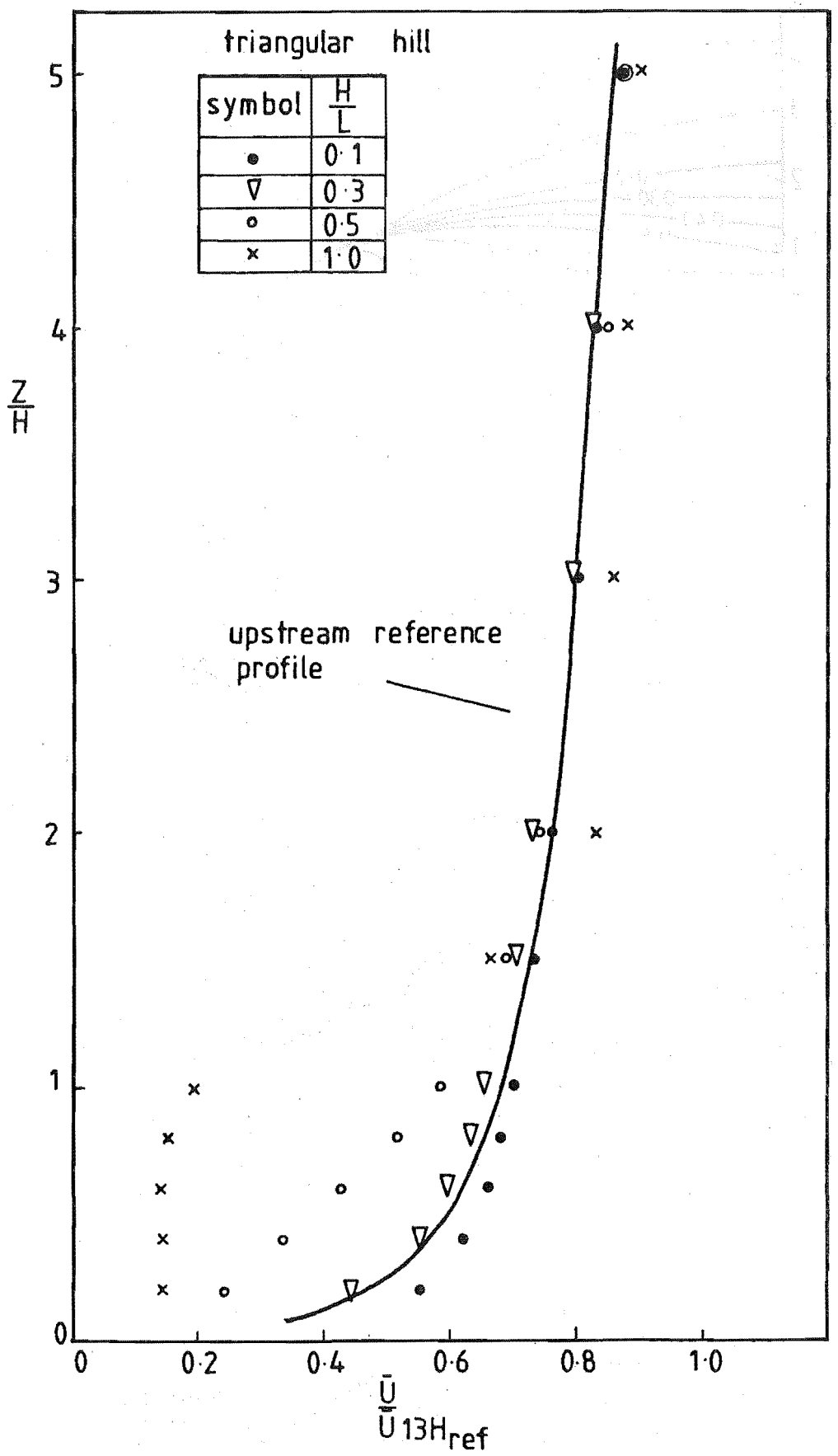

FIG 4·5 MEAN VELOCITY PROFILES AT $\frac{x}{L} = 2$

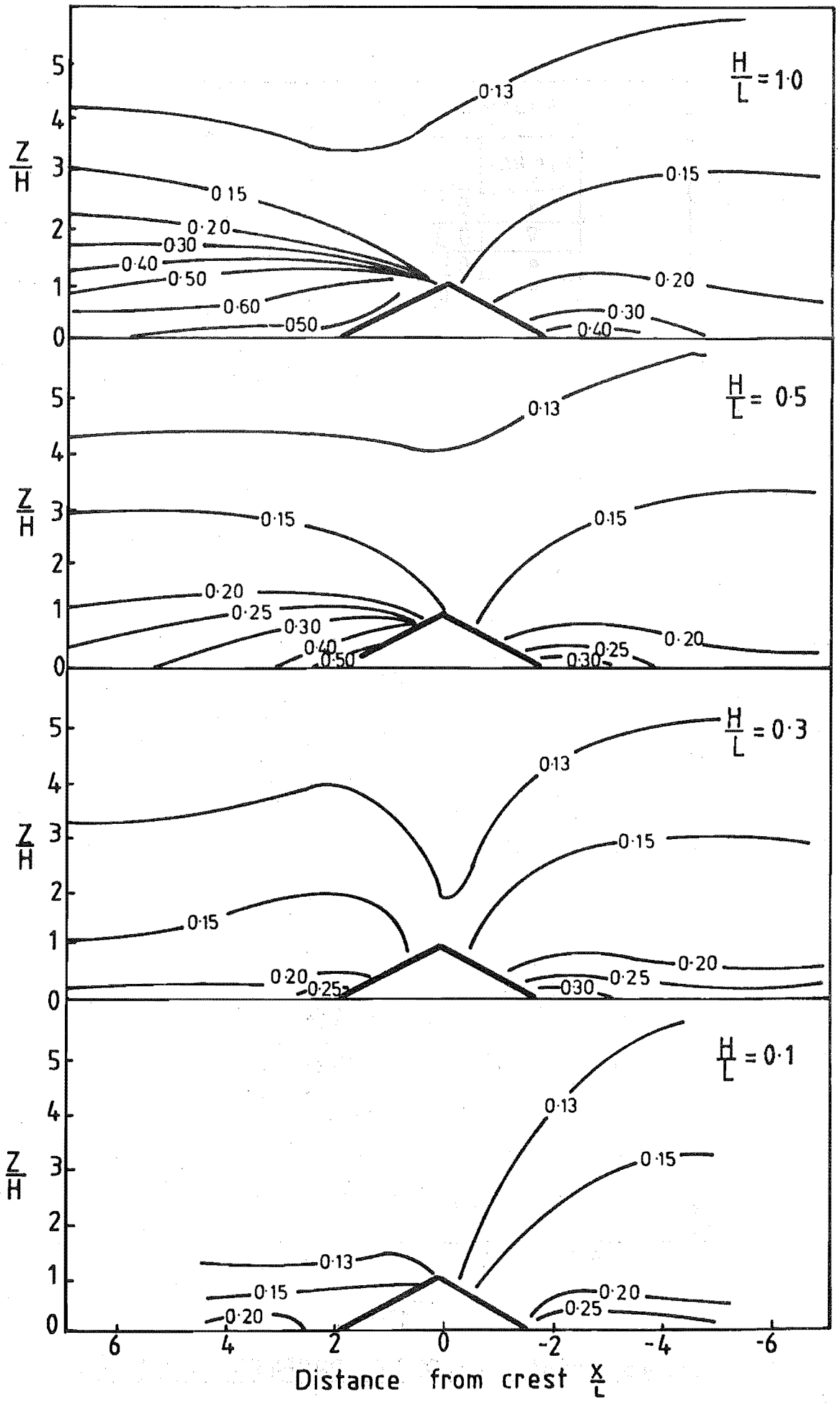

FIG 4·6 ISOTURBS FOR THE TRIANGULAR HILLS

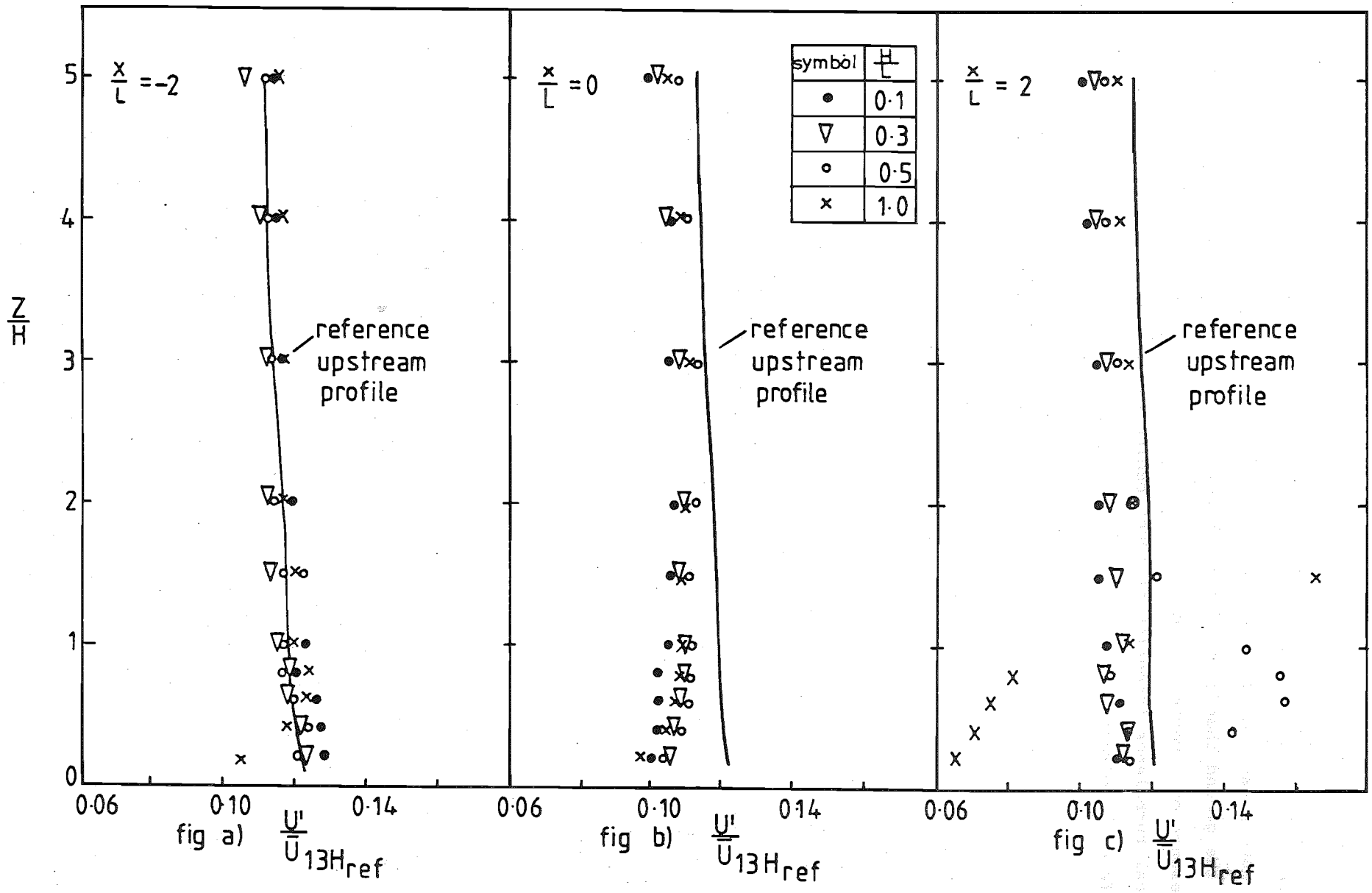

FIG 4·7 TURBULENCE INTENSITY PROFILES OVER TRIANGULAR HILLS

Downstream of the hill crests there is an increase in the local turbulence intensity for all the hills as may be seen from figure 4.6. For the hills with an aspect ratio of 0.5 and 1.0 the local turbulence intensity is higher close to the ground than in the upstream reference approach profile due to the presence of a vortex. For the hills with an aspect ratio of 0.1 and 0.3 the local turbulence intensity is lower behind the crest than in the upstream reference approach flow.

The velocity fluctuations u' downstream of the hill crests at $\frac{x}{L} = 2$ are illustrated in figure 4.7c. For the hills with $\frac{H}{L}$ of 0.5 and 1.0 the value of u' is greater than the upstream reference value up to two hill heights above the ground. The maximum value of u' is always larger and occurs at a greater height for the hill with $\frac{H}{L}$ of 1.0 than for the hill with $\frac{H}{L}$ of 0.5.

4.4.3 u velocity component energy spectra and autocorrelation coefficients

The spectra and autocorrelation functions for the flow over the four triangular hills were measured at the upstream reference position, at the hill crest, and 10H downstream of the hills at heights of $\frac{z}{H} = 0.2$, 1.0 and 2.0. The spectral peak values are summarised in table 4.1 and the spectra at the hill crests at a height of $\frac{z}{H} = 0.2$ are compared in figure 4.8.

Figure 4.8 shows that at the hill crests the spectral peak wave number has decreased relative to the upstream reference value for all the hills. This indicates an increase in the average eddy size. The largest decrease in the spectral peak wave number at the crest at any height occurs for the hills with $\frac{H}{L} = 0.3$ and 0.5 as illustrated at a height of $\frac{z}{H} = 0.2$ in figure 4.8. The largest changes in the spectral peak wave number at the hill crests occur close to the ground. For example at $\frac{z}{H} = 0.2$ the spectral peak wave number is 30% to 40% of the upstream reference value whereas at $\frac{z}{H} = 2.0$ the spectral peak wave number is 85% to 100% of the upstream reference value.

At 10H downstream of the hills the spectral peak wave number has increased close to the ground relative to the upstream reference value. The largest increase occurs for the hill of $\frac{H}{L} = 1.0$ where even at $\frac{z}{H} = 2.0$ the spectral peak is twice its upstream reference value. The only changes in the spectral shape occurred at the hill crest at a height of $\frac{z}{H} = 0.2$ where the spectra became more peaked. Figure 4.8 shows that the hills with $\frac{H}{L}$ of 0.3 and 0.5 have the largest changes in the spectral shape.

$\frac{H}{L}$	$\frac{z}{H}$ = 0.2									$\frac{z}{H}$ = 1.0									$\frac{z}{H}$ = 2.0								
	10H upstream of the hill			crest			10H downstream of the hill			10H upstream of the hill			crest			10H downstream of the hill			10H upstream of the hill			crest			10H downstream of the hill		
	k_p	n_p	T_E	k_p	n_p	T_E	k_p	n_p	T_E	k_p	n_p	T_E	k_p	n_p	T_E	k_p	n_p	T_E	k_p	n_p	T_E	k_p	n_p	T_E	k_p	n_p	T_E
	m^{-1}	H_z	ms	m^{-1}	H_z	ms	m^{-1}	H_z	ms	m^{-1}	H_z	ms	m^{-1}	H_z	ms	m^{-1}	H_z	ms	m^{-1}	H_z	ms	m^{-1}	H_z	ms	m^{-1}	H_z	ms
0.10	0.82	6.36	17.7	0.28	3.56	29.2	0.96	7.90	22.2	0.37	4.09	27.6	0.30	4.03	34.5	0.39	4.63	32.2	0.35	4.29	28.0	0.34	4.76	34.2	0.34	4.25	32.0
0.30	0.82	6.36	17.7	0.29	4.07	32.7	1.00	8.15	22.7	0.37	4.09	27.6	0.27	3.69	32.0	0.34	3.92	30.9	0.35	4.29	28.0	0.29	4.09	33.4	0.29	3.66	32.5
0.50	0.82	6.36	17.7	0.25	3.48	32.8	1.60	12.32	18.6	0.37	4.09	27.6	0.27	3.76	31.2	0.35	3.68	26.2	0.35	4.29	28.0	0.29	4.05	31.4	0.29	3.47	29.5
1.00	0.82	6.36	17.7	0.34	4.30	25.6	2.90	15.89	12.9	0.37	4.09	27.6	0.33	4.47	28.7	1.10	8.72	15.6	0.35	4.29	28.0	0.33	4.57	29.9	0.70	7.67	20.9

TABLE 4.1 Integral time scales and spectral peak values for the triangular hills.

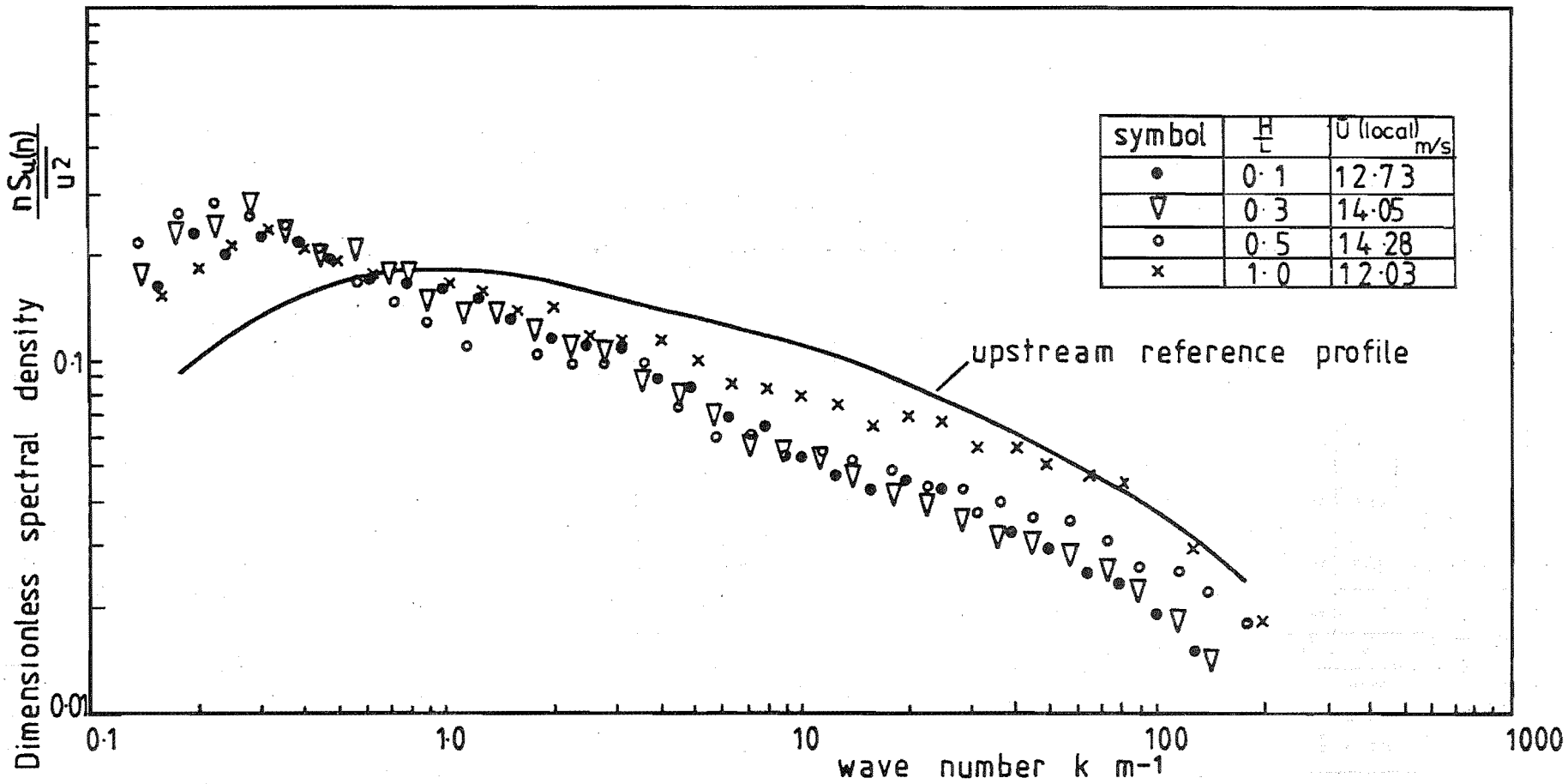

FIG. 4·8 SPECTRA AT THE CREST AT $\frac{Z}{H} = 0·2$

The integral time scales calculated from the measured autocorrelation functions are presented in table 4.1. Taylor's hypothesis cannot be used to calculate length scales from the integral time scales because the flow is changing appreciably with streamwise distance.

At the hill crests the integral time scale T_E was considerably larger than at the corresponding height in the upstream reference position, matching the decrease in the spectral peak wave number at the hill crests. The largest increase occurs close to the ground and is largest for the hills with an aspect ratio of 0.3 and 0.5. For example at the hill crests at a height of $\frac{z}{H} = 0.2$:

$\frac{H}{L}$	0.1	0.3	0.5	1.0
% increase in T_E	165	185	185	145

At 10H downstream of the hills the only significant difference in the integral time scale relative to the upstream reference value occurred for the hill with $\frac{H}{L}$ of 1.0 where the integral time scale was considerably reduced.

4.5 Discussion of the experimental results

4.5.1 Mean velocity characteristics over the hills

As the flow approached the foot of the triangular hills the mean velocity decreased and was followed by an increase in the mean velocity towards the crest. The maximum mean velocity over each hill was at the hill crest and the maximum crest velocity occurred for the hill with $\frac{H}{L} = 0.5$ which had a uniform mean velocity profile at the crest. After the crest the mean velocity decreased for all four hills. A wake region grew after the crest for the hills with an aspect ratio of 0.5 and 1.0 and extended to lengths greater than 10H downstream of the hills. The wake region was an area of low mean velocities and large velocity fluctuations.

For the steeper hills an upstream vortex and downstream wake region produced the equivalent of a taller potential flow ridge with a gradual slope for the main flow outside the separation region. This was responsible for the reduced crest velocities for the steepest hill compared to the more gentle hills.

Taylor and Gent (1974) performed numerical solutions for their equations for curved hills with maximum values of $\frac{H}{L}$ equal to 0.035, 0.070 and 0.16. Their results show a rapid increase in shear stress and pressure and therefore mean velocity at the hill crest as the hill slope increased over the range of values used. This trend is shown by the results obtained in the present work presented in section 4.4.1 and in particular by figure 4.3.

Jackson and Hunt (1975) using their analytical theory predicted that the maximum speedup would occur at the hill crest at the height of the inner region which is given by equation 2.7. At this height the speedup is given by equation 2.8. The analysis strictly applies to bell-shaped hills with a very gentle slope, a condition which is not met by the triangular hills used.

The measured amplification factors at the crest of the four triangular hills at the height of the inner region obtained from figure 4.3 are compared with the predictions of Jackson and Hunt in the table below:

$\frac{H}{L}$	ℓ	$\frac{\ell}{H}$	A_z at $z = \frac{\ell}{H}$	Jackson and Hunt	
	cm		present work	ΔS_{max}	$A_{z\,max}$
0.1	10.1	2.02	1.13	0.2	1.2
0.3	4.2	0.82	1.26	0.6	1.6
0.5	2.8	0.56	1.38	1.0	2.0
1.0	1.6	0.32	1.35	2.0	3.0

The above table shows that the speedup is consistently over-estimated by the theory of Jackson and Hunt. The best agreement is obtained for the hill with the smallest slope which best satisfies the assumptions of the theory as discussed in section 2.1.1.

Counihan (1973) tested three sinusoidal hill shapes with $\frac{H}{L}$ = 0.33, 0.67 and 1.34 in a simulated rural boundary layer. Two values of the hill height to boundary layer height ratio were used. Because the mean velocity over the hills is dependent on the boundary layer height and the hill shape, close agreement with the measurements over the triangular hills presented in section 4.4.1 should not be expected.

The mean velocity profiles obtained by Counihan at the crest of the hills for the ratio of $\frac{H}{\delta}$ closest to that used in the measurements over the triangular hills are shown in figure 4.9. Counihan's results show the same trend as the mean velocity profiles obtained in the present work shown in figure 4.3. At the crest the mean velocity is larger and the mean velocity profile more uniform for the hill with $\frac{H}{L} = 0.33$ than for the hill with $\frac{H}{L} = 0.67$.

Values of the amplification factor obtained by Counihan are compared to those obtained for the triangular hills in the table below. In all cases the values obtained in the present work were interpolated from figure 4.4.

A_z at $z = H$

$\frac{H}{L}$	Counihan $\frac{H}{\delta} = 0.083$	Present work $\frac{H}{\delta} = 0.056$
0.33	1.21	1.22
0.67	1.17	1.20
1.34	1.13	<1.14

Close correspondence is shown between the two columns in the above table which illustrates that the speedup phenomena is relatively insensitive to the shape of the hill.

Bowen and Lindley (1977) present the results of measurements over escarpment shapes with approach ramps of aspect ratio 0.50, 1.0, 1.5 and a cliff escarpment subjected to exactly the same approach profile as was used in the present work. Because of the similarity of the potential flow fields around the leading parts of bodies irrespective of their downstream shape it was considered reasonable to compare the mean velocity profiles obtained by Bowen and Lindley with those measured over the triangular hills. Bowen and Lindley found that for the range of escarpment slope angles considered the mean velocity profiles at the crest of the escarpments was insensitive to the value of $\frac{H}{L}$. Their single mean velocity profile at the crest is compared to the mean velocity profiles at the crest of the triangular hills in figure 4.3. The maximum velocity at the crest of the triangular hills appears to be a limiting condition for the speedup and is the same as that obtained over the escarpments.

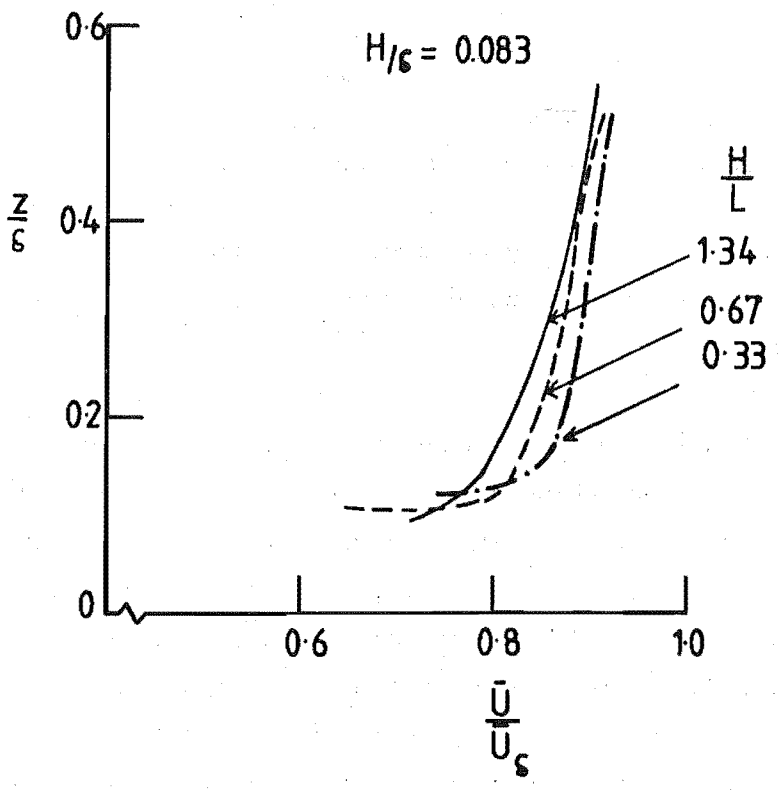

FIG. 4·9 VELOCITY PROFILES AT HILL CRESTS AFTER COUNIHAN (1973)

The approach mean velocity profile used in the present work is compared to that used by Bouwmeester et.al. (1978) in figure 4.10 and shows that the approach mean velocity profile used by Bouwmeester et.al. is slightly dependent on the hill slope. This is because the hill crests were placed in the same position in the wind tunnel and as the flow appears to be slowly changing with streamwise distance the approach profile changes as the hill length changes. The log-linear plot in figure 4.10 accentuates the differences between the mean velocity profiles, all of which are reasonably well represented by a 1/6 power law.

Bouwmeester et.al. used a lower roughness length ($\frac{Z_o}{H} = 1.3 \times 10^{-3}$) than that used in the present work ($\frac{Z_o}{H} = 4.6 \times 10^{-3}$). The slightly higher $\frac{Z_o}{H}$ ratio used in the present work would tend to increase the amplification factors at the hill crest as discussed in Chapter Ten.

Similarly, Bouwmeester et.al. used a hill height to boundary layer height ratio of 0.090 whereas a corresponding value of 0.056 was used in the present tests. The lower $\frac{H}{\delta}$ ratio used in the present work would also tend to increase the amplification factors at the hill crests as discussed in Chapter Eight.

The amplification factors at the hill crest for the triangular hill with $\frac{H}{L} = 1.0$ are compared to those obtained by Bouwmeester et.al. for the same hill in figure 4.11. Close to the ground the agreement is excellent. Further out in the boundary layer Bouwmeester's amplification factors are a little larger than those obtained in the present work but the difference is small.

The amplification factors at the hill crest for the hill with $\frac{H}{L} = 0.1$ are compared to those obtained by Bouwmeester et.al. in figure 4.12. Close to the ground the amplification factors obtained by Bouwmeester et.al. are lower than those obtained in the present work, whereas further out in the boundary layer the agreement is better. While the discrepancy close to the ground is consistent with the lower ratio of $\frac{H}{\delta}$ and the larger roughness length used in the present work, it could also be due to the roughness change from the Torro roughness elements over which the boundary layer had developed to the smooth hill surface used in the present tests. In the work performed by Bouwmeester et.al. such a roughness change did not occur and the hill surface roughness appeared to be similar to the roughness over which the boundary layer had grown. Better agreement with Bouwmeester's work was obtained for the hill covered with roughness (the results for which are presented in Chapter Six)

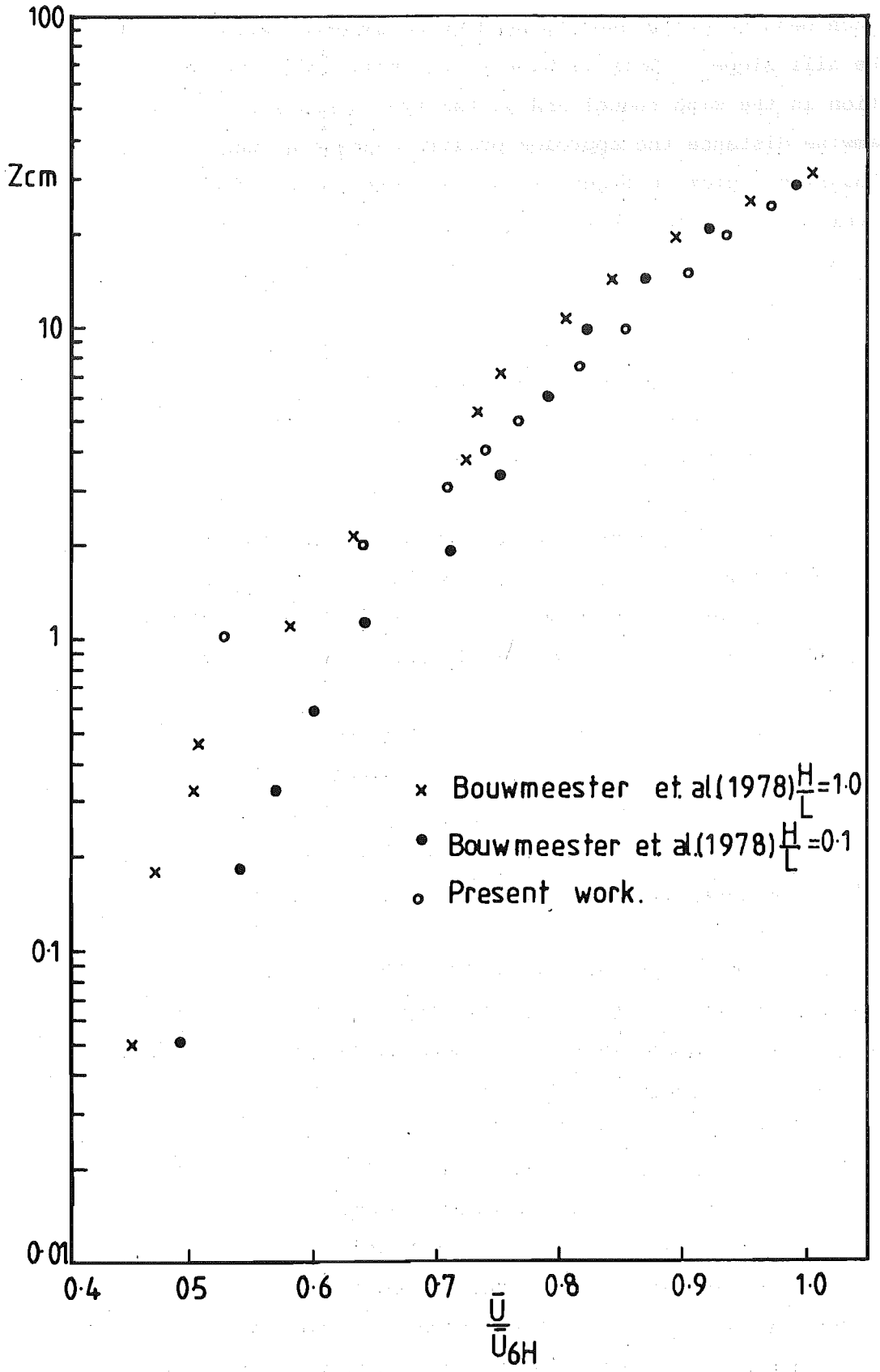

FIG 4·10 COMPARISON OF APPROACH VELOCITY PROFILES

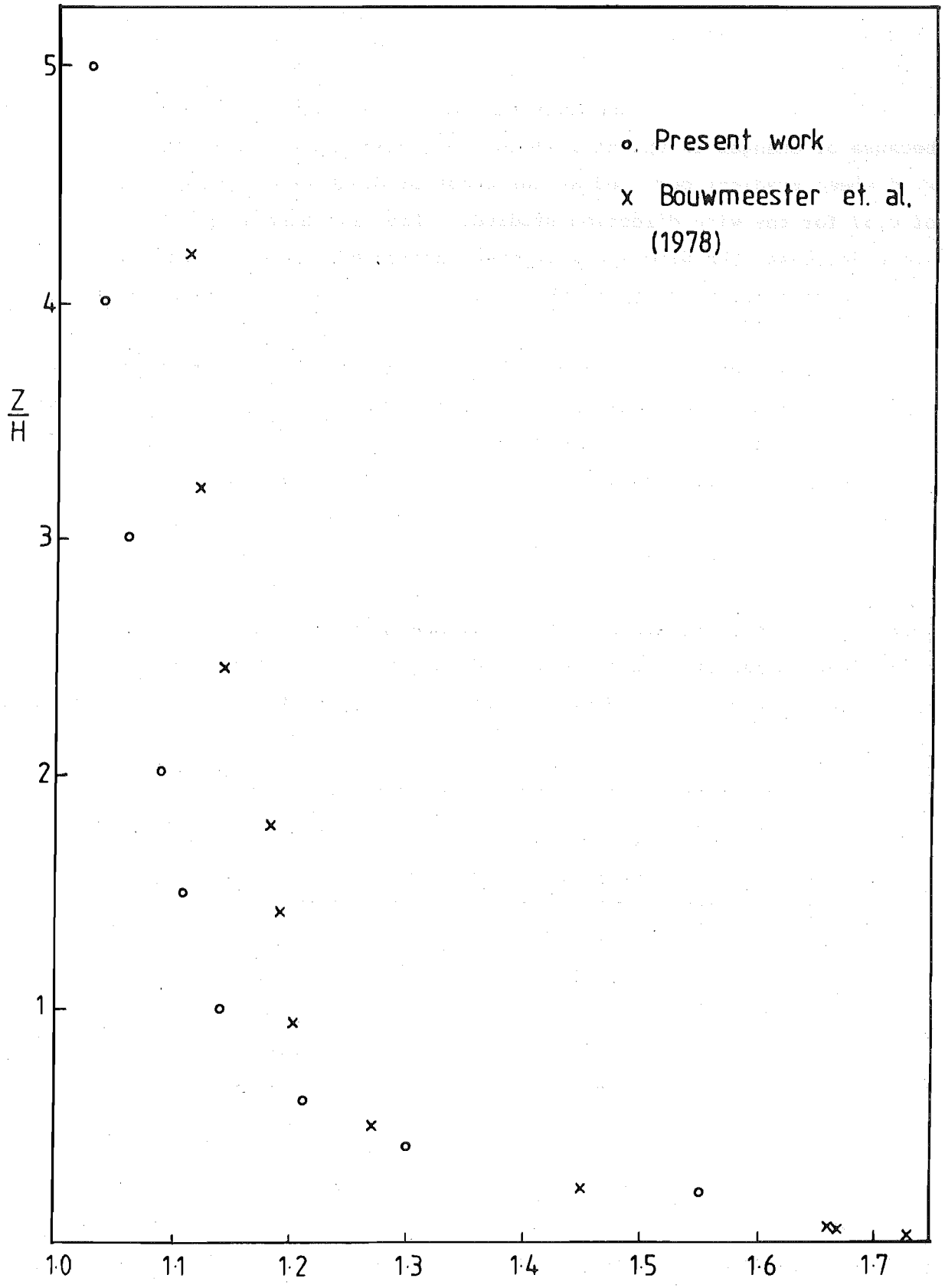

FIG 4·11 COMPARISON OF AMPLIFICATION FACTORS AT THE CREST FOR HILL $\frac{H}{L} = 1.0$

as shown in figure 4.12.

Frenkiel (1962) found that the wind speed ratios vary with wind direction because of changes in the hill slope. Frenkiel found that a vertical mean wind speed gradient occurred at the crest of Givat Hamore which had an $\frac{H}{L}$ value of 0.57 for the wind direction studied. Frenkiel also found that as the hill slope decreased the wind speed gradient decreased. These trends are shown by the mean velocity profiles at the crest of the triangular hills in figure 4.3.

From measurements at his hill site for a number of directions, Sacre (1978) showed that the greater the upwind slope the smaller the wind speed gradient at the crest. From his results Sacre concluded that the amplification factor at the crest up to a height of 0.5H could be expressed by:

$$A_z = 1.02 + 2.75\ \Delta P \qquad (4.1)$$

where ΔP is the local slope at the hill crest. The values of the measured amplification factor at the crest at a height of $\frac{z}{H} = 0.5$ for the triangular hills are compared to the amplification factor predicted by Sacre in the table below:

$\frac{H}{L}$	A_z at z = 0.5H present work	A_z from equation 4.1
0.1	1.33 (1.26)	1.16
0.3	1.40	1.43
0.5	1.41	1.71
1.0	1.25	2.40

As discussed above, the amplification factor for the hill with $\frac{H}{L} = 0.1$ may be appreciably influenced by the roughness change from the rough surface over which the boundary layer had developed to the smooth hill surface. The value for the triangular hill with $\frac{H}{L} = 0.1$ which was covered with the upstream roughness, as presented in Chapter Six is included in brackets in the above table. This value shows better agreement with the results of Sacre. Sacre's predictions are close to the measured values for the gentle hills which avoid flow separation, but fail to predict the amplification factor for the steeper

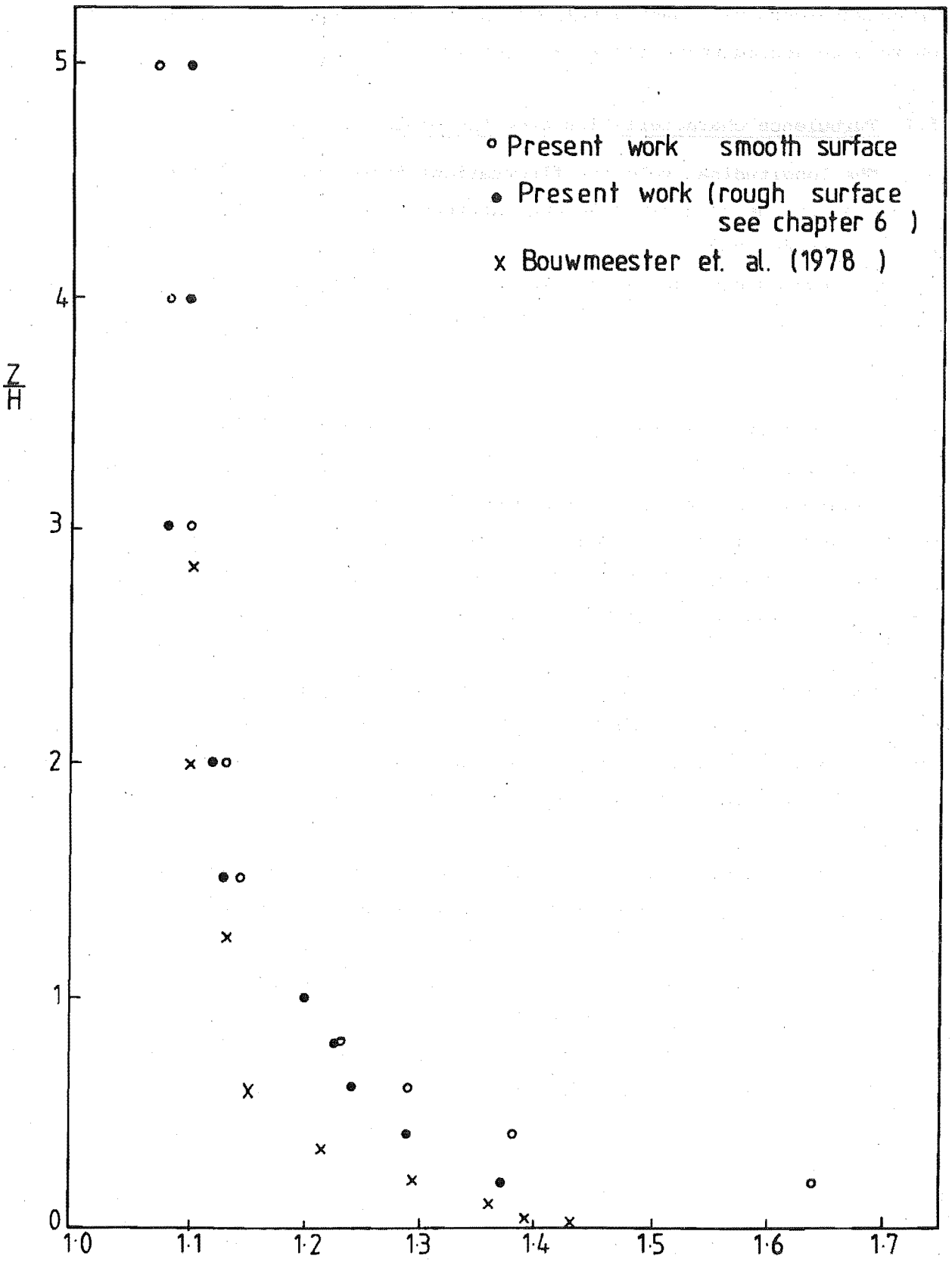

FIG 4·12 COMPARISON OF AMPLIFICATION FACTORS AT THE CREST FOR HILL $\frac{H}{L} = 0.1$

hills. This is not surprising considering that the relation was derived from measurements made over a hill which had an $\frac{H}{L}$ value which varied from 0.06 to 0.20 according to the wind direction.

4.5.2 Turbulence characteristics over the hills

The longitudinal velocity fluctuations at the foot of the hills were the same as in the upstream reference approach flow but the velocity fluctuations decreased towards the crest. In the region after the crest the velocity fluctuations increased, the largest increases occurred for the hills with an aspect ratio of 0.5 and 1.0 for which a large wake region grew from the hill crest.

The spectral peak shifted to a lower wave number at the hill crest compared to the spectral peak wave number in the upstream reference approach flow. There was a corresponding increase in the integral time scale calculated from the autocorrelation functions. This is due to the contracting streamlines over the hill causing the average gust length to increase. The changes were largest for the hills with $\frac{H}{L} = 0.3$ and 0.5.

Counihan (1973) tested three sinusoidal hill shapes with $\frac{H}{L} = 0.33$, 0.67 and 1.34 in a simulated rural boundary layer. Because different hill shapes and a smaller hill height to boundary layer height ratio were used in the present work only limited comparisons are possible.

Counihan presents contours of equal velocity fluctuations u' over some of the sinusoidal hills. One such diagram for the hill with $\frac{H}{L} = 0.33$ is shown in figure 4.13. This figure illustrates the same trends in the velocity fluctuations as were found in the present work. The decrease in u' at the hill crest is clearly evident as is the increase in u' in the post-crest region. The maximum value of u' in the post-crest region occurs at some height above the ground as found in the present work and shown in figure 4.7c.

Counihan predicted that flow separation would occur when $\frac{H}{L} > 0.43$ (for $\frac{H}{\delta} = 0.125$) and $\frac{H}{L} > 0.54$ (for $\frac{H}{\delta} = 0.083$). The value of $\frac{H}{\delta}$ used in the present work was 0.056, so separation would be expected to occur for $\frac{H}{L} > 0.54$. The triangular hill with $\frac{H}{L} = 0.50$ showed flow separation because the sharp crested triangular hills would exhibit earlier flow separation than the round crested hills used by Counihan.

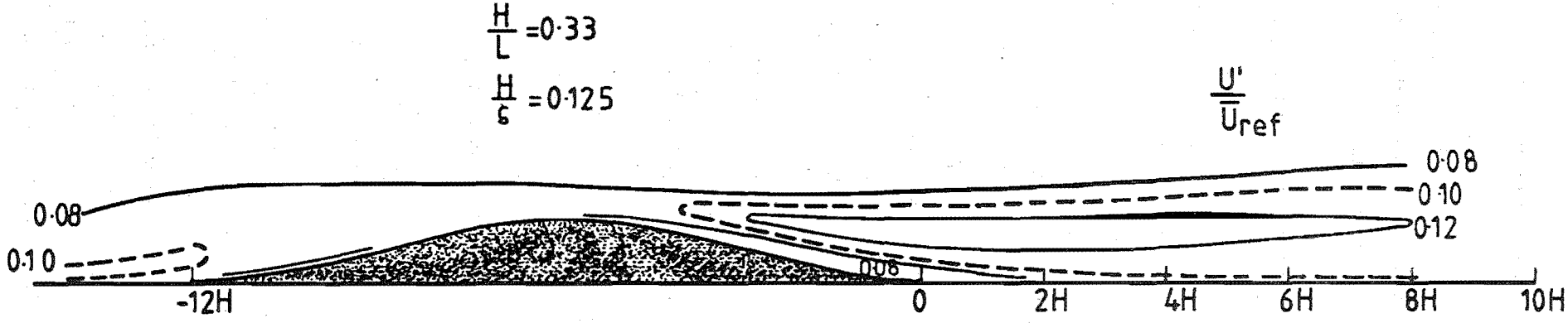

FIG 4·13 ISOTURBS OVER A SINUSOIDAL HILL AFTER COUNIHAN (1973)

Taylor and Gent (1974) used their numerical method to predict that flow separation would occur over their hill shapes when $\frac{H}{L}$ was greater than 0.66. Flow separation occurred over the triangular hill with $\frac{H}{L} = 0.5$ but as discussed above, the sharp crested triangular hills would be expected to exhibit earlier flow separation than the round crested hill shapes studied by Taylor and Gent.

The approach turbulence intensity profile used in the present work is compared to that used by Bouwmeester et.al. (1978) in figure 4.14. As for the approach mean velocity profile the approach turbulence intensity profile used by Bouwmeester et.al. is slightly dependent on the hill slope. This is because the hill crests were placed in the same position in the wind tunnel and as the flow appears to be slowly changing with streamwise distance, the approach turbulence intensity profile changes as the hill length changes.

Figure 4.14 also shows that the approach turbulence intensity profiles used by Bouwmeester et.al. are considerably lower than those used in the present work. The turbulence intensity profiles used by Bouwmeester et.al. are representative of flow over large expanses of water.

Bouwmeester et.al. present isoturbs for the flow over triangular hills with $\frac{H}{L} = 0.1$, 0.33, 0.5 and 1.0. As in the present work, Bouwmeester et.al. found that the velocity fluctuations decreased towards the hill crest, and that the minimum values of u' occurred at the hill crest. Figure 4.15 shows that the u' values measured by Bouwmeester et.al. at the hill crest are smaller than those in the upstream reference approach flow. This is the same trend found in the present work as may be seen from figure 4.7. Rider and Sandborn (1977) showed that the vertical velocity fluctuations increased towards the hill crest.

Bouwmeester et.al. present spectra measured at various positions in the flow over a triangular hill of $\frac{H}{L} = 0.5$. These spectra were not measured at a constant height above the ground, but rather along a streamline. There was a slight increase in the spectral peak frequency from the upstream foot of the hill at a height of $\frac{z}{H} = 0.28$ to the crest of the hill at a height of $\frac{z}{H} = 0.08$. The increase in the mean velocity at the crest was more than sufficient to cause the spectral peak wave number to decrease at the crest relative to the upstream reference value as was found in the present work, discussed in section 4.4.3. Spectral measurements were also made by Bouwmeester

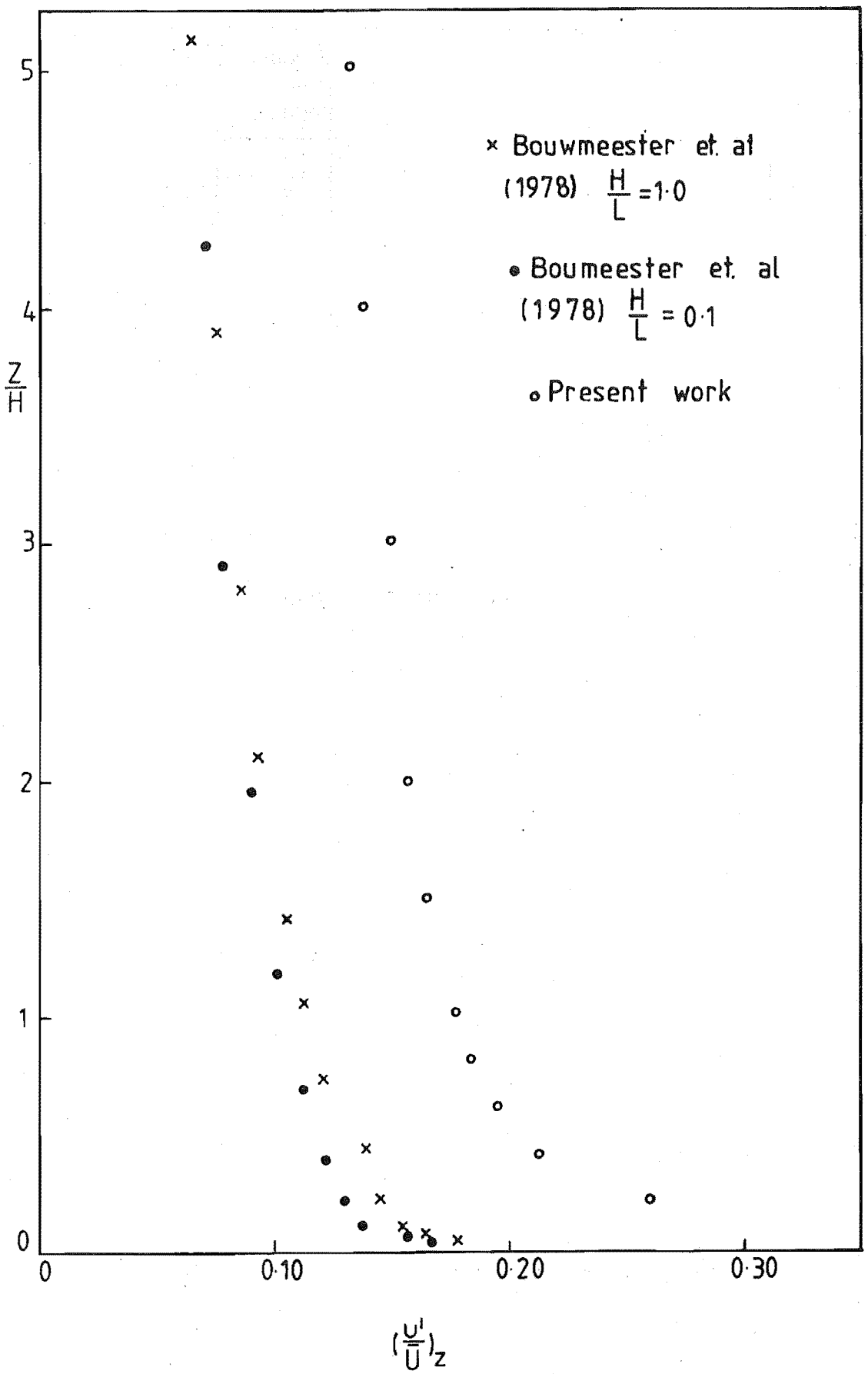

FIG 4·14 COMPARISON OF APPROACH TURBULENCE PROFILES

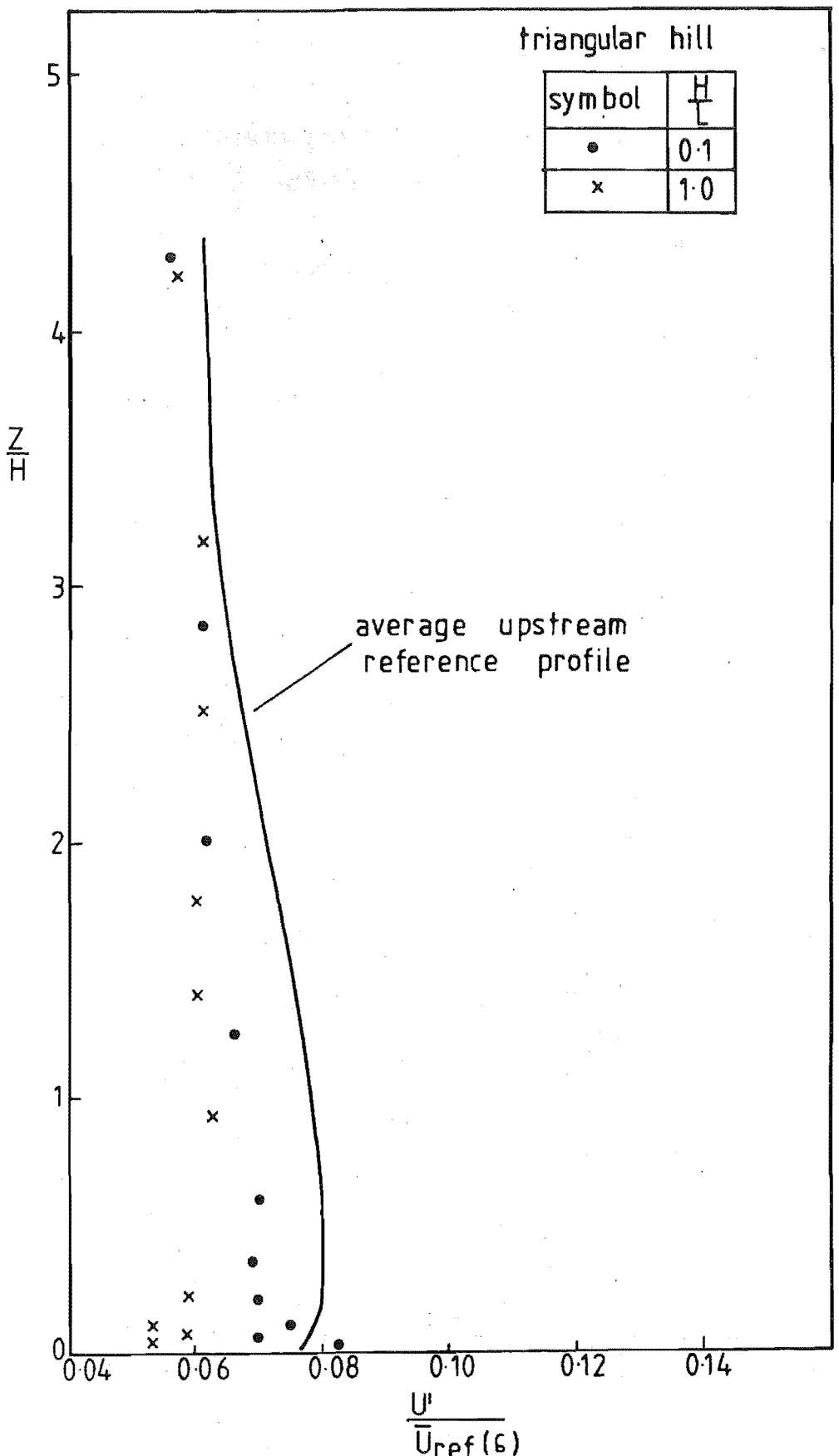

FIG4·15 TURBULENCE INTENSITY PROFILES AT $\frac{x}{L}=0$ AFTER BOUWMEESTER ET. AL. (1978)

et.al. further out in the boundary layer: at the upstream foot of the hill ($\frac{z}{H}$ = 0.72), at the hill crest ($\frac{z}{H}$ = 0.33) and downstream of the foot of the hill ($\frac{z}{H}$ = 0.75). The results show that the spectral peak frequency remains in the same position. If the mean velocity changes are considered as the flow moves over the hill then these spectra also show the same trends as those discussed in section 4.4.3.

4.5.3 Predicting the mean velocity profile at the hill crest

Bouwmeester et.al. (1978) developed a technique for predicting the mean velocity profile at the crest of a hill. The method involves representing the mean velocity profiles at the upwind reference position and at the hill crest by a power law. As was shown in Chapter Three the approach mean velocity profile is well described by a power law. The measured mean velocity profiles at the crest of the hills can also be described closely by a power law as shown in figure 4.16. The prediction technique of Bouwmeester et.al. should therefore work well.

The prediction method involves determining the amplification factor at one hill height above the crest using a graphical relation between the upwind and downwind slope and the amplification factor. Measurements made in the present work do not fit the graphical relation very well. The prediction method makes no allowance for the effect of different ridge shapes but allowance is made for different incident mean velocity power law profiles.

The predicted mean velocity profiles at the hill crests are shown in figure 4.17 which may be compared with the measured mean velocity profiles at the hill crests as presented in figure 4.3. The prediction method yields velocities which are too low close to the surface and too high well above the surface.

4.6 Conclusions from the study of the influence of the hill slope on the wind flow over hills

(a) The mean velocity decreased as the flow approached the upwind foot of the hills, after which the velocity increased. The maximum velocity for all the hills occurred at the hill crest. The mean velocity decreased in the region after the crest where a wake region formed for the steeper hills.

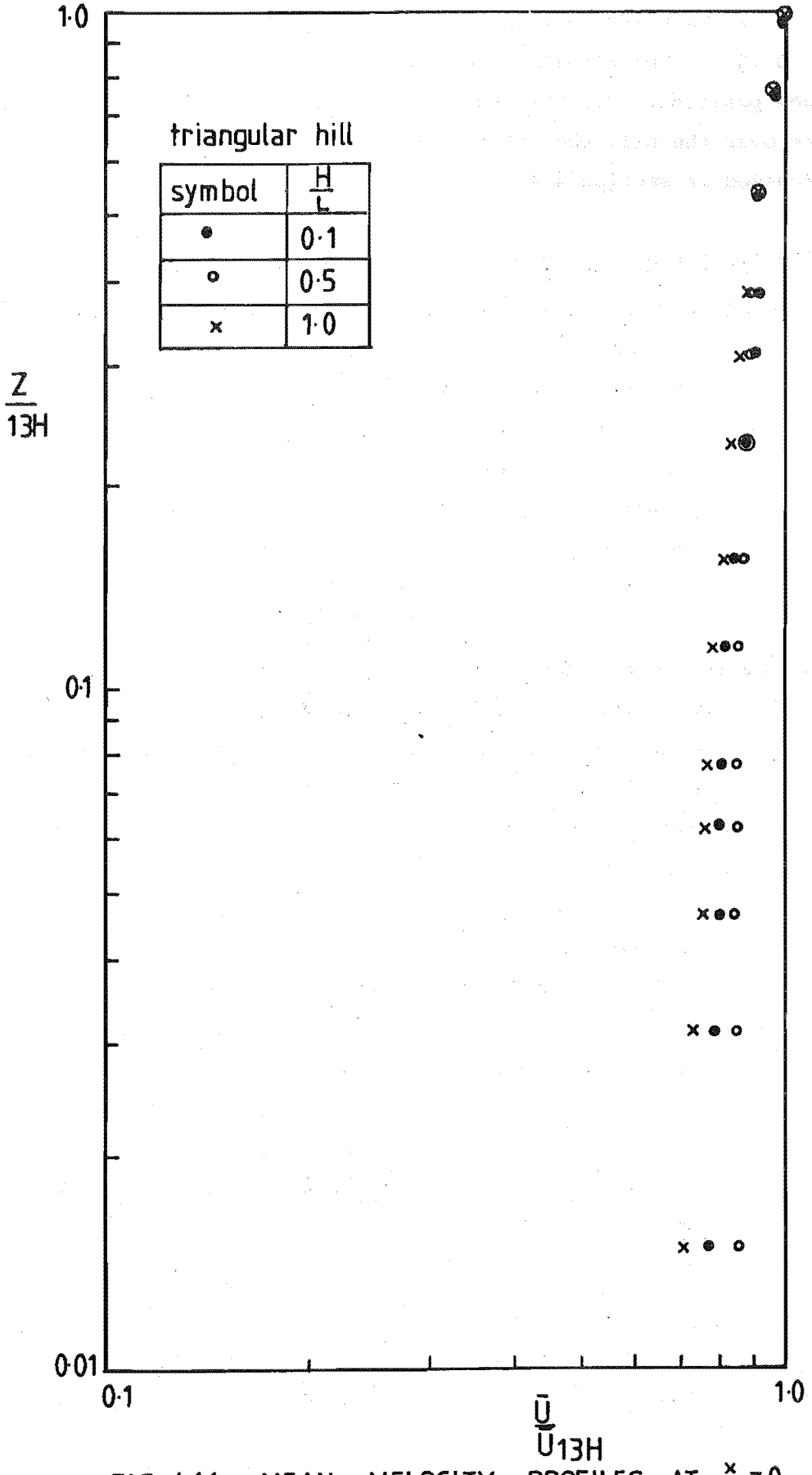

FIG 4·16 MEAN VELOCITY PROFILES AT $\frac{x}{L} = 0$

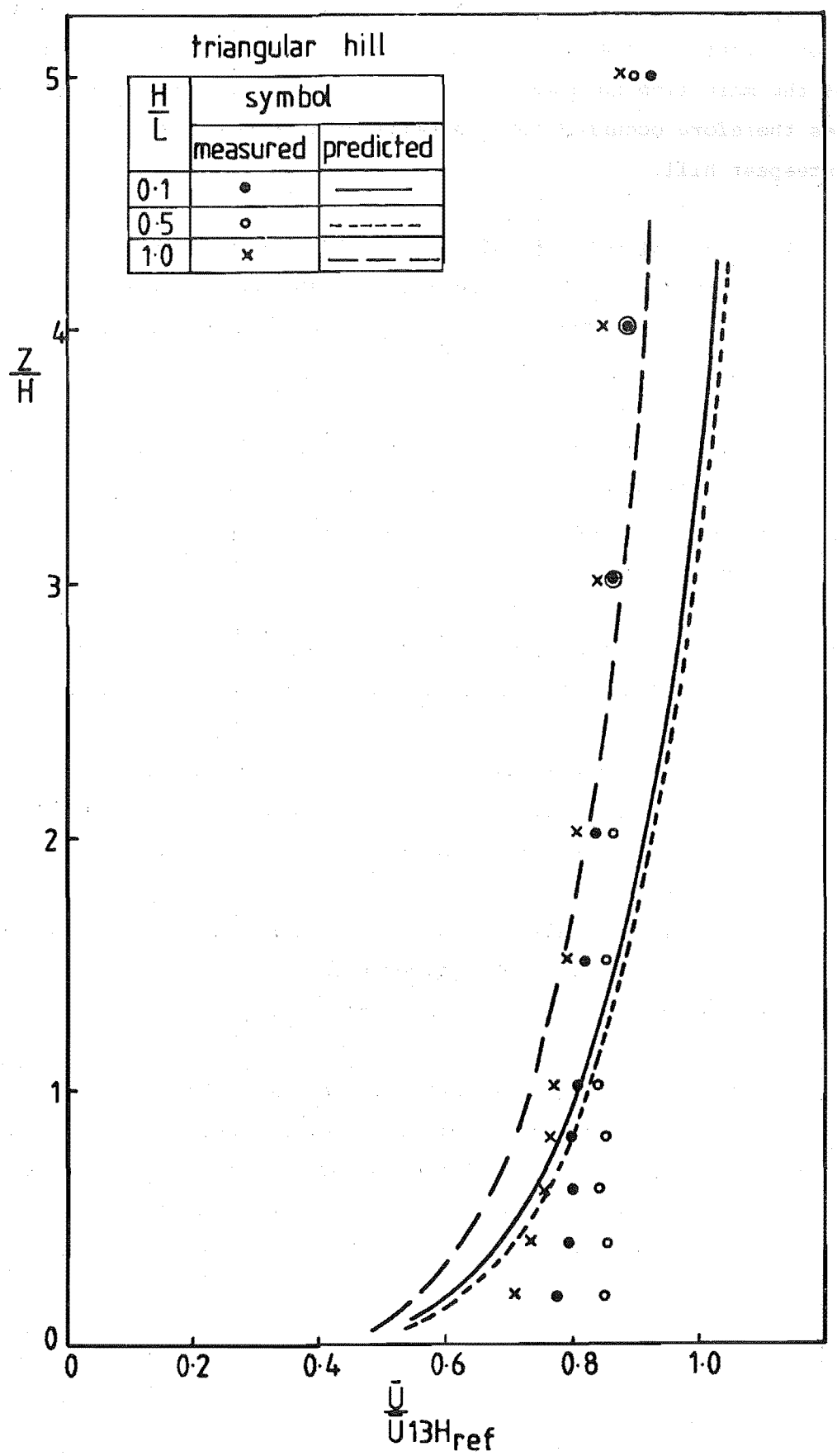

FIG 4·17 PREDICTED MEAN VELOCITY PROFILES AT $\frac{x}{L} = 0$

(b) The upstream vortex and downstream wake region produced the equivalent of a higher potential flow hill for the steeper hills and an effective gradual slope for the main flow outside the separation region. The largest mean velocities therefore occurred for the hills of intermediate slope rather than for the steepest hill.

(c) The longitudinal velocity fluctuations decreased towards the hill crests and increased in the region after the crest. The largest increase in the velocity fluctuations occurred for the steeper hills which exhibited a wake region.

(d) The spectral peak frequency shifted to lower frequencies at the hill crest compared to the upstream reference approach flow. The largest changes in the spectral peak frequency occurred for the hills with the largest mean velocities at the hill crest.

(e) The trends shown in the theoretical approaches to wind flow over hills fail for the steeper hills where the assumptions of the theories are invalid.

The measured flow quantities over the hills show similar trends to the available laboratory and field tests but close comparisons are difficult because of different approach flow conditions.

There are very few rigorous field tests with which to compare the results. The available field work covers a very small range of hill slopes and the approach wind conditions are frequently not measured.

(f) The prediction techniques reported in the literature are not satisfactory. A power law fits the measured mean velocity profiles well but the prediction methods only allow for the affect of the upwind and downwind slope and changes in the approach mean velocity power law exponent on the wind flow over the hills. Other parameters such as the boundary layer height and the hill profile shape are not considered.

CHAPTER 5

INFLUENCE OF THE HILL SHAPE ON THE WIND FLOW OVER HILLS

5.1 Introduction

To investigate the effect of the hill shape on the wind flow over hills three symmetrical bell-shaped hills were constructed. Measurements were made in the flow over the bell-shaped hills of the mean velocity, the longitudinal velocity fluctuations and the energy spectra and autocorrelation functions.

The measurements over the bell-shaped hills were compared with those made over triangular hills with the same value of $\frac{H}{L}$.

5.2 Experimental apparatus

5.2.1 The model hills

Three symmetrical bell-shaped hills were made with $\frac{H}{L}$ values equal to 0.3, 0.5 and 1.0. The hill height H was 5.0 cm as for the triangular hills described in Chapter four. The values of $\frac{H}{L}$ were chosen so the measurements over the bell-shaped hills could be compared to the measurements over the triangular hills with the same value of $\frac{H}{L}$, presented in Chapter four.

The shape of the symmetrical bell-shaped hills was defined by:

$$y = \frac{H}{1 + \left(\frac{x}{L}\right)^2} \qquad (5.1)$$

where y was measured vertically upwards and x was measured from the hill crest. This shape is the same as that used by Corby (1954) and Jackson and Hunt (1975), and is a good approximation to the bell-shaped hills considered by Taylor and Gent (1974), Deaves (1975) and Derickson and Meroney (1977).

Because the hill shape defined by equation 5.1 extends to infinity, the hill length used was 4L from the hill crest for the hills with $\frac{H}{L}$ equal to 0.3 and 0.5 and 6L for the hill with $\frac{H}{L}$ equal to 1.0. The bell-shaped hill with $\frac{H}{L}$ equal to 0.3 was constructed from acrylic sheet, the two remaining bell-shaped hills were made from aluminium. As for the triangular hills described in section 4.2.1 the bell-shaped hills were also constructed in two halves so the

traversing system could be moved between the hills to aid streamwise traversing. The two hill sections consisted of a number of rib sections covered with an 0.3 cm thickness of the construction material so the hill shape was defined by equation 5.1. Figure 5.1 shows the bell-shaped hill with $\frac{H}{L}$ equal to 0.3 mounted in the wind tunnel. The aluminium sheet proved superior to the acrylic sheet in the ease of construction, and was also more robust in use.

5.3 Experimental procedure

The experimental procedure was exactly the same as was followed for the tests using the triangular hills, described in section 4.3.

The bell-shaped hills were placed in the simulated atmospheric boundary layer described in Chapter three so that the start of the hills were at X = 9.5 m. In this way the bell-shaped hills were subjected to exactly the same approach profile as the triangular hills.

Traverses were made at the same vertical and streamwise locations as were made over the triangular hills using the same flow measuring and flow traversing equipment.

5.4 Experimental results

5.4.1 Mean velocity profiles and amplification factors

Lines of equal amplification factor for the flow over the three bell-shaped hills are shown in figure 5.2. Figure 5.2 may be compared to figure 4.2 which shows the lines of equal amplification factor for the same flow incident on the triangular hills with the same values of $\frac{H}{L}$.

In the region before the crest the bell-shaped hills have larger velocities than the corresponding triangular hills. The maximum difference in the velocities occurs at $\frac{x}{L} = -2$ (i.e. the upwind foot of the triangular hills) close to the ground and the increase in velocity is larger the greater the value of $\frac{H}{L}$:

e.g. at $\frac{z}{H} = 0.2$, $\frac{x}{L} = -2$:

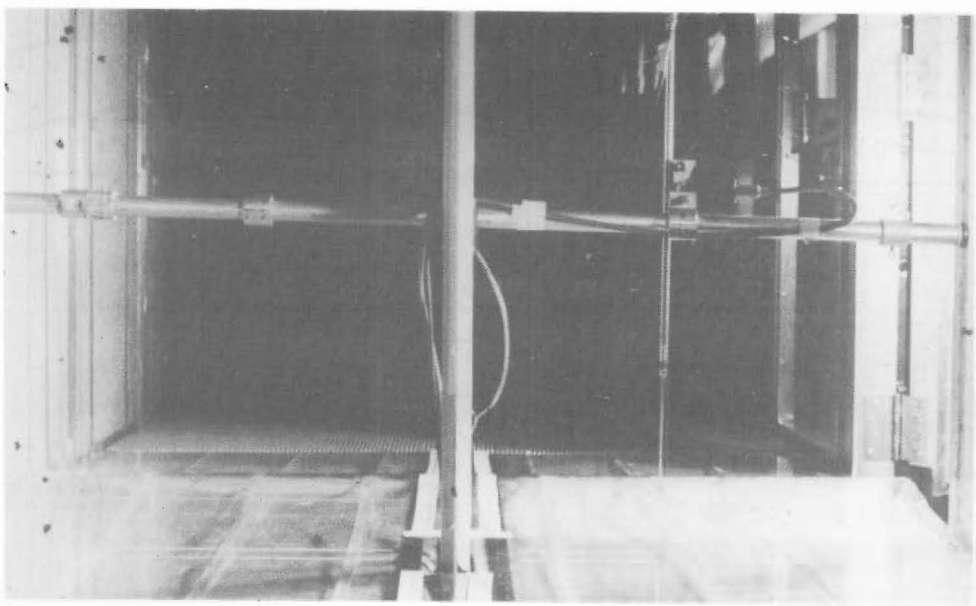

Fig. 5.1 Photograph of a model hill mounted in the wind tunnel

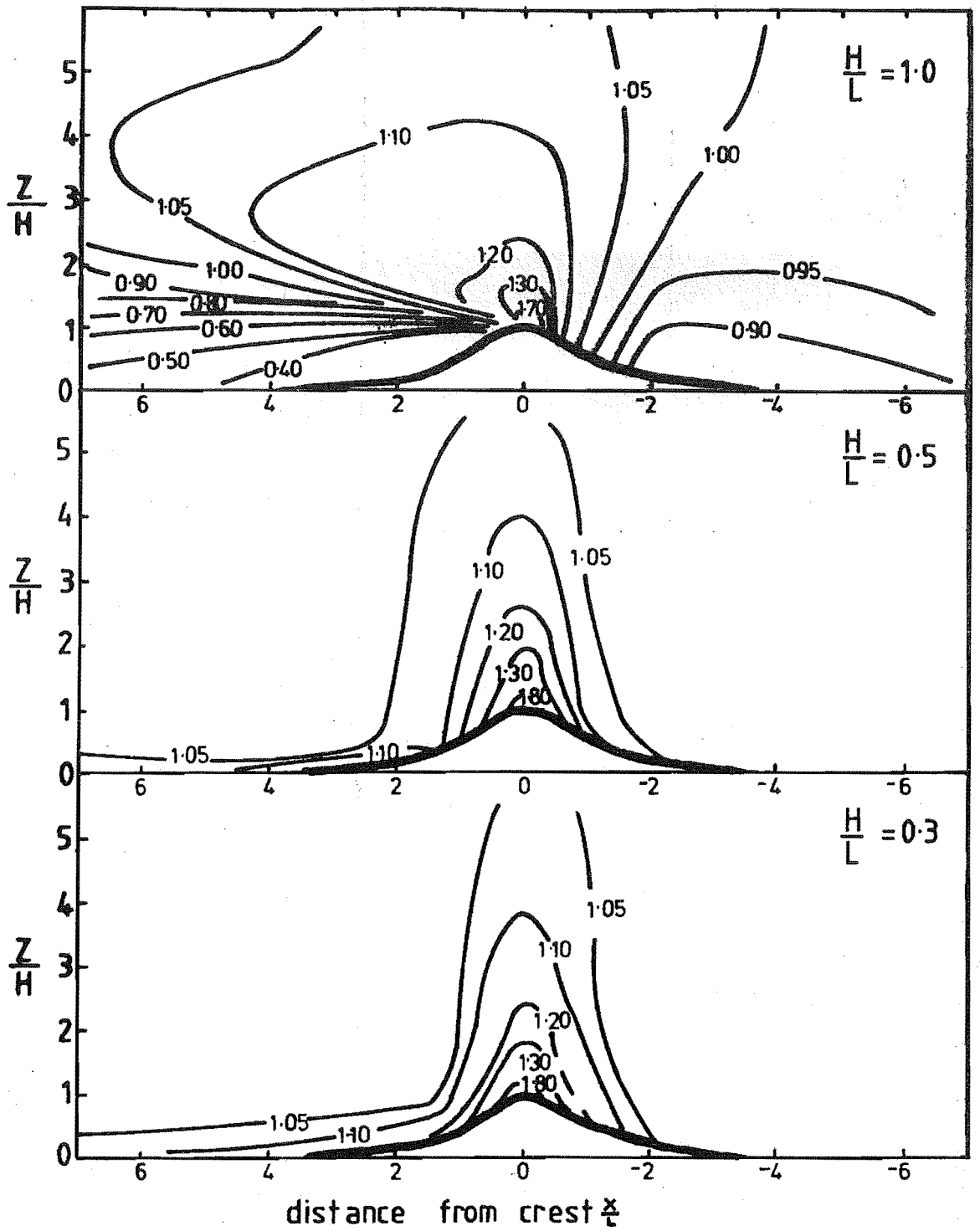

FIG. 5·2 LINES OF EQUAL AMPLIFICATION FACTOR.

$\frac{H}{L}$	0.3	0.5	1.0
$\frac{\bar{U}_{\text{bell-shaped hill}}}{\bar{U}_{\text{triangular hill}}}$	1.30	1.53	1.79

The amplification factors at the crest of the bell-shaped hills are compared to those for the triangular hills with the same value of $\frac{H}{L}$ in figure 5.3. For the hills with $\frac{H}{L}$ equal to 0.3 there is little difference between the crest amplification factors. The bell-shaped hills with $\frac{H}{L}$ equal to 0.5 and 1.0 have amplification factors about 5% larger than the values for the corresponding triangular hills.

In the region after the crest the bell-shaped hills have larger velocities than the corresponding triangular hills at any value of $\frac{x}{L}$. The bell-shaped hills had approximately twice the length of hill surface of the triangular hills and some of the increased velocity could be attributed to the longer distance of smooth surface and consequent speedup. The effect of the length of smooth hill surface on the boundary layer developed over a rough surface is discussed in Chapter six. The largest changes at any point occur for the hills with $\frac{H}{L}$ equal to 0.5 where the bell-shaped hill has lines of equal amplification factor completely different to those of the corresponding triangular hill because of the absence of a downstream vortex for the bell-shaped hill.

5.4.2 Turbulence intensity profiles

Lines of equal local turbulence intensity for the flow over the three bell-shaped hills are presented in figure 5.4 which may be compared to figure 4.6 which shows the isoturbs over the corresponding triangular hills.

In the region before the crest the local turbulence intensity is much higher close to the ground for the triangular hills than for the bell-shaped hills. For all $\frac{H}{L}$ values the largest difference in the local turbulence intensity occurs at the upwind foot of the triangular hills. Changes in the velocity fluctuations u' are very small so the changes in the local turbulence intensity are due to changes in the local velocity.

The longitudinal velocity fluctuations at the hill crest for the triangular and bell-shaped hills are compared in figure 5.5 for each $\frac{H}{L}$ value.

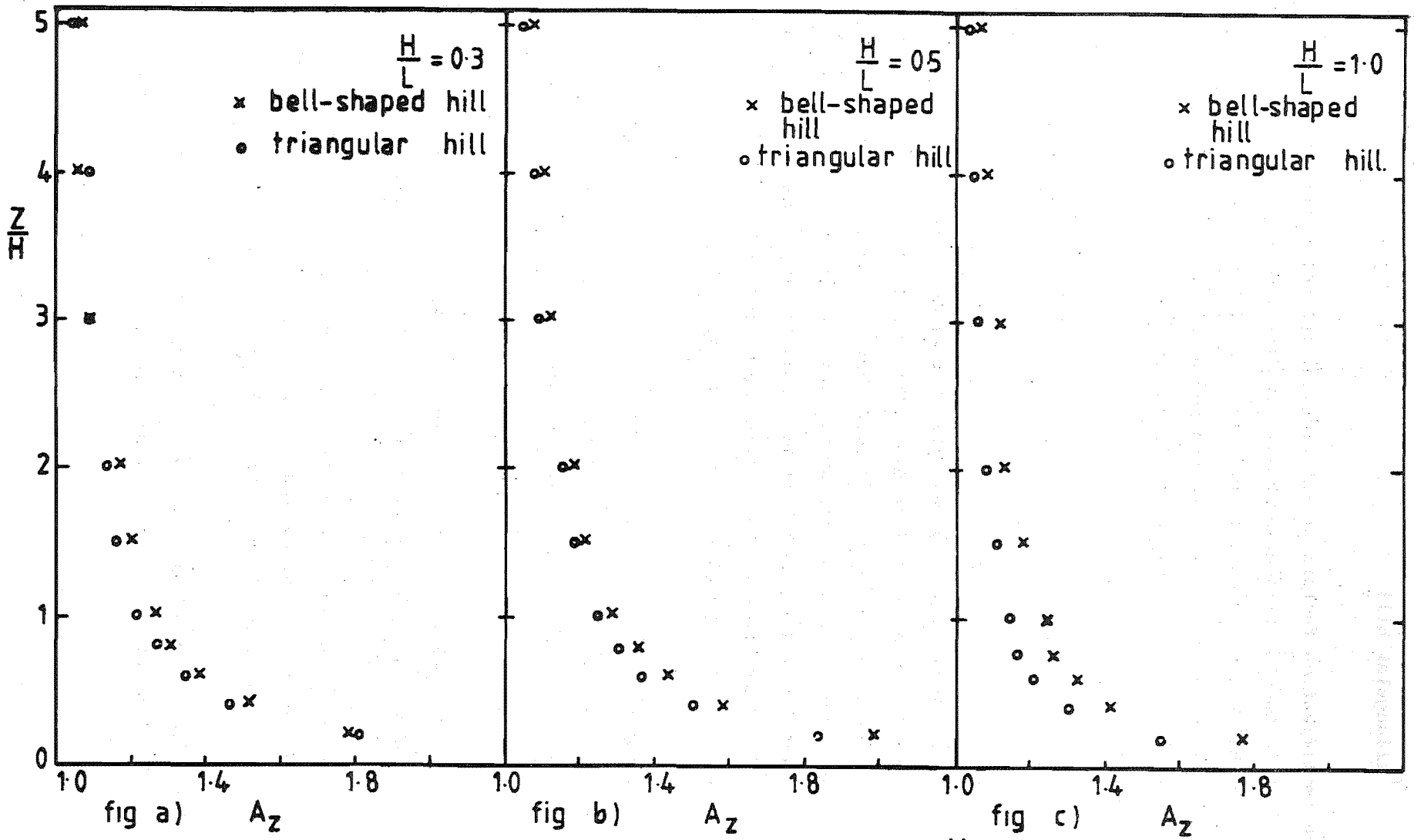

FIG 5·3 COMPARISON OF AMPLIFICATION FACTORS AT $\frac{X}{L} = 0$

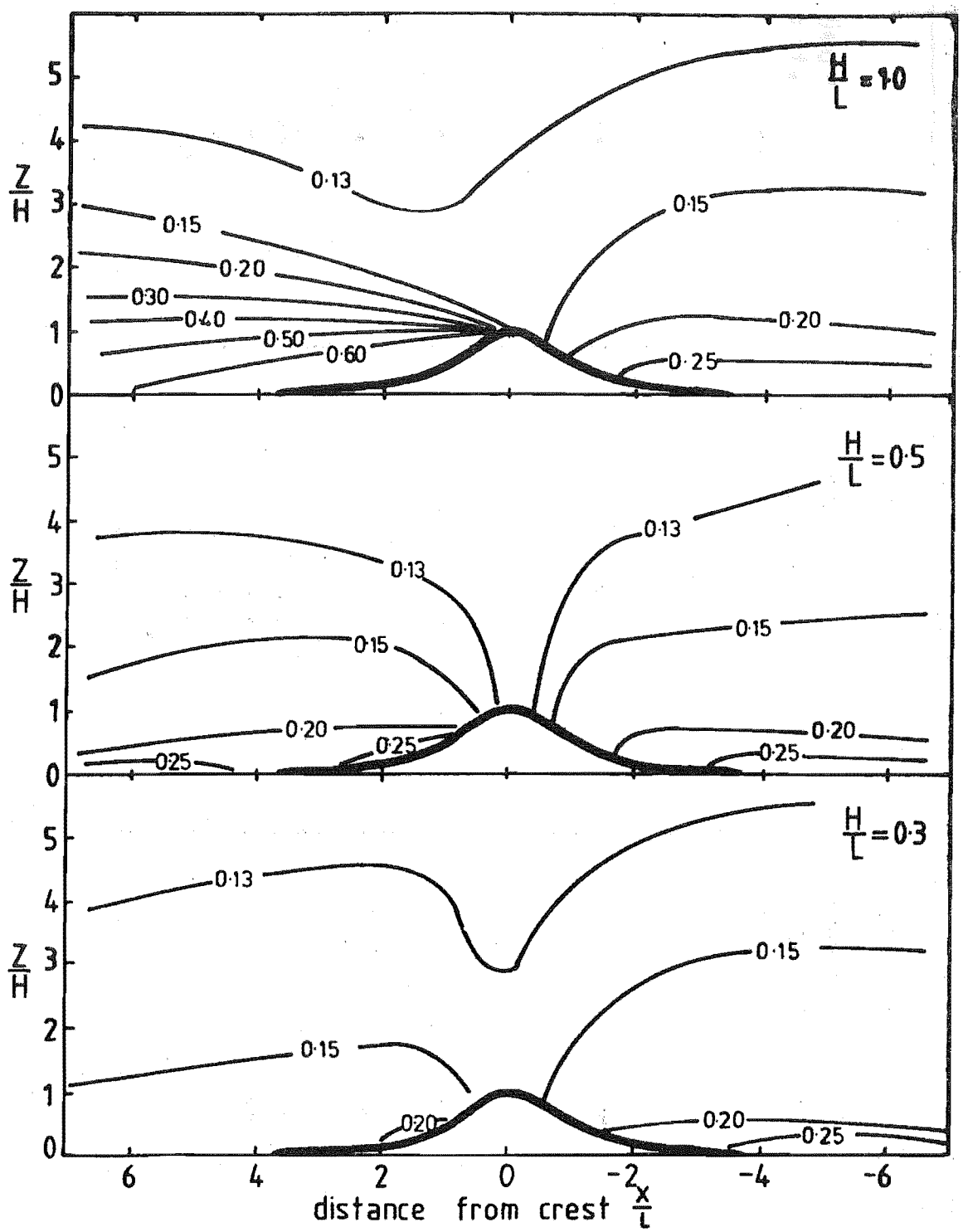

FIG 5·4 ISOTURBS FOR THE BELL-SHAPED HILLS

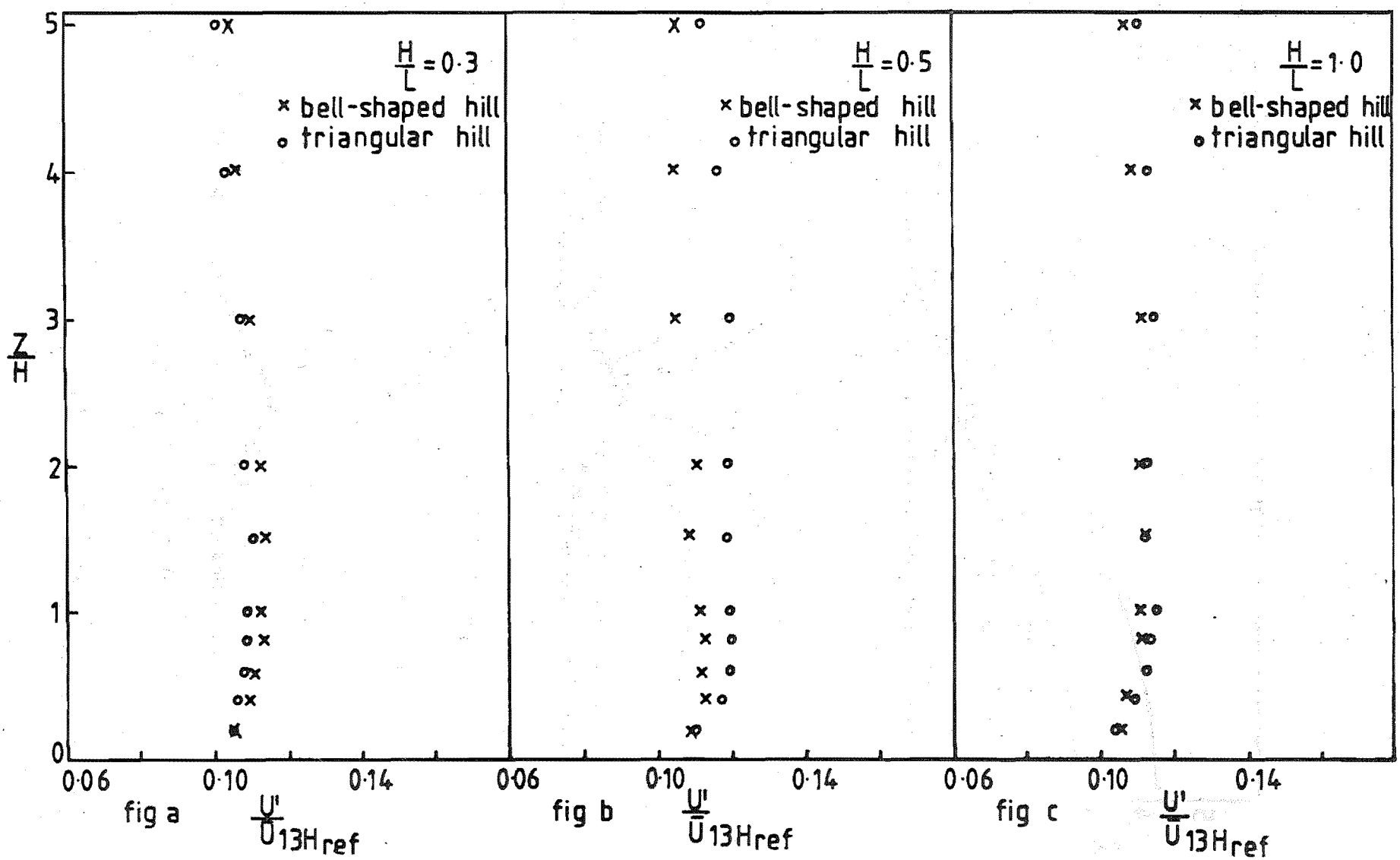

FIG 5·5 COMPARISON OF TURBULENCE INTENSITY PROFILES AT $\frac{X}{L} = 0$

For the hills with $\frac{H}{L}$ equal to 0.3 and 1.0 the velocity fluctuations u' and the local turbulence intensity are within 5% for the triangular and bell-shaped hills. For the hill with $\frac{H}{L}$ = 0.5 the velocity fluctuations u' are up to 10% lower for the bell-shaped hill, as may be seen from figure 5.5b.

In the region after the crest there is little difference between the values of the local turbulence intensity or the velocity fluctuations u' for the triangular and bell-shaped hills with $\frac{H}{L}$ equal to 0.3. For the hills with $\frac{H}{L}$ equal to 0.5 the local turbulence intensity is up to 50% higher for the triangular hill at any position compared to the bell-shaped hill. For example compare the position of the 0.20 isoturb in figures 5.4 and 4.6. As may be seen from figure 5.6b the velocity fluctuations are also very much higher for the triangular hill. For the hills with $\frac{H}{L}$ = 1.0 opposite trends are present to those for the hills with $\frac{H}{L}$ = 0.5. The local turbulence intensity is up to 15% lower for the triangular hill than for the corresponding bell-shaped hill. For example compare the position of the 0.50 isoturb in figures 5.4 and 4.6. As illustrated in figure 5.6c the velocity fluctuations are also very much lower for the triangular hill with $\frac{H}{L}$ = 1.0 than for the corresponding bell-shaped hill.

5.4.3 u velocity component energy spectra and autocorrelation coefficients

The energy spectra for the flow over the bell-shaped hills were measured at the upstream reference position, at the hill crest and 10H downstream of the end of the hills at heights above the surface of $\frac{z}{H}$ = 0.2, 1.0 and 2.0. These spectra were compared with the corresponding spectra measured over the triangular hills. As the digital data acquisition system described in Appendix two had not been commissioned when these measurements were made, comparisons cannot be made for regions below the spectral peak. Spectral peak values obtained from the measured spectra are presented in table 5.1. Estimates of the location of the spectral peak must be regarded as approximate because of the flat-topped spectra and the fluctuating signal from the frequency analyser.

The spectral peak wave number at the hill crest has decreased relative to the upstream reference value at the same height. The decrease is larger for the bell-shaped hills than for the corresponding triangular hills as illustrated in figures 5.7, 5.8 and 5.9 and shown in the table below:

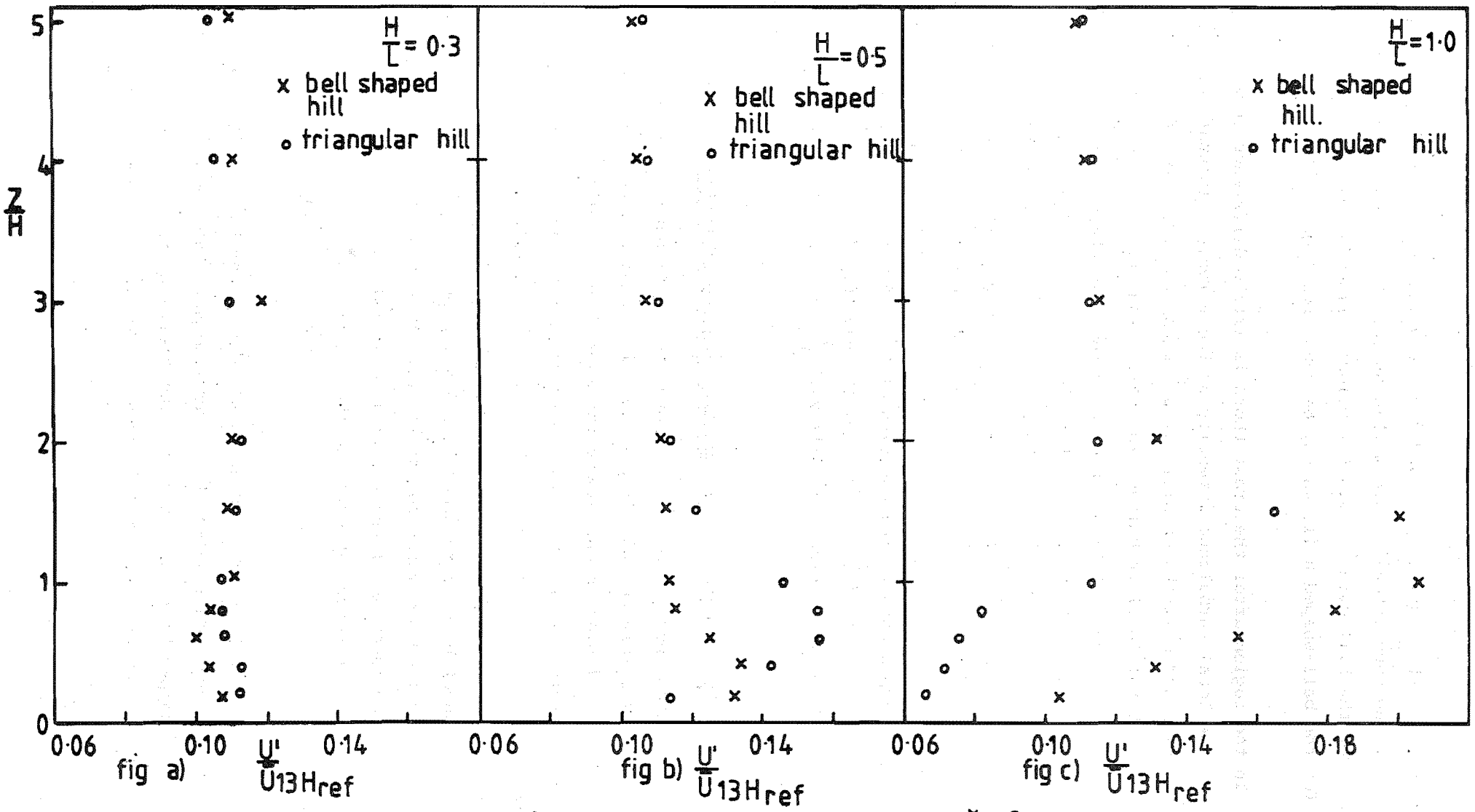

FIG 5·6 COMPARISON OF TURBULENCE INTENSITY PROFILES AT $\frac{x}{L}=2$

Hill Shape	$\frac{H}{L}$	$\frac{z}{H}$ = 0.2									$\frac{z}{H}$ = 1.0									$\frac{z}{h}$ = 2.0								
		10H upstream of the hill			crest			10H downstream of the hill			10H upstream of the hill			crest			10H downstream of the hill			10H upstream of the hill			crest			10H downstream of the hill		
		k_p	n_p	T_E	k_p	n_p	T_E	k_p	n_p	T_E	k_p	n_p	T_E	k_p	n_p	T_E	k_p	n_p	T_E	k_p	n_p	T_E	k_p	n_p	T_E	k_p	n_p	T_E
		m^{-1}	H_z	ms	m^{-1}	H_z	ms	m^{-1}	H_z	ms	m^{-1}	H_z	ms	m^{-1}	H_z	ms	m^{-1}	H_z	ms	m^{-1}	H_z	ms	m^{-1}	H_z	ms	m^{-1}	H_z	ms
Bell-shape	0.30	0.82	6.36	17.7	0.27	3.74	29.7	0.82	6.57	17.2	0.37	4.09	27.6	0.27	3.73	30.3	0.36	4.20	27.5	0.35	4.29	28.0	0.28	3.95	28.5	0.28	3.53	28.5
	0.50	0.82	6.36	17.7	0.17	2.61	37.0	1.00	7.92	21.8	0.37	4.09	27.6	0.24	3.47	34.3	0.42	4.89	31.4	0.35	4.29	28.0	0.28	4.02	34.2	0.32	4.00	32.0
	1.00	0.82	6.36	17.7	0.29	3.78	29.4	1.18	8.08	17.9	0.37	4.09	27.6	0.27	3.66	30.0	0.67	6.32	20.5	0.35	4.29	28.0	0.28	3.91	31.8	0.46	5.00	23.0
Triangular	0.30	0.82	6.36	17.7	0.29	4.07	32.7	1.00	8.15	22.7	0.37	4.09	27.6	0.27	3.69	32.0	0.34	3.92	30.9	0.35	4.29	28.0	0.29	4.09	33.4	0.29	3.66	32.5
	0.50	0.82	6.36	17.7	0.25	3.48	32.8	1.60	12.32	18.6	0.37	4.09	27.6	0.27	3.76	31.2	0.35	3.68	26.2	0.35	4.29	28.0	0.29	4.05	31.4	0.29	3.47	29.5
	1.00	0.82	6.36	17.7	0.34	4.30	25.6	2.90	15.89	12.9	0.37	4.09	27.6	0.33	4.47	28.7	1.10	8.72	15.6	0.35	4.29	28.0	0.33	4.57	29.9	0.70	7.67	20.9

TABLE 5.1 Integral time scales and spectral peak values for the bell-shaped hills.

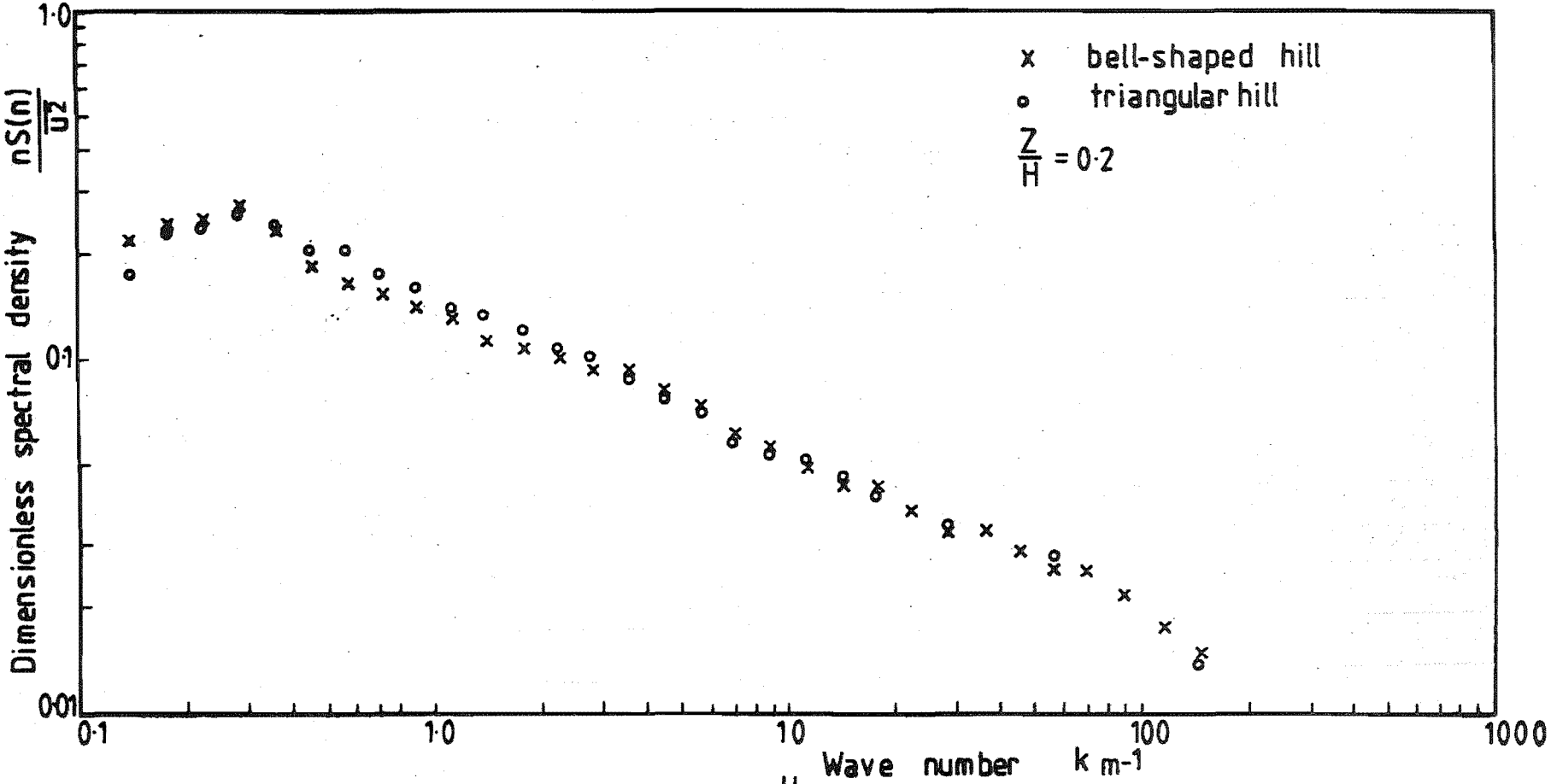

FIG. 5·7 SPECTRA AT THE CREST FOR $\frac{H}{L}$ = 0·3

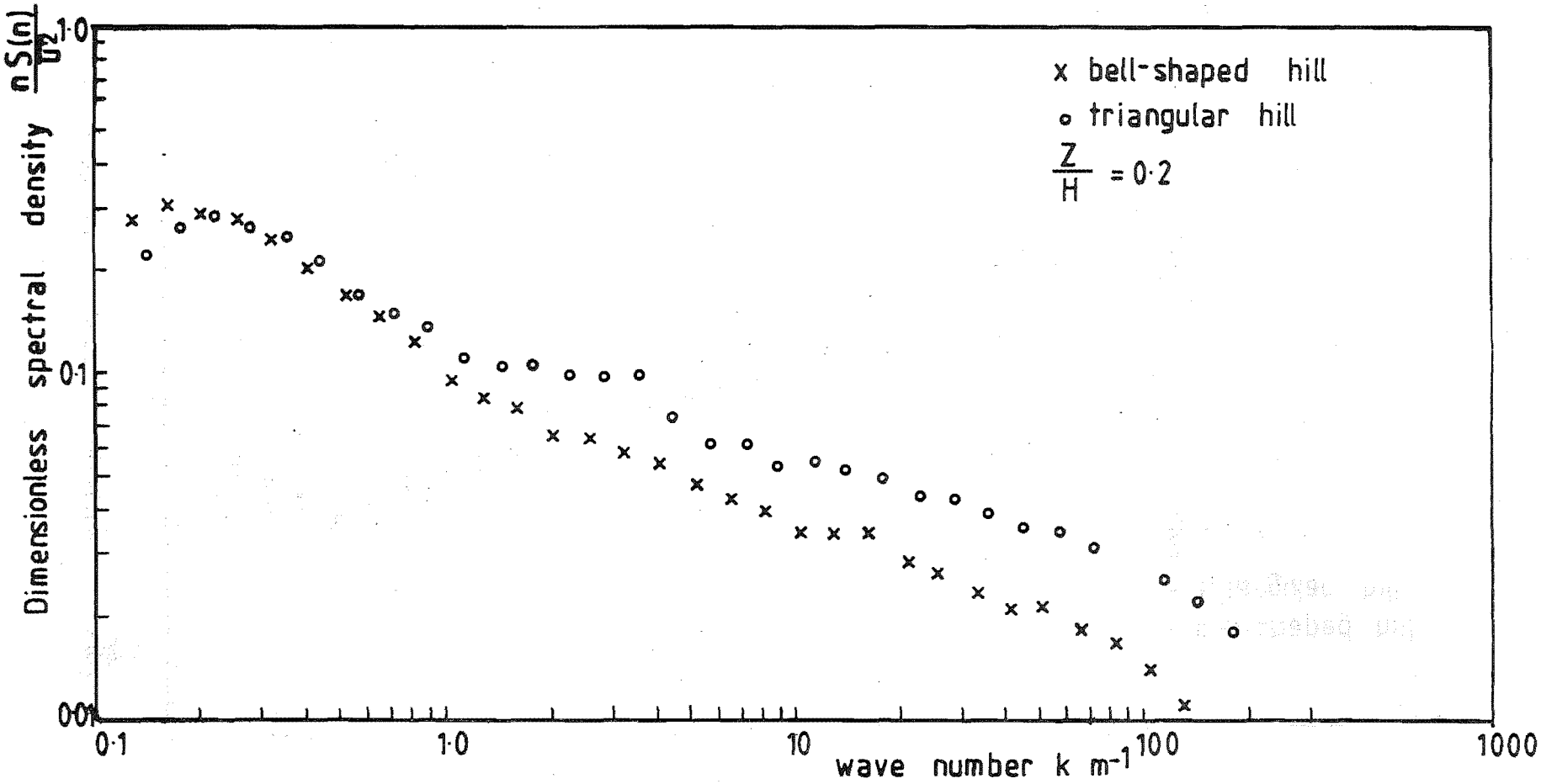

FIG 5·8 SPECTRA AT THE CREST FOR $\frac{H}{L}$ = 0·5

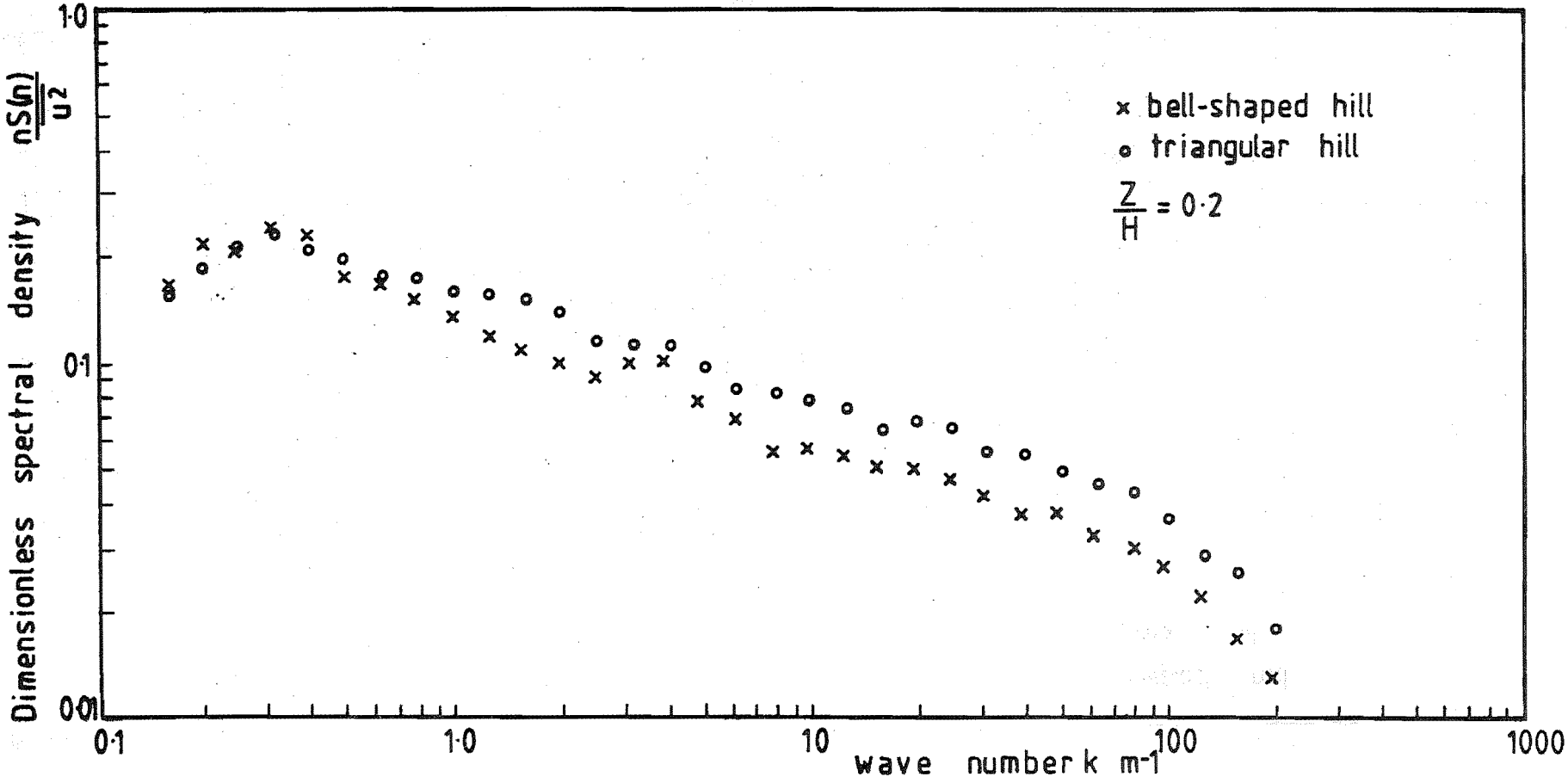

FIG 5·9 SPECTRA AT THE CREST FOR $\frac{H}{L} = 1{\cdot}0$

$\frac{z}{H} = 0.2, \frac{x}{L} = 0$

$\frac{H}{L}$	% reduction in the location of the spectral peak wave number for the bell-shaped hill compared to the corresponding triangular hill
0.3	6%
0.5	30%
1.0	15%

As for the triangular hills the only changes in the spectral shape occurred at the crest of the bell-shaped hills at a height of $\frac{z}{H} = 0.2$ where the spectra at the crest were more peaked compared to the upstream reference spectra. Figures 5.8 and 5.9 show that the spectral slope in the region after the spectral peak is steeper for the bell-shaped hills than for the triangular hills indicating that more high frequency energy is present in the flow at the crest for the triangular hills.

Downstream a distance 10H from the end of the hills the spectral peak does not shift to such a high frequency for the bell-shaped hills compared to the shift for the corresponding triangular hills. This could be due to the much longer distance of smooth hill surface after the crest for the bell-shaped hills compared to the triangular hills, as well as the different hill shape.

The integral time scales calculated from the measured autocorrelation functions in the flow over the bell-shaped hills are presented in table 5.1 where they may be compared with the corresponding values for the triangular hills as presented in table 4.1. Errors in the calculated integral time scales arose because of the fluctuating autocorrelation functions and the occasional failure of the function to decrease to zero within the maximum delay time of 100 ms obtainable with the analog signal processing equipment.

For the bell-shaped hills with $\frac{H}{L}$ of 0.5 and 1.0 the integral time scale is up to 15% larger both at the crest and 10H downstream of the end of the hills compared to the corresponding values for the triangular hills. The bell-shaped hill with $\frac{H}{L}$ of 0.3 has integral time scales slightly less than those for the corresponding triangular hills at all locations.

5.5 Discussion of the experimental results

In this section the experimental results presented in section 5.4 are compared with the available literature.

Bouwmeester et.al. (1978)

Bouwmeester et.al. compared the velocity fields over symmetric triangular and sinusoidal hills with $\frac{H}{L}$ values of 0.5 and 0.67, and found the velocity fields were almost identical. The sinusoidal hills used by Bouwmeester et.al. were only half-sine hills and their abrupt start and finish compared to the bell-shaped hills used in the present work gave much better correspondence with the triangular hills upstream and downstream of the hill crest.

The mean velocity profiles of Bouwmeester et.al. at the hill crests are compared for the sinusoidal and triangular hills with $\frac{H}{L}$ of 0.5 in figure 5.10. Except for a small region close to the ground the triangular hill had a slightly reduced velocity compared to the sinusoidal hill. This is the same trend as found in the present work for the triangular and bell-shaped hills with $\frac{H}{L}$ of 0.5 as shown in figure 5.3.

Bouwmeester et.al. do not present any turbulence data over their sinusoidal hills so a comparison of the turbulence over their sharp and round-crested hills with the present work cannot be made.

Rider and Sandborn (1977)

Rider and Sandborn subjected a single approach boundary layer profile to six different ridge shapes which varied from a triangular shape to a box shape. Each hill had the same distance from the hill crest to the hill base and consequently the ratio $\frac{H}{L}$ varied by a factor of two. The speedup at the hill crests varied markedly from which it was apparent that the ratio of the hill height to the hill base length does not characterise the hill accurately. The triangular and sinusoidal hills were found to have the largest speedup.

The approach mean velocity profile used by Rider and Sandborn had a power law exponent of 0.22 and their approach turbulence profile was similar to that used in the present work. The mean velocity profiles obtained by Rider and Sandborn at the crest of their triangular and sinusoidal hills with $\frac{H}{L}$ of 0.5 are compared in figure 5.11. The corresponding turbulence intensity

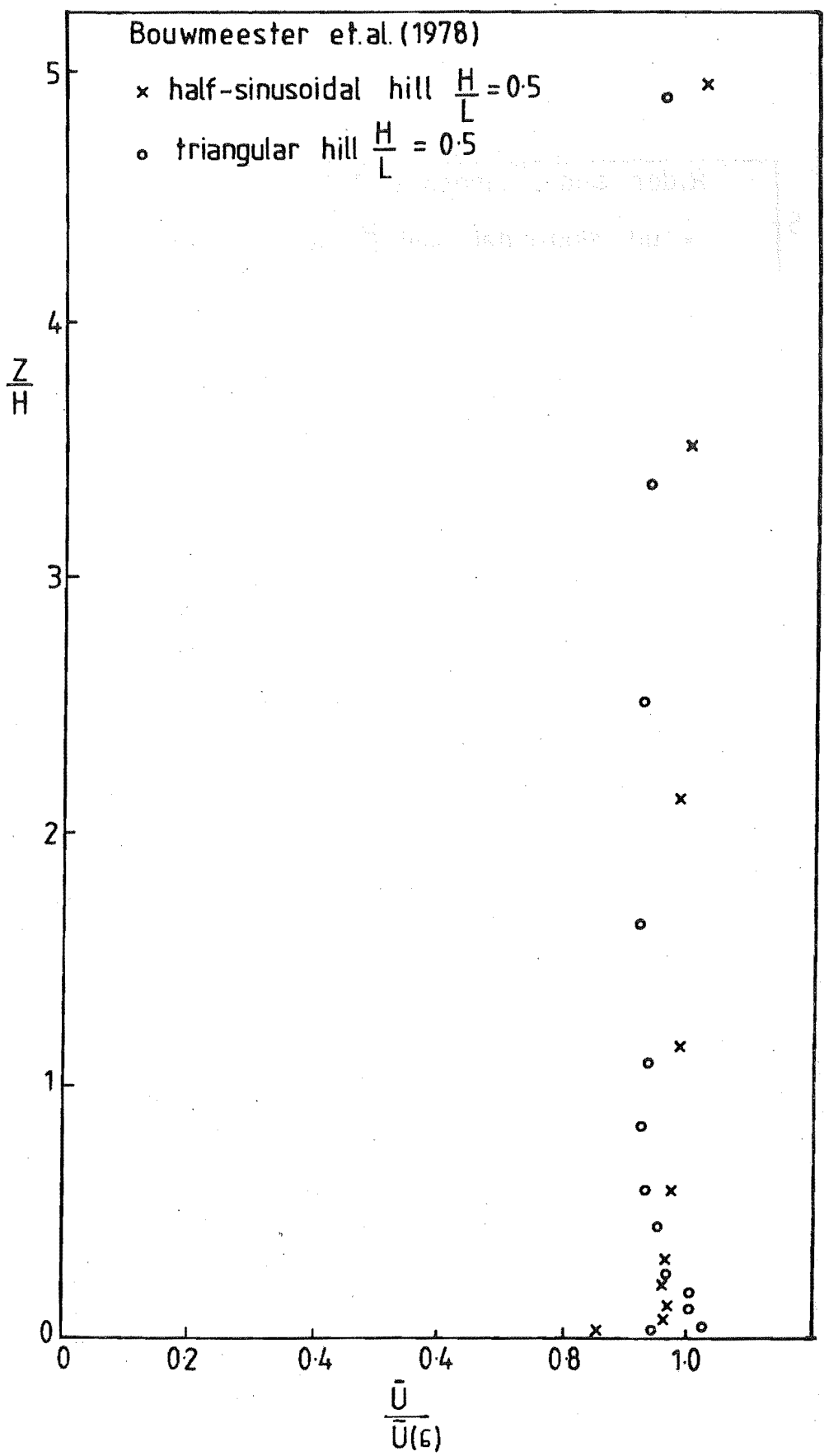

FIG 5·10 COMPARISON OF VELOCITY PROFILES AT THE CREST.

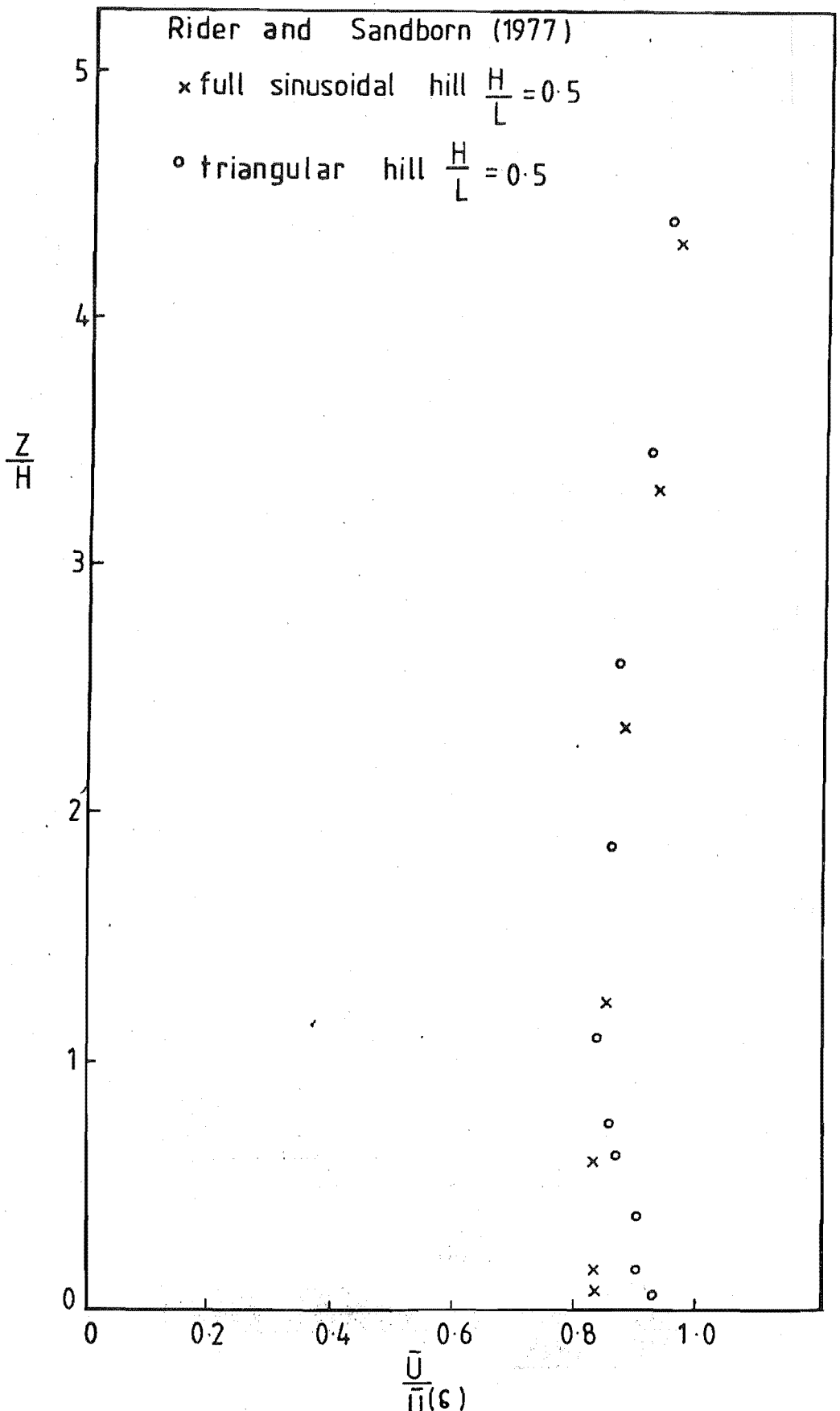

FIG 5·11 COMPARISON OF VELOCITY PROFILES AT THE CREST.

profiles are shown in figure 5.12. As was found in the present work, the triangular and round-crested hills with the same value of $\frac{H}{L}$ have similar mean velocity profiles at the crest. Figure 5.12 shows that Rider and Sandborn obtained almost identical turbulence profiles at the crest of their triangular and round-crested hill. This was in contrast to the present work where the triangular hill with $\frac{H}{L}$ of 0.5 had turbulence intensity values about 10% larger than for the corresponding round-crested hill.

5.6 Conclusions to the study of the influence of the hill shape on the wind flow over hills

(a) The bell-shaped hills had larger velocities upstream and downstream of the hill crest compared to the triangular hills with the same value of $\frac{H}{L}$. But at the crest the velocity profiles for the triangular and bell-shaped hills were found to be similar, a conclusion that is supported by the available literature.

(b) The only significant difference in the velocity fluctuations over the triangular and bell-shaped hills occurred for the hill which had a slope close to the slope at which flow separation occurred. In this case the triangular hill exhibited flow separation but the bell-shaped hill did not. This led to an increase in the velocity fluctuations at the crest and downstream of the crest for the triangular hill compared to the bell-shaped hill with the same aspect ratio.

(c) At the crest of the bell-shaped hills there was a larger decrease in the spectral peak wave number and a larger increase in the integral time scale relative to the upstream reference flow than for the triangular hills.

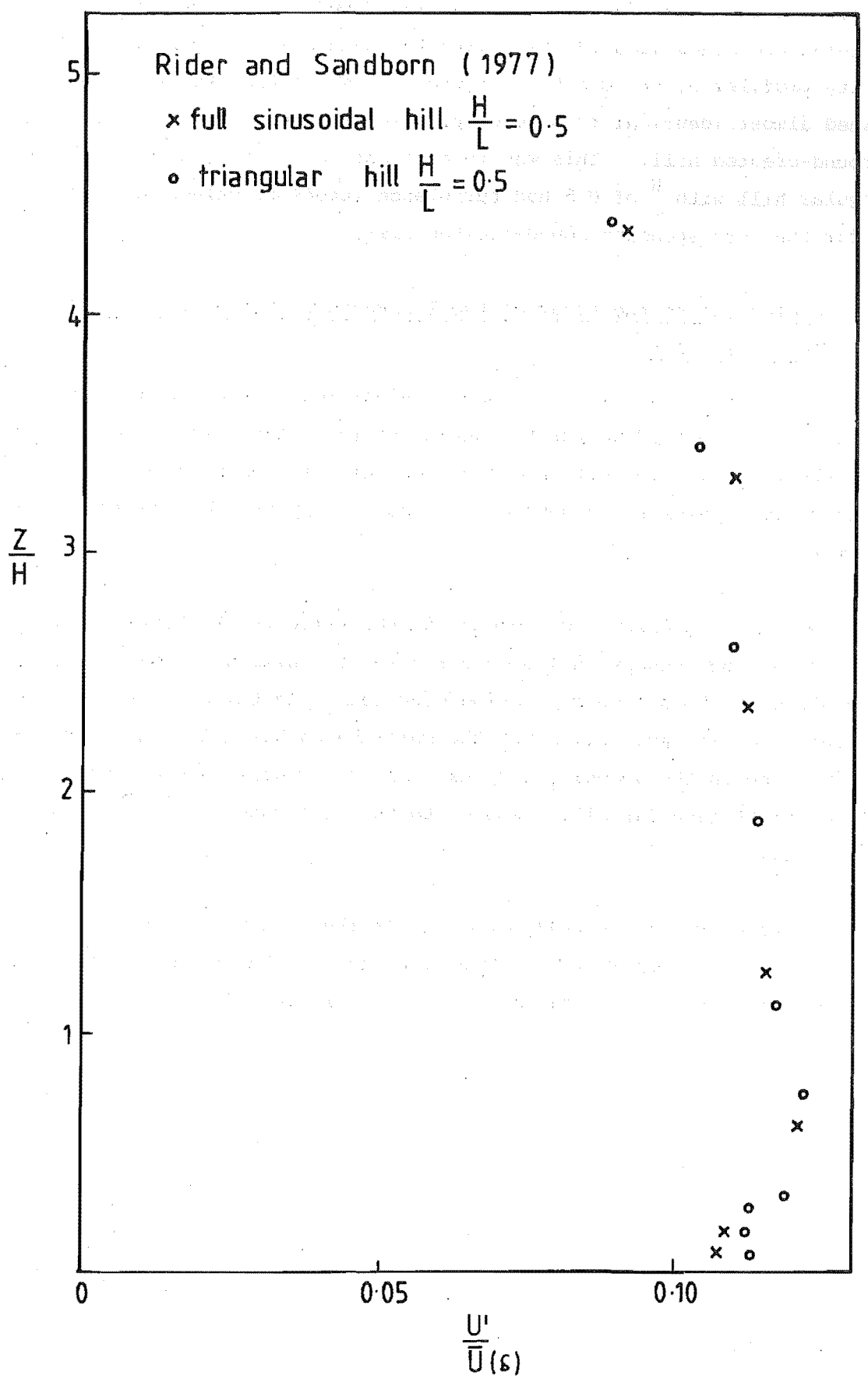

FIG 5·12 COMPARISON OF TURBULENCE INTENSITY PROFILES AT THE CREST

CHAPTER 6

INFLUENCE OF THE HILL SURFACE ROUGHNESS ON THE WIND FLOW OVER HILLS

6.1 Introduction

The purpose of the tests described in this chapter was to examine the effect of the roughness change associated with the boundary layer developed over a rough surface passing over the smooth two-dimensional hills. The simulated atmospheric rural boundary layer used in the work described so far had developed over a surface consisting of Torro roughness elements where each roughness element was 6% of the model hill height.

The experimental work of Freeston (1974) and Bouwmeester et.al.(1978) used smooth hills or escarpments in simulated atmospheric boundary layers established over a rough surface. Other wind tunnel investigations performed by Counihan (1973), (1974) and Bowen and Lindley (1977) used hills or escarpments covered with the upstream surface roughness. The author is aware of no direct comparison of the effect of using rough and smooth hill surfaces in boundary layers established over a rough surface.

6.2 Experimental apparatus

6.2.1 The model hills

Two triangular hills with aspect ratios of 0.1 and 1.0 were constructed and covered with Torro baseboard. All the dimensions were measured from the base of the Torro roughness elements. The rough-surfaced hill dimensions therefore corresponded to the dimensions of two smooth-surfaced triangular hills used in the work described in Chapter four.

The triangular hills with an aspect ratio of 0.1 and 1.0 were selected because they had the largest and smallest length of hill surface respectively of those smooth-surfaced hills used in the tests reported in Chapter four. The effect of the hill surface roughness was expected to be proportional to the length of the hill surface. The model hills chosen for the investigation were therefore expected to be sufficient to indicate any trends in the effect of the hill surface roughness on the flow over the model hills.

6.2.2 Flow measuring equipment and signal processing

The work described in this chapter and in the remainder of the project was performed when the digital data acquisition system described in Appendix two had been commissioned. The mean and standard deviation of the fluctuating hot wire anemometer signal were still read from the DISA 55D30 and DISA 55D35 DC and RMS voltmeters but autocorrelations and energy spectra were measured using the digital system. The faster processing times and extended frequency range obtained with the digital system were a considerable improvement over those obtained using the analog system.

6.3 Experimental procedure

The rough-surfaced triangular hills were placed in the same position in the 1:300 rural atmospheric boundary layer simulation described in Chapter three as the corresponding smooth-surfaced triangular hills. Measurements in the flow over the hills were made at the same vertical and streamwise positions as were made over the corresponding smooth-surfaced triangular hills, and the same traversing procedure was used. Any vertical traverse over a rough triangular hill therefore had a corresponding traverse over a smooth triangular hill.

The following quantities were measured:

(i) mean velocity $\overline{U}$,

(ii) longitudinal velocity fluctuations u',

(iii) u component energy spectra,

(iv) u component autocorrelation coefficients.

6.4 Experimental results

6.4.1 Mean velocity profiles and amplification factors

Lines of equal amplification factor are plotted for the smooth and rough triangular hills with an aspect ratio of 0.1 and 1.0 in figure 6.1.

Comparing first the results for the rough and smooth triangular hills with an aspect ratio of 0.1 the effect of the surface roughness is to cause a reduction in the amplification factor at any position over the hill. At any given height within the region affected by the hill surface roughness the reduction in the value of the amplification factor for the hill with surface roughness progressively increases as the distance from the start of

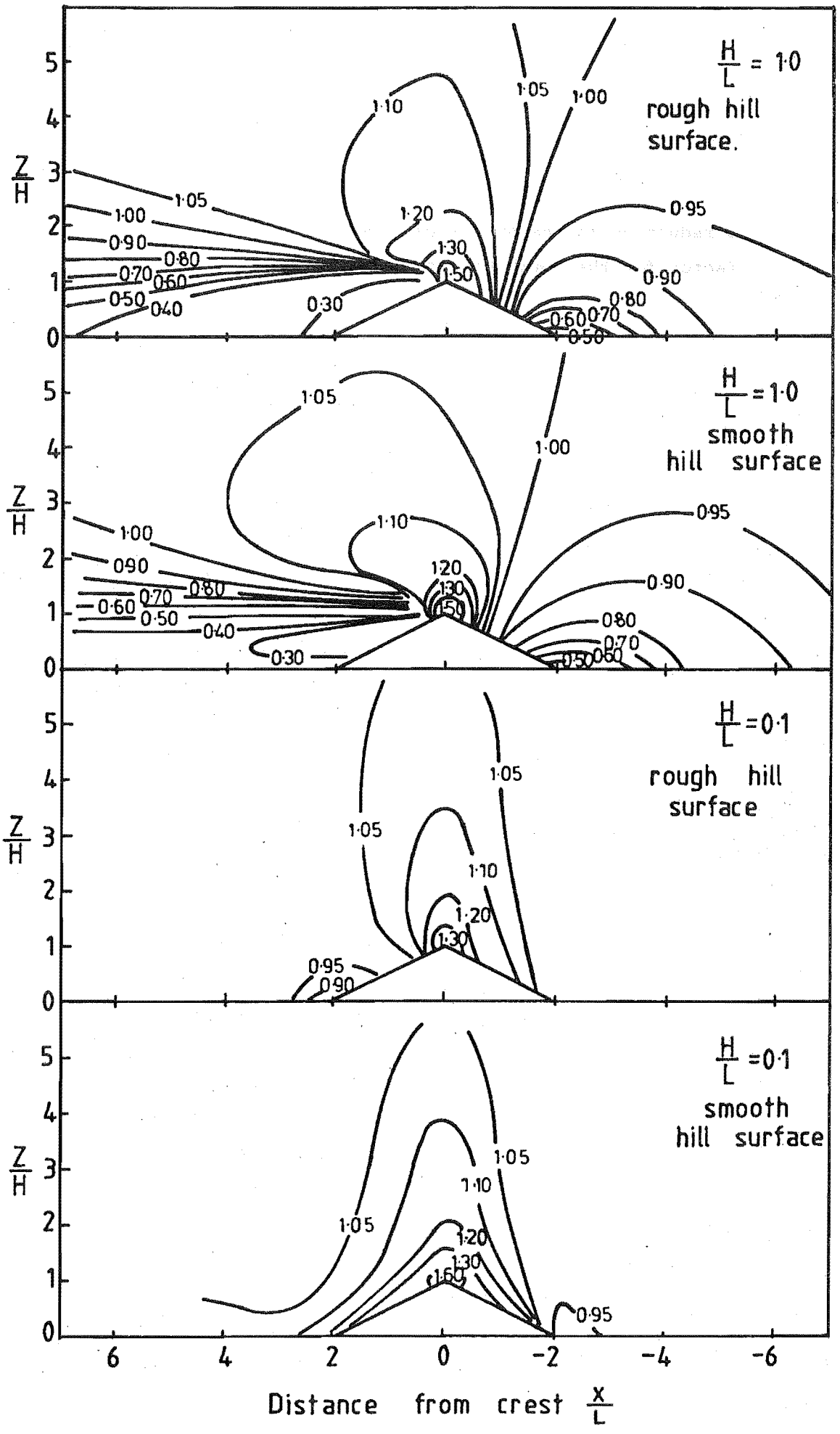

FIG. 6·1 LINES OF EQUAL AMPLIFICATION FACTOR

the hill increases. For example at a height of $\frac{z}{H} = 0.2$:

$\frac{x}{L}$	-1.5	0	1.5
% reduction in the amplification factor for the rough hill surface	15%	19%	30%

The velocity profiles at the crest of the rough and smooth triangular hills with an aspect ratio of 0.10 are compared in figure 6.2. The reduction in velocity caused by the hill surface roughness decreases rapidly as the distance above the hill increases.

For the triangular hill with an aspect ratio of 1.0 the roughness on the hill surface causes the velocity and hence the amplification factor at any location to increase slightly. Figure 6.3 compares the velocity profiles at the hill crest for the rough and smooth hills with an aspect ratio of 1.0. The rough hill has slightly higher mean velocities, although strictly the increase in the mean velocity is within the measurement uncertainty of ± 2%.

In the region behind the hill crest velocities are up to 20% higher for the rough hill except in the region close to the hill surface immediately behind the hill crest where the velocities are lower.

6.4.2 Turbulence intensity profiles

Lines of equal local turbulence intensity are presented for the rough and smooth triangular hills in figure 6.4. In analysing the results trends in the velocity fluctuations u' alone were also examined.

Comparing firstly the results for the rough and smooth triangular hills with an aspect ratio of 0.10, the effect of the hill surface roughness is to cause an increase in the value of the longitudinal velocity fluctuations at any location. The maximum increase in the velocity fluctuations occurs at the hill crest at a height of $\frac{z}{H} = 0.2$ where u' is up to 30% higher than the corresponding value for the smooth hill as may be seen from figure 6.5. As for the mean velocity the largest changes in the velocity fluctuations u' occur close to the ground and the height over which the changes occur increases as the distance over the hill surface increases. At a distance 10 H beyond the end of the hill the major changes in u' occur at a height of $\frac{z}{H} = 1.5$

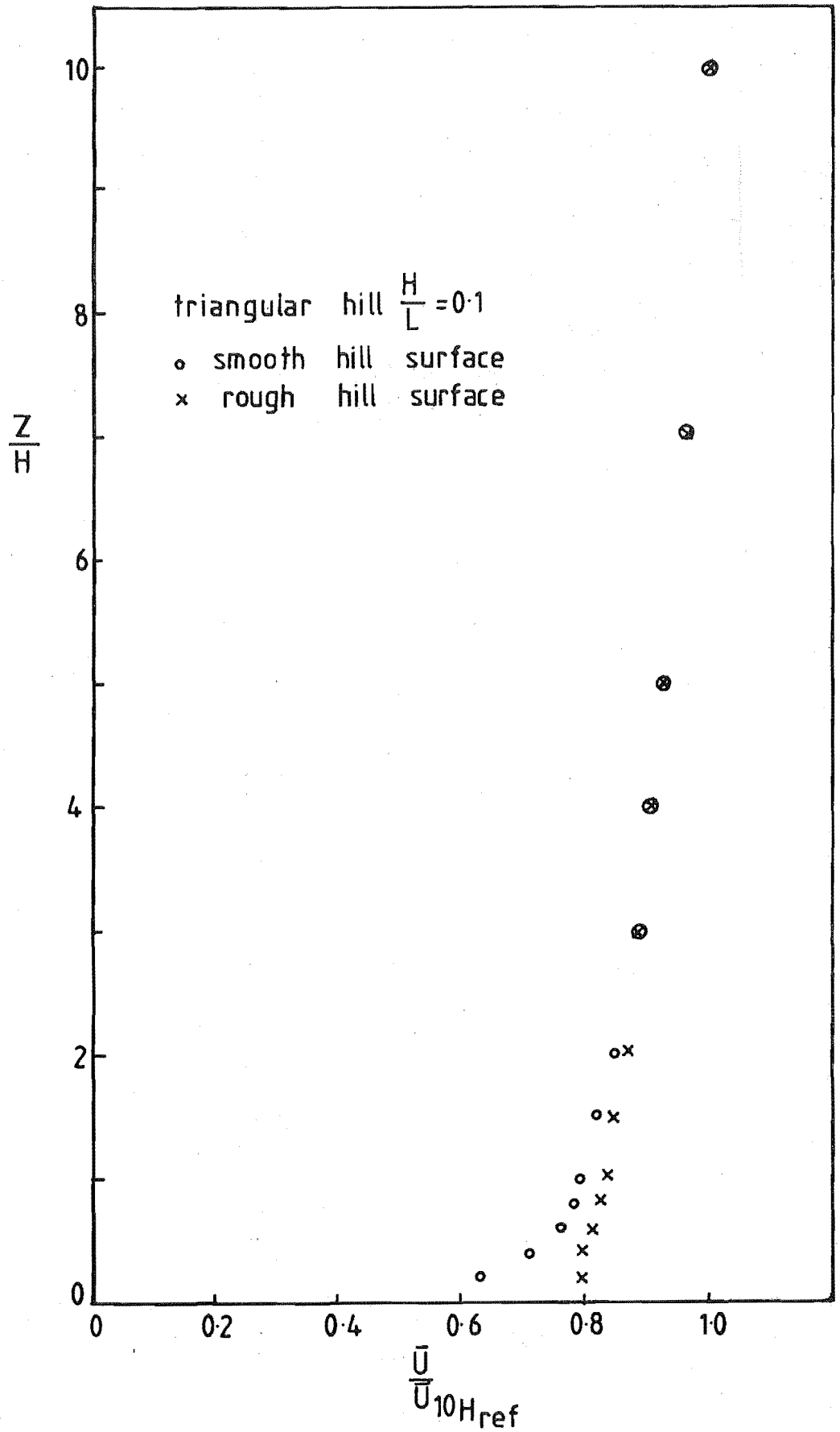

FIG 6·2 VELOCITY PROFILES AT THE CREST.

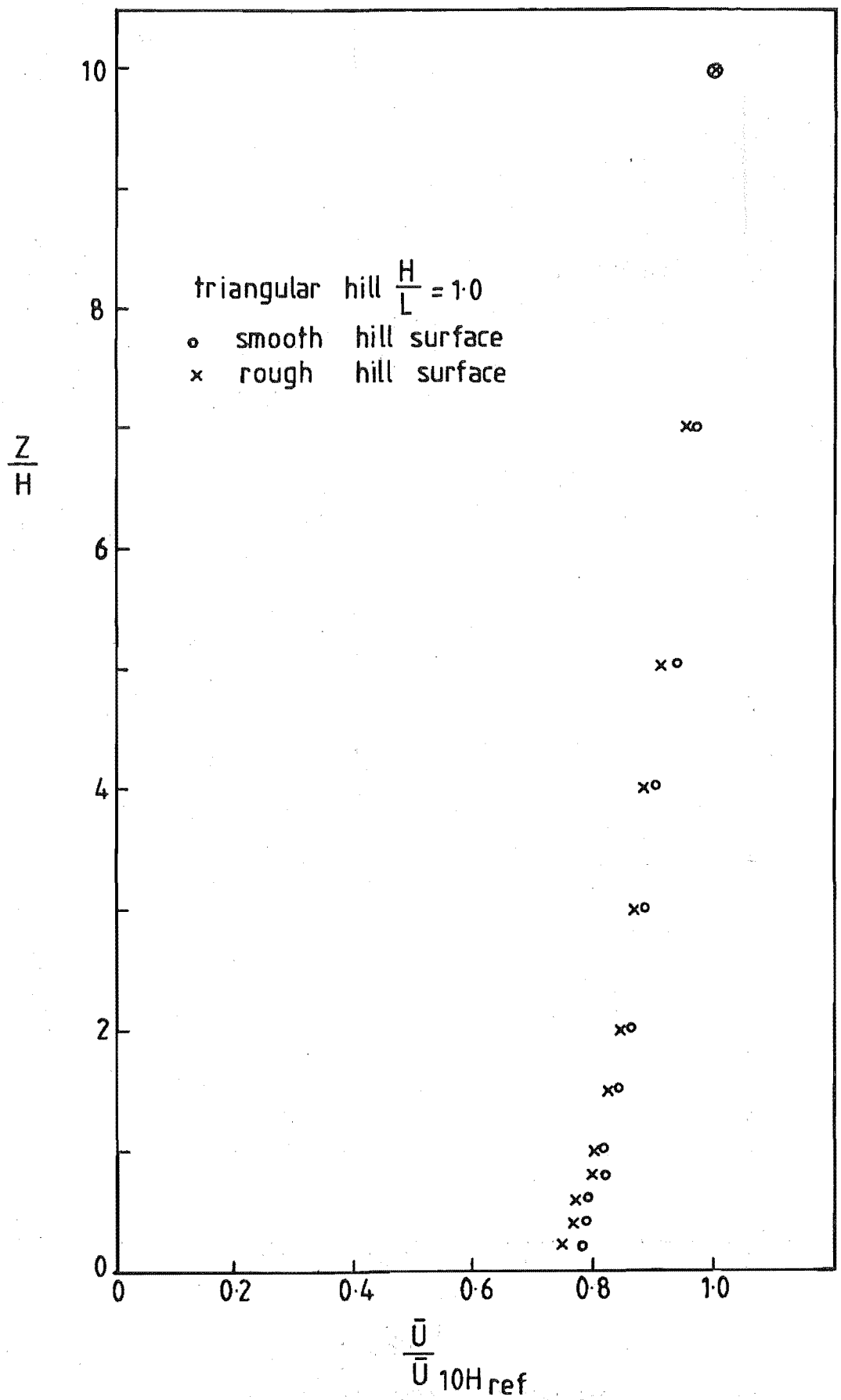

FIG 6·3 VELOCITY PROFILES AT THE CREST.

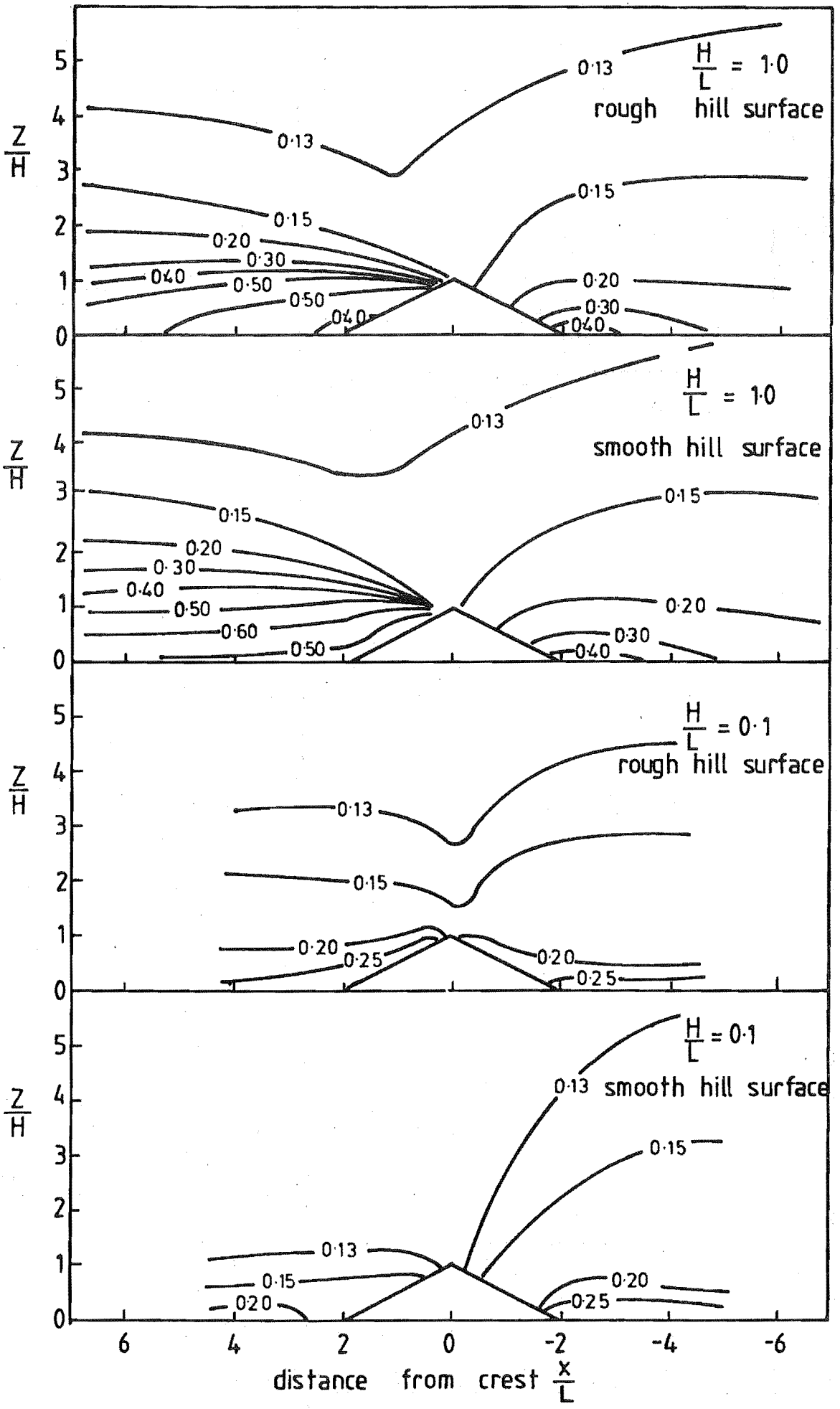

FIG 6·4 ISOTURBS OVER ROUGH TRIANGULAR HILLS

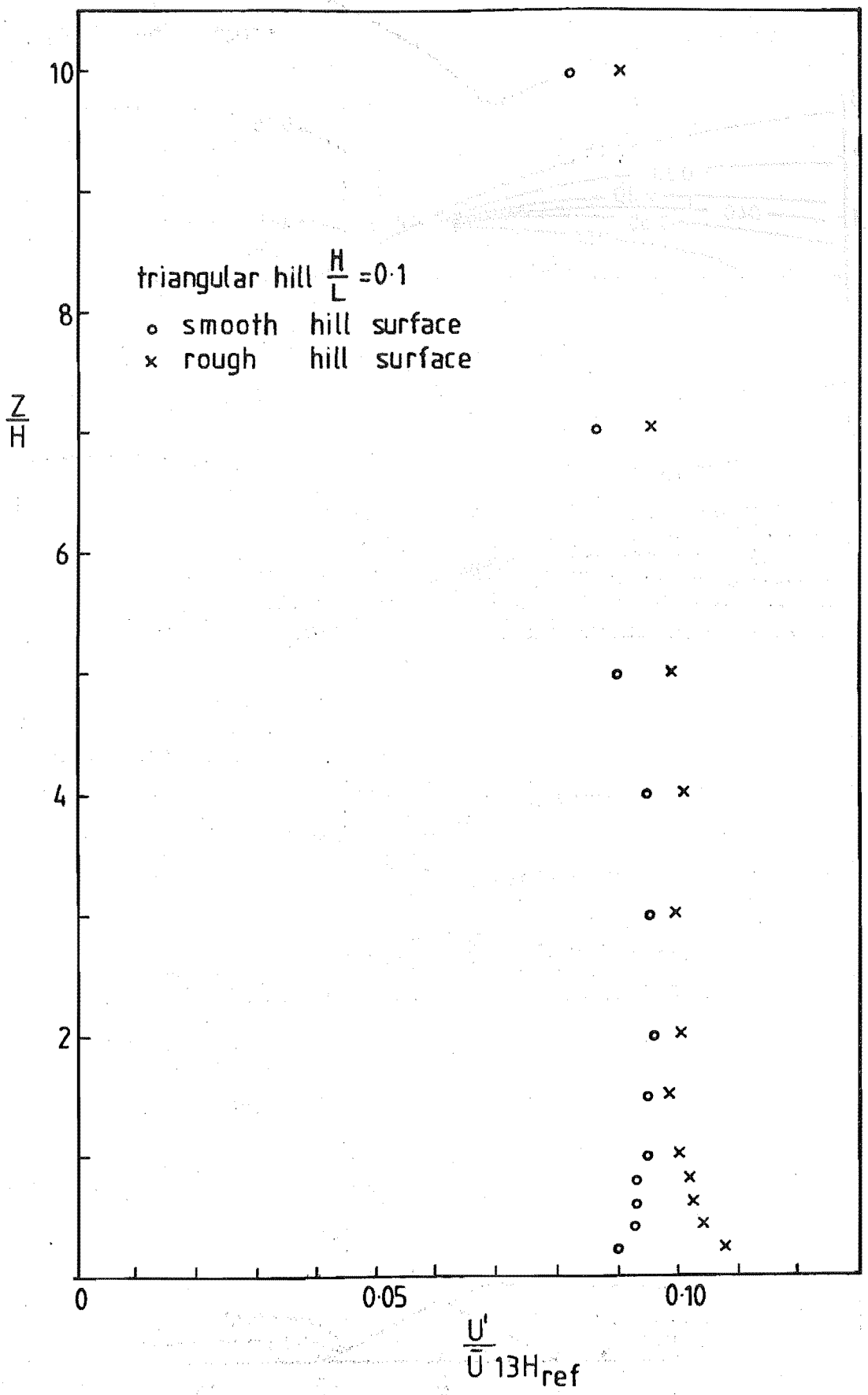

FIG 6·5 TURBULENCE INTENSITY PROFILES AT THE CREST.

because close to the ground the boundary layer has been re-established by the Torro roughness in the case of the smooth hill. Because the longitudinal velocity fluctuations increase as the mean velocity decreases, increases in the local turbulence intensity of up to 50% occur close to the ground.

For the triangular hill of aspect ratio 1.0 the velocity fluctuations are the same everywhere within the experimental measurement uncertainty as illustrated in figures 6.4 and 6.6. An exception is in the region immediately behind the hill crest where the velocity fluctuations u' are up to 20% lower for the rough hill. Mean velocity measurements in this region were also found to be low as recorded in section 6.4.1.

6.4.3 u velocity component energy spectra and autocorrelation coefficients

Energy spectra and autocorrelation coefficients in the flow over each hill were measured at the upstream reference position, at the hill crest and 10 H downstream of the end of the hill at heights above the surface of $\frac{z}{H}$ = 0.2, 1.0 and 2.0.

Energy spectra

The locations of the spectral peaks are summarised in table 6.1 and a number of the spectra measured over the rough and smooth hills are compared in figures 6.7, 6.8 and 6.9.

At the hill crest for both rough hills there is a predictable increase in high frequency energy compared to the corresponding smooth hills which is indicative of a decrease in the average eddy size. This effect is clearly more pronounced for the hill with an aspect ratio of 0.1. For example consider the ratio of the spectral peak frequencies at the hill crest for the smooth and rough hills at a height of $\frac{z}{H}$ = 0.2.

$\frac{H}{L}$	$\frac{\text{spectral peak frequency for the rough hill}}{\text{spectral peak frequency for the smooth hill}}$
0.1	2.4
1.0	1.2

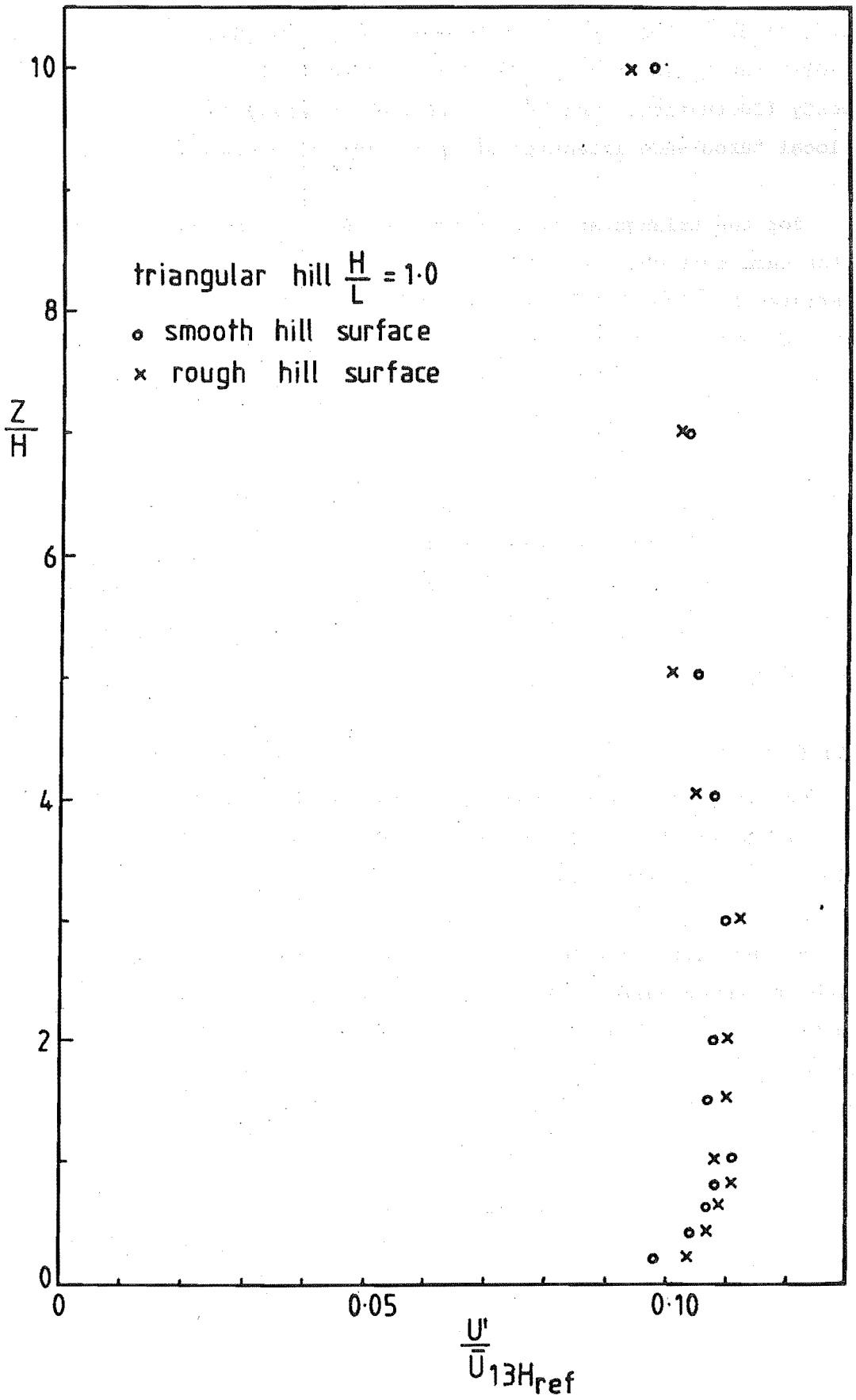

FIG 6·6 TURBULENCE INTENSITY PROFILES AT THE CREST

		$\frac{z}{H}$ = 0.2									$\frac{z}{H}$ = 1.0									$\frac{z}{H}$ = 2.0								
	$\frac{H}{L}$	10H upstream of the hill			crest			10H downstream of the hill			10H upstream of the hill			crest			10H downstream of the hill			10H upstream of the hill			crest			10H downstream of the hill		
		k_p	n_p	T_E	k_p	n_p	T_E	k_p	n_p	T_E	k_p	n_p	T_E	k_p	n_p	T_E	k_p	n_p	T_E	k_p	n_p	T_E	k_p	n_p	T_E	k_p	n_p	T_E
		m^{-1}	H_z	ms	m^{-1}	H_z	ms	m^{-1}	H_z	ms	m^{-1}	H_z	ms	m^{-1}	H_z	ms	m^{-1}	H_z	ms	m^{-1}	H_z	ms	m^{-1}	H_z	ms	m^{-1}	H_z	ms
rough hills	0.10	0.82	6.36	17.7	0.80	8.50	22.4	1.30	9.98	18.3	0.37	4.09	27.6	0.40	5.33	22.7	0.44	4.88	24.7	0.35	4.29	28.0	0.35	4.85	26.5	0.37	4.83	26.5
	1.00	0.82	6.36	17.7	0.42	5.35	26.2	1.70	10.56	10.2	0.37	4.09	27.6	0.34	4.69	32.6	1.40	12.54	9.2	0.35	4.29	28.0	0.27	3.75	25.7	0.55	6.47	17.3
smooth hills	0.10	0.82	6.36	17.7	0.28	3.56	29.2	0.96	7.90	22.2	0.37	4.09	27.6	0.30	4.03	34.5	0.39	4.63	32.2	0.35	4.29	28.0	0.34	4.76	34.2	0.34	4.25	32.0
	1.00	0.82	6.36	17.7	0.34	4.30	25.6	2.90	15.88	12.9	0.37	4.09	27.6	0.33	4.47	28.7	1.10	8.72	15.6	0.35	4.29	28.0	0.33	4.57	29.9	0.70	7.67	20.9

TABLE 6.1 Integral time scales and spectral peak values for the rough-surfaced triangular hills.

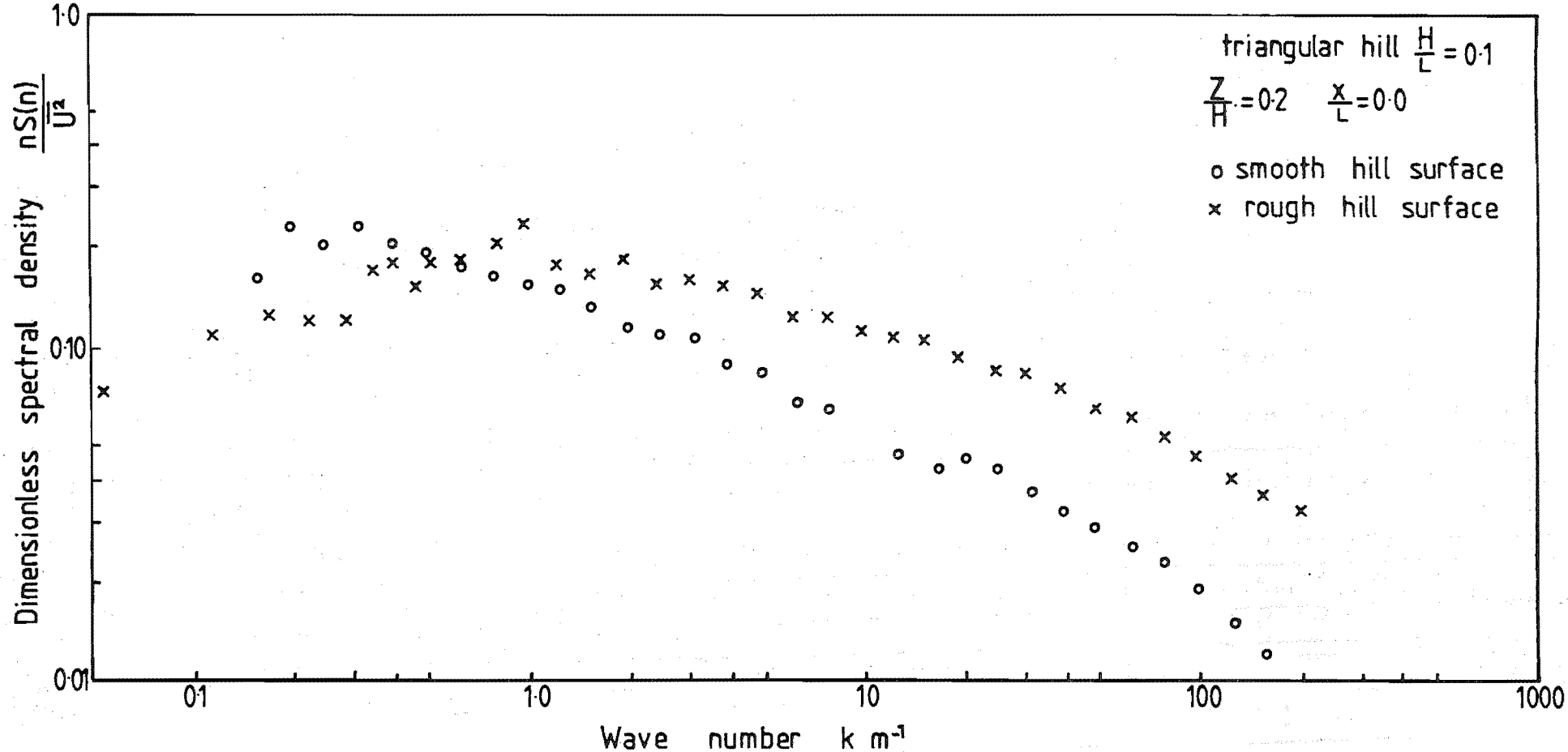

FIG 6·7 SPECTRA AT THE CREST FOR $\frac{H}{L} = 0{\cdot}10$

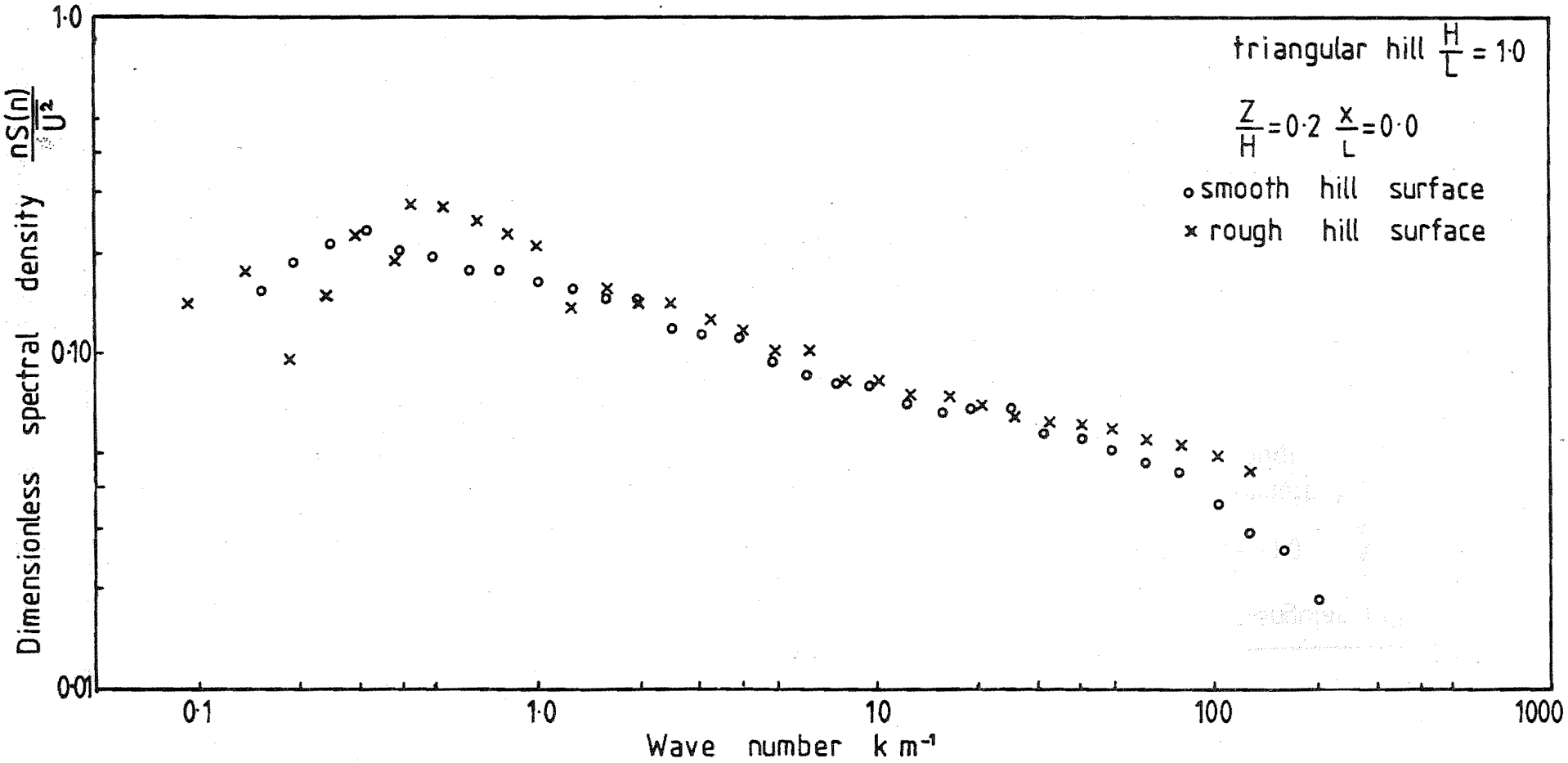

FIG 6·8 SPECTRA AT THE CREST FOR $\frac{H}{L}$=1·0

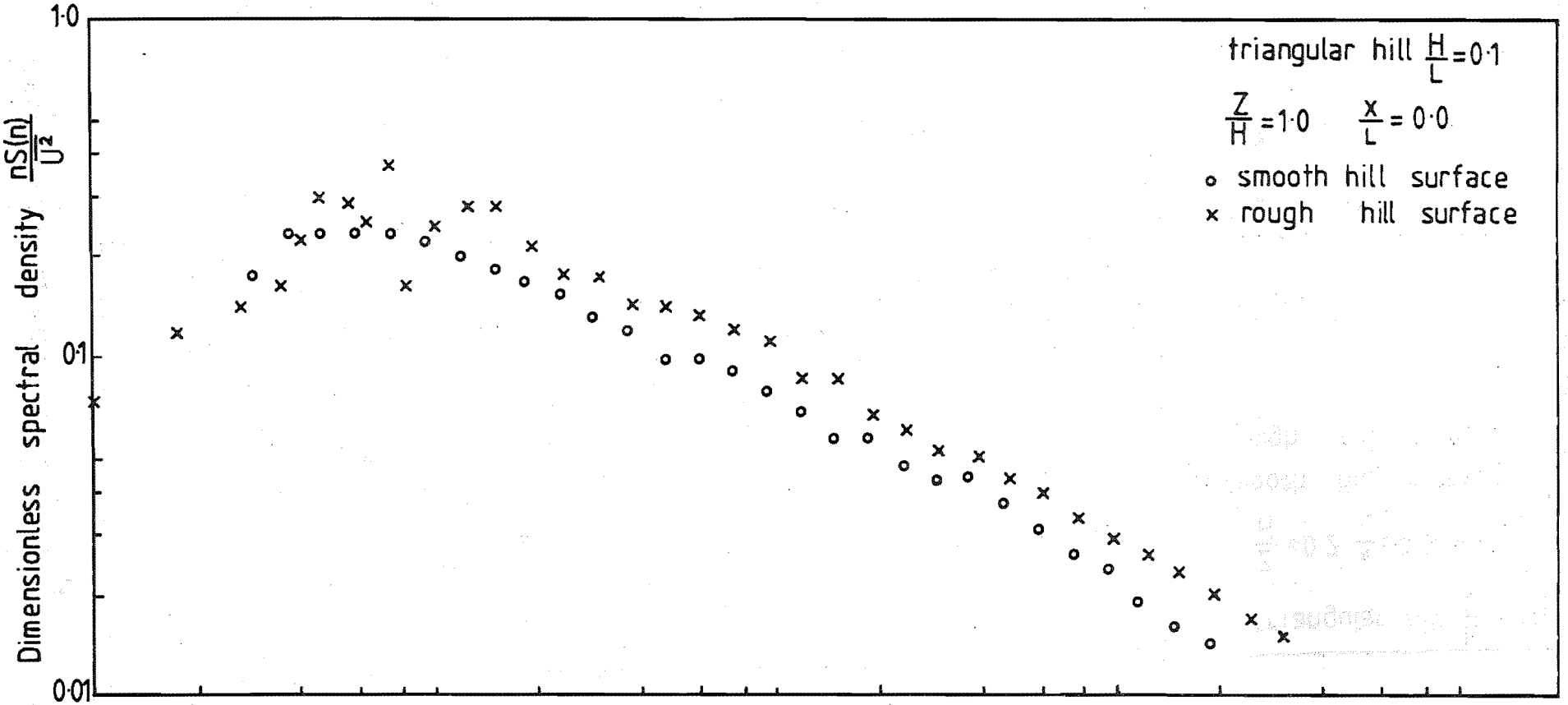

FIG. 6·9 SPECTRA AT THE CREST FOR $\frac{H}{L}$ = 0·10

The trend for an increase in high frequency energy at the hill crest extends to greater heights for the hill with an aspect ratio of 0.1 than for the hill with an aspect ratio of 1.0.

At the hill crest at a height of $\frac{z}{H} = 0.2$ the spectrum for the rough hill with an aspect ratio of 0.1 is slightly less peaked than the spectrum for the corresponding smooth hill as illustrated in figure 6.7. No other changes in the spectral shape were observed at the hill crests.

In the region downstream of the hill crest the spectrum at a height of $\frac{z}{H} = 0.2$ for the rough hill with an aspect ratio of 1.0 is more peaked and shows more low frequency energy than the spectrum for the corresponding smooth hill. For the rough hill with an aspect ratio of 0.1 the spectra show more high frequency energy compared to the smooth hill spectra downstream of the hill crest.

Autocorrelations

The values of the integral time scale calculated from the autocorrelation curves measured over the rough hills are shown in table 6.1 where they are compared to the values for the corresponding smooth hills as presented in table 4.1.

For the triangular hill with an aspect ratio of 0.1 the value of the integral time scale for the rough hill is up to 35% lower than the corresponding value for the smooth hill at any location.

For the hill with an aspect ratio of 1.0 the values of the integral time scale for the rough and smooth hills show no significant difference at the crest but are very much lower for the rough hill downstream of the hill crest.

6.5 Discussion of the experimental results

The hill surface roughness has a very significant affect on the flow parameters. Changes in the mean velocity and local turbulence intensity of up to 20% and 50% respectively were observed close to the ground.

The changes in the measured flow quantities were larger for the hill with an aspect ratio of 0.1. This triangular hill had a hill surface length

of 2 m compared to a hill surface length of 0.17 m for the triangular hill with an aspect ratio of 1.0. The longer hill surface allowed larger changes to occur in the flow close to the ground and therefore more appreciable differences were observed between the rough and smooth hills.

When the hill surface roughness was increased the velocity close to the ground decreased. This was caused by the surface protrusions associated with the rough surface causing increased drag and larger shear brought about by the more turbulent eddying motion and small scale boundary layer separation. The roughness elements over the hill surface caused a greater loss of momentum over the hill surface than occurred for the smooth hill surface. The effect of the roughness change was not immediately felt but diffused outwards as the flow progressed over the smooth hills forming an internal boundary layer.

There are a large number of theories which model the effect on boundary layer flow of rough to smooth and smooth to rough transitions on a flat surface: Townsend (1965), Peterson (1969), Shir (1972), Rao et.al.(1974). Measurements have been made in regions of a change in surface roughness by Rider, Philip and Bradley (1963), Bradley (1968), Antonia and Luxton (1971) and more recently by Mulhearn (1978). The trend indicated by these theoretical models and experimental measurements made over flat surfaces is for the velocity to increase close to the ground over the smooth surface after a rough to smooth transition. Precisely the same trend was seen in the flow over the smooth hills when compared to the flow over the rough hills.

The only theoretical or experimental work obtained which related topographic effects and roughness changes was that of Lo (1977). The governing equations in Lo's model are derived in a curvilinear coordinate system which allowed the inclusion of elevation changes without complicating the mathematics further. Lo compared his results to those of Taylor (1969) who modelled a roughness change on a flat surface.

A comparison of Lo and Taylor's results show that for a rough to smooth transition the presence of the hill reduces the affect of the roughness transition. At large distances from the change in topography the effect of the topography is negligible, as expected.

Lo's model is not applicable to the cases studied in the present work because his model omits the pressure gradient term in the x - momentum equation. Therefore the model only applies to extremely gentle topography.

A comparison of the energy spectra obtained over the rough hills and over the smooth hills indicated a trend for the spectra over the rough hills to shift to a higher wave number. This indicates a decrease in the average eddy size and is consistent with the assumption that the roughness elements over the hill surface cause larger shear and a more turbulent eddying motion which will be at a higher wave number than for the smooth hill surface.

In analysing the results obtained for the smooth hills it is possible that a change in the surface level at the roughness change should be allowed for. Results obtained by Mulhearn (1978) over a flat surface show that an effective change in the surface level at a roughness change has only a small influence on wind speed changes and a negligible influence on changes in the velocity fluctuations. The effective change in the surface level in going from the rough hill surface to the smooth hill surface was therefore not considered significant.

In an effort to separate the influences of topography and surface roughness changes, mean velocities were measured over a 2 m length of flat acrylic sheet. The acrylic sheet was placed in the wind tunnel working section so it had the same upstream reference profile as the model hills. The speedup due to the flow over the 2 m length of flat sheet was calculated. A 2 m length of flat acrylic sheet was chosen as this corresponded to the length of hill surface for the triangular hill with an aspect ratio of 0.1. The amplification factors calculated for the flow over the flat sheet are compared with the amplification factors obtained for the rough and smooth triangular hills of aspect ratio 0.1 in table 6.2 .

In comparing the amplification factors over the flat sheet with those over the hill surface it was assumed that there would be no pressure effect from the change in surface roughness alone and that the hill slope by itself had no effect on the stress distribution except for displacing it along with the flow. This may not be quite correct since a change in the roughness of the surface may have at least some minor effect on the pressure distribution, (see Shir (1972)).

The close correspondence between the two columns on the right hand side of the table 6.2 suggests that the effect of the smooth hill surface is exactly the same as the effect of the same length of flat smooth surface.

Height $\frac{z}{H}$	Amplification factor over the hill $\frac{H}{L} = 0.1$ at $\frac{x}{L} = 2$		Difference in amplification factors	Fractional speedup due to 2 m of flat acrylic sheet
	no surface roughness	surface roughness		
0.2	1.17	0.87	0.30	0.31
0.4	1.10	0.92	0.18	0.16
0.6	1.06	0.92	0.14	0.10
0.8	1.04	0.97	0.07	0.07
1.0	1.03	0.97	0.06	0.06
1.5	1.01	0.99	0.02	0.03
2.0	1.01	1.00	0.01	0.02
3.0	1.01	1.00	0.01	0.00
4.0	1.01	1.03	0.02	0.01
5.0	1.01	1.02	0.01	0.01
7.0	1.01	1.01	0.00	0.00
10.0	0.99	1.01	0.02	0.00
13.0	1.00	1.01	0.01	0.00

TABLE 6.2 Comparison of the amplification factors over a flat surface and over a rough and smooth hill.

6.6 Conclusions to the study of the influence of the hill surface roughness on the wind flow over hills.

(a) The effect of the surface roughness change associated with the simulated atmospheric boundary layer developed over a rough surface passing over a smooth hill surface was examined by comparing the measurements made over two hills of the same shape with rough and smooth surfaces. The two hills used had the longest and shortest length of hill surface of those used in the tests over the smooth hills reported in Chapter four. The hill surface roughness was found to have a very significant effect on the flow parameters causing changes of up to 20% in the mean velocity and 50% in the local turbulence close to the ground.

(b) The velocity at all locations over the hill with the longer hill surface was reduced by an increase in the hill surface roughness. The velocity over the shorter hill showed little change between the smooth and rough hills. The decrease in the mean velocity was caused by increased drag induced by the roughness elements. The region of influence of the hill surface roughness increased as the distance over the hill increased which is consistent with the concept of an internal boundary layer growing and slowly diffusing outwards at the roughness change associated with the smooth hill surface. The results obtained were therefore consistent with the trends shown in the literature for a rough to smooth transition over a flat surface.

(c) The longitudinal velocity fluctuations u' over the longest hill surface increased with an increase in the hill surface roughness. The largest increases occurred close to the hill surface. This was caused by the more turbulent eddying motion associated with the rough surfaced hills. The shorter hill showed no measurable change in the values of the velocity fluctuations.

(d) The difference in the amplification factors for the hills with the rough and smooth surfaces was very similar to the fractional speedup measured over the same length of smooth flat surface subjected to the same approach profile as the model hills. The pressure effect resulting from the change in the surface roughness therefore appears to be negligible as does the effect of the hill on the stress distribution.

CHAPTER 7

A 1:3000 RURAL ATMOSPHERIC BOUNDARY LAYER SIMULATION

The object of the work described in this chapter was to generate a simulated neutrally stable rural atmospheric boundary layer of about 1:3000 scale. This boundary layer would be used to investigate the wind flow over the two-dimensional triangular hills used in the tests in the 1:300 rural atmospheric boundary layer simulation reported in Chapter four. A comparison of the results obtained in each boundary layer should enable conclusions to be drawn on the effect of the boundary layer height on the wind flow over the simple hill shapes.

Only two simulated atmospheric boundary layers had been previously established in the atmospheric boundary layer wind tunnel in the Department of Mechanical Engineering at the University of Canterbury. A 1:300 rural atmospheric boundary layer simulation was initially established by Raine (1974) and subsequently re-established as part of the present project as described in Chapter three. Meroney et.al. (1978) established a 1:5000 atmospheric boundary layer simulation for use with topographical models. This 1:5000 simulation was not considered satisfactory for the present work. The turbulence intensities were low close to the ground compared to the 1:300 simulation previously used and the mean velocity profile power law exponent was 0.14 rather than 0.16 as in the 1:300 simulation. It was considered desirable that the small scale simulation should be as faithful as possible a reproduction of the larger scale 1:300 simulation.

For the simulation described in this chapter a second honeycomb was installed at the entrance to the working section of the atmospheric boundary wind tunnel described in section 3.1.1. The purpose of this honeycomb was to provide flow straightening, remove large lateral and vertical fluctuations in the flow and reduce the streamwise velocity fluctuations.

7.1 Experimental procedure

A simulated rural atmospheric boundary layer of about 1:3000 scale characteristic of the flow over terrain of roughness length Z_o = 5 cm and with a mean velocity profile power law exponent of 0.16 was required.

A step change and boundary layer growth scheme consisting of a coarse grid, trip fence and surface roughness was used. This system was successfully employed in establishing the rural atmospheric boundary layer of 1:300 scale described in Chapter three. The grid bar spacings, trip fence height and surface roughness were altered until the mean velocity profile and turbulence intensity at the reference measurement position were considered satisfactory.

The reference measurement position was at X = 3 m, 25 cm south of the wind tunnel centreline. All the measurements were made at a wind tunnel speed of 9.1 m/s measured using the reference pitot-static probe. The reference pitot-static probe was located in the boundary layer free stream at X = 1.8 m at a height of 61 cm, 30 cm in from the north wall of the wind tunnel and was continuously monitored. The wind tunnel speed was set by adjusting the fan pitch blade settings until the desired wind tunnel speed was reached. By moving the reference position close to the grid and reducing the wind tunnel speed a smaller boundary layer height was immediately achieved compared to that measured in the 1:300 simulation described in Chapter three.

The wind tunnel roof was set at a height of 1.23 m at the grid and a divergence of 0.6°, and was therefore left unchanged from that used in the 1:300 simulation.

7.1.1 The grid

The grid was situated at X = 0 m. The purpose of the grid was to produce large scale turbulence at all heights. It was possible to control the velocity profile to a small degree by adjusting the grid bar spacing, although large changes in the grid bar spacing were found to have only a small effect on the mean velocity profile.

The grid consisted of 1.9 cm square bars. The initial grid arrangement was 14 uniformly spaced horizontal bars and 14 uniformly spaced vertical bars.

7.1.2 The trip fence

The trip fence was situated at X = 0.61 m. The purpose of the trip fence was to cause an initial thickening of the boundary layer and an increase in the turbulence levels at all heights.

The trip fence was made of wooden strips 0.7 cm thick and 1.9 cm wide which spanned the width of the wind tunnel. Wooden strips were added or removed from the initial trip fence to obtain the desired turbulence levels. Small changes in the trip fence height were found to affect the flow markedly.

The initial trip fence height was set at 4.9 cm.

7.1.3 Surface roughness

The surface roughness extended from immediately behind the trip fence to X = 7.5 m.

The Torro roughness described in section 3.2.3 which was used in the 1:300 rural atmospheric boundary layer simulation showed unsatisfactory trends in the turbulence intensity profile close to the ground in the reference position at X = 3 m and it was decided to use a different surface roughness. The velocity profile and turbulence intensity at X = 3 m were measured using an expanded polystyrene foam and various types of carpet and packing materials as surface roughness. The surface roughness used was found to dominate the velocity profile and turbulence intensity throughout the boundary layer and especially close to the ground.

The final roughness chosen was a cardboard, widely used as a protective material in the packing industry. The roughness dimensions of the cardboard are shown in figure 7.1.

The cardboard was glued to 2.3 m lengths of 0.3 cm thick hardboard which were in turn lightly nailed to the wind tunnel floor. Packing was inserted under the hardboard so the height of the base of the roughness elements above the wind tunnel floor was 0.6 cm corresponding to the height of the foot of the two-dimensional model hills.

It is especially important in small scale atmospheric boundary layer simulations that the roughness element height is sufficient to ensure that the flow is aerodynamically rough. Atmospheric flows are always aerodynamically rough and it is essential that the simulated atmospheric flow is also aerodynamically rough since in aerodynamically rough flow the molecular

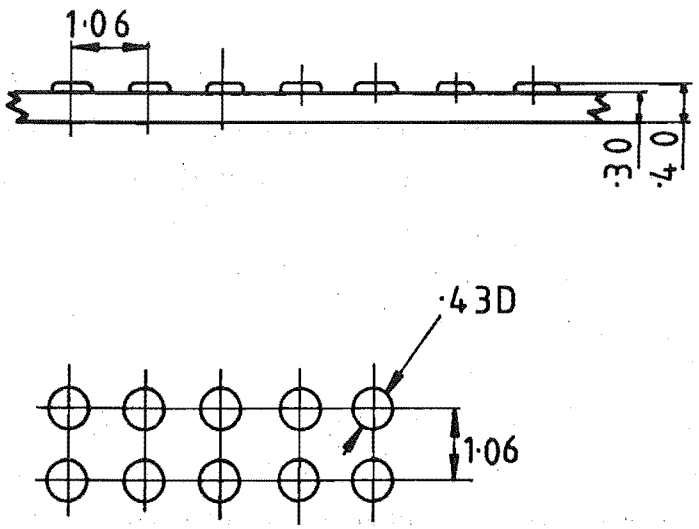

All dimensions in cm

FIG. 7.1 SURFACE ROUGHNESS

viscosity is minimized and the Reynolds number similarity requirement may be relaxed.

Schlichting (1968) has shown that aerodynamically rough flow on a flat surface will occur if the roughness elements have an average height k_r such that:

$$k_r > \frac{100\ \nu}{\bar{U}_\infty} \tag{7.1}$$

For the simulation described in this chapter $\bar{U}_\infty \doteqdot 9.0$ m/s and at 15°C the kinematic viscosity of air is 1.5×10^{-5} m^2/s so the right-hand side of equation 7.1 is 0.017 cm and Schlichting's criteria for fully aerodynamically rough flow is satisfied since $k_r = 0.1$ cm in this simulation.

Sundaram, Ludwig and Skinner (1972) also discuss the necessity for aerodynamically rough flow in atmospheric boundary layer simulations. They show that for fully aerodynamically rough flow the test height z must satisfy the relation:

$$z \geq \left(\frac{3\ \nu}{\kappa \bar{U}_z}\right) \left(\frac{H_a}{Z_o}\right) \log_e \left(\frac{H_a}{Z_o}\right) \tag{7.2}$$

The value of the von Karman constant κ is about 0.4 and the kinematic viscosity of air at 15°C is 1.5×10^{-5} m^2/s. The value of $\frac{H_a}{Z_o}$ is 2000 since the height of the surface layer is about 100 m (Panofsky (1969)) and the roughness length Z_o is about 5 cm. For the simulation at z = 0.5 cm, $\bar{U} = 5.1$ m/s assuming a $\frac{1}{6}$ power law, and so the right-hand side of equation 7.2 is equal to 0.034 mm and we see that the criteria of Sundaram, Ludwig and Skinner is satisfied. At z = 8.0 cm, $\bar{U} = 9.1$ m/s and the criteria is also satisfied. Therefore it appears that fully aerodynamically rough flow can be maintained in the atmospheric boundary layer simulation described in this chapter at all times.

7.1.4 Wind modelling procedure

The trip fence height and grid bar spacings were adjusted until the mean velocity and turbulence intensity profiles at X = 3 m were considered satisfactory for a small scale rural atmospheric boundary layer simulation with a roughness length Z_o of about 5 cm.

This was achieved with a trip fence height of 2.1 cm and the grid arrangement shown in Table 7.1. Detailed measurements of the final simulation are presented in section 7.2.

7.2 Detailed evaluation of the final layout

In this section detailed measurements are presented for the final simulation.

The following measurements were made:

(i) mean velocity $\overline{U}$,

(ii) u, v and w velocity component turbulence intensities,

(iii) u and w velocity component energy spectra,

(iv) autocorrelation coefficients of the u velocity component,

(v) lateral cross-correlations of the u velocity component.

(vi) Reynolds stress.

(vii) self preservation of the flow at X = 5 m.

7.2.1 Mean velocity profiles

The mean velocity profile at X = 3 m is shown in figures 7.2 and 7.3. Figure 7.2 indicates that the worst non-uniformity is ± 3.7% about the lateral mean at z = 0.5 cm. This was considered satisfactory especially in view of the uniformity throughout the remainder of the boundary layer.

Figure 7.2 shows the close agreement of the mean velocity profile to the $\frac{1}{6}$ power law which is representative of flow over rural terrain. Close to the ground the expected logarithmic nature of the velocity profile is illustrated in figure 7.3. Extrapolation of the logarithmic portion of the velocity profile gives a value of Z_o equal to 0.03 cm.

It is possible that the measured mean velocity profile should be plotted using some value for a zero plane displacement. Antonia and Luxton (1971) advocate fitting the measured mean velocity profile to the logarithmic law:

$$\overline{U} = 2.5\ u_* \log_e \left[\frac{z - d}{Z_o} \right] \qquad (7.3)$$

by an error-in-origin method. This involves choosing successive values for

bar number	bar breadth = 1.9 cm		horizontal grid bars	vertical grid bars
	bar width		distance from the top of the iron clamping frame at the floor to the centre of the bar.	distance from the outer edge of the iron clamping frame on the north wall to the centre of the bar.
	horizontal grid bars	vertical grid bars		
1	3.8 cm	1.9 cm	10.8 cm	3.6 cm
2	3.8	1.9	24.4	13.0
3	3.8	1.9	39.3	22.0
4	1.9	1.9	48.9	30.9
5	1.9	1.9	56.4	39.8
6	1.9	1.9	62.5	48.8
7	1.9	1.9	68.0	57.8
8	1.9	1.9	75.1	66.6
9	1.9	1.9	82.3	75.5
10	1.9	1.9	90.4	84.5
11	1.9	1.9	98.0	93.4
12	1.9	1.9	105.7	102.4
13	1.9	1.9	115.0	111.4
14		1.9		120.4

TABLE 7.1 Final grid arrangement

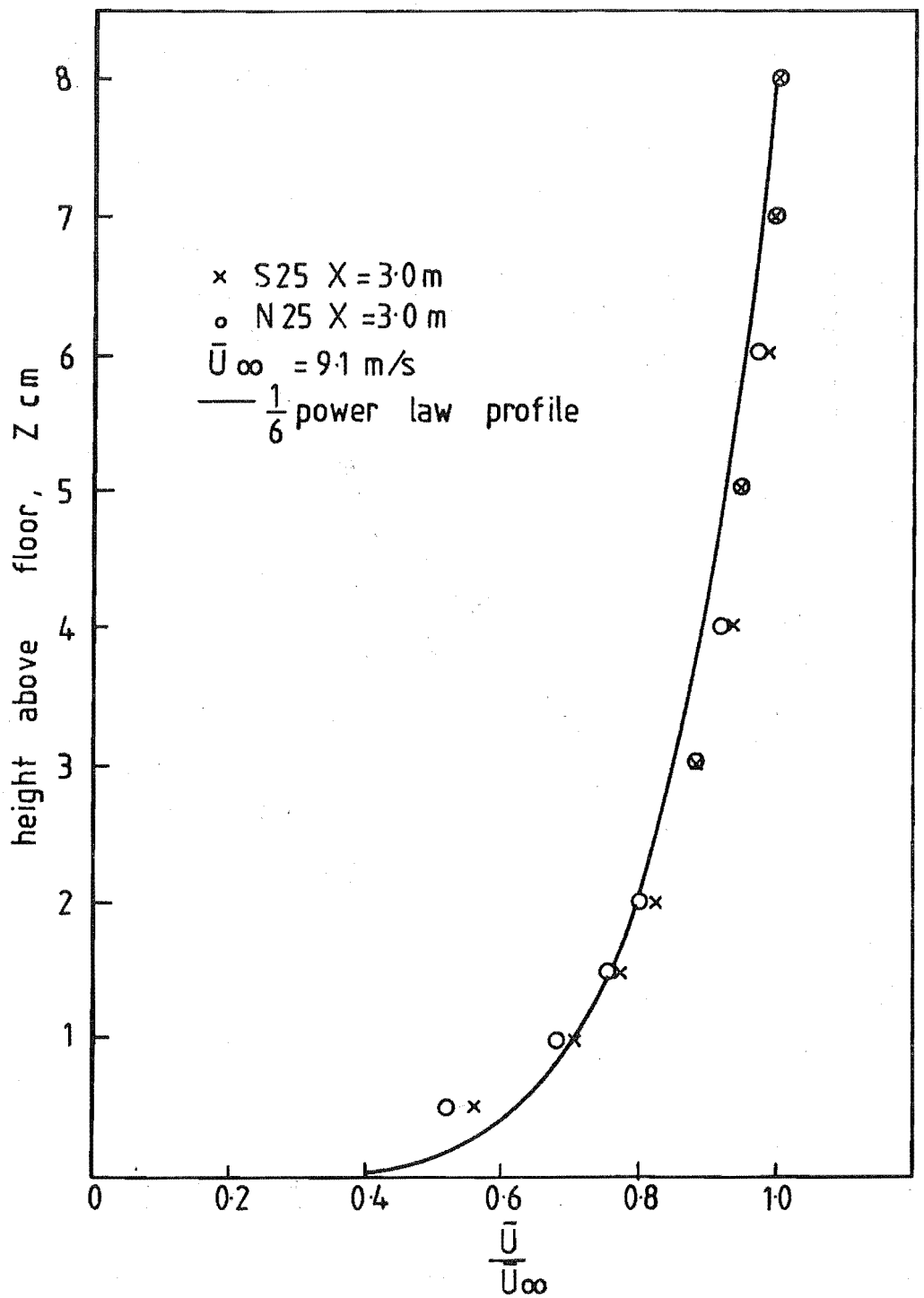

FIG 7.2 MEAN VELOCITY PROFILE AT X = 3m

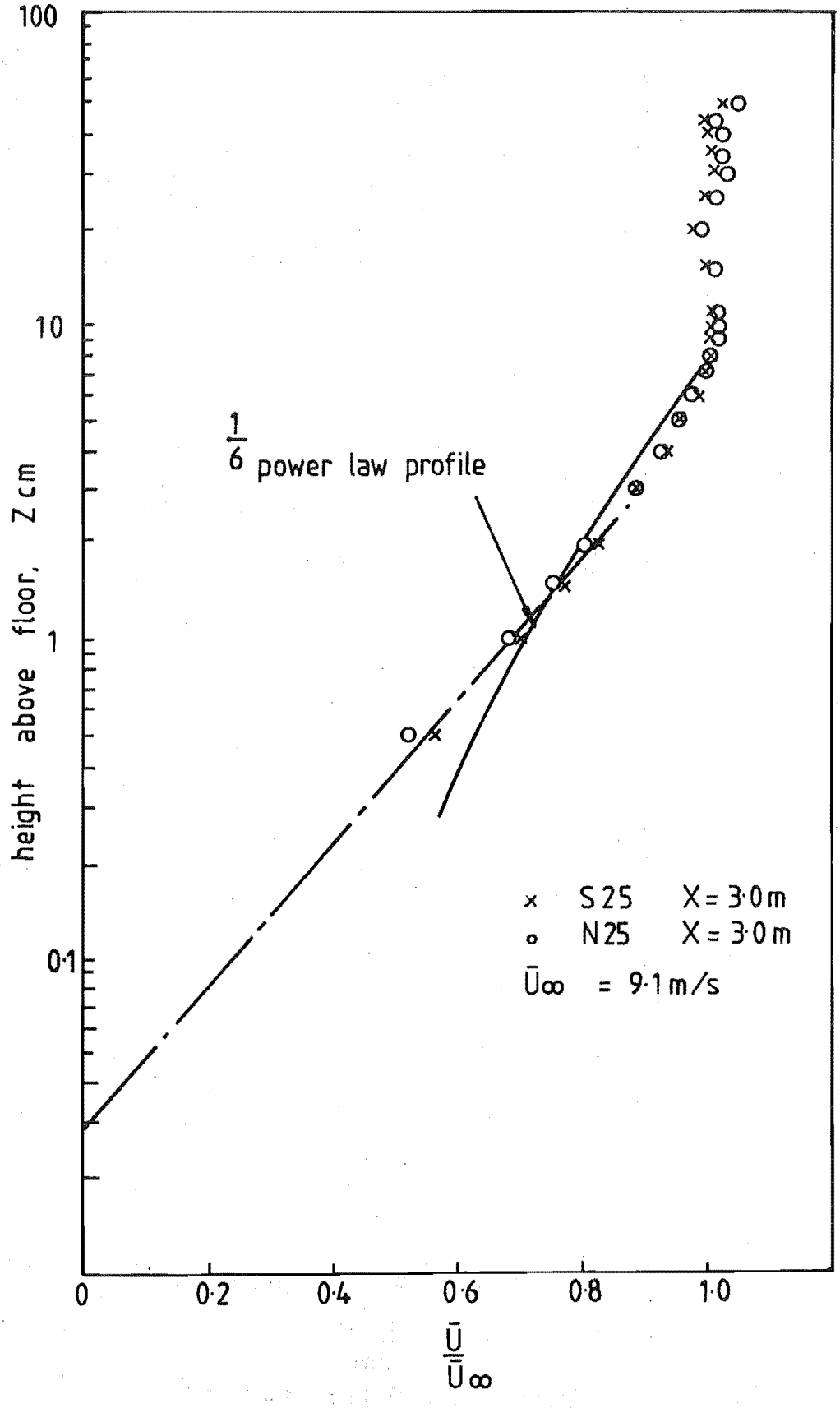

FIG 7.3 MEAN VELOCITY PROFILE AT X= 3m

the zero plane displacement d until a straight line is obtained over the region expected to be logarithmic.

Cook (1978) suggests that a better method of fitting the measured mean velocity profile to the logarithmic law is to fit to a known value of u_* determined by an independent method. The Reynolds stress profile presented in section 7.2.3 yields a value of $u_* = 0.48$ ms^{-1} and this fixes the slope of the line. From figure 7.4 this value of u_* gives a zero plane displacement of 0.25 cm and a value for z_o of 0.004 cm. The resulting mean velocity profile in figure 7.4 is logarithmic over a far larger portion of the boundary layer than can be reasonably expected.

In conclusion it was felt that the mean velocity profile was best plotted with no zero plane displacement since a reasonable logarithmic region close to the ground was obtained, but remembering that the value of z_o so obtained may be too high.

A boundary layer height of about 8.0 cm is indicated by figure 7.3. Above the edge of the boundary layer the velocity remains essentially constant up to at least 50 cm as required.

7.2.2 Turbulence intensity profiles

Figure 7.5 shows that the measured values of the local turbulence intensity compare favourably with the E.S.D.U. (1972) design curve for Z_o of 5 cm and scaled 1:3750. The lateral uniformity was also considered satisfactory.

Close to the floor the ratio u':v':w' = 1.80 : 1.39 : 1.00 is obtained from figure 7.6. This compares well with the atmospheric model presented by Teunissen (1972) which gives u':v':w' = 1.92 : 1.54 : 1.00. Further out in the boundary layer the ratio of u':v':w' = 0.86 : 1.07 : 1.00 which indicates that w' is high in the outer part of the boundary layer. This is common in accelerated growth boundary layers as reported by previous investigators (Counihan (1969), Cook (1973), Raine (1974)).

Close to the floor a single mean turbulence intensity value for each velocity component was expressed in terms of the friction velocity u_*.

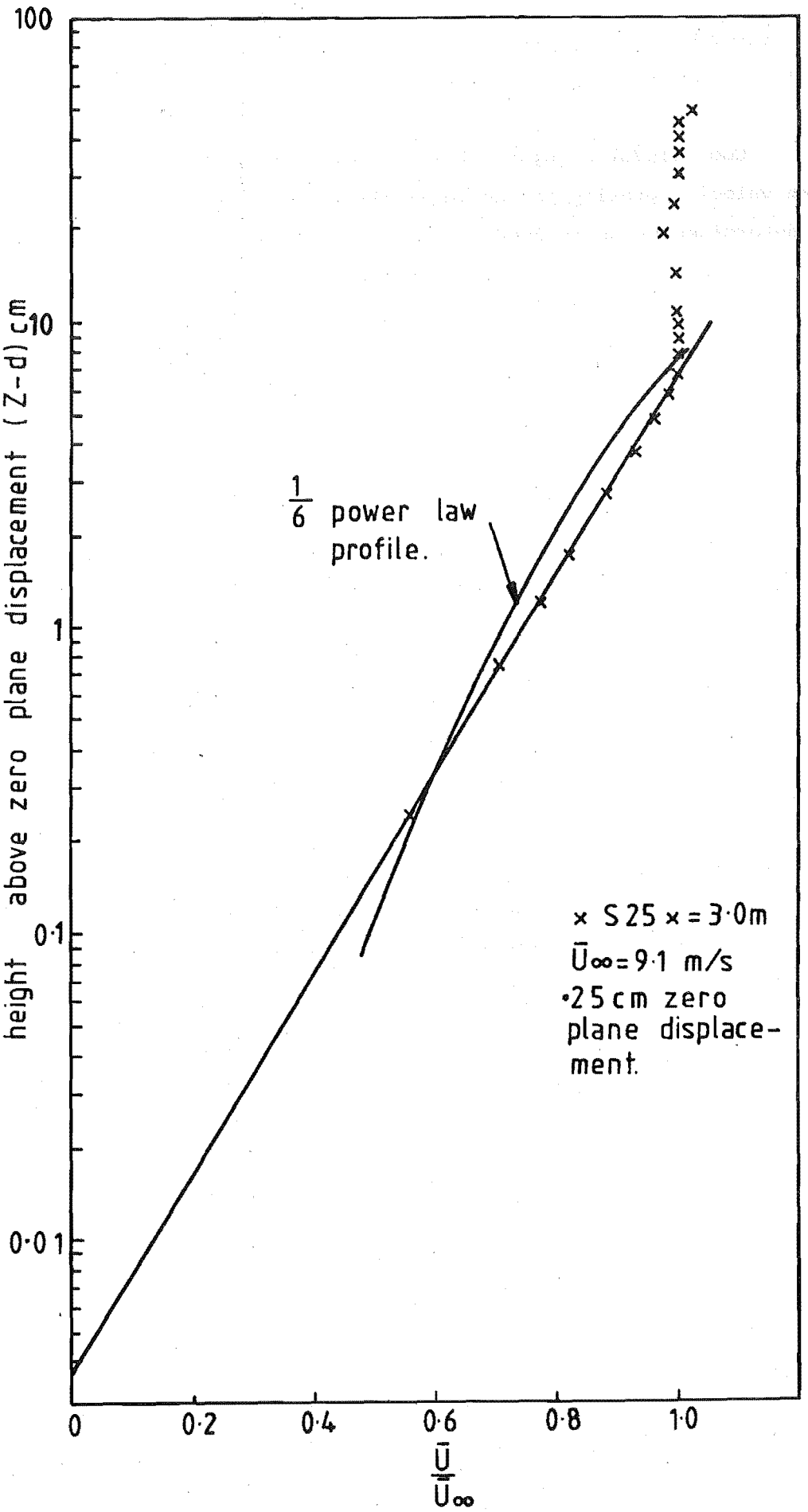

FIG. 7.4 MEAN VELOCITY PROFILE AT X = 3m

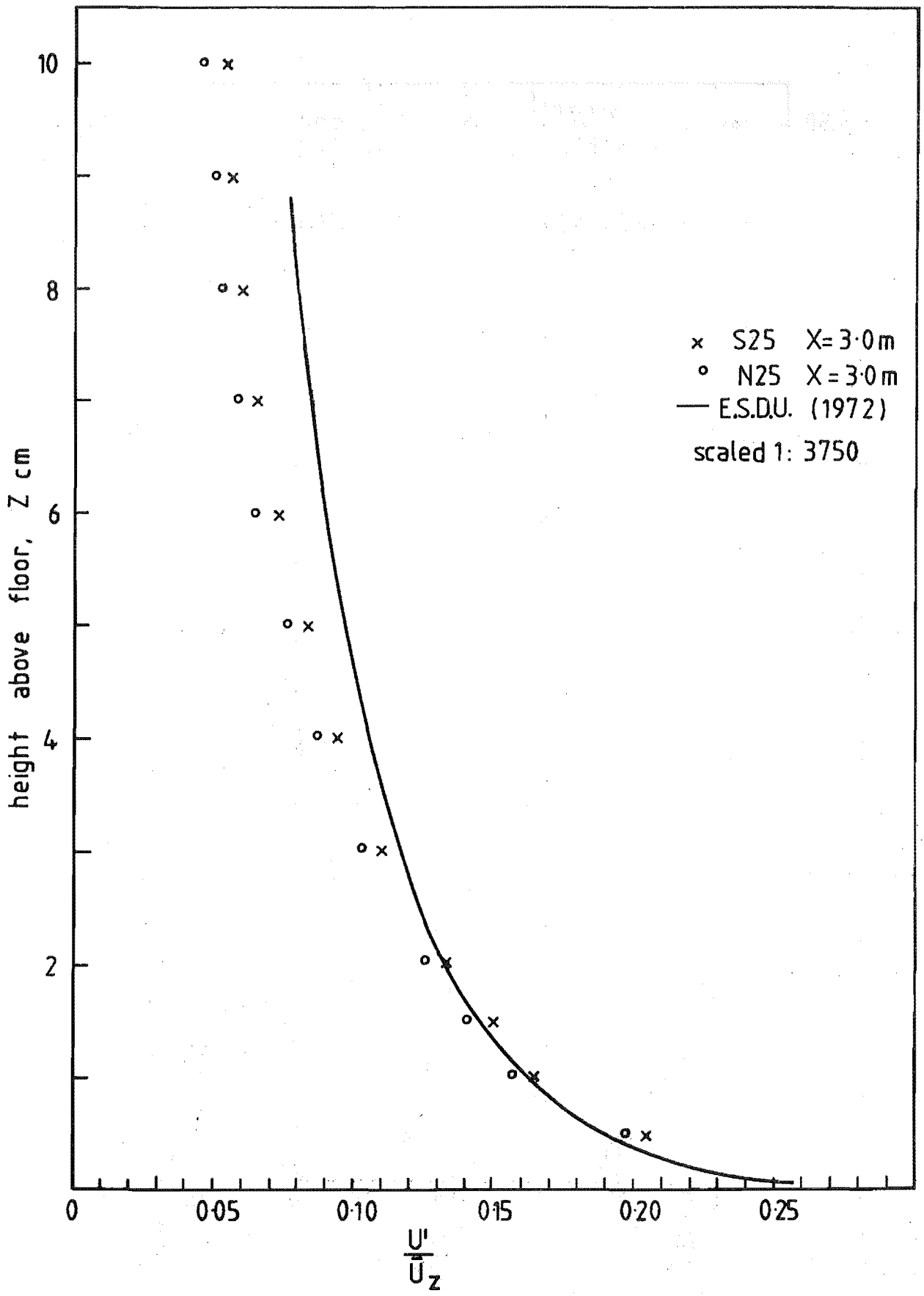

FIG 7.5 LOCAL TURBULENCE INTENSITY PROFILE AT X = 3m

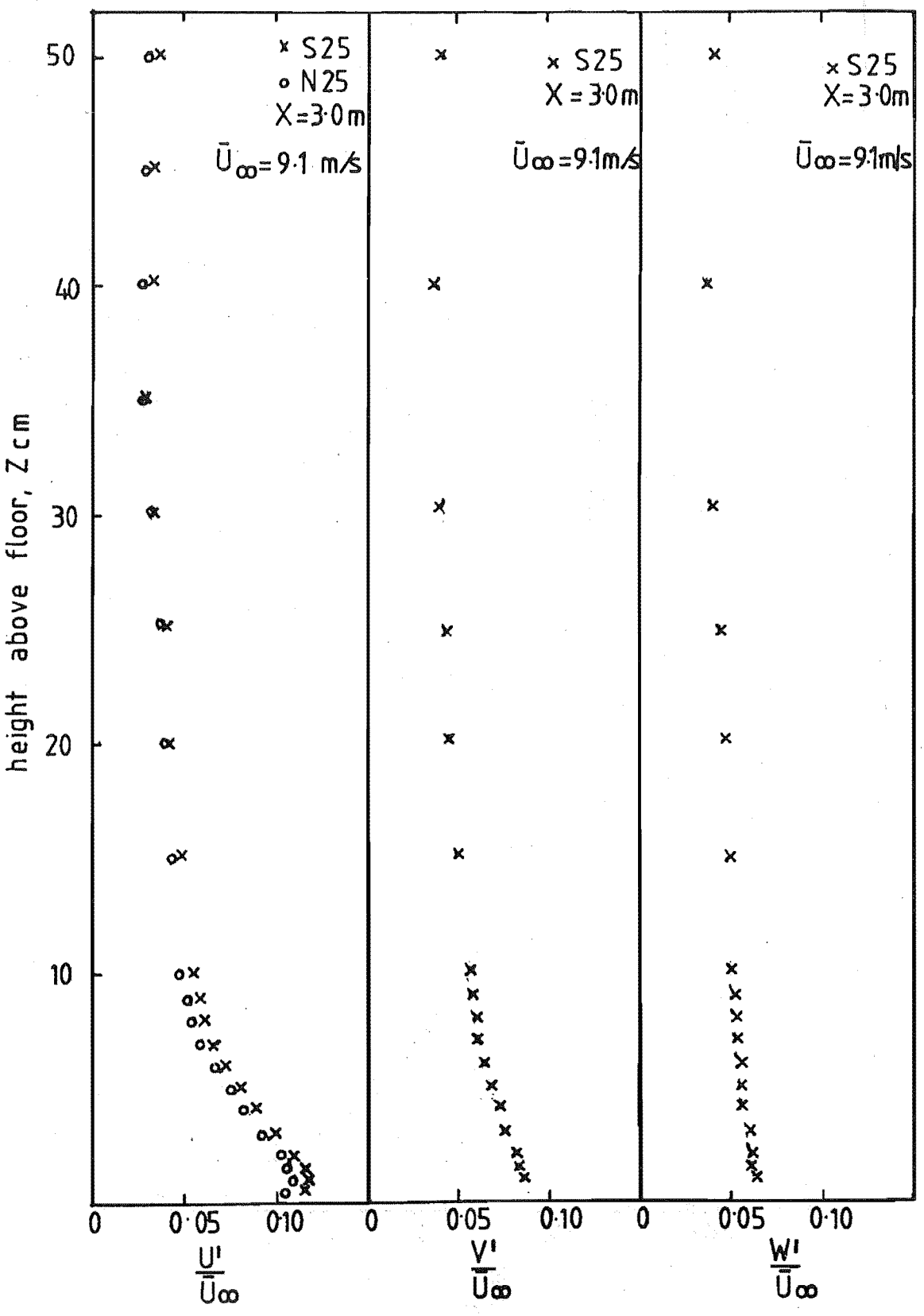

FIG 7.6 TURBULENCE INTENSITY PROFILES AT X=3m

The friction velocity was obtained from the slope of the logarithmic velocity profile near the ground. These values are compared with full scale values for the same region in adiabatic conditions as presented by Panofsky (1969) and recorded in the table below:

	Panofsky (1969)	Present Work
$\frac{u'}{u_*}$	2.5	2.5
$\frac{v'}{u_*}$	2.0	2.0
$\frac{w'}{u_*}$	1.3	1.4

7.2.3 Reynolds stress profile

The Reynolds stress was measured using the DISA TCA system which is described in Appendix one.

Plate (1971) suggests that the lowest 100 m of the atmosphere constitutes an approximately constant stress layer. Figure 7.7 shows that the simulation also displays this characteristic. The existence of a constant shear stress region from close to the floor to z = 2.0 cm vindicates the use of a logarithmic mean velocity profile for this region. Figure 7.8 shows that the measured Reynolds stress values compare well to the atmospheric data given by E.S.D.U. (1974) for Z_o = 5 cm, scaled 1:3750.

The Reynolds stress measurements made in the simulated rural boundary layer were considered to show satisfactory characteristics.

7.2.4 u and w velocity component energy spectra

In figure 7.9 the measured u component energy spectra are compared to the model spectrum of Harris (1968). The measured spectra display the desired + 1.0 and - $\frac{2}{3}$ slope on either side of the spectral peak which is characteristic of the von Karman isotropic spectrum. At a height of 1.5 cm and 5.0 cm the measured spectra compare well to the Harris model spectrum. At a height of 0.5 cm the broad band spectral shape reflects the definite

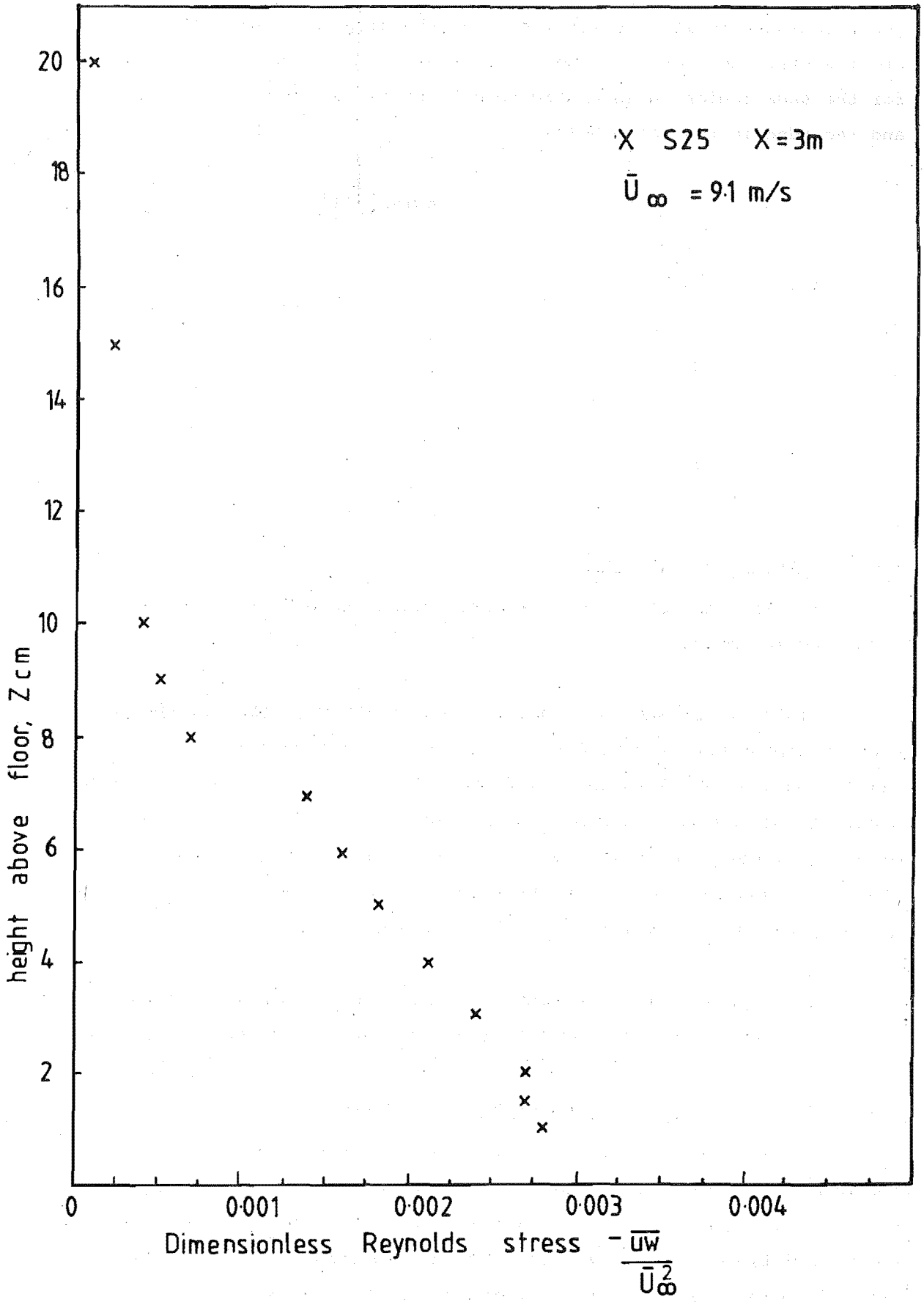

FIG 7.7 REYNOLDS STRESS AT X= 3m

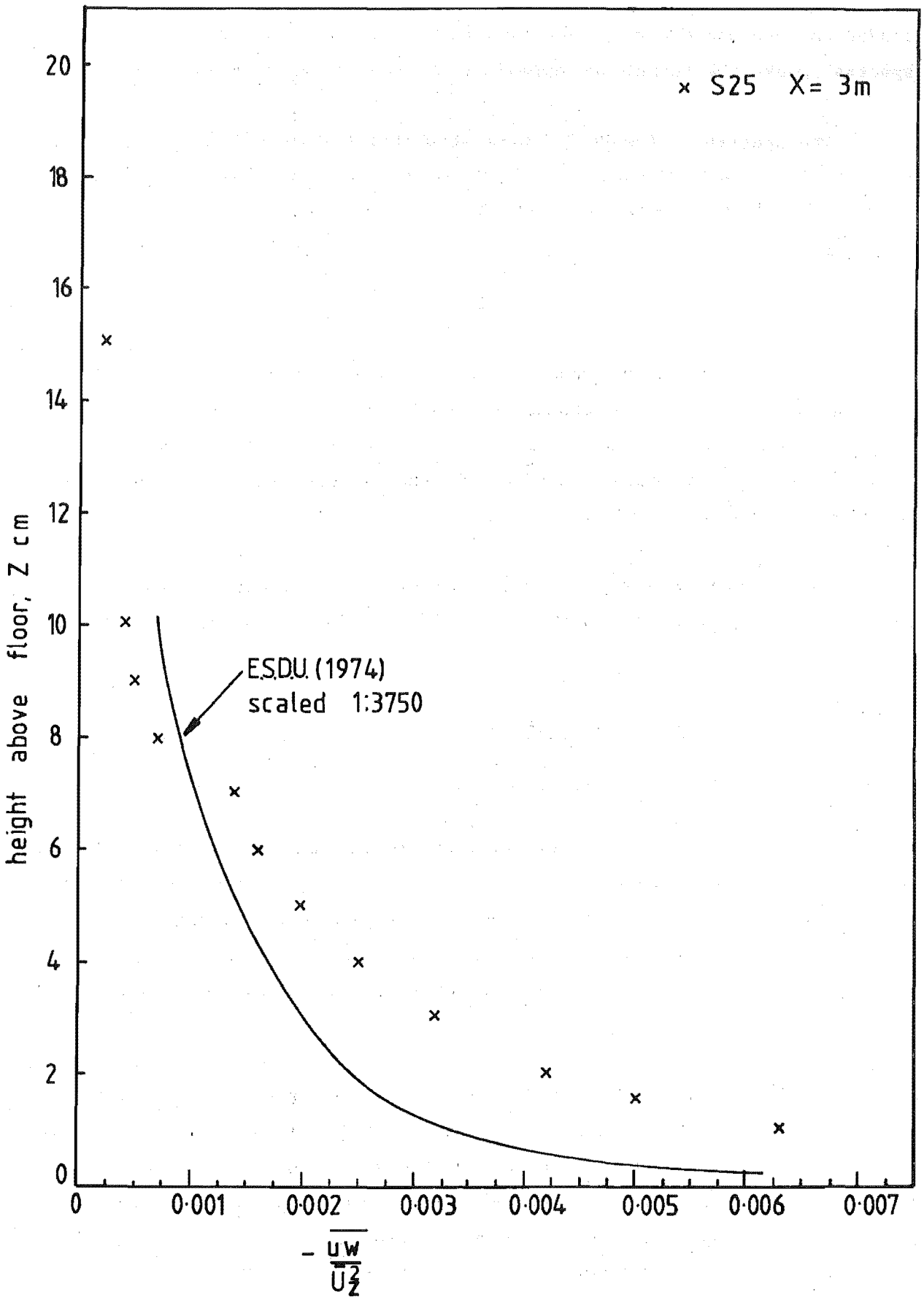

FIG. 7.8 REYNOLDS STRESS PROFILE AT X= 3m

anisotropy which will exist close to the floor, and comparison with the Harris model spectrum is poor. In figure 7.9 the model spectrum of Harris is scaled 1:3750 and because the model spectral peak is to the right of the measured spectral peaks the turbulence appears to be scaled larger than 1:3750.

The spectra in figure 7.9 also show that viscous effects are unlikely to be important in the range of energy containing eddies using the criteria of Templin (1969). Templin states that viscous effects are unlikely to be important if:

$$\frac{k_v}{k_p} > 10 \text{ or } 100 \tag{7.4}$$

where k_v is the reduced frequency at which viscous cut off of the energy spectrum of the turbulence becomes noticeable and k_p is the location of the spectral peak. At z = 0.5 cm, $\frac{k_v}{k_p}$ is between 10 and 100 but at z = 1.5 cm and z = 5.0 cm $\frac{k_v}{k_p}$ is greater than 100 and the viscous cut off is beyond the range of interest using Templin's criteria.

The measured w velocity component energy spectra were compared to the model spectrum advanced by Busch and Panofsky (1968) which is given by:

$$\frac{n\, S_w(n)}{\overline{w^2}} = \frac{0.636\, \frac{f}{f_m}}{1 + (\frac{f}{f_m})^{5/3}} \tag{7.5}$$

This expression is a reasonably good fit to neutral atmospheric field data except at low frequencies where the energy is systematically underestimated. The measured w spectra show an acceptable shape when compared with the model spectrum of Busch and Panofsky in figure 7.10. As expected, the measured w spectra show a considerable variation with height as found in field data.

Length scales were obtained from the measured spectra using equations 3.3, 3.4 and 3.5. These equations are an estimate of the true integral scale only in so far as the actual spectra have the same shape as the von Karman spectrum. The calculated length scales are presented in table 7.2 together with the length scales derived from the correlation curves. Large variations are apparent in the values obtained by the different methods. Similar vari-

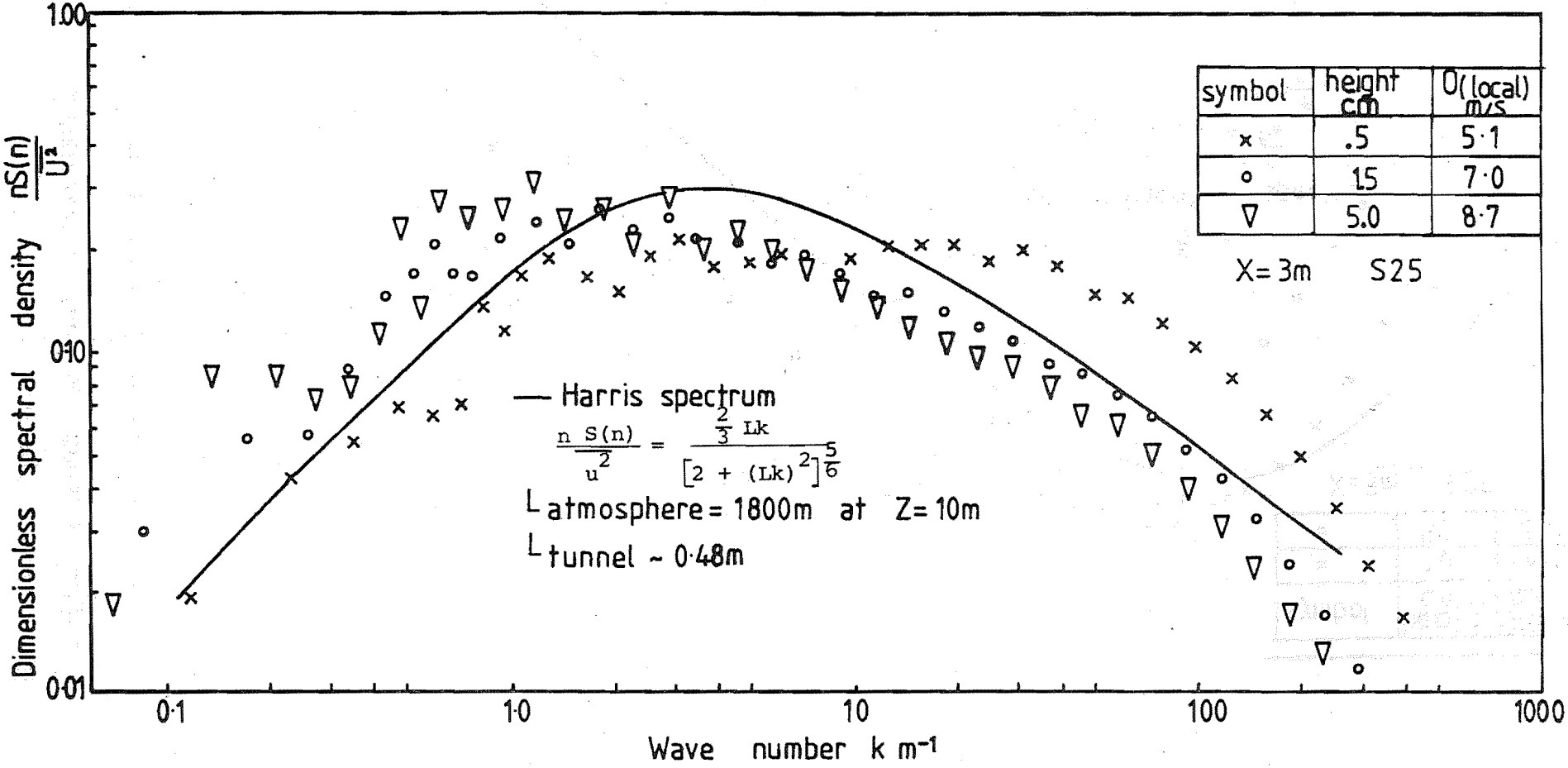

FIG. 7.9 ENERGY SPECTRA FOR THE U VELOCITY COMPONENT.

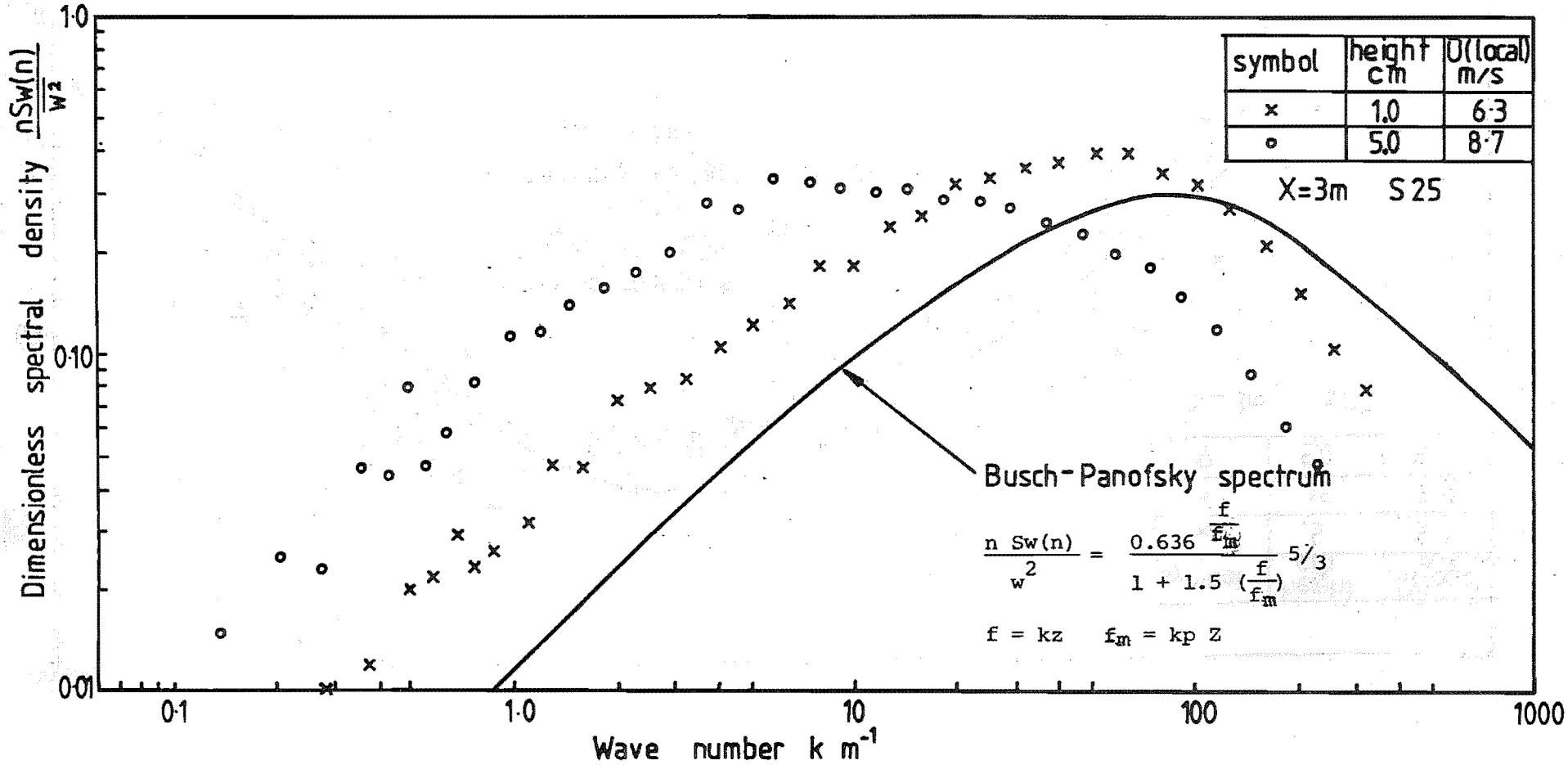

FIG 7.10 ENERGY SPECTRA FOR THE W VELOCITY COMPONENT.

Location		Spectral peak wave number u component	Spectral peak wave number w component	Integral length scales of turbulence, cm				
				Derived from spectra			Derived from correlation curves	
x m	z cm	k_{p_u} m^{-1}	k_{p_w} m^{-1}	$Lu_x = \frac{0.146}{k_{p_u}}$	$Lu_x = \frac{0.212}{k_{p_w}}$	$Lw_x = \frac{0.106}{k_{p_w}}$	Lu_x	Lu_y
3	0.5	15		0.97			2.91	
3	1.0		54		0.39	0.20		
3	1.5	1.8		8.11			6.03	1.33
3	3.0							1.90
3	5.0	1.3	7	11.23	3.03	1.51	7.22	2.43

TABLE 7.2 Tabulated length scale data

ations are found in the work of other investigators (Teunissen (1972), Raine (1974)).

7.2.5 Correlation coefficients

The autocorrelation coefficients were measured using a signal from a DISA 55F31 single wire probe. The signal was digitised and the autocorrelation function calculated using digital fast Fourier transform techniques described in Appendix two.

Turbulence length scales were calculated from the autocorrelation curves presented in figure 7.11 using the area under the curves to the first zero crossing. In obtaining the length scales it was assumed that Taylor's hypothesis (i.e. frozen flow) is valid. Taylor's hypothesis was originally made for homogeneous isotropic turbulence for which $\overline{U} >> u'$. However it is generally assumed to apply in the atmospheric boundary layer. Length scales obtained from the autocorrelation curves are summarised in table 7.2.

The lateral length scales were obtained by integration of the appropriate lateral correlation curve obtained using the analog signal processing equipment described in Appendix one. The lateral correlation curves are presented in figure 7.12 together with the calculated lateral length scales. The length scales obtained show a steady increase with height as has been found in the atmosphere by Harris (1968). Harris found that $Lu_x = 4\ Lu_y$ close to the ground and $Lu_x = 2\ Lu_y$ in the middle to outer part of the boundary layer. This behaviour is approximately shown by the curves in figure 7.12.

The lateral length scales are summarised in table 7.2 for comparison with the length scales obtained from the spectra.

7.2.6 Linear scaling of the simulation

In figure 7.13 the measured length scales of turbulence are compared with atmospheric models assuming for the atmosphere a $\frac{1}{6}$ power law mean velocity profile and a gradient height of 300 m. The variation of Lu_x at a height of 0.5 cm is adequate, further out in the boundary layer the values of Lu_x are all too large.

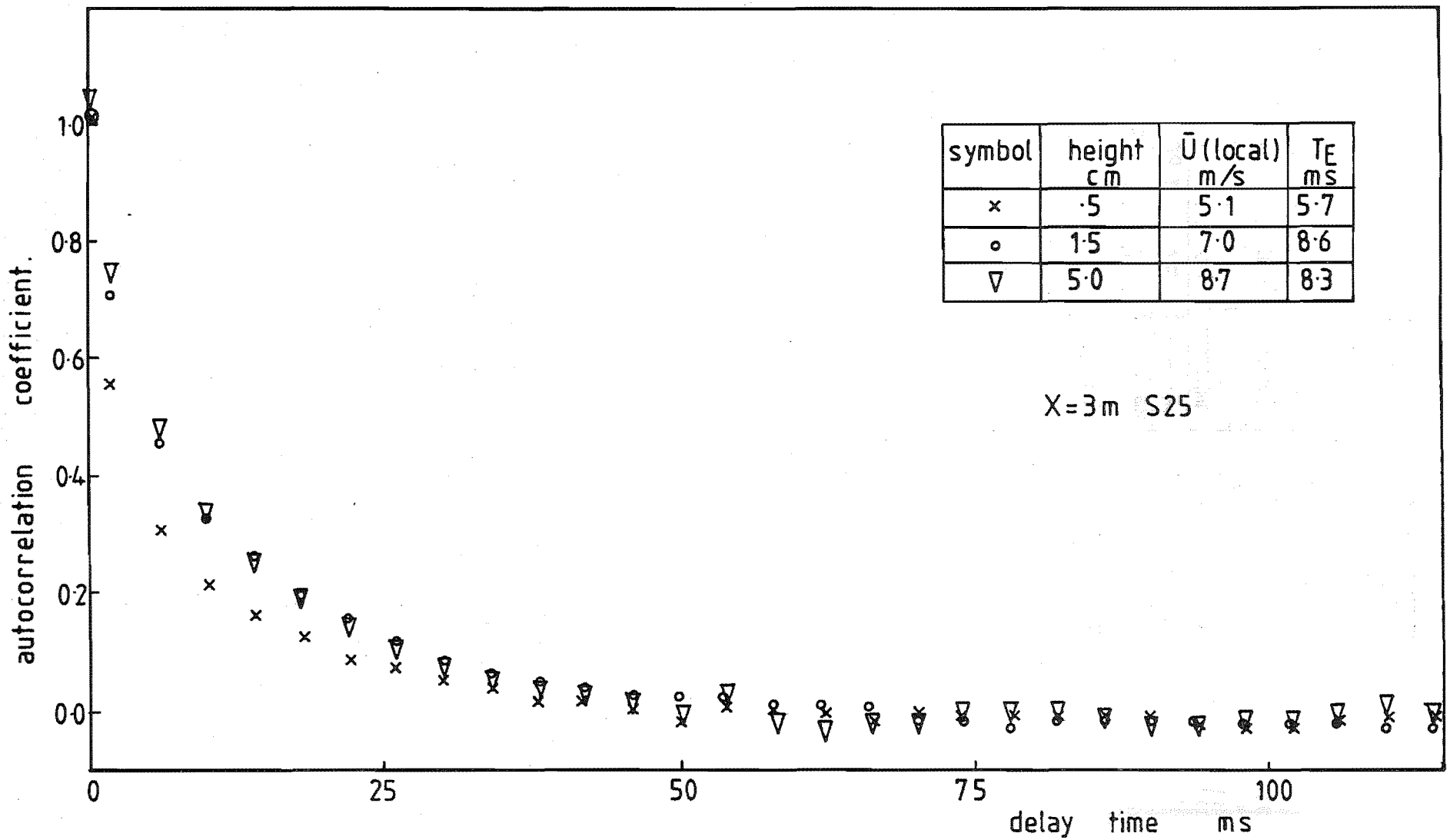

FIG 7.11 AUTOCORRELATION FUNCTIONS AT X=3m

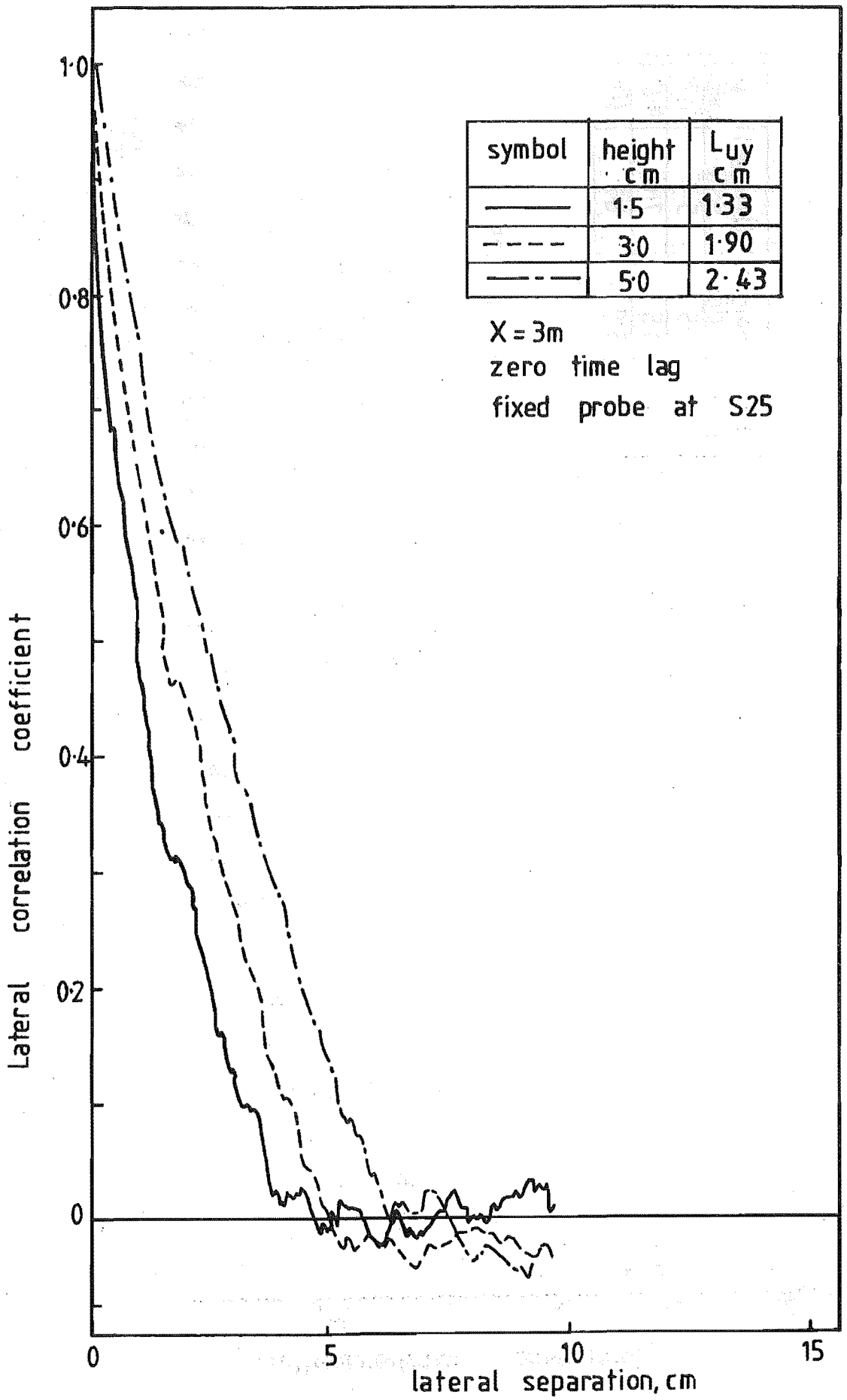

FIG. 7·12 LATERAL CORRELATION FUNCTIONS AT X=3m

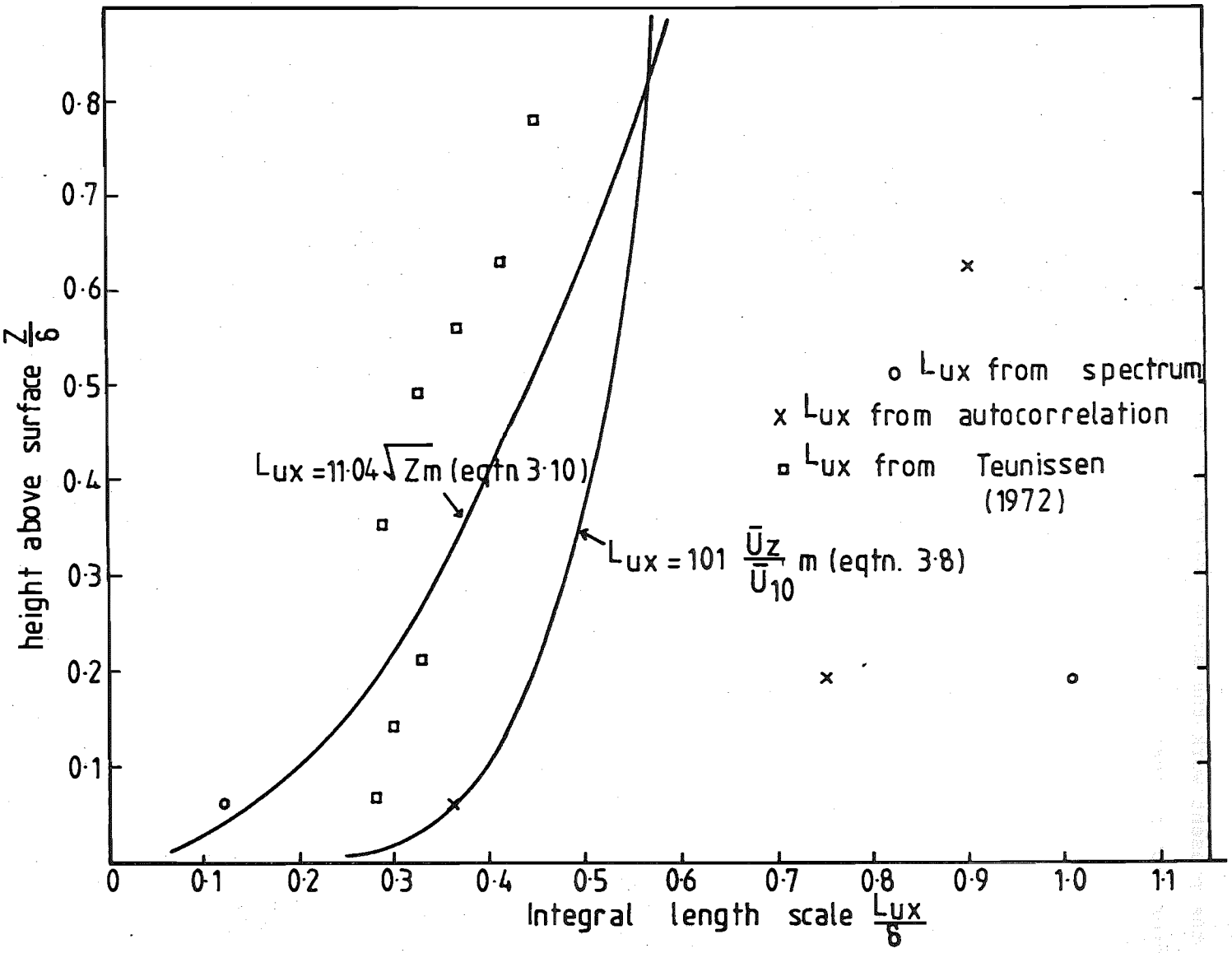

FIG 7.13 VARIATION OF LENGTH SCALE WITH HEIGHT.

A number of previous simulations such as those reported by Davenport and Isyumov (1967), Campbell and Standen (1969) and Counihan (1969) show length scales decreasing with height and little attention has usually been paid to obtaining the correct variation of the length scale with height. In the present work the actual values of the length scale are not very satisfactory but at least the desirable trend of increasing length scale with height is shown.

Estimates of the linear scaling of the simulation were made using the methods described by Raine (1974) and Cook (1977) and are summarised in table 7.3 and discussed below.

Raine (1974)

Estimates of the linear scale for the simulation were made using the method presented by Raine (1974) and are summarised in table 7.3.

Comparison of boundary layer depths (assuming a gradient height of 300 m in the atmosphere) and turbulence intensity profiles between the simulation and atmospheric data leads to a linear scaling of about 1:3750. Based on turbulence length scales a scale factor of about 1:25,000 is indicated close to the ground whereas further out in the boundary layer table 7.3 shows a scale factor of about 1:2000. Comparison of roughness lengths leads to a linear scaling of 1:170.

Raine's method of estimating the linear scaling of the simulation leads to a scale factor of about 1:4000.

Cook (1977)

Cook (1977) describes a method for determining the model scale factor in wind tunnel simulations. The method involves using a design curve for the variation of the length scale with height given by E.S.D.U. (1972):

$$S = \frac{91.3 \; (z-d)_m^{0.491}}{Lu_{x_m}^{1.403} \; z_{o_m}^{0.088}} \qquad (7.6)$$

where the subscript m refers to the model values. For Z_o = 5 cm which is a reasonable value for the roughness length for a rural atmospheric boundary layer (E.S.D.U. (1972)) and if the value for the zero plane displacement d

Location		Linear scaling $\frac{d_m}{d_a}$ based on			Turbulence length scale Lu_x from spectra	Linear scaling $\frac{d_m}{d_a}$ based on				Turbulence length scale Lu_x from autocorr.	Linear scaling $\frac{d_m}{d_a}$ based on		
X m	z cm	$\frac{\delta_m}{\delta_a}$	$\frac{z_{o_m}}{z_{o_a}}$	Turb. intensity profile		eqtn 3.8	eqtn 3.9	eqtn 3.10	Cook (1977)		eqtn 3.8	eqtn 3.10	Cook (1977)
3	0.5	1:3750	1:167	1:3750	0.97 cm	1:50,000	1:75,000	1:6,480	1:2,758	2.91 cm	1:5,300	1:7,200	1:920
3	1.5	1:3750	1:167	1:3750	8.11 cm	1: 1,600	1: 3,000	1: 280	1: 485	6.03 cm	1:2,500	1: 500	1:652
3	5.0	1:3750	1.167	1:3750	11.23 cm	1: 1,350	1, 2,500	1: 475	1: 533	7.22 cm	1:2,800	1:1,150	1:830

TABLE 7.3 Estimates of the linear scale of the simulation

is assumed to be zero then equation 7.6 becomes:

$$S = \frac{170.9\ z_m^{0.35}}{Lu_{x_m}} \qquad (7.7)$$

The results of applying equation 7.7 to the calculated values of the length scales are presented in table 7.3. The values of the scale factor are much less than those given by Raine's method and suggest a linear scaling of about 1:1000. The effect of the rapid increase in the length scale of the simulation as the height above the ground increases is apparent from the tabulated values of the scale factor S.

In conclusion it was felt that the simulation was scaled at about 1:3000.

7.2.7 Flow self preservation at X = 5 m

Figure 7.14 shows the obvious acceleration of the flow close to the ground. An increase in the boundary layer height was expected from X = 3 m to X = 5 m and figure 7.14 shows that the boundary layer height has increased from 8.0 cm at X = 3 m to 10.0 cm at X = 5 m. Lateral uniformity was similar to that at X = 3 m and was considered satisfactory.

The u component turbulence intensity profile at X = 5 m is illustrated in figure 7.15 and shows almost no change to that measured at X = 3 m except for the small decrease in the turbulence intensity close to the ground.

From figure 7.16 the spectral peak wave numbers have increased close to the ground reflecting an increase in the longitudinal length scale of the turbulence. The spectral peak wave numbers and corresponding length scales at X = 5 m are summarised in table 7.4.

The flow at X = 5 m was considered acceptable. The small increase in the linear scale of the simulation because of the increased boundary layer growth and increased length scales was not considered significant in view of the approximate methods used to calculate the linear scale of the simulation.

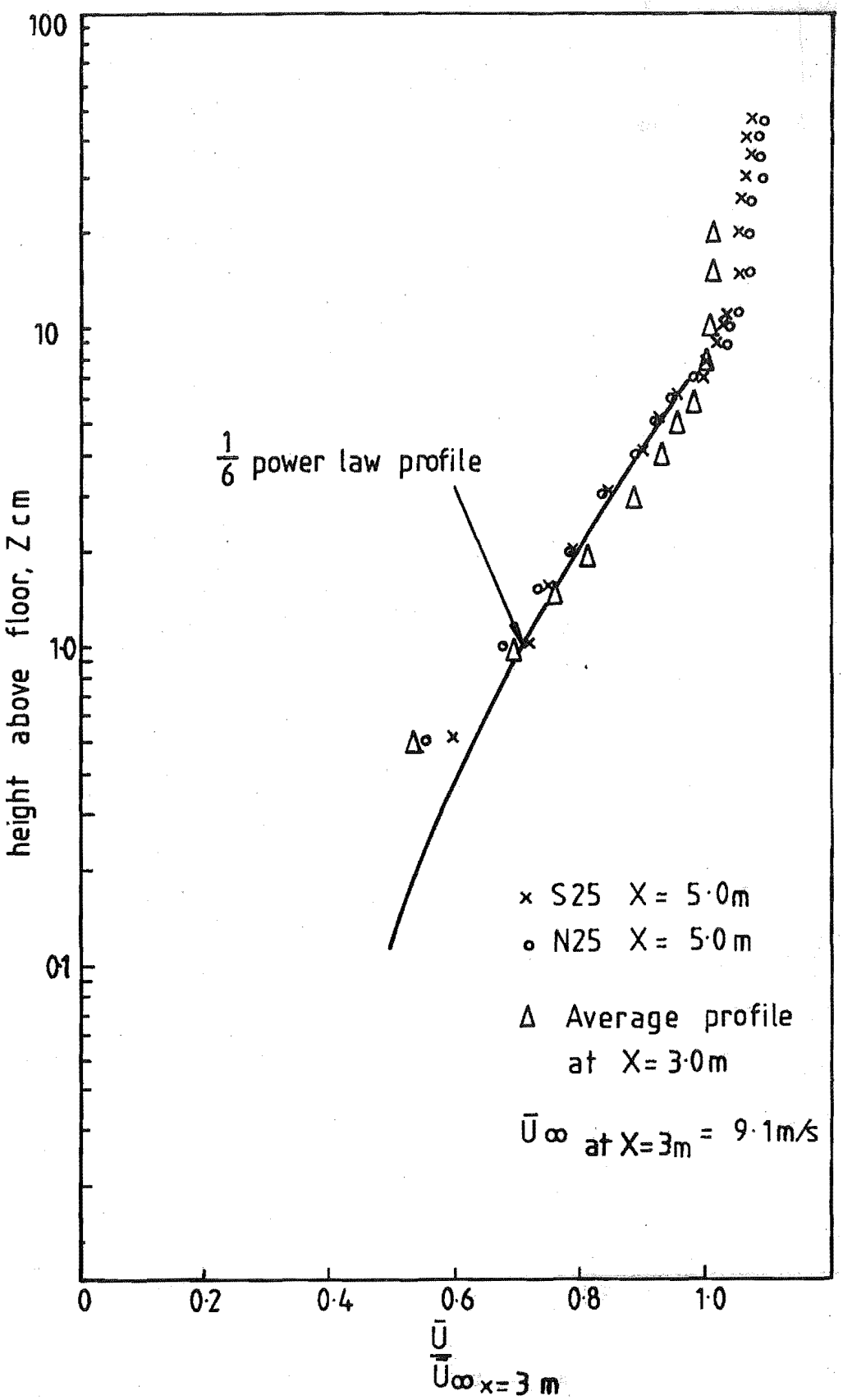

FIG 7.14 MEAN VELOCITY PROFILE AT X=5 m

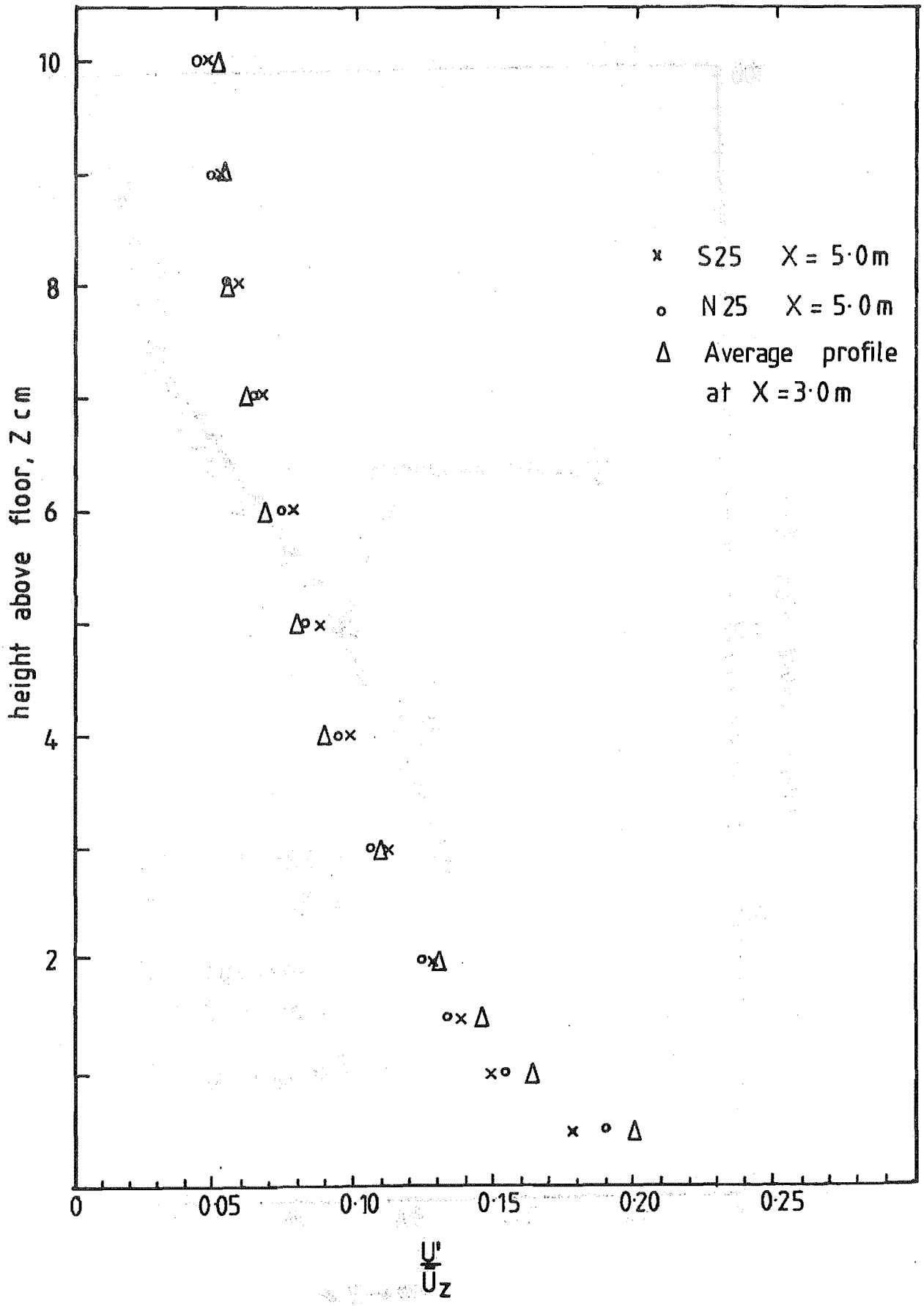

FIG 7.15 TURBULENCE INTENSITY PROFILE AT X=5 m

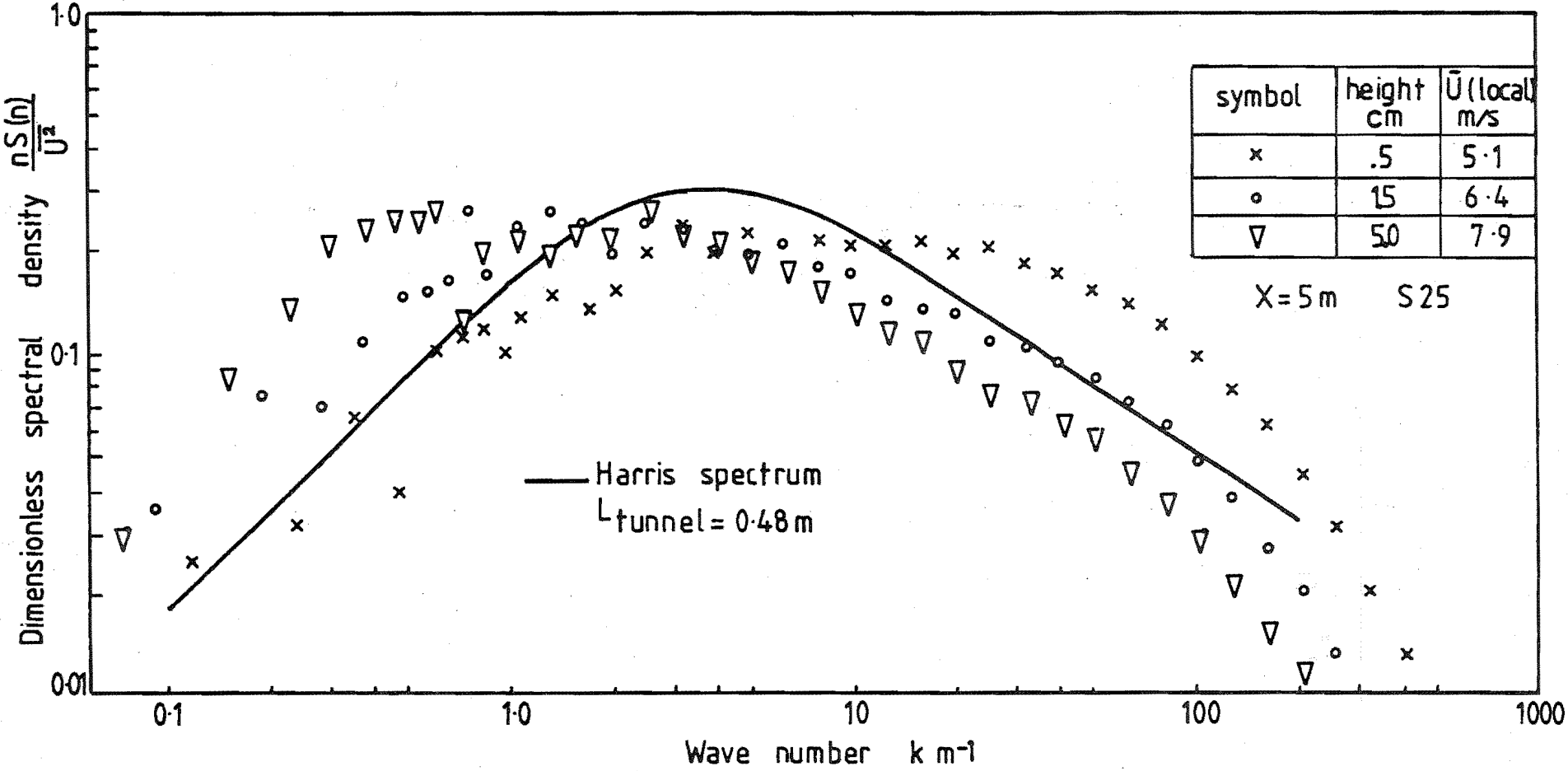

FIG 7·16 ENERGY SPECTRA FOR THE U VELOCITY COMPONENT X = 5 m

Height	X = 3 m		X = 5 m	
z cm	Spectral peak wave number u component k_{p_u} m^{-1}	Turbulence length scale $Lu_x = \frac{0.146}{k_p}$	Spectral peak wave number u component k_{p_u} m^{-1}	Turbulence length scale $Lu_x = \frac{0.146}{k_p}$
0.5	15	0.97 cm	12	1.22 cm
1.5	1.8	8.11 cm	1.7	8.59 cm
5.0	1.3	11.23 cm	1.4	10.43 cm

TABLE 7.4 Tabulated length scale data (X = 5 m)

7.2.8 Static pressure gradient

The longitudinal static pressure gradient was measured at the flush wall mounted static pressure taps which are located as described in section 3.1.1. The longitudinal static pressure variation was less than 0.25 mmH_2O about the mean.

The static pressure variation across the working section at X = 3 m and X = 5 m was measured with the pitot-static rake illustrated in figure 3.7 and was found to be within the accuracy of the measuring equipment.

Considering the small variation in the static pressure along the working section, the wind tunnel roof setting was not adjusted from that initially set as described in section 7.1.

7.3 Conclusions

In this chapter experimental results from a small scale laboratory simulation of the atmospheric surface layer were presented. The simulation was achieved using a coarse grid, trip fence and surface roughness in common with other similar simulations. Measurements of the flow properties were made and compared with full scale data from the neutrally stable atmosphere.

Most of the measured boundary layer properties compared well with full scale data for a rural atmospheric boundary layer. Satisfactory simulation of the mean velocity, turbulence intensity and spectral shape were achieved. Flow uniformity was good, there were no appreciable static pressure gradients in the working section and aerodynamically rough flow was maintained at all heights. However the trend in length scales was unsatisfactory with the length scales being much too large outside a small region close to the ground.

The boundary layer was considered a reasonable representation of a neutrally stable rural atmospheric boundary layer of approximately 1:3000 scale.

CHAPTER 8

INFLUENCE OF THE HILL HEIGHT ON THE WIND FLOW OVER HILLS

8.1 Introduction

The purpose of the tests described in this chapter was to examine the affect of the ratio of the hill height H to the boundary layer height δ on the wind flow over hills.

Measurements were made over three smooth triangular hills with aspect ratios of 0.1, 0.5 and 1.0 which were placed in turn in the 1:3000 model rural boundary layer described in Chapter seven. The hill height to boundary layer height ratio in this boundary layer was 0.625. The tests in a model rural boundary layer described in Chapters four, five and six used a value of $\frac{H}{\delta}$ equal to 0.056.

Comparison of the measurements in each boundary layer were made to enable conclusions to be drawn on the influence of the hill height on the wind flow over hills.

8.2 Experimental procedure

The smooth surfaced triangular hills with $\frac{H}{L}$ = 0.1, 0.5 and 1.0 used in the work reported in Chapter four were placed in the 1:3000 rural atmospheric boundary layer simulation. The upstream foot of each hill was located at X = 4.0 m, and the model hills were screwed to the wind tunnel floor.

As for all the previous tests no measurable change in the static pressure gradient at mid-tunnel height was observed after the installation of the hills. Therefore no pressure correction by means of the wind tunnel roof was necessary.

It was anticipated that the reduced boundary layer height would lead to a smaller region of influence of the model hills on the wind flow. More velocity measurements were therefore made close to the ground in the work presented in this chapter than in the work previously described.

Measurements were made at the following vertical and streamwise locations:-

vertical locations: $\frac{z}{H}$ = 0.1, 0.2, 0.3, 0.4, 0.6, 0.8, 1.0, 1.2, 1.6, 2.0, 3.0, 4.0, 5.0, 7.0, 10.0.

streamwise locations: $\frac{x}{L}$ = 0, ±0.5, ±1.0, ±1.5, ±2.0.

x = 10H upstream of the start of the hill (reference approach flow).

x = 10H downstream of the end of the hill.

x = 1H, 2H and 5H upstream and downstream of the hill as required.

Energy spectra and autocorrelation functions of the u velocity component were measured at a height of $\frac{z}{H}$ = 0.1, 0.2 and 1.0, 10H upstream of the start of the hills, at the hill crests and 10H downstream of the end of the hills.

Measurements were made at one lateral position, 25 cm south of the wind tunnel centreline.

In order to normalise the velocity measurements at each streamwise location with those in the approach flow a streamwise traverse at a height of $\frac{z}{H}$ = 10 was made over each hill.

8.3 Experimental results

8.3.1 Mean velocity profiles and amplification factors

Lines of equal amplification factor for the flow over the three triangular hills in the 1:3000 simulated rural atmospheric boundary layer are presented in figure 8.1. Figure 8.1 may be compared to figure 4.2 which shows the lines of equal amplification factor for the same hills in the model rural boundary layer of 1:300 scale.

In the region before and at the hill crest the value of the amplification factor has decreased as the boundary layer height has decreased. The maximum reduction in the amplification factor occurs at the ground and the reduction in the amplification factor decreases as the distance above the hill increases. The largest reduction in the amplification factor in the region before and at the hill crest occurs for the hill with an aspect ratio of 0.1 at the crest

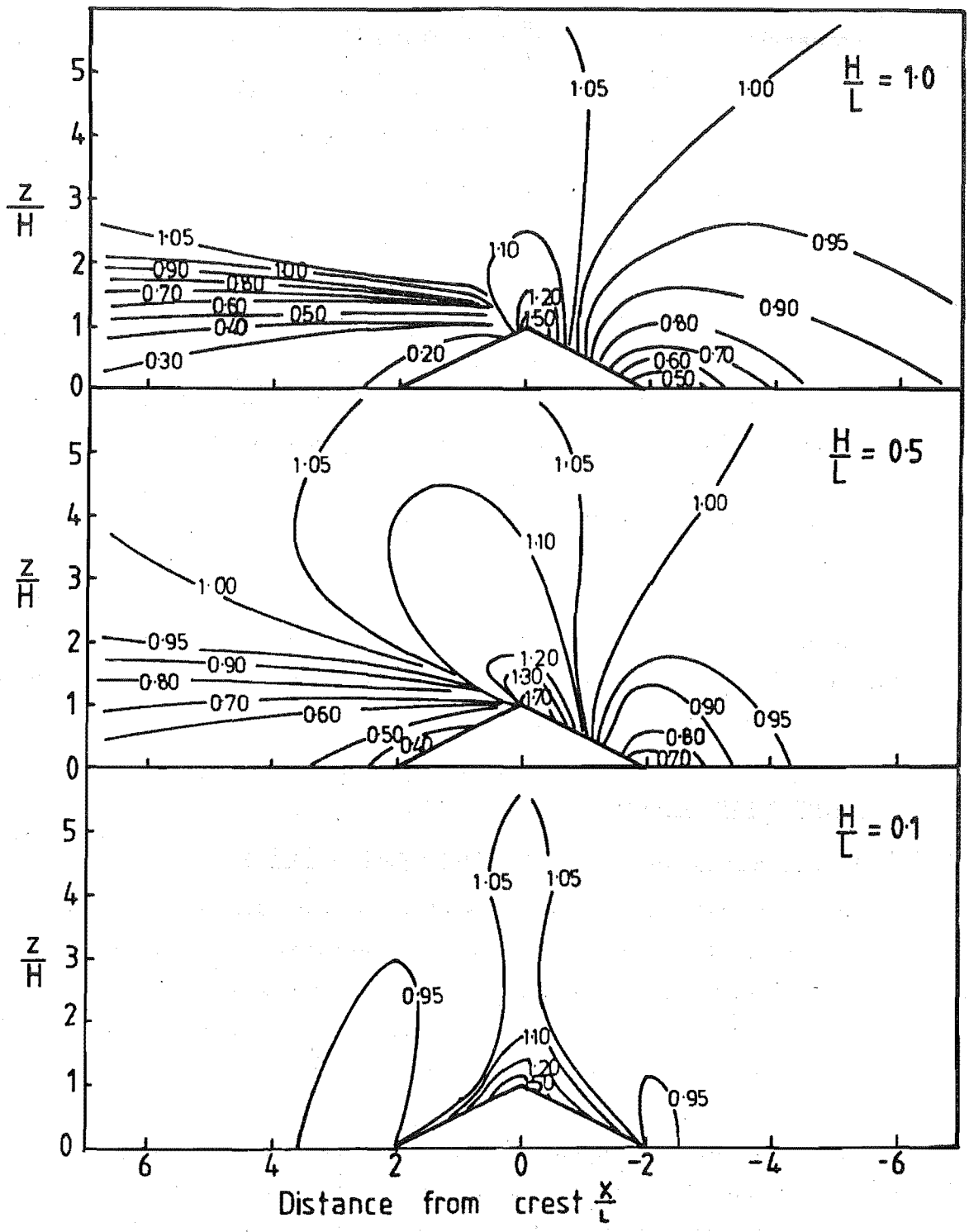

FIG 8·1 LINES OF EQUAL AMPLIFICATION FACTOR

at $\frac{z}{H}$ = 0.2 where the amplification factor has been reduced by 19%. For the hill of aspect ratio 1.0 the reduction in the amplification factor at the same position is 10%. The fractional speedup profiles at the crest are shown in figure 8.2.

After the crest between 2H and 5H above those hills with an aspect ratio of 0.5 and 1.0 there is a small but consistent increase in the value of the amplification factor as the hill height to boundary layer height ratio is increased. The maximum increase in the amplification factor is about 10%. For the hill with an aspect ratio of 0.1 this trend is not evident.

After the crest between the ground and 2H above the ground the amplification factor is reduced when the boundary layer height is reduced for all the three hills used. The maximum reduction occurs in different places for each hill and there is no clear trend either in the magnitude or the location of the maximum reduction as may be seen from the table below:

$\frac{H}{L}$	maximum reduction in amplification factor	location of the maximum reduction
0.1	37%	foot of the downwind slope at $\frac{z}{H}$ = 0.2.
0.5	58%	immediately after the crest at $\frac{z}{H}$ = 0.2.
1.0	24%	all along the downwind slope at $\frac{z}{H}$ = 0.2

Well downstream of the end of the hills the velocity profiles have been largely re-established by the surface roughness and the values of the amplification factor in each boundary layer are similar.

8.3.2 Turbulence intensity profiles

Lines of equal local turbulence intensity $\frac{u'}{U}$ in the flow over the model hills in the 1:3000 rural atmospheric boundary layer simulation are shown in figure 8.3. Figure 8.3 may be compared to the isoturbs in figure 4.6 for the flow over the same hills in the 1:300 model rural boundary layer.

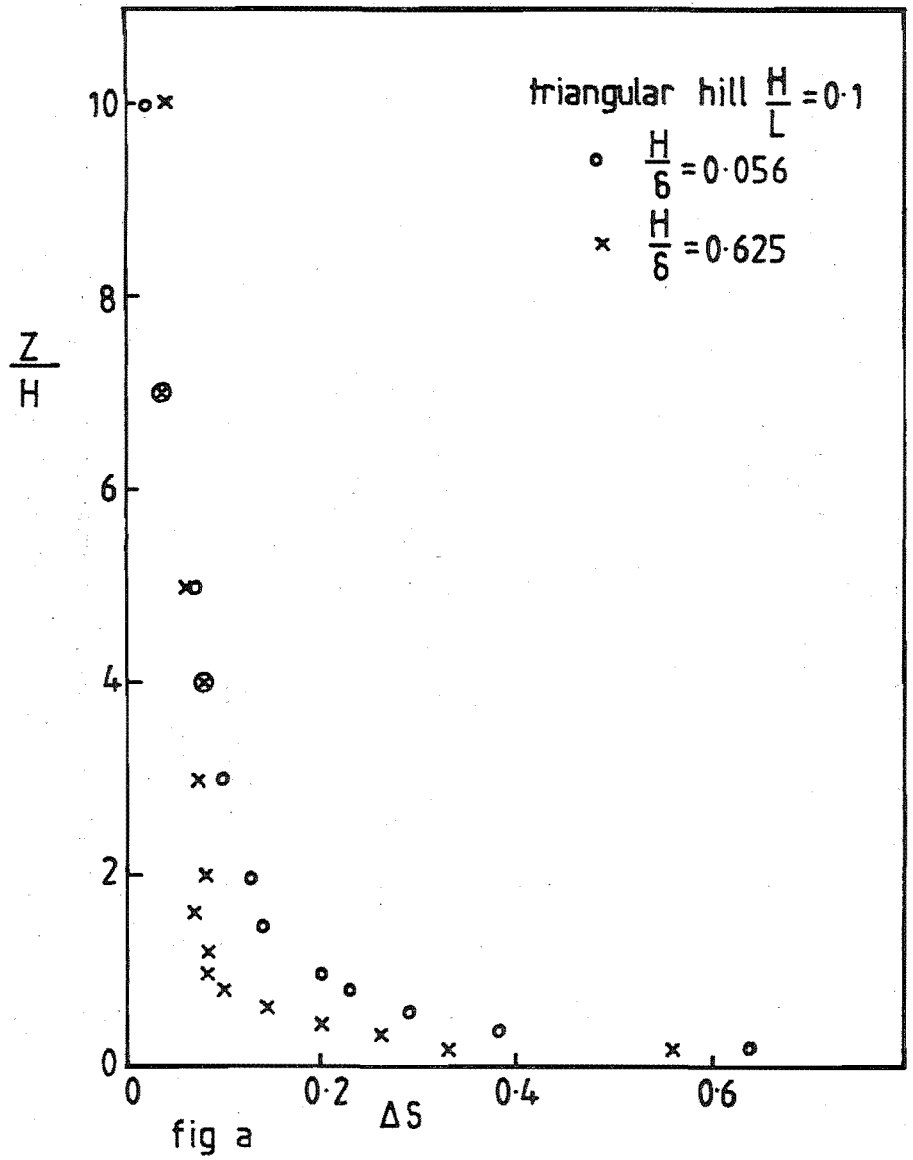

fig a

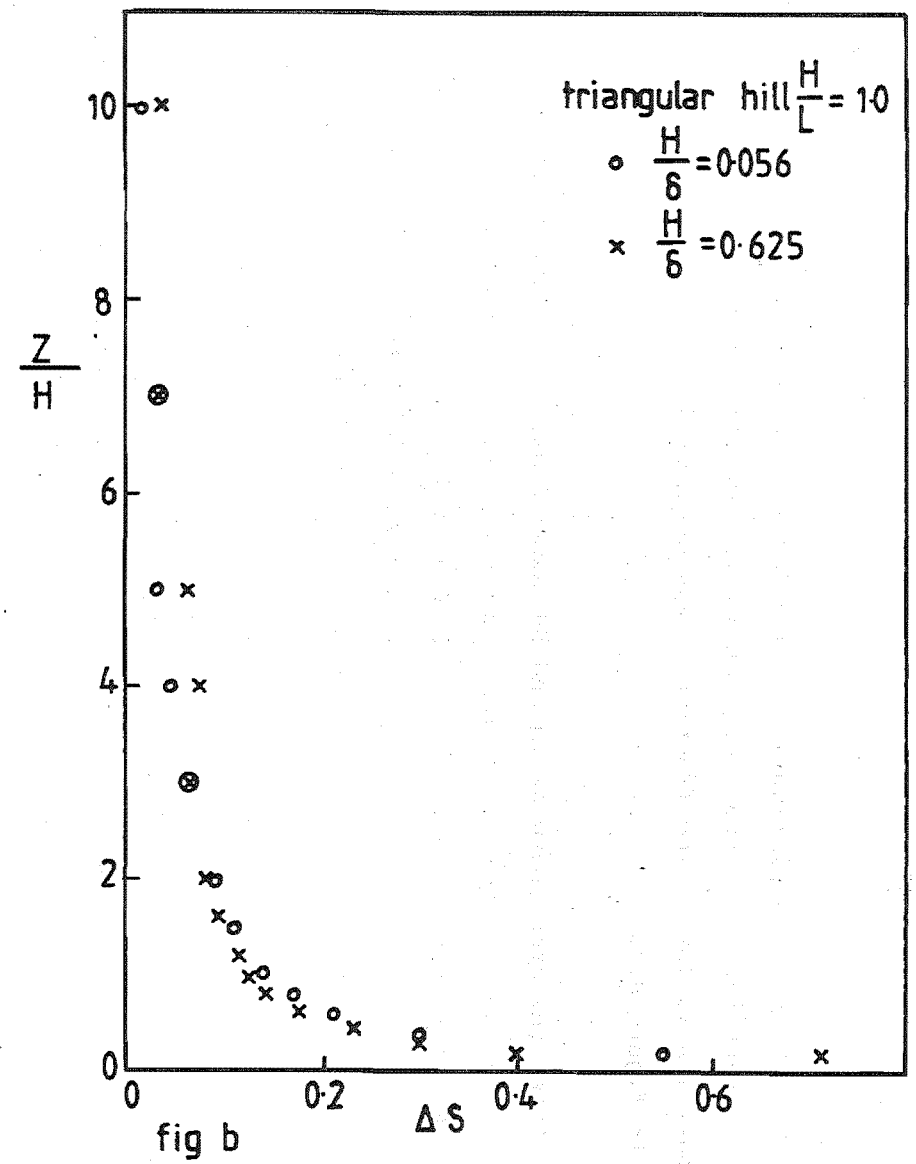

fig b

FIG 8·2 FRACTIONAL SPEEDUP AT THE CREST.

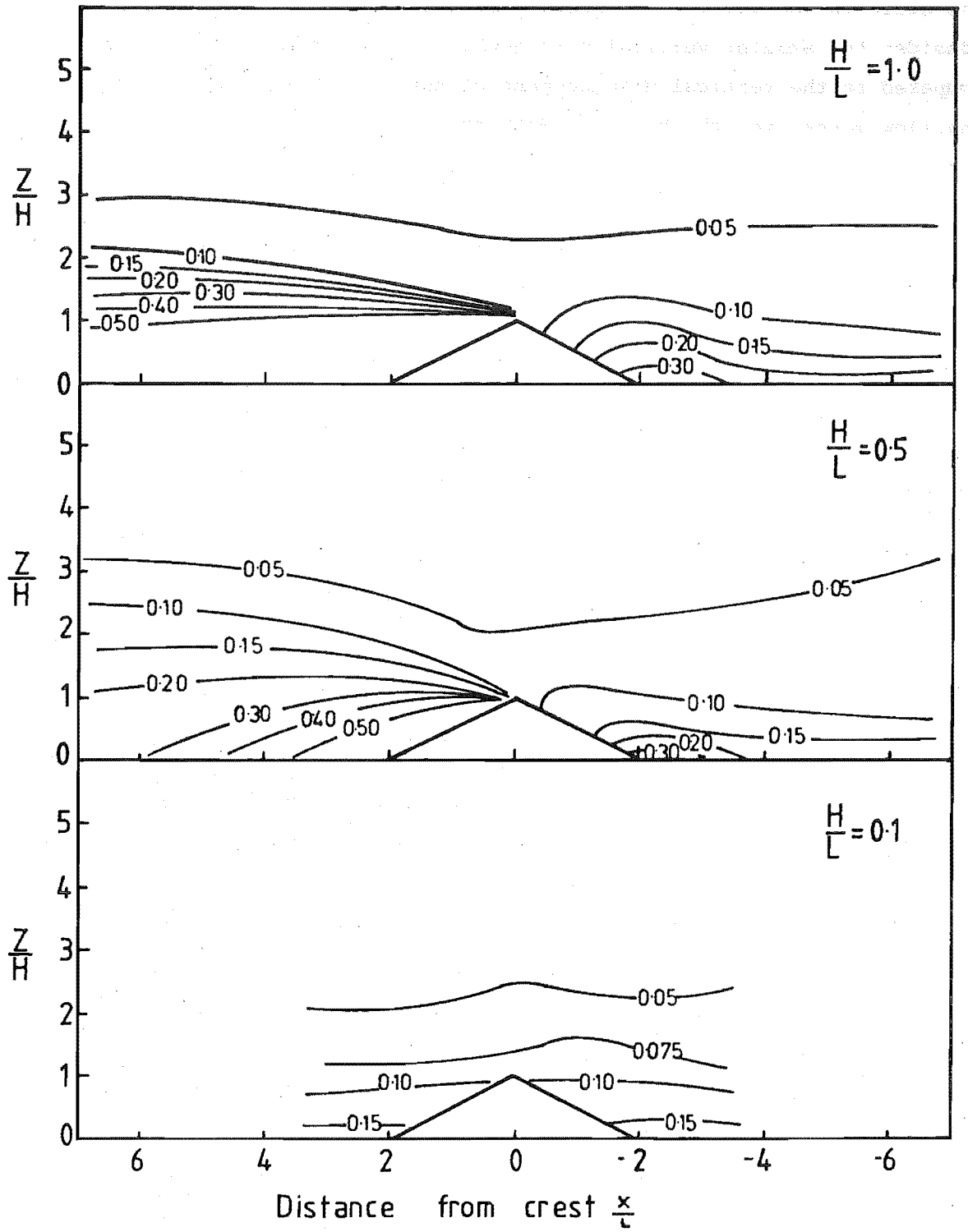

FIG 8·3 ISOTURBS OVER THE TRIANGULAR HILLS

From these figures at any given height above the hills there is a less rapid change in the local turbulence intensity as the flow moves over the hills in the 1:3000 atmospheric boundary layer simulation. For example consider the smaller vertical displacement of the 0.05 isoturb in figure 8.3 compared to the vertical displacement of the 0.13 isoturb in figure 4.6 as the flow moves over the hills. Both the 0.05 and 0.13 isoturbs are at similar heights above the ground in each boundary layer.

In the region before the hill crest the local turbulence intensity in the flow over the model hills in the 1:3000 rural boundary layer simulation has increased relative to that in the larger-scale 1:300 model rural boundary layer. This may be seen by comparing the position of the 0.30 isoturb in figures 4.6 and 8.3. This isoturb is in a similar position in the flow over each hill despite a very much reduced value of the incident local turbulence intensity for those hills in the smaller scale boundary layer.

The ratio of the local turbulence intensity in the approach flow to the local turbulence intensity at the hill crests is very similar for the two boundary layers as illustrated for the hill with an aspect ratio of 0.5 in the table below:

Height $\frac{z}{H}$	$\left[\begin{array}{l}\text{ratio of the local turbulence intensity in the approach} \\ \text{flow to the local turbulence intensity at the hill crest}\end{array}\right]_{\frac{H}{\delta} = 0.625}$	$\left[\begin{array}{l}\text{ratio of the local turbulence intensity in the approach} \\ \text{flow to the local turbulence intensity at the hill crest}\end{array}\right]_{\frac{H}{\delta} = 0.056}$
0.2	1.00	
0.4	0.98	
0.6	1.04	
0.8	1.04	
1.0	1.13	

When flow separation occurs at the hill crest as for the model hills with an aspect ratio of 0.5 and 1.0 the values of the local turbulence intensity are similar in the separation region behind the hills in both boundary layers. This may be seen by comparing the positions of the 0.20 and 0.50 isoturbs for this region in figures 4.6 and 8.3.

Outside the separation region after the hill crests the ratio of the local turbulence intensity to the local turbulence intensity in the approach flow at any given height is similar.

Only changes in the local turbulence intensity $\frac{u'}{U}$ have been considered above. In analysing the results the variation in the velocity fluctuations u' alone were also examined, and the same trends as discussed for $\frac{u'}{U}$ were evident, although to a reduced extent.

8.3.3 u velocity component energy spectra and autocorrelation coefficients

The energy spectra for the flow over the model hills in the 1:3000 rural atmospheric boundary layer simulation were measured at the upstream reference position, at the hill crest and 10H downstream of the end of the hills at heights above the surface of $\frac{z}{H}$ = 0.2, 1.0 and 2.0. These spectra were compared with the spectra measured over the same hills in the 1:300 rural atmospheric boundary layer simulation. Spectral peak values obtained from the measured spectra are presented in table 8.1.

The spectral peak wave numbers at the hill crests have decreased relative to the upstream reference values at the same height in both boundary layers. This trend is larger for those hills in the 1:300 rural atmospheric boundary layer simulation, ($\frac{H}{\delta}$ = 0.056). This is illustrated in the table below where values of the spectral peak are compared for the two boundary layers at a height of $\frac{z}{H}$ = 0.2

$\frac{z}{H}$ = 0.1										$\frac{z}{H}$ = 0.2									$\frac{z}{H}$ = 1.0								
$\frac{H}{L}$	10H upstream of the hill			crest			10H downstream of the hill			10H upstream of the hill			crest			10H downstream of the hill			10H upstream of the hill			crest			10H downstream of the hill		
	k_p	n_p	T_E	k_p	n_p	T_E	k_p	n_p	T_E	k_p	n_p	T_E	k_p	n_p	T_E	k_p	n_p	T_E	k_p	n_p	T_E	k_p	n_p	T_E	k_p	n_p	T_E
	m^{-1}	H_z	ms	m^{-1}	H_z	ms	m^{-1}	H_z	ms	m^{-1}	H_z	ms	m^{-1}	H_z	ms	m^{-1}	H_z	ms	m^{-1}	H_z	ms	m^{-1}	H_z	ms	m^{-1}	H_z	ms
0.10	15	76.8	5.7	1.0	7.99	9.4	18	85.7	6.9	1.8	11.4	7.9	1.2	10.1	14.8	2.3	30.3	14.8	1.3	11.4	8.3	1.3	12.3	13.5	1.3	10.3	18.1
0.50	15	76.8	5.7	1.0	8.86	8.3	2.3	10.6	8.0	1.8	11.4	7.9	0.7	6.60	9.7	2.3	12.8	12.8	1.3	11.4	8.3	1.1	11.2	8.7	2.2	15.2	14.9
1.00	15	76.8	5.7	2.0	17.5	7.0	3.8	9.54	13.4	1.8	11.4	7.9	1.2	10.6	7.8	3.6	10.5	12.8	1.3	11.4	8.3	1.0	10.4	9.5	2.1	10.6	9.3

TABLE 8.1 Integral time scales and spectral peak values for the triangular hills ($\frac{H}{\delta}$ = 0.625)

$\frac{z}{H} = 0.2$	$\frac{\left(\frac{n}{U}\right)_p \text{ crest}}{\left(\frac{n}{U}\right)_p \text{ approach flow}}$	
$\frac{H}{L}$	$\frac{H}{\delta} = 0.625$	$\frac{H}{\delta} = 0.056$
0.1	0.67	0.34
0.5	0.39	0.30
1.0	0.67	0.41

Downstream a distance 10H from the end of the hills the spectral peak does not shift to such a high frequency for those hills in the smaller scale simulation. This is illustrated in the table below at a height of $\frac{z}{H} = 0.2$:

$\frac{z}{H} = 0.2$	$\frac{\left(\frac{n}{U}\right)_p \text{ 10H downstream}}{\left(\frac{n}{U}\right)_p \text{ approach flow}}$	
$\frac{H}{L}$	$\frac{H}{\delta} = 0.625$	$\frac{H}{\delta} = 0.056$
0.1	1.28	1.17
0.5	1.28	1.95
1.0	2.00	3.54

The integral time scales calculated from the measured autocorrelation functions in the flow over the triangular hills in the 1:3000 rural atmospheric boundary layer simulation are presented in table 8.1. These values may be compared with the corresponding values for the same hills in the 1:300 model rural boundary layer presented in table 4.1.

In both boundary layers the integral time scale is greater at the crest than in the upstream reference position. Downstream of the hills the integral time scale is much larger relative to the upstream reference values for those hills in the 1:3000 rural atmospheric boundary layer simulation.

8.4 Discussion of the experimental results

When the boundary layer height was reduced the amplification factors over the hill decreased. The lower turbulence intensity values at the hill crest when the boundary layer height was reduced reflected the lower turbulence intensity in the approach flow. Relative to the approach flow there were similar changes in the turbulence intensity over the hills in both boundary layers. Smaller changes in the spectral peak wave number relative to the upstream reference values occurred when the boundary layer height was reduced.

There are very few comments in the literature on the affect of the hill height on the wind flow over hills. Field programmes have obvious limitations in such an investigation and it is up to theoretical and laboratory approaches to provide an insight to the influence of the height of the hill on the wind flow over hills.

In discussing the general theoretical background for their wind tunnel programme aimed at measuring the wind flow over some simple hill shapes, Rider and Sandborn (1977) write:

"In general the effect of a small hill in a deep boundary layer will depend on the energy distribution within the approach flow. The thicker the boundary layer the less the energy will be distributed in the region near the surface; thus the less will be the speedup effect of the hill". . . ."It is apparent that the higher the hill compared to the boundary layer thickness the larger will be the speedup."

The above comments of Rider and Sandborn are not confirmed by the measurements made in the present work presented in section 8.3.

Bouwmeester et.al. (1978) used ratios of $\frac{H}{\delta} = 0.09$ and 0.11 in their wind tunnel experiments. Because of the small range of $\frac{H}{\delta}$ little information can be deduced from their measurements on the affect of the hill height on the wind flow over hills. However they report some results on the affect of the hill height obtained from an inviscid flow model developed by Derickson and Meroney (1977). The inviscid flow model was used to investigate the affect of the ratio $\frac{H}{\delta}$ on the flow over a bell-shaped hill of $\frac{H}{L} = 0.1$, similar in shape to the bell-shaped hills considered in Chapter five and defined by

equation 5.1. A logarithmic approach velocity profile was used in the model with approximately the same surface roughness in each case for $\frac{H}{\delta}$ values of 0.012, 0.04, 0.4 and 4. The upstream approach velocity profile and corresponding fractional speedup profiles at the hill crest are presented in figures 8.4 and 8.5. These figures show that the speedup decreases as $\frac{H}{\delta}$ increases and that the largest changes occur close to the ground. This is the same trend obtained in the present work as shown in the results presented in section 8.3.

The decrease in the fractional speedup for a tenfold increase in $\frac{H}{\delta}$ ($\frac{H}{\delta}$ = 0.04 to $\frac{H}{\delta}$ = 0.4) for the bell-shaped hill with $\frac{H}{L}$ = 0.1 considered by Bouwmeester et.al. (1978) is tabulated below. Comparison is made with the values obtained in the present work for the triangular hill with $\frac{H}{L}$ = 0.1 for a similar increase in $\frac{H}{\delta}$ ($\frac{H}{\delta}$ = 0.056 to $\frac{H}{\delta}$ = 0.625).

Height	Decrease in fractional speedup	
$\frac{z}{H}$	Bouwmeester et.al. (1978)	Present work
0.2	0.05	0.15
0.4	0.04	0.07
1.0	0.01	0.05

The results obtained by Bouwmeester et.al. show the same trend as found in the present work, but the change in the fractional speedup was larger in the present work.

8.5 Conclusions to the study of the influence of the hill height on the wind flow over hills.

The purpose of the tests reported in this chapter was to examine the influence of the hill height on the wind flow over some simple hill shapes. This was achieved by comparing flow measurements over the same triangular hills in two model rural boundary layers of different scale.

The amplification factors in the flow over the model hills decreased as the ratio $\frac{H}{\delta}$ increased. The size of the reduction increased as $\frac{H}{L}$ decreased. Relative to the approach flow there were similar changes in the velocity fluctuations in both boundary layers. The results obtained agree qualitatively

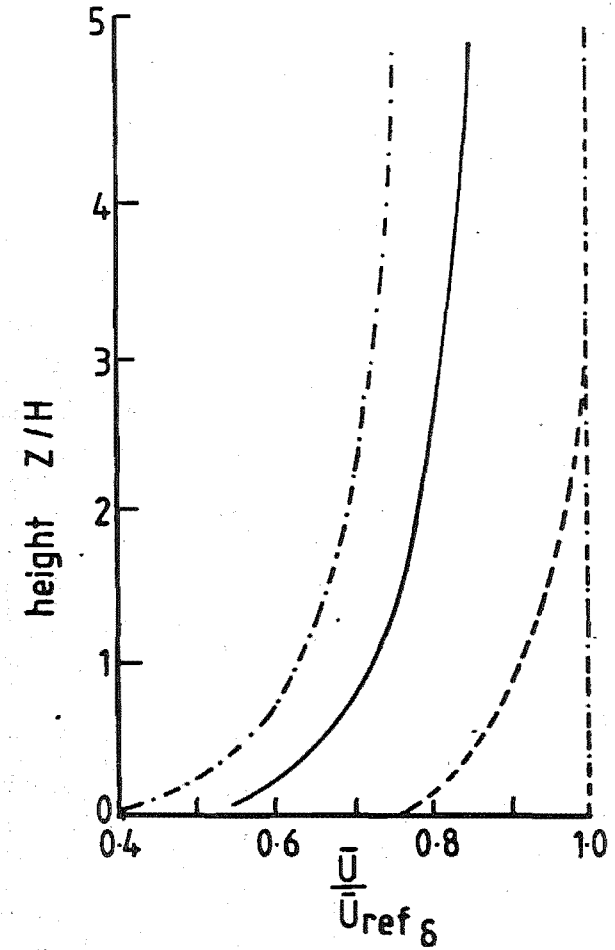

FIG 8·4 UPSTREAM REFERENCE APPROACH MEAN VELOCITY PROFILES FOR NUMERICAL INVISCID FLOW CALCULATIONS AFTER BOUWMEESTER et.al. (1978)

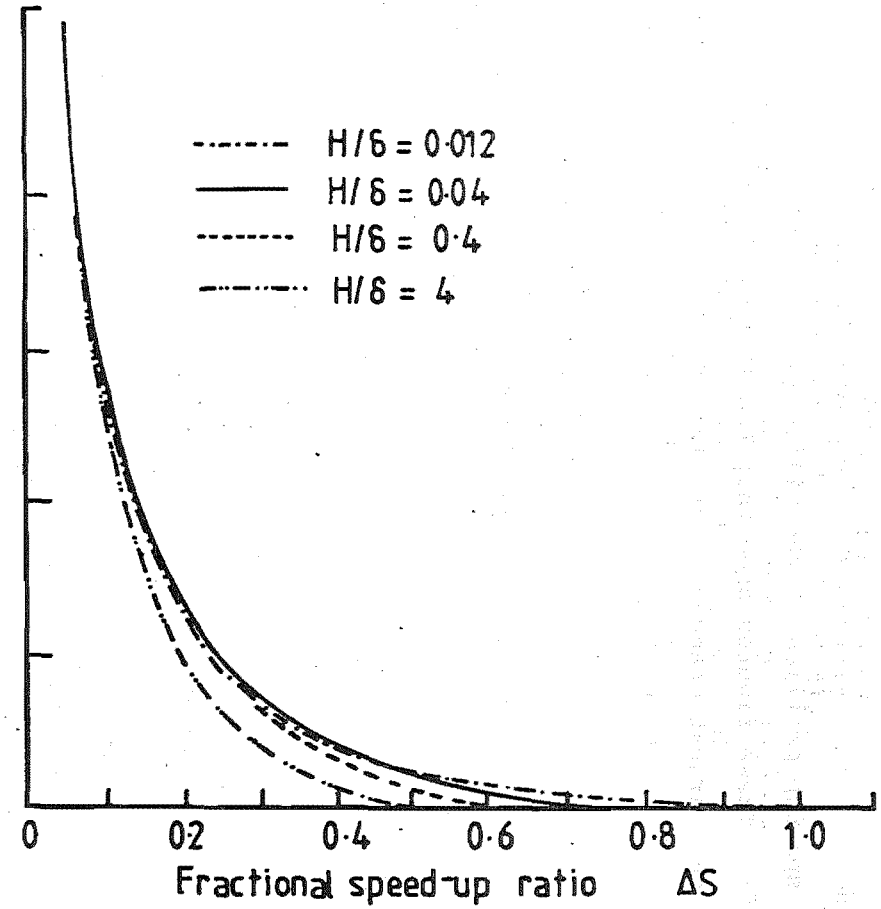

FIG 8·5 FRACTIONAL SPEEDUP PROFILES AT THE CREST OF A BELL-SHAPED HILL, $\frac{H}{L}$ = 0·1 AFTER BOUWMEESTER et. al. (1978)

with the predictions of an inviscid flow model reported in the literature.

Reports in the literature on the affect of the hill height on the wind flow over hills are very scarce and those that are available were shown to be conflicting.

CHAPTER 9

A 1:400 URBAN ATMOSPHERIC BOUNDARY LAYER SIMULATION

The object of the part of the experimental programme described in this chapter was to simulate a neutrally stable urban atmospheric boundary layer of scale as large as 1:300. This simulation was required to investigate the affect of the incident mean velocity profile and turbulence on the wind flow over model hills. The equilibrium state, defined as no change in the boundary layer with streamwise distance would not occur in an urban area due to insufficient fetch being available. However as a basis from which to work the equilibrium state is considered here.

9.1 Experimental procedure

To achieve the simulation a modified version of the system previously employed to produce a rural atmospheric boundary layer simulation was used. This system produced accelerated boundary layer growth as the available wind tunnel working section was too short to rely entirely upon natural boundary layer growth.

All measurements were made at the maximum wind tunnel speed of 19 m/s at X = 9 m, 90 cm above the floor. The wind tunnel speed was continuously monitored using a reference pitot-static probe located at X = 9 m, at a height of 1 m, 15 cm in from the north wall of the wind tunnel.

For the simulation described in this chapter a second honeycomb was installed at the entrance to the working section of the atmospheric boundary layer wind tunnel described in section 3.1.1.

The roof of the working section of the wind tunnel was set at a height of 1.23 m at the grid and a divergence of 0.6^{o}. This was the same roof position as was used in the 1:300 rural atmospheric simulation described in Chapter three.

9.1.1 The grid

The coarse grid acts as a mixing device by reproducing as much of the atmospheric turbulence spectra as is practical. The grid was left unchanged from the model rural boundary layer described in Chapter three as urban and rural boundary layers have the same energy spectra, (Counihan (1975)). The grid bar spacings are therefore given in table 3.1.

9.1.2 The trip fence

The trip fence was situated 0.61 m downstream of the coarse grid and is described in section 3.2.2. The fence height was adjusted to 24 cm as this height was found to give satisfactory turbulence levels in the boundary layer.

9.1.3 The surface roughness

After passing over the trip fence the boundary layer was allowed to grow over a rough surface consisting of large blocks placed on the Torro baseboard described in section 3.2.3. A single Torro block is shown in figure 9.1 and each block roughness element consisted of a number of these single Torro blocks joined together so the blocks were 6.4 cm x 3.2 cm and 5.6 cm high. These blocks were arranged on the wind tunnel floor in a diamond shaped grid as shown in figures 9.2 and 9.3. The first row of blocks were placed 8.0 cm downstream of the trip fence and the blocks extended to X = 9.5 m. This block arrangement gave a brick plan area to total area ratio of 0.09.

9.2 Detailed evaluation of the urban boundary layer simulation

In this section the boundary layer characteristics measured at X = 9 m are compared with those made in other urban boundary layer simulations and with the design data of E.S.D.U. (1972), (1974) and Counihan (1975).

9.2.1 Mean velocity profiles

The mean velocity profile at X = 9 m is plotted in figures 9.4 and 9.5. Measurements were made at a number of lateral and longitudinal positions relative to a particular element whose centre was at X = 8.98 m and 16 cm south of the wind tunnel centreline. These measurements were made in order to assess the local effects of the large roughness elements. The scatter in figures 9.4 and 9.5 and subsequent figures is indicative of the variation

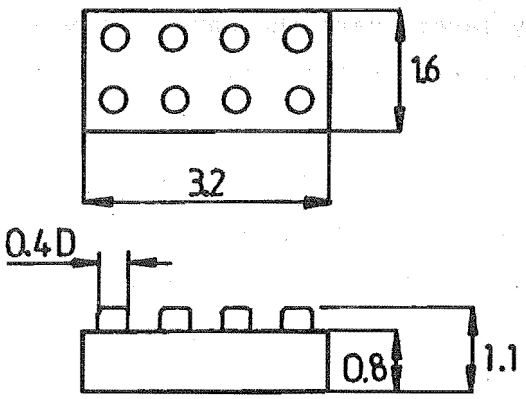

All dimensions in cm.

FIG 9·1 A TORRO BLOCK

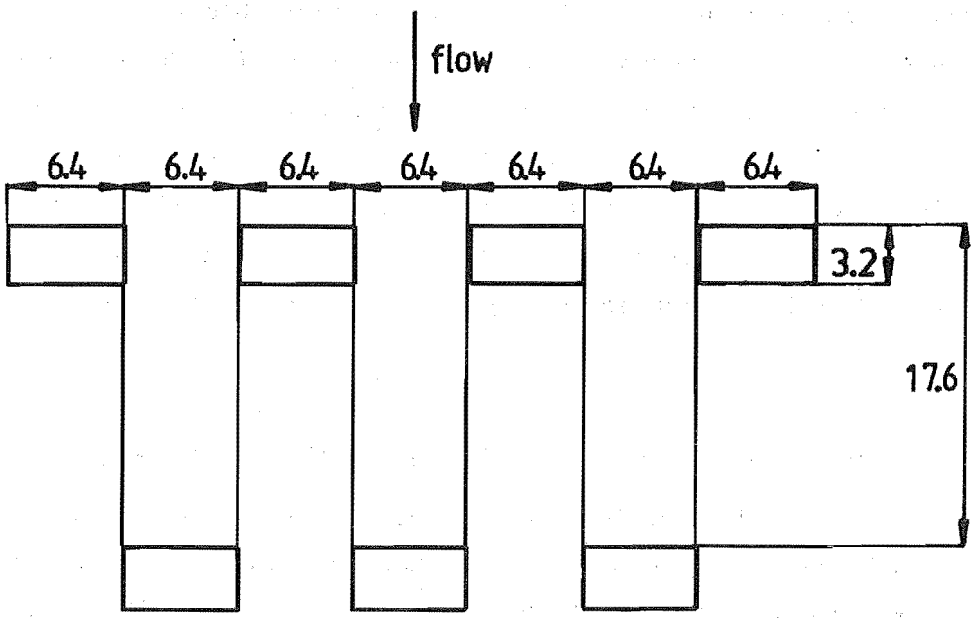

All dimensions in cm.

FIG 9·2 TORRO BLOCK PATTERN

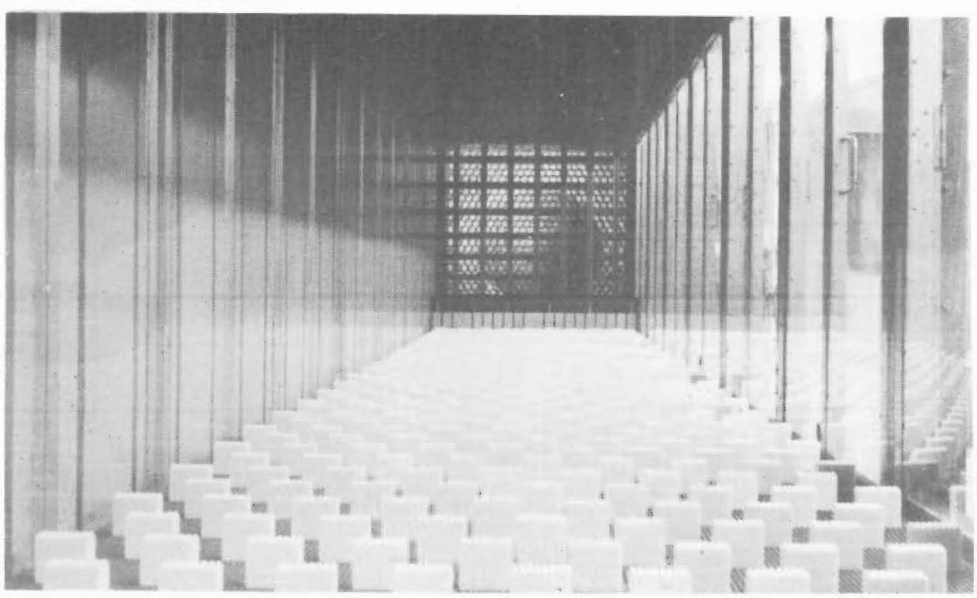

Fig. 9.3 Photograph of the working section

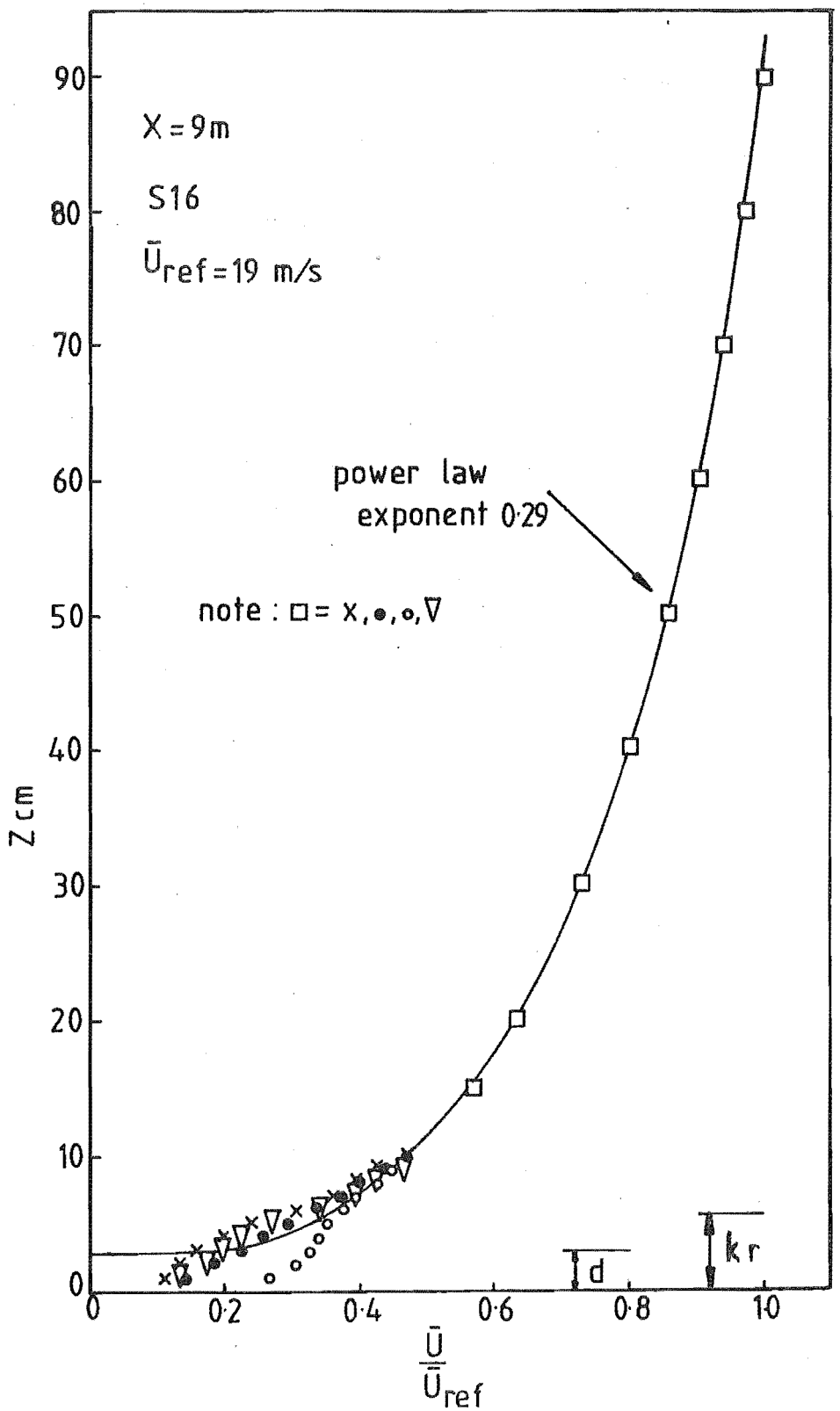

FIG. 9·4 MEAN VELOCITY PROFILE

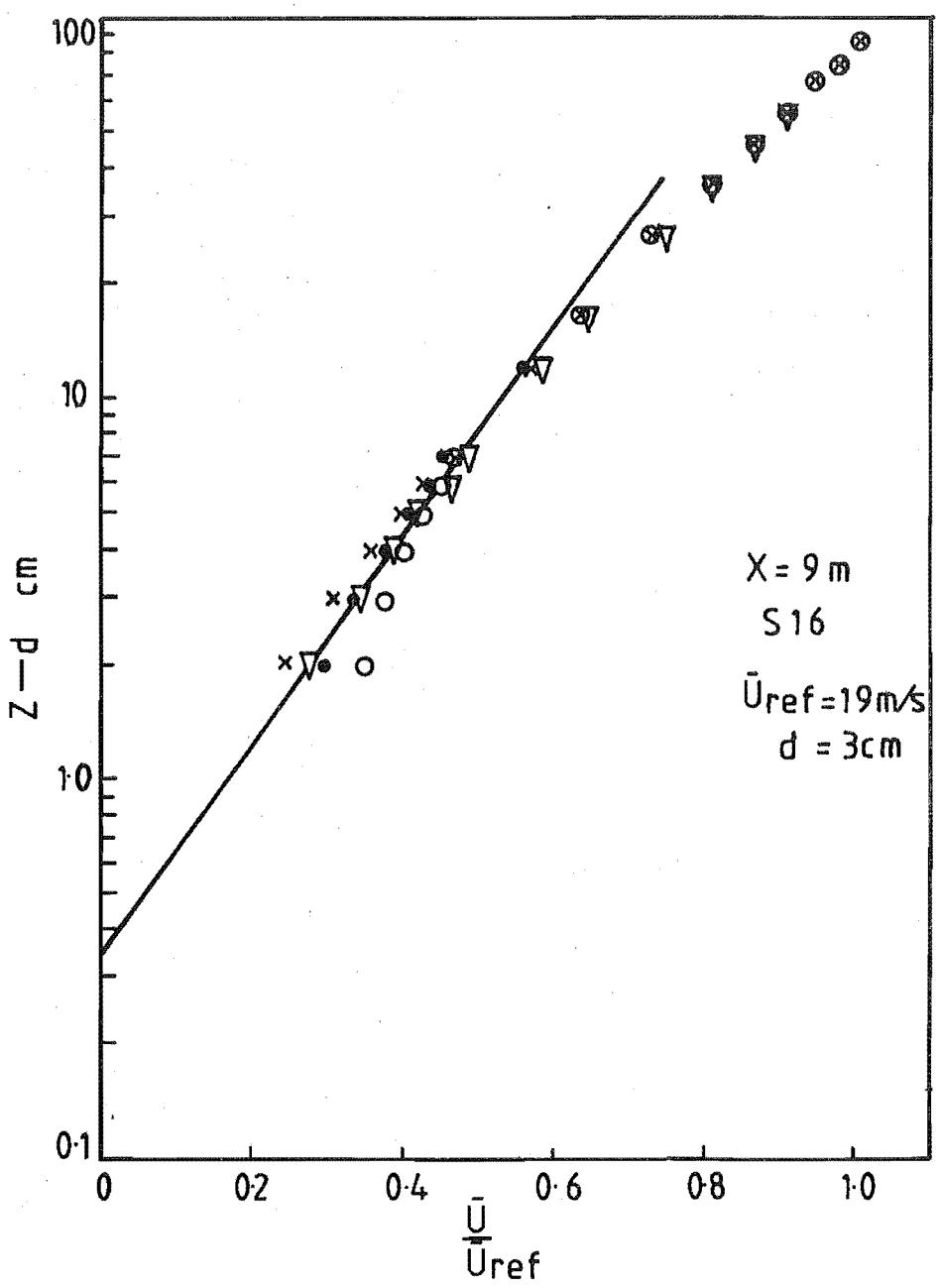

FIG 9·5 MEAN VELOCITY PROFILE

relative to a particular roughness element. Variations in the mean velocity are fairly large up to about 1.5 roughness element heights.

In figure 9.4 the mean velocity profiles are compared to a power law:

$$\frac{\overline{U}}{\overline{U}_{\delta}} = \left(\frac{z - d}{\delta - d}\right)^{\alpha} \tag{9.1}$$

In terms of reference quantities equation 9.1 becomes:

$$\frac{\overline{U}}{\overline{U}_{ref}} = \left(\frac{z - d}{z_{ref} - d}\right)^{\alpha} \tag{9.2}$$

The mean velocity profile is seen to fit a power law with an exponent of 0.29 in figure 9.4. This compares favourably with the 0.28 power law exponent in the urban simulations described by Counihan (1973) and Cook (1973). The review of field data by E.S.D.U. (1972) quotes power law exponents of 0.26 for suburbs of large towns and cities and 0.35 for the centres of large towns and cities. In his review paper Counihan (1975) suggests power law exponents of 0.24 to 0.30 for very rough terrain. Figure 9.4 indicates a zero plane displacement of 3 cm.

In figure 9.5 the measured velocity profiles are compared to the standard logarithmic law:

$$\frac{\overline{U}}{\overline{U}_{ref}} = 2.5 \frac{u_*}{\overline{U}_{ref}} \log_e \left[\frac{z - d}{Z_o}\right] \tag{9.3}$$

The straight line portion of figure 9.5 near the ground vindicates the value of 3 cm chosen for the zero plane displacement. Figure 9.5 yields a value for the roughness length Z_o of 0.35 cm and a value for the friction velocity u_* of 0.063 $\overline{U}_{ref}$ = 1.20 m/s. The value of Z_o must be regarded as approximate as Z_o is slowly changing with downstream distance as shown in section 9.2.8 and Z_o is very sensitive to the value of the zero plane displacement. Counihan (1975) suggests a value of Z_o between 1 m and 4 m for very rough urban terrain. According to the review of field data by E.S.D.U. (1972) the value of Z_o appropriate to the centres of large towns and cities is between 1 m and 1.5 m. If a full scale value for Z_o of 1.5 m is assumed, then based on Z_o the simulation is scaled at 1:430.

9.2.2 Turbulence intensity profiles

The measured turbulence intensity profiles are presented in figures 9.6 and 9.7.

In the region between 7 cm and 40 cm above the floor the turbulence intensity profiles in figure 9.6 are reasonably constant. The shear stress and friction velocity in this region were also shown to be effectively constant (figure 9.5 and 9.8). For this region a single mean intensity value for each velocity component can therefore be expressed in terms of the friction velocity u_*. These values are compared in the table below with full scale values from Panofsky (1969):

	Panofsky (1969)	Present work
$\frac{u'}{u_*}$	2.6	2.3
$\frac{v'}{u_*}$	2.0	1.8
$\frac{w'}{u_*}$	1.3	1.6

The measured values indicate that the vertical turbulence is too high in the boundary layer simulation. This is common in accelerated growth boundary layers and similar characteristics are shown in the simulations described by Counihan (1969) and Tieleman et.al. (1978).

As for the mean velocity measurements the turbulence intensity profiles in figures 9.6 and 9.7 show considerable variation up to a height of about 1.5 roughness element heights. This variation illustrates the difficulty in defining mean values of measurements made in urban areas.

In figure 9.7 the turbulence measurements are presented in terms of the local velocity $\left(\frac{u'}{\bar{U}}\right)_Z$ for ease of comparison with other data. All the data with which the measured values are compared were scaled at 1:400 between the wind tunnel and the atmosphere. The data of Cook (1973), Counihan (1975) and Feasey (1978) were plotted assuming the simulation in the present work had a 3 cm zero plane displacement. No adjustment was made to the E.S.D.U.

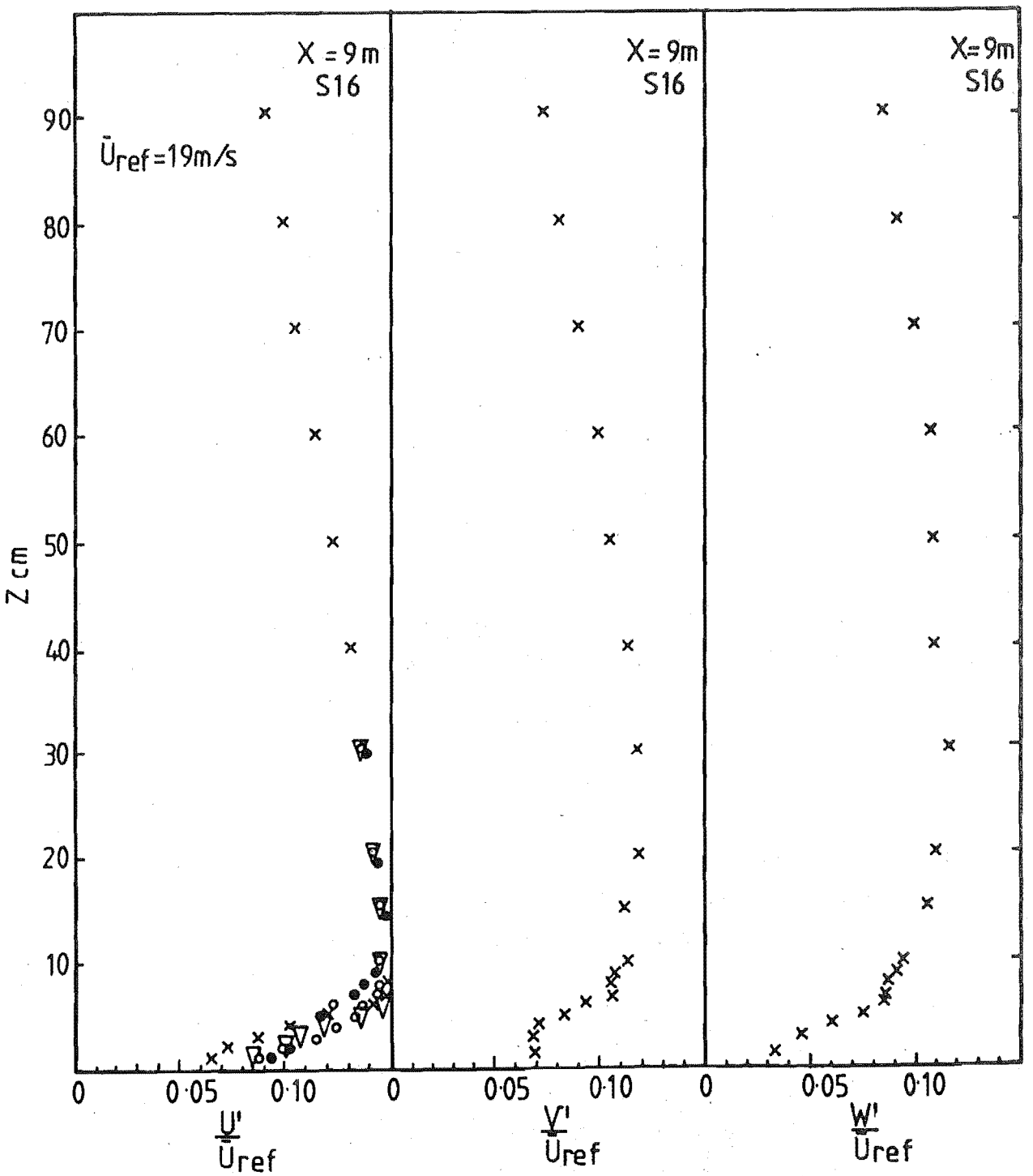

FIG 9·6 TURBULENCE INTENSITY PROFILES AT X=9m

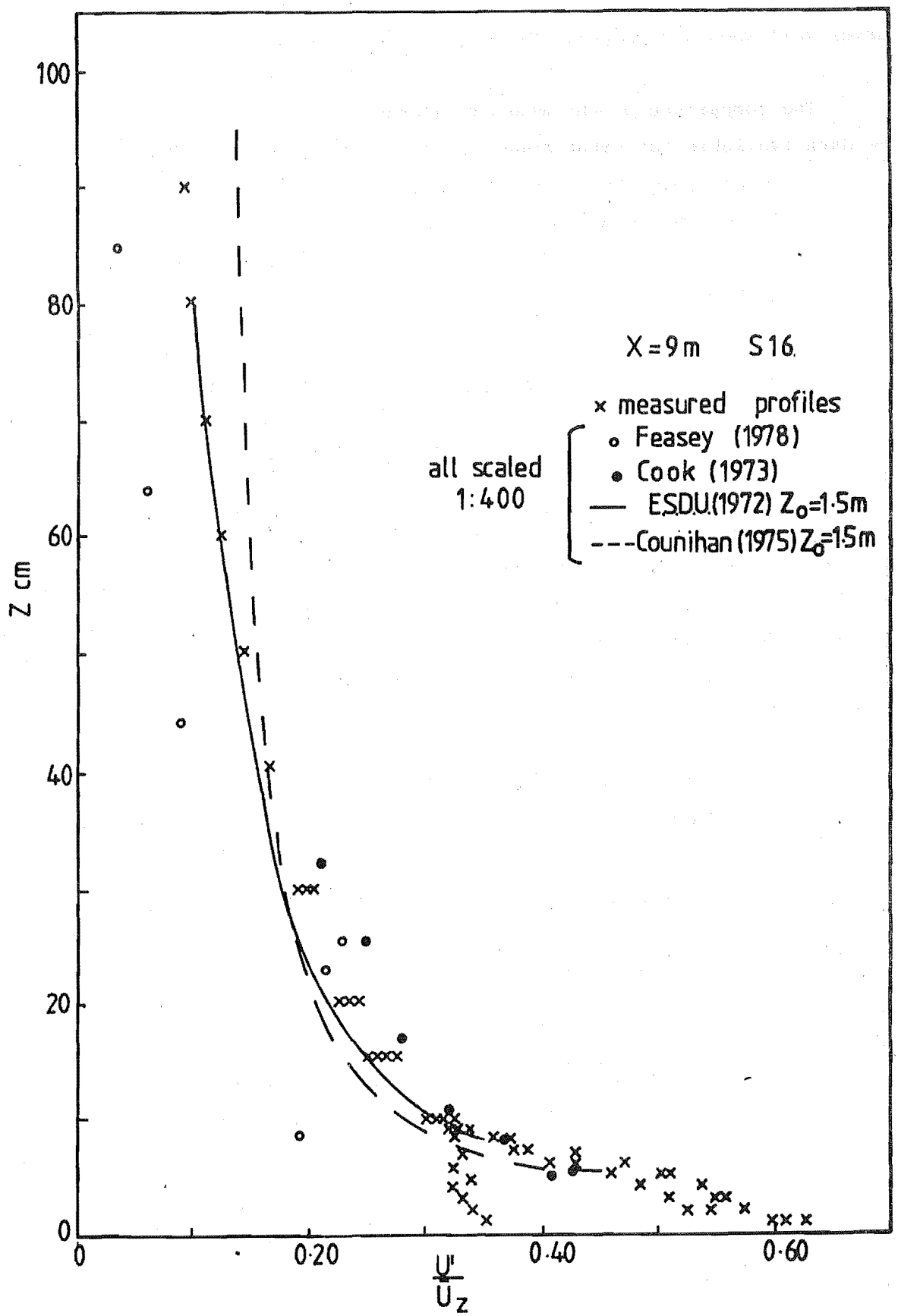

FIG 9·7 TURBULENCE INTENSITY PROFILES

(1972) data since this design curve already incorporates a zero plane displacement. The measured turbulence intensity profiles fit the design curves well when a 3 cm zero plane displacement is used.

The comparison of the measured turbulence intensity profiles with the data available for urban boundary layers was considered reasonable. It was therefore concluded that the turbulence intensity profiles were scaled at about 1:400 between the wind tunnel and the atmosphere.

9.2.3 Reynolds stress profile

The measured Reynolds stress profile is plotted in figure 9.8 and is compared with the Reynolds stress profiles in the urban simulations described by Cook (1973) and Counihan (1973). The height coordinate has not been normalised in order to show the scale differences between the simulations.

The measured shear stress profile confirms the existence of a constant shear stress region from approximately 5 cm to 50 cm and justifies the use of a logarithmic mean velocity profile in this region. The shape of the profiles compared in figure 9.8 is similar in all cases. All the profiles show relatively high values of the Reynolds stress at the roughness element height.

Comparing the Reynolds stress profile with that measured in the rural boundary layer simulation described in Chapter three, the larger roughness elements in the urban simulation give significantly higher values of the Reynolds stress reflecting the difference in the exponent of the mean velocity profile. Counihan (1973) showed that the ratio of urban to rural stresses derived on a semi-theoretical basis is 1.50. Using the maximum value of the Reynolds stress in each simulation, the ratio of urban to rural stresses in the present work is 1.10. This reflects the high Reynolds stress values in the 1:300 simulated atmospheric rural boundary layer described in Chapter three.

The value of the atmospheric surface drag coefficient k_{10} can be derived from the Reynolds stress profile using the relations:

$$k_{\infty} = -\left(\frac{\overline{uw}}{\overline{U_{\infty}}^2}\right)_{max} = 0.00274 \text{ here} \qquad (9.4)$$

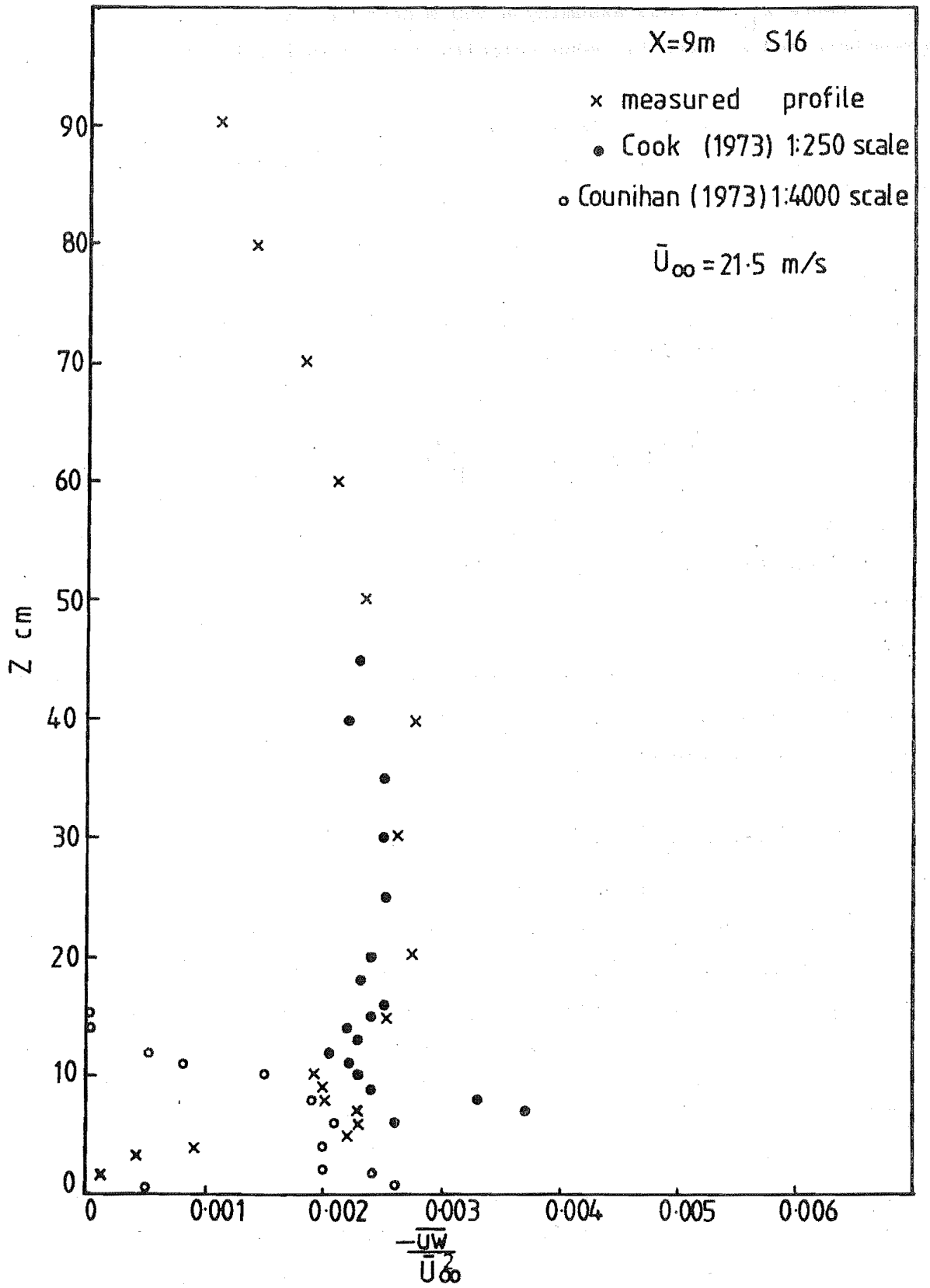

FIG 9·8 REYNOLDS STRESS PROFILE

and k_{10} can be found from

$$\frac{k_{10}}{k_\infty} = \left(\frac{\overline{U}_\infty}{\overline{U}_{10}} \right)^2 \qquad (9.5)$$

Hence $k_{10} = 0.033$ assuming a 550 m boundary layer height in the atmosphere and a power law mean velocity profile with exponent 0.29.

Davenport (1963) gives a value for k_{10} of 0.037 for $Z_o = 1.5$ m . Harris (1970) gives values for k_{10} of 0.03 to 0.05 for urban boundary layers. The value of k_{10} was therefore considered acceptable for an urban boundary layer simulation.

A value for the shear velocity u_* can also be derived from the Reynolds stress profile using the relation:

$$\left(\frac{u_*}{\overline{U}_\infty} \right)^2 = k_\infty = -\left(\frac{\overline{uw}}{\overline{U}_\infty 2} \right)_{max} \qquad (9.6)$$

which gives $u_* = 1.13$ m/s. This agrees well with a value of $u_* = 1.20$ m/s obtained from the slope of the logarithmic mean velocity profile near the ground.

The measured Reynolds stress profile was considered acceptable for an urban boundary layer simulation considering the lack of full scale Reynolds stress measurements in urban terrain.

9.2.4 u, v and w velocity component energy spectra

u velocity component energy spectra

Counihan (1975) suggests that the form of rural and urban spectra should be similar. In figure 9.9 the measured u component spectra is therefore compared to the atmospheric model spectrum proposed by Harris (1968). The measured spectra show good agreement with the curve proposed by Harris when the simulation is scaled at 1:400 between the atmosphere and the wind tunnel.

The spectra generally collapse onto a single curve, except close to the ground where there is a shift to higher frequencies. The spectra all show an inertial subrange of at least two orders of magnitude on the k axis

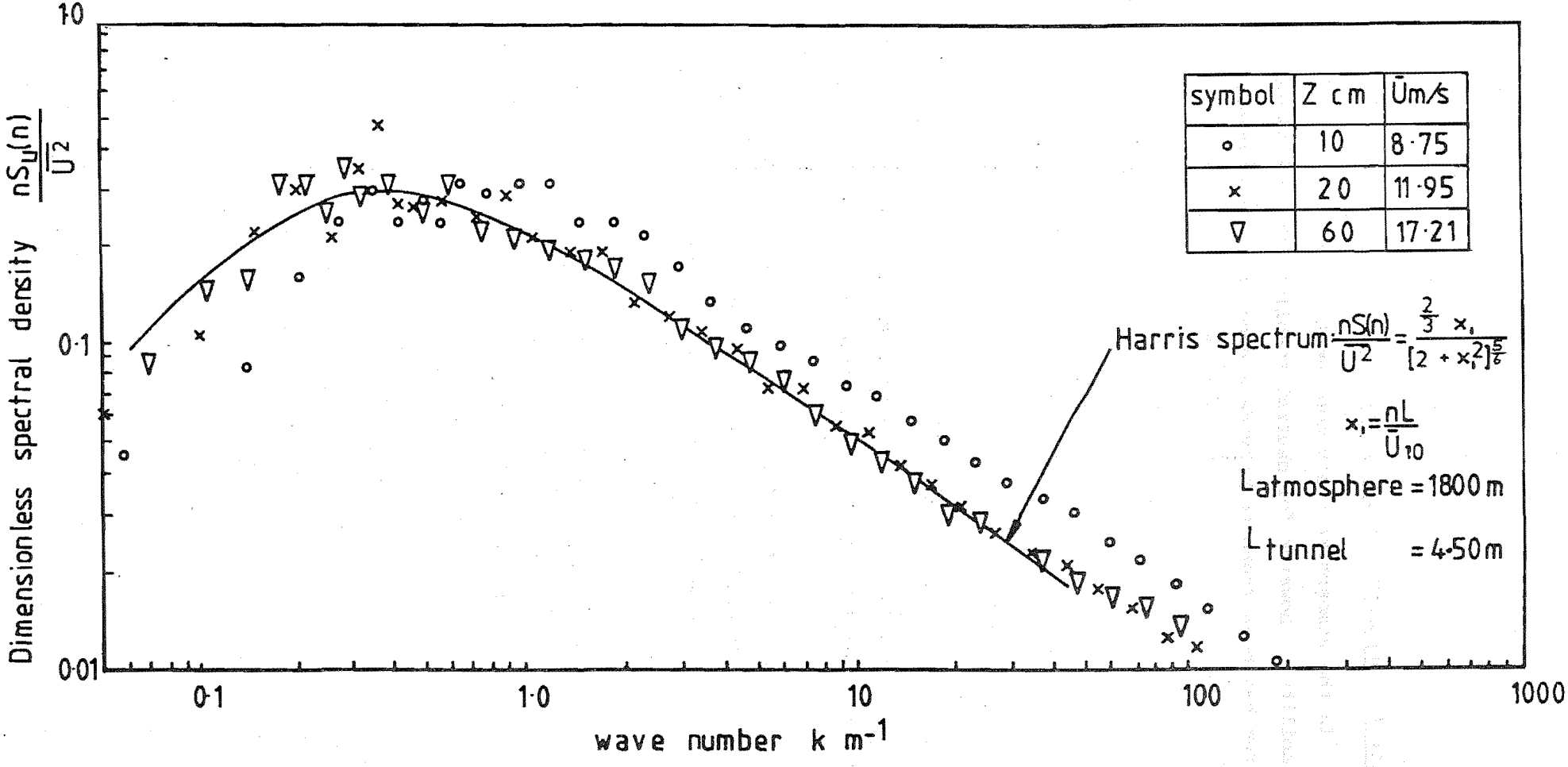

FIG 9·9 ENERGY SPECTRA FOR THE U VELOCITY COMPONENT AT X=9 m

and it is therefore unlikely that viscous effects will be important.

v velocity component energy spectra

In the atmosphere the v component energy spectra is strongly dependent on stability. However for neutral stability the von Karman isotropic spectrum has been found to provide a good fit to atmospheric data (Teunissen (1970)). This model shows good agreement with the measured spectra in figure 9.10.

As for the u component spectra the position of the spectral peak is approximately invariant with height except close to the ground, where the peak shifts to higher frequencies.

w velocity component energy spectra

The measured w component energy spectra presented in figure 9.11 shows considerable variation with height above the ground as found in the atmosphere.

Close to the ground the flatter peak of the spectrum advanced by Busch and Panofsky (1968) fits the measured spectra well. Further out in the boundary layer the von Karman isotropic spectrum provides a better fit to the measured spectra.

The length scales obtained from the spectral peaks are presented in table 9.1 and are plotted in figure 9.12 where they are compared with the variation in atmospheric length scales. The ill-defined spectral peaks make determination of the length scales uncertain.

9.2.5 Autocorrelation coefficients

The autocorrelation coefficients at X = 9 m are presented in figure 9.13. The areas under the correlation curves to the first zero crossing are summarised in table 9.1 together with turbulence length scales calculated using Taylor's hypothesis:

$$Lu_x = \overline{U} \int_0^\infty \rho_{uu_\tau} \, d\tau \qquad (9.7)$$

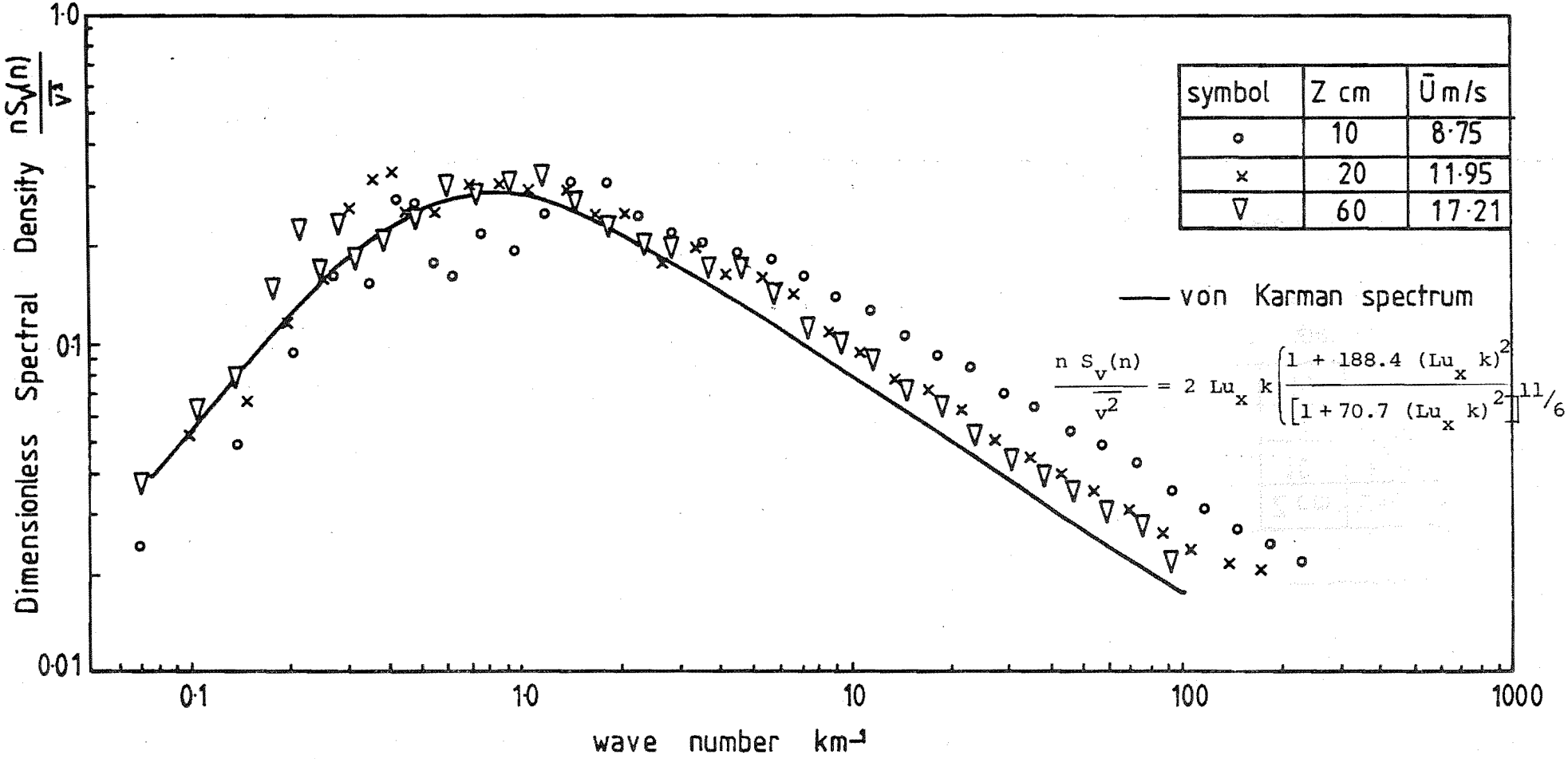

FIG 9·10 ENERGY SPECTRA FOR THE V VELOCITY COMPONENT AT X= 9m

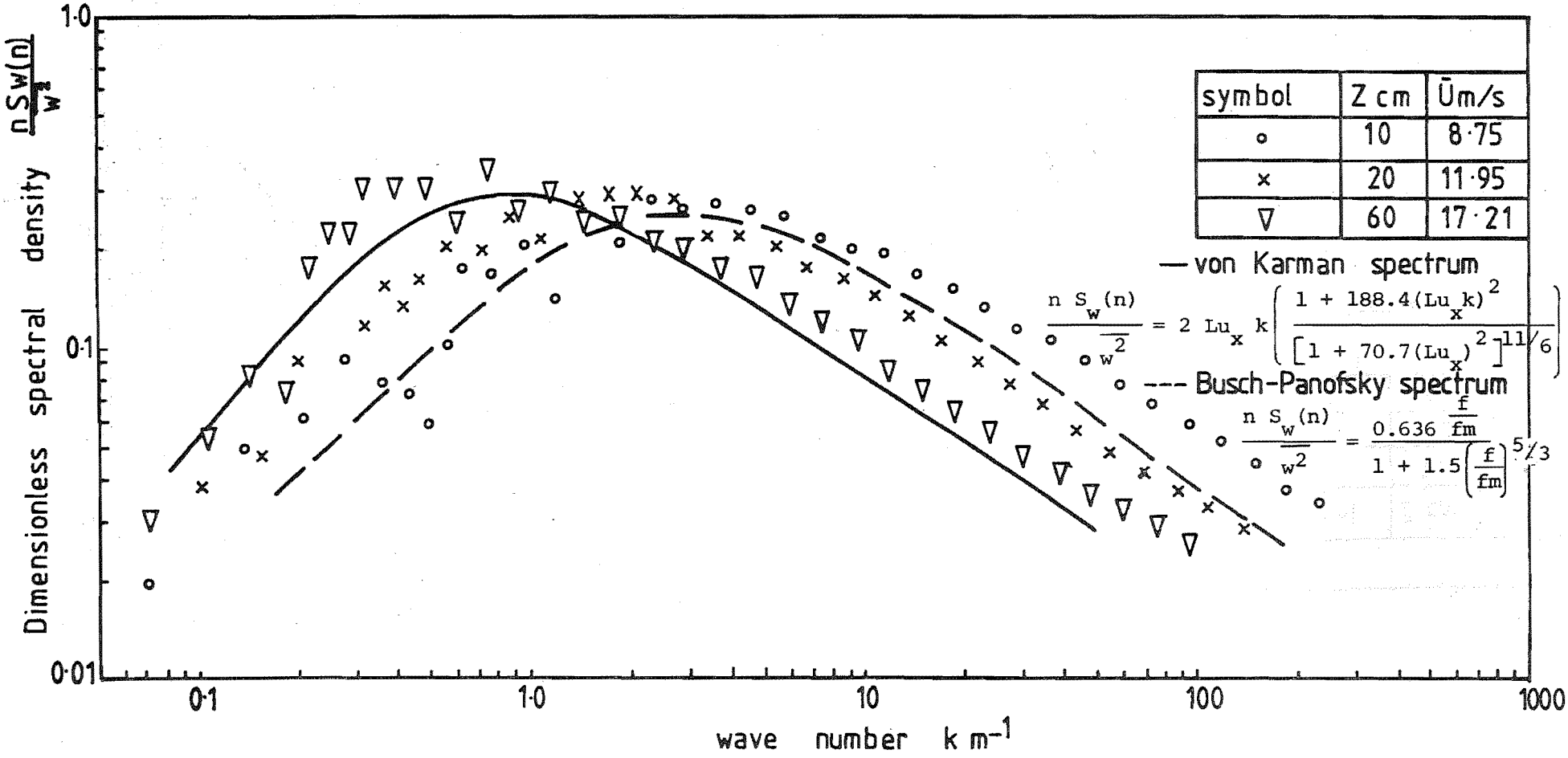

FIG 9·11 ENERGY SPECTRA FOR THE W VELOCITY COMPONENT AT X=9m

Location		Spectral peak wave number k_p m^{-1}			Area under autocorrelation curve	Integral length scales of turbulence, cm				
						Derived from spectra				Derived from autocorrelation
X m	z cm	u component	v component	w component	ms	$Lu_x = \frac{0.146}{k_{p_u}}$	$Lu_x = \frac{0.212}{k_{p_w}}$	$Lw_x = \frac{0.106}{k_{p_w}}$	$Lv_x = \frac{0.106}{k_{p_v}}$	Lu_x
9	10	0.70	1.30	3.00	27.5	20.9	7.1	3.5	8.2	24.1
9	20	0.38	0.58	1.80	34.3	38.4	11.8	5.9	18.3	41.0
9	60	0.34	0.95	0.60	27.2	42.9	35.3	17.7	11.2	46.8

TABLE 9.1 Tabulated length scale data

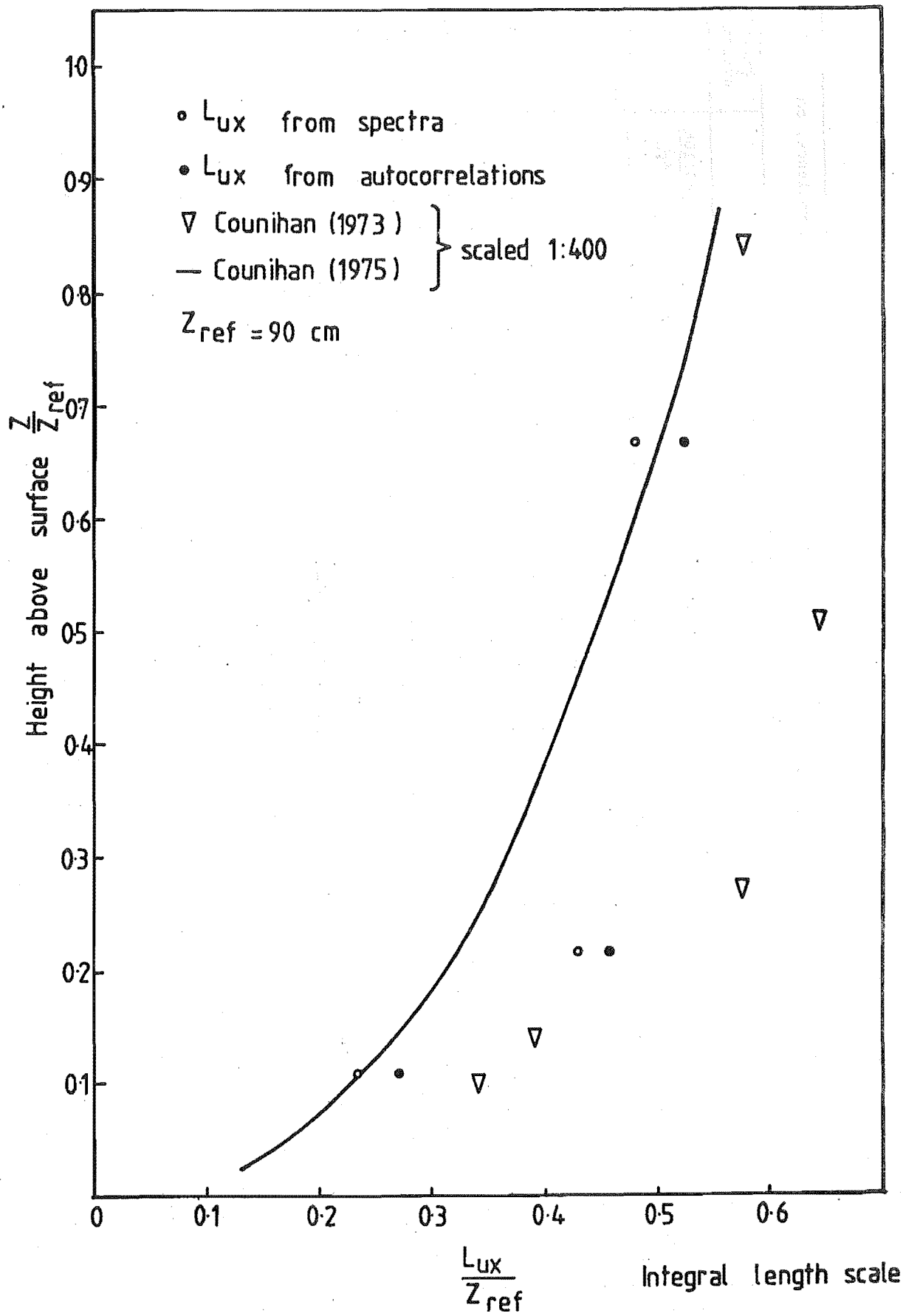

FIG 9·12 VARIATION IN TURBULENCE LENGTH SCALES WITH HEIGHT

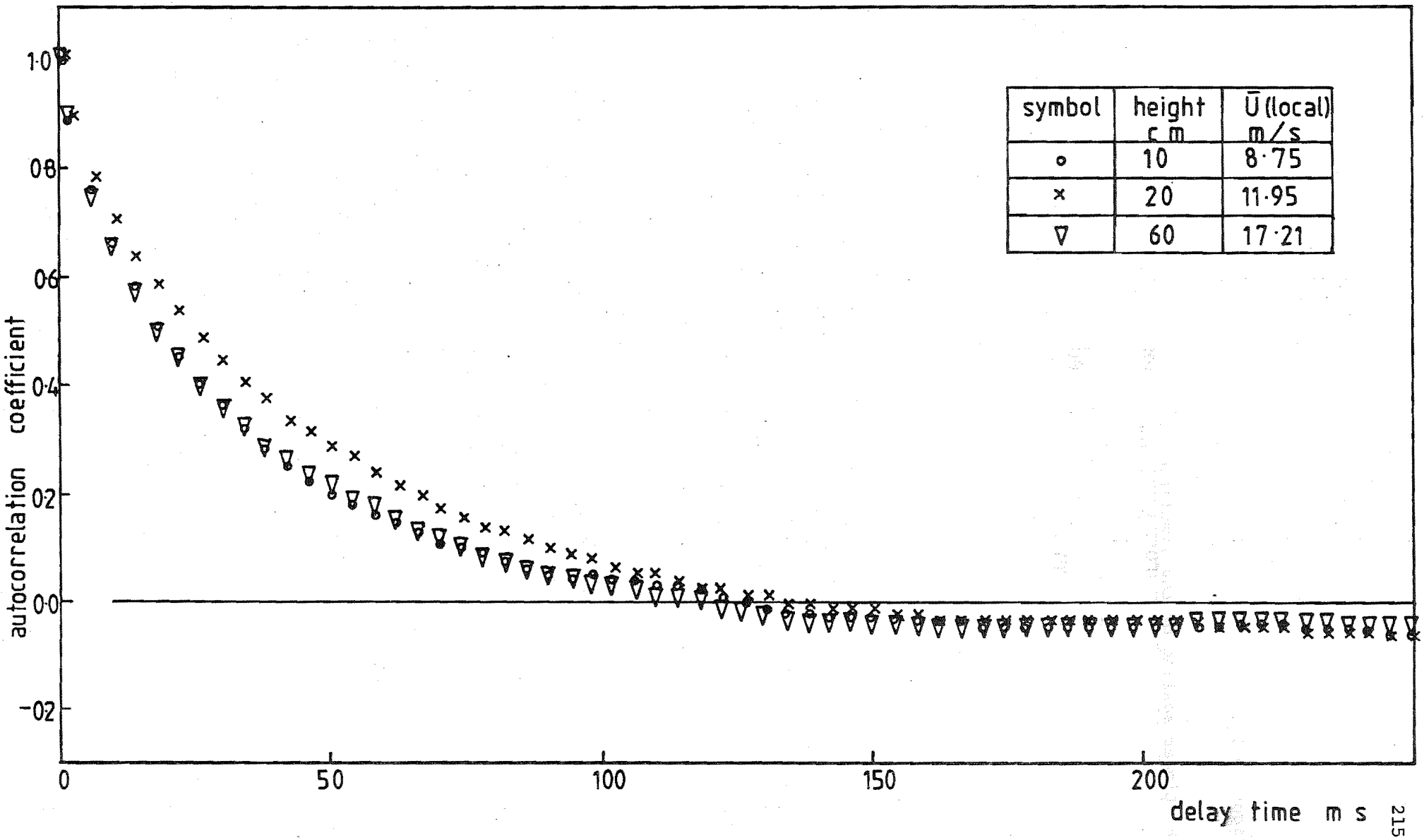

FIG 9·13 AUTOCORRELATION FUNCTIONS AT X=9m

The calculated turbulence length scales show the desired increase with height above the ground and are compared with atmospheric length scales in figure 9.12.

9.2.6 Linear scaling of the simulation

The turbulence length scales calculated from the autocorrelation curves and spectral peaks are presented in table 9.1. There is a considerable amount of scatter in the calculated values obtained using the two methods and it is uncertain whether the values obtained using the autocorrelation curves or spectral peaks are more accurate.

The vertical distribution of the measured turbulence integral scales are shown in figure 9.12. These show the desired increase in length scale with height but the measured turbulence length scale at z = 20 cm appears a little high relative to the length scales at z = 10 cm and z = 60 cm. However the measured length scales in figure 9.12 show reasonable agreement with the design curve presented by Counihan (1975) and the simulated urban boundary layer described by Counihan (1973). These have been scaled at 1:400.

The height of the urban boundary layer is a function of the fetch of urban development upwind of the site as the internal boundary layer grows from the roughness change to displace the previous boundary layer. Cook (1973) chose a value of 417 m for the height of the atmospheric boundary layer. Counihan (1975) cites 600 m as the average height of both urban and rural boundary layers. Davenport (1961) suggests an urban boundary layer height of 520 m. An atmospheric urban boundary layer height of 550 m was selected and the simulation described in this chapter is therefore only a partial depth simulation. Assuming an 0.29 mean velocity profile power law exponent, $\overline{U}_{ref}$ (the mean velocity at z_{ref} = 90 cm) is therefore 0.884 $\overline{U}_{\infty}$.

Estimates of the linear scales of the simulation are summarised in table 9.2 (page 217). The linear scale based on the turbulence length scales was calculated using the equation:

$$S = \frac{91.3\ (z-d)_m^{0.491}}{Lu_{x_m}^{1.403}\ z_{o_m}^{0.088}} \qquad (9.8)$$

Location		Linear scaling $\frac{d_m}{d_a}$ based on		Turbulence length scale Lu_x from spectra	Linear scaling $\frac{d_m}{d_a}$ based on eqtn 9.8	Turbulence length scale Lu_x from autocorrelation	Linear scaling $\frac{d_m}{d_a}$ based on eqtn 9.8
x m	z cm	$\frac{z_{o_m}}{z_{o_a}}$	Turb. intensity profile				
9	10	1:430	1:400	20.9 cm	1:370	24.1 cm	1:300
9	20	1:430	1:400	38.4 cm	1:240	41.0 cm	1:200
9	60	1:430	1:400	42.9 cm	1:370	46.8 cm	1:330

TABLE 9.2 Estimates of the linear scale of the simulation

where the subscript m refers to model values and $Z_{o_m} = 3.5 \times 10^{-3}$ m and $d = 3 \times 10^{-3}$ m. Equation 9.8 was presented by Cook (1977) and is based on the design curves of E.S.D.U. (1972). Comparison of the turbulence intensity profiles and roughness lengths leads to a linear scaling of about 1:400. Based on the turbulence length scales the linear scaling was about 1:350. It was considered that the simulation was scaled at about 1:400 between the atmosphere and the wind tunnel.

9.2.7 Static pressure gradient

The static pressure gradient along the working section was measured using the flush wall mounted static pressure taps described in section 3.1.1. The maximum variation about the mean longitudinal static pressure was 3% so the wind tunnel roof position was left unchanged from that used in the 1:300 rural atmospheric boundary layer simulation reported in Chapter three.

The static pressure gradient across the working section at X = 9 m was measured using the pitot-static rake shown in figure 3.7. The lateral static pressure was constant, within the measurement uncertainty.

9.2.8 Flow self preservation

To investigate the self preservation of the flow, all the Torro blocks beyond the row of blocks at X = 8.97 m were removed and measurements were made at a number of lateral and longitudinal positions behind the last row of blocks. The longitudinal position was always measured from the face of the Torro blocks furthest downstream.

The lateral uniformity of the mean velocity at multiples of the Torro block width W downstream of the last row of blocks is illustrated in figures 9.14 and 9.15. The logarithmic plot exaggerates the non-uniformity close to the ground. Figure 9.14 shows that 1 W downstream of the last row of roughness elements there is considerable lateral variation in the mean velocity below about 7.0 cm. At 5 W (16.0 cm) downstream the lateral uniformity appears to be excellent.

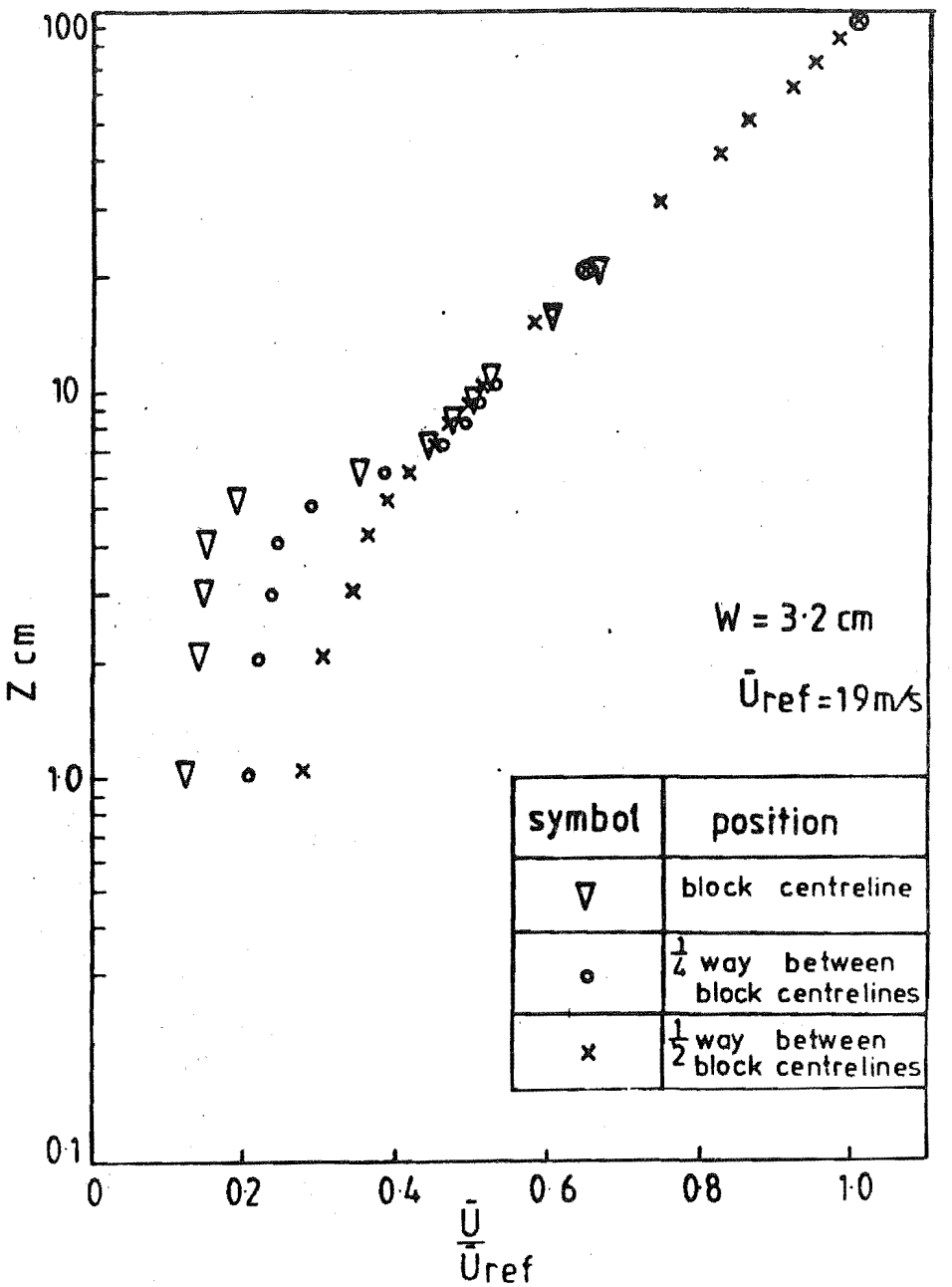

FIG 9·14 VELOCITY PROFILES AT 1W DOWNSTREAM OF THE LAST ROW OF BLOCKS

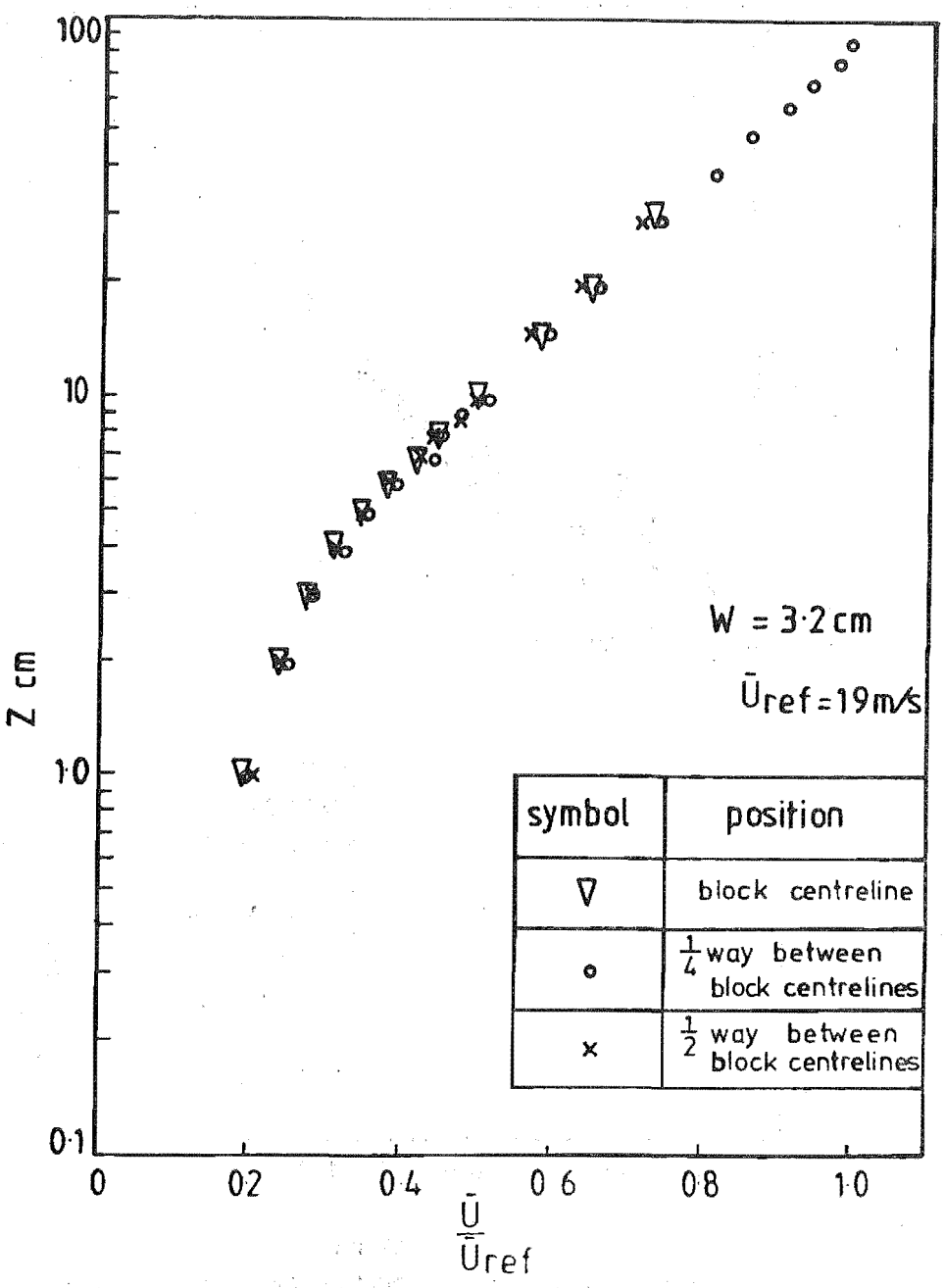

FIG 9·15 VELOCITY PROFILES AT 5W DOWNSTREAM OF THE LAST ROW OF BLOCKS

The mean velocity and turbulence intensity profiles at a fixed lateral position but a number of longitudinal positions downstream of the last row of roughness elements are illustrated in figures 9.16 and 9.17 respectively. These figures illustrate the increase in the mean velocity and decrease in the turbulence intensity close to the ground following the rough to smooth change in surface roughness.

To consider the results further, reference was made to some of the published literature on the flow of boundary layers over a sudden roughness change. The problem of an atmospheric turbulent flow above a sudden change in surface roughness has been studied by a number of authors, most of whom have developed numerical solutions to the problem.

Figure 9.18 shows a schematic representation of the rough to smooth transition based on the models of Wood (1971), Shir (1972) and Rao et.al. (1974). The flow adjusts to the new surface roughness by forming an internal layer the height of which denotes the outward extent of the velocity field affected by the new surface.

δ_u is the "velocity boundary layer" depth at which $\bar{U}_2$ is within 1% of $\bar{U}_1$. The predicted internal boundary layer depth δ_u depends on which analytical model of the flow is chosen. The model of Shir (1972) suggests a value of 18 cm for a 1.9 m (60W) fetch. The model of Rao et.al.(1974) also yields a value of 18 cm for a 1.9 m fetch. Wood (1971) suggests a value of 17 cm for a 1.9 m fetch and 5.7 cm for an 0.48 m fetch, corresponding to a fetch of 15 W in figure 9.16. From figure 9.16 the velocity boundary layer depth at an 0.48 m (15 W) fetch is about 6.5 cm and at a 1.9 m fetch, about 25 cm. The predicted estimates appear to be of the right order.

The simulated urban atmospheric boundary layer characteristics described in sections 9.2.1 to 9.2.5 were measured among the Torro block roughness elements as in the atmospheric urban boundary layer simulations of Counihan (1973) and Cook (1973). Feasey (1978) measured his boundary layer characteristics 0.5 m beyond the last roughness elements. Tieleman et.al. (1978) also measured their boundary layer characteristics 0.5 m behind the last roughness element. In both the simulations of Feasey and Tieleman et.al. the increase in mean velocity close to the ground associated with the change in surface roughness is obvious. The simulation of Tieleman et.al.

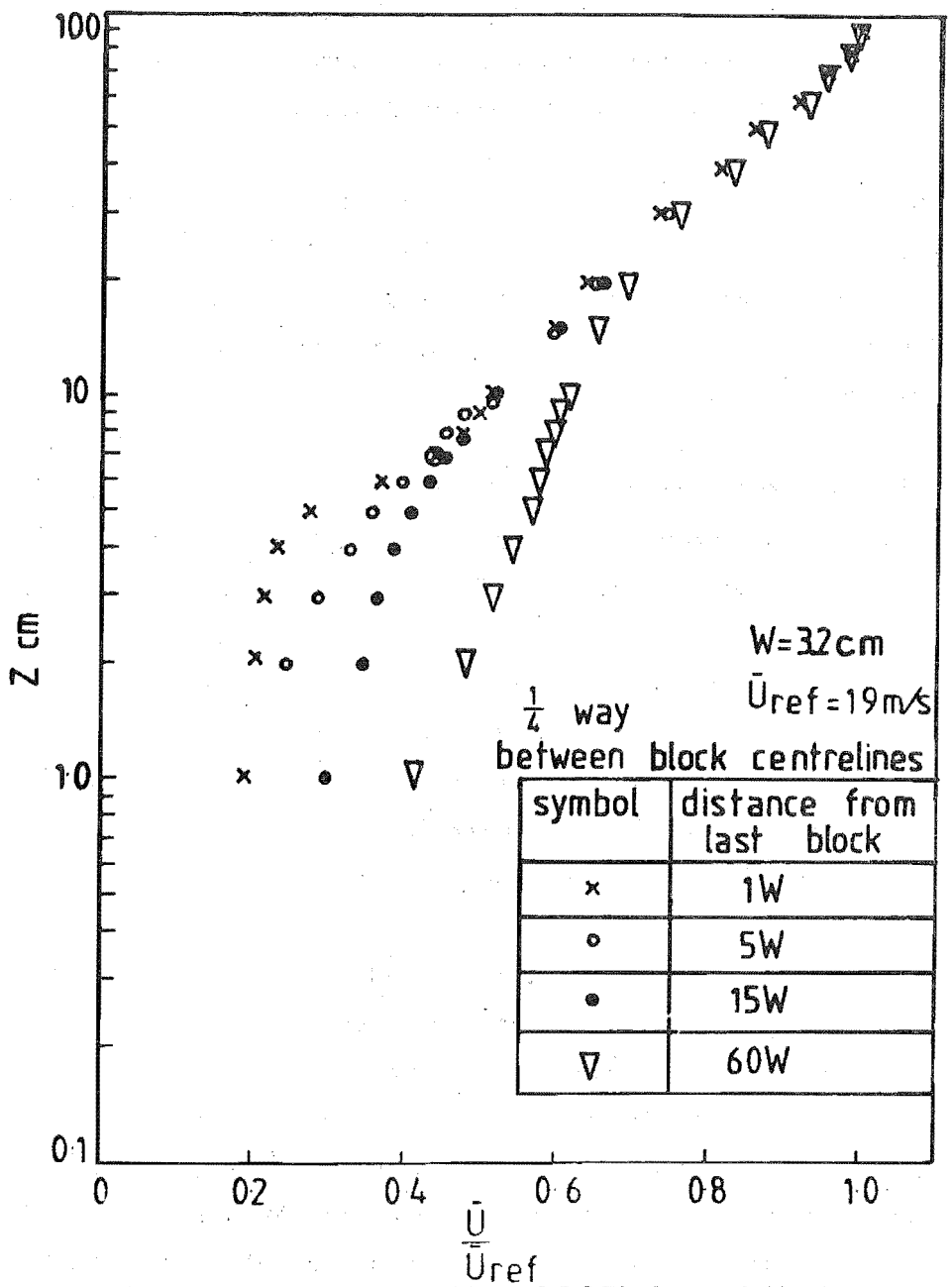

FIG 9·16 VELOCITY PROFILES DOWNSTREAM OF THE LAST ROW OF BLOCKS

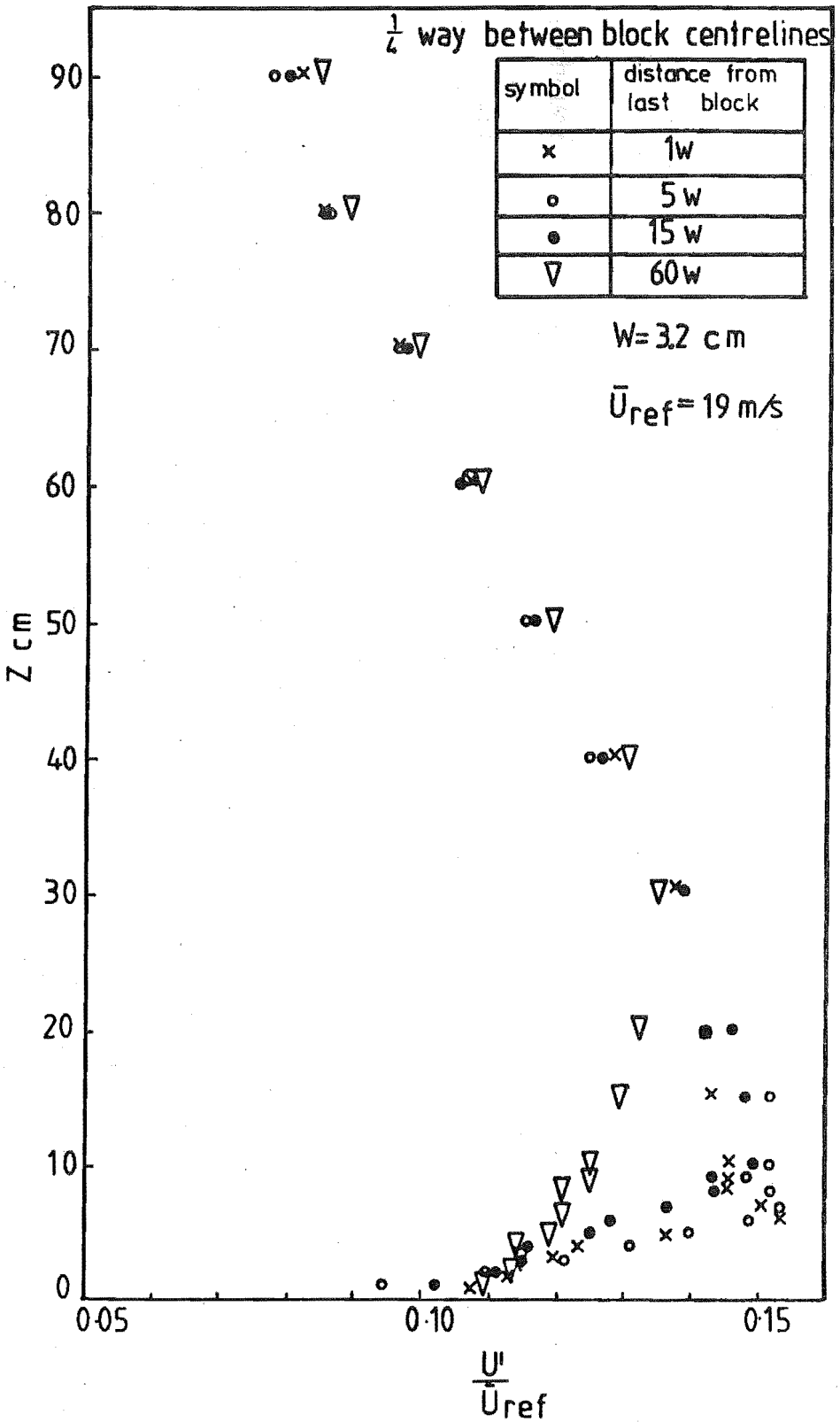

FIG 9·17 TURBULENCE INTENSITY PROFILES DOWNSTREAM OF THE LAST ROW OF BLOCKS

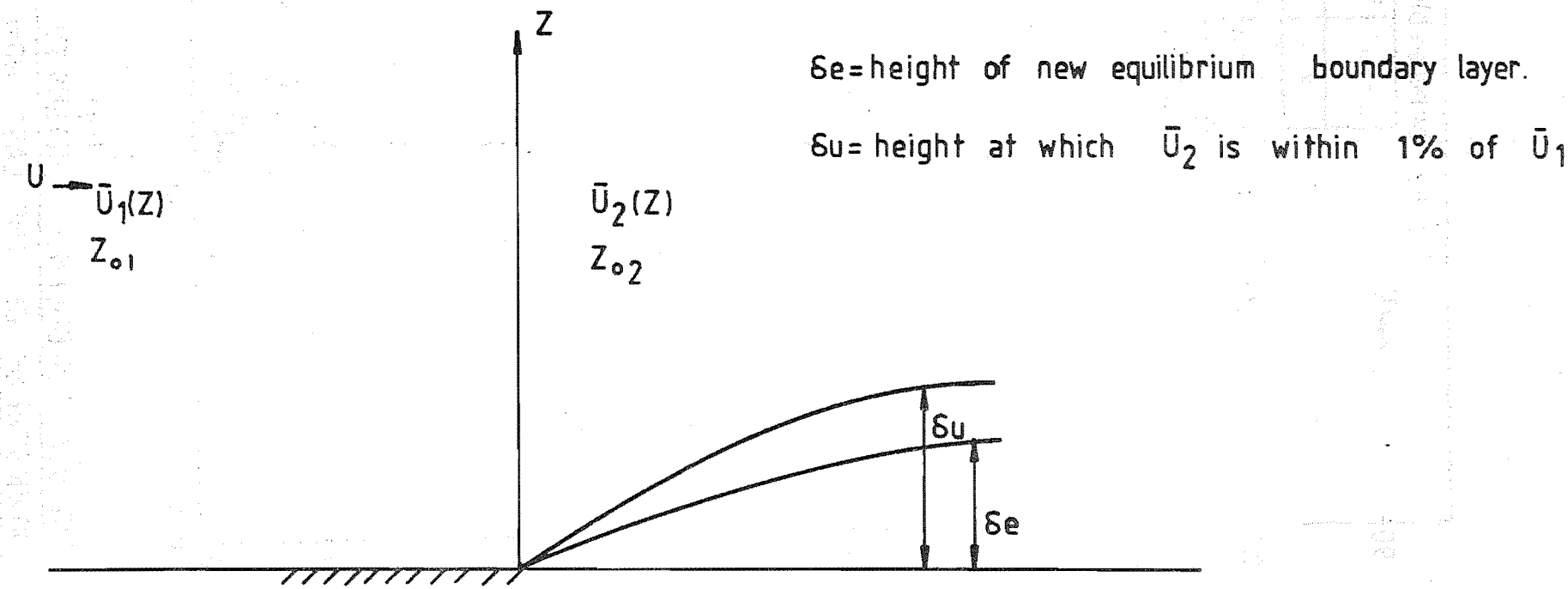

FIG 9·18 SCHEMATIC REPRESENTATION OF THE ROUGH TO SMOOTH CHANGE IN SURFACE ROUGHNESS.

has a kinked velocity profile indicative of the two surface roughnesses.

9.3 Conclusions

In this chapter the development and evaluation of a neutrally stable urban atmospheric boundary layer simulation of linear scale about 1:400 has been described.

The simulation was generated using a coarse grid, a trip fence and large blocks as surface roughness in common with a number of similar urban boundary layer models reported in the literature. The boundary layer characteristics measured among the large roughness elements were compared with those made in other urban simulations and with the design data of E.S.D.U. (1972), (1974) and Counihan (1975).

The mean velocity profiles, turbulence intensity profiles and the Reynolds stress profile were all satisfactory. The length scales of turbulence were reasonably correct except that the length scale at a height of 20 cm was a little high compared to those measured at 10 cm and 60 cm. The measured boundary layer characteristics were considered to be a good representation of a 1:400 model urban boundary layer.

In the region after the roughness elements used to achieve the simulation, measurements were made to examine the effect of the change in surface roughness. Following the rough to smooth transition the mean velocity increased and the velocity fluctuations decreased. The resulting internal boundary layer growth was well predicted by the literature.

CHAPTER 10

INFLUENCE OF THE BOUNDARY LAYER CHARACTERISTICS ON THE WIND FLOW OVER HILLS

10.1 Introduction

The purpose of the tests described in this chapter was to examine the effect of the approach mean velocity and turbulence profiles on the wind flow over model hills.

All the work presented in the preceeding chapters used approach boundary layer characteristics which modelled the flow over rural terrain. In the atmosphere the mean velocity and turbulence profiles vary over a wide range depending on the surface roughness. The work presented in this chapter should assist the application of the results obtained in the present work to various terrain types.

To examine the effect of the incident boundary layer characteristics on the wind flow over the model hills, measurements were made over triangular hills with aspect ratios of 0.1 and 1.0. These model hills were placed in the 1:400 simulated urban boundary described in Chapter nine. The measurements were compared with those made over the same hills in the 1:300 rural boundary layer model. Conclusions were therefore able to be made on the effect of the incident mean velocity and turbulence profiles on the wind flow over the model hills. The small difference in the scale of the simulations was not believed to be significant considering the results presented in Chapter eight.

10.2 Experimental procedure

The two model triangular hills with $\frac{H}{L}$ values of 0.1 and 1.0 were placed in turn in the simulated urban boundary layer described in Chapter nine. The model hills were covered with Torro baseboard and were the same as those used in the work described in Chapter six.

Covering the model hills with the block roughness elements used in the urban model boundary layer was considered. In this case the measured flow characteristics would be dependent on the measurement position relative

to the roughness elements. It was therefore decided to use the model hills covered with only the Torro baseboard and accept the internal boundary layer growth due to the roughness change as discussed in section 9.2.8.

The last row of Torro blocks were therefore placed in the wind tunnel at X = 9.32 m and the model hills were installed in the wind tunnel so that their upstream foot was at X = 9.5 m. After the model hills were placed in the wind tunnel the approach reference profiles were unchanged from those measured before the hills were installed.

Measurements over the two triangular hills were made at the same vertical and streamwise locations as were used in the tests in the model rural boundary layer. These locations are recorded in section 4.3. The vertical locations were measured above the zero plane displacement height of 3 cm instead of above the hill surface. Measurements were made at only one lateral position, 25 cm south of the wind tunnel centreline.

No measurable changes in the static pressure gradient at mid-tunnel height were observed after the installation of the hill models. Pressure corrections by means of the wind tunnel roof adjustment were therefore not made.

The mean velocity, velocity fluctuations, energy spectra and autocorrelation functions measured over the two model hills are presented below. The results are discussed in section 10.4 in relation to the literature reviewed in Chapter two.

10.3 Experimental results

10.3.1 Mean velocity profiles and amplification factors

Lines of equal amplification factor for the two hills in the 1:400 simulated atmospheric urban boundary layer are presented in figure 10.1. These may be compared to the lines of equal amplification factor for the flow over the same shaped hills in the model rural boundary layer which are also presented in figure 10.1. At any point over the two hills the amplification factor was always larger when the hills were placed in the urban boundary layer.

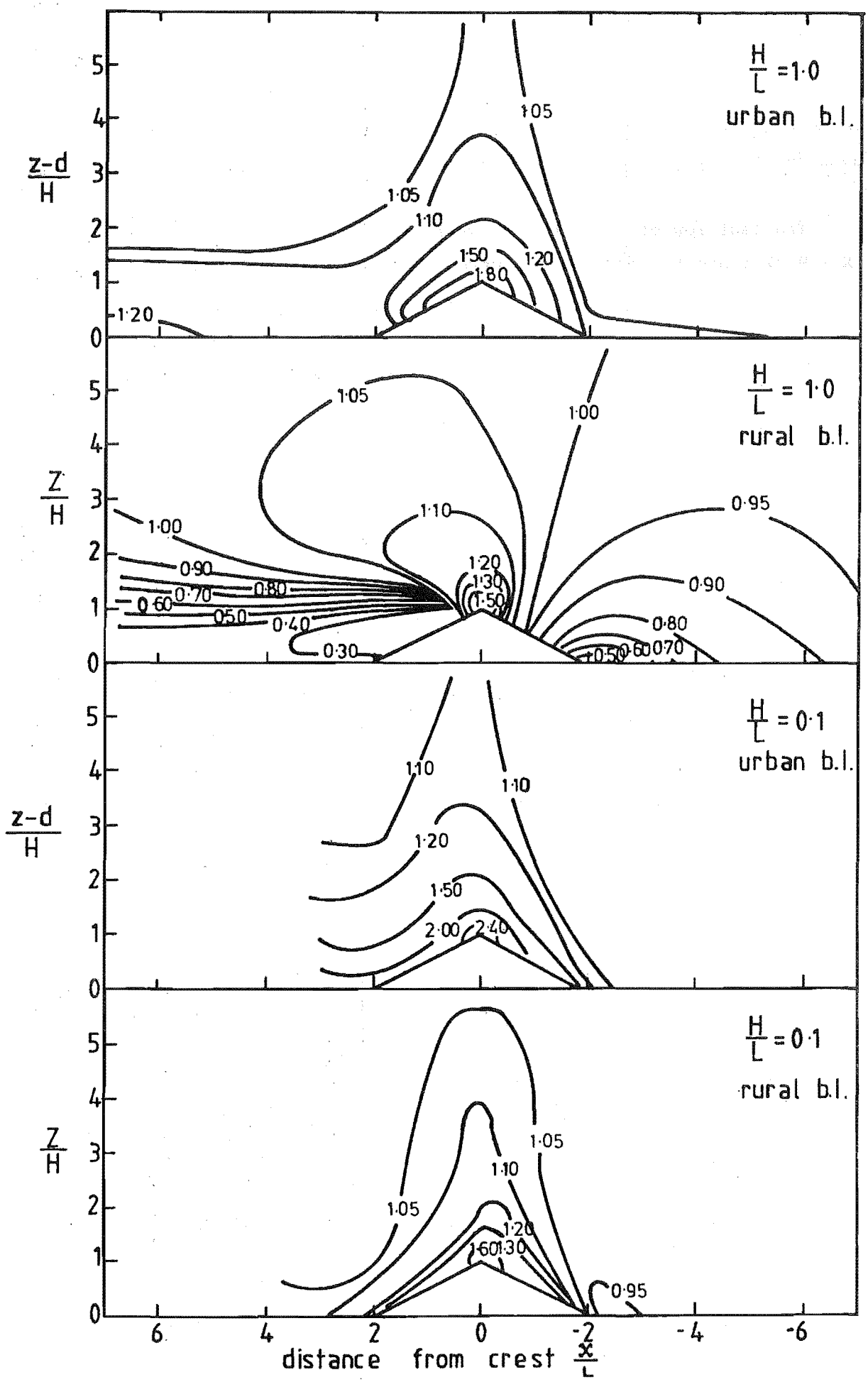

FIG. 10.1 LINES OF EQUAL AMPLIFICATION FACTOR

In the region before the crest the largest changes in the amplification factor occur for the hill with $\frac{H}{L} = 1.0$ as illustrated in the table below:

$\frac{z - d}{H} = 0.2$	$\frac{H}{L} = 1.0$		$\frac{H}{L} = 0.1$	
$\frac{x}{L}$	-1.0	-2.0	-1.0	-2.0
Increase in the amplification factor between the rural and urban model boundary layers.	1.46	1.98	1.29	1.26

In figure 10.2 the amplification factors at the crest for the two hills in the rural and urban model boundary layers are compared. The largest difference in the amplification factors between the two boundary layers occurs close to the ground and the difference between the amplification factors decreases rapidly as the distance above the ground increases. Close to the ground at the crest the amplification factor for the hill with $\frac{H}{L} = 1.0$ is about 30% greater in the urban boundary layer and for the hill with $\frac{H}{L} = 0.10$ about 45% greater.

After the crest the largest difference in the amplification factors between the urban and rural boundary layers occurs for the hill with $\frac{H}{L} = 1.0$. A large region of low amplification factors behind the hill did not occur for this hill in the urban model boundary layer. This was probably due to the reduced effect of the sharp edged crest in the urban model boundary layer as all the measurements were made above the zero plane displacement height of 3 cm.

10.3.2 Turbulence intensity profiles

Isoturbs for the two hills in the simulated urban boundary layer are shown in figure 10.3. These may be compared with the corresponding figures for the same shaped hills in the simulated rural boundary layer which are also illustrated in figure 10.3.

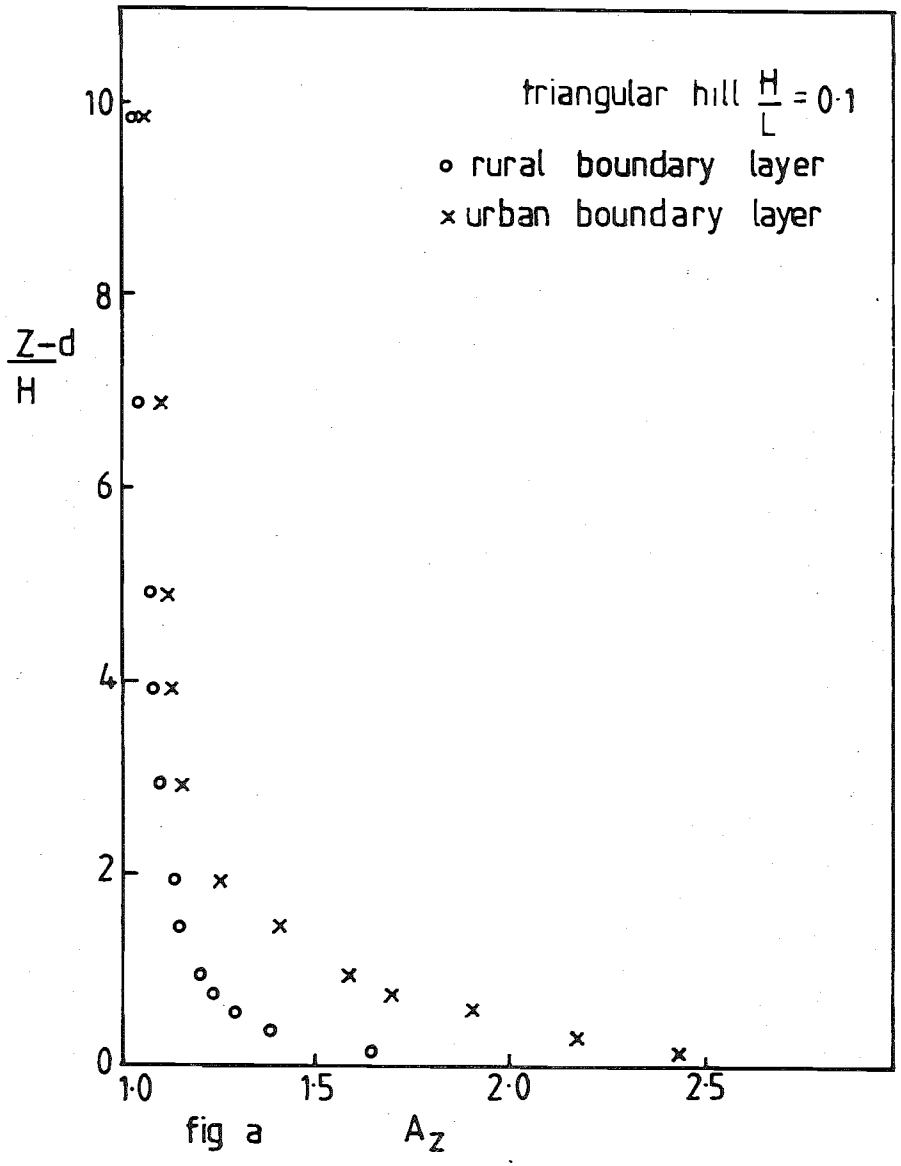

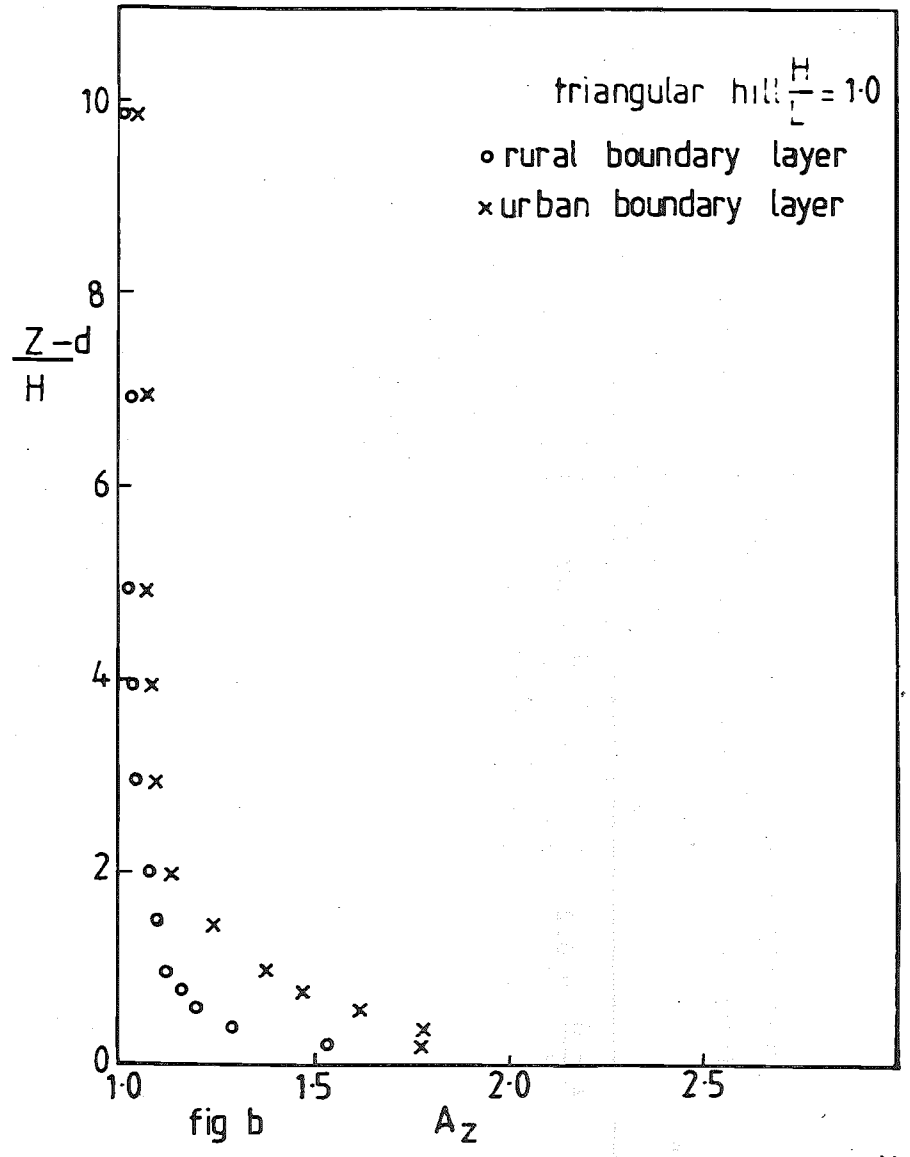

FIG 10.2 COMPARISON OF AMPLIFICATION FACTORS AT THE CREST

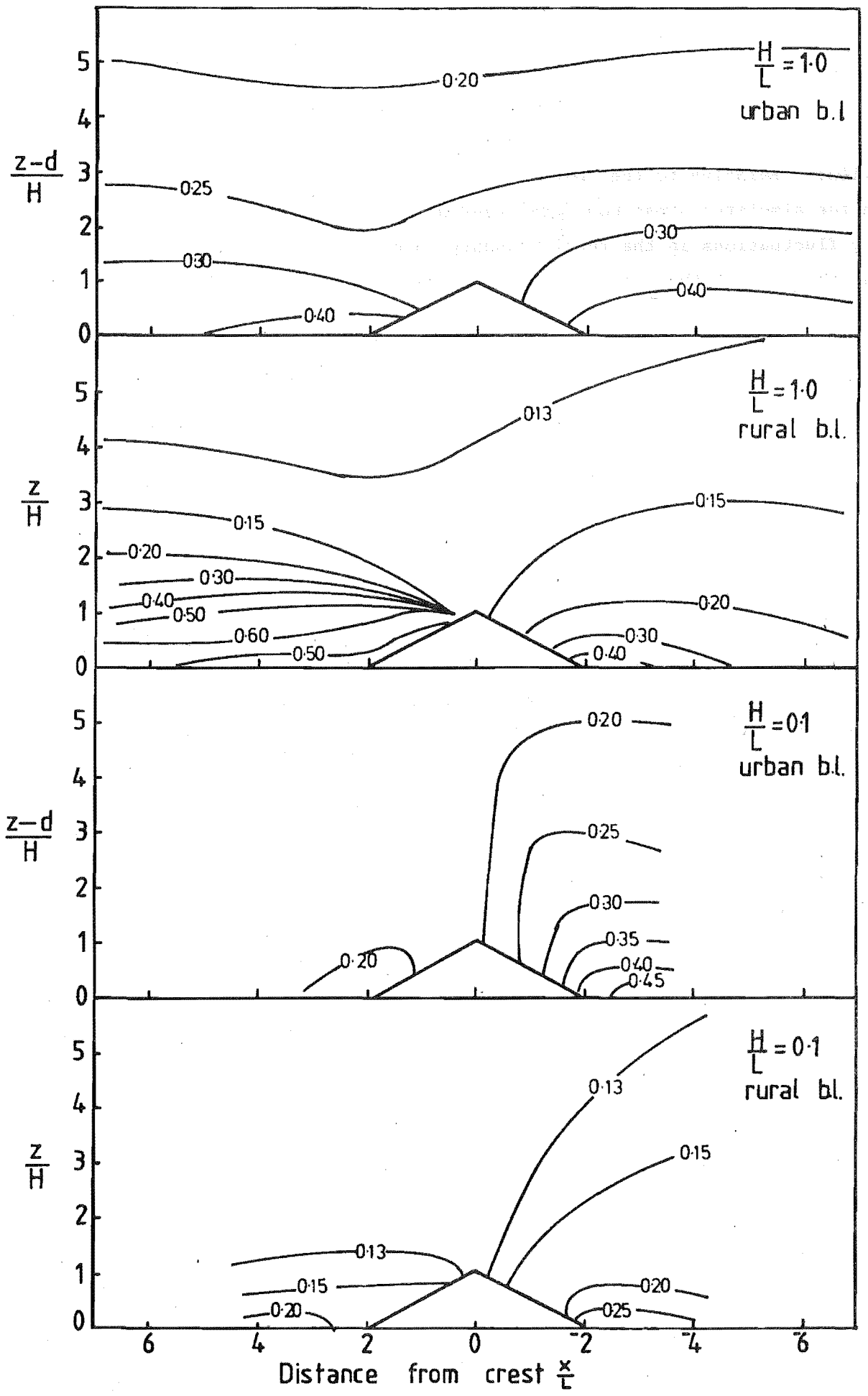

FIG. 10.3 ISOTURBS OVER THE TRIANGULAR HILLS

In both model atmospheric boundary layers the velocity fluctuations u' and the local turbulence intensity $\frac{u'}{U}$ decrease towards the crest of the hills. Relative to the upstream reference values the velocity fluctuations in the simulated urban boundary layer do not decrease as much as the velocity fluctuations in the rural boundary layer in the region before the crest. But the local turbulence intensity decreases more rapidly for the hills in the urban boundary layer in this region reflecting the greater relative increase in the mean velocity in the model urban boundary layer relative to the rural boundary layer.

At the hill crests the velocity fluctuations have decreased less in the urban boundary layer for the hill with $\frac{H}{L} = 1.0$ and more for the hill with $\frac{H}{L} = 0.1$ as shown in figures 10.4 and 10.5.

In the region after the crest for both hills in both boundary layers the velocity fluctuations relative to the upstream values are similar. But the local turbulence intensity is much lower relative to the upstream values in the urban boundary layer. This reflects the relatively higher mean velocity in this region in the urban model boundary layer.

Changes in the local turbulence intensity well above the hill are much more pronounced when the hills were in the model rural boundary layer. This may be seen by comparing the vertical distance moved by the 0.20 and 0.13 isoturbs for the hill with $\frac{H}{L} = 1.0$ in figure 10.3.

10.3.3 u velocity component energy spectra and autocorrelation coefficients

The u component energy spectra and autocorrelation functions for the flow over the hills in the simulated urban atmospheric boundary layer were measured at heights of $\frac{z-d}{H}$ equal to 0.2, 1.0 and 2.0. The spectrum at a height of $\frac{z-d}{H} = 0.2$ in the urban boundary layer upstream reference position was measured at a height which was below the height of the roughness elements. It is therefore likely that the spectrum at this height was dependent on the measuring position relative to the roughness elements. The spectral peak values are summarised in table 10.1. These values may be compared to the corresponding values for the same hills in the model rural boundary layer which are presented in table 4.1.

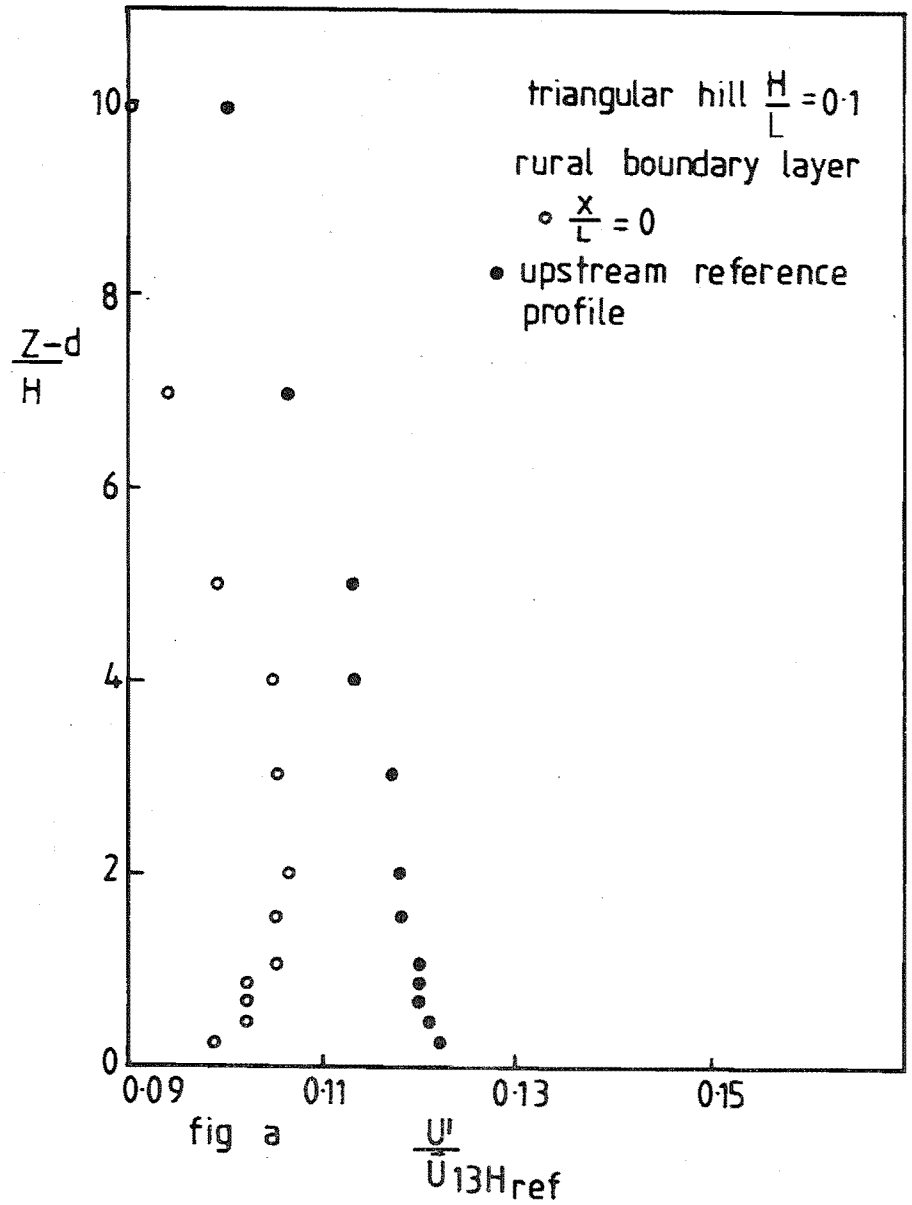

fig a

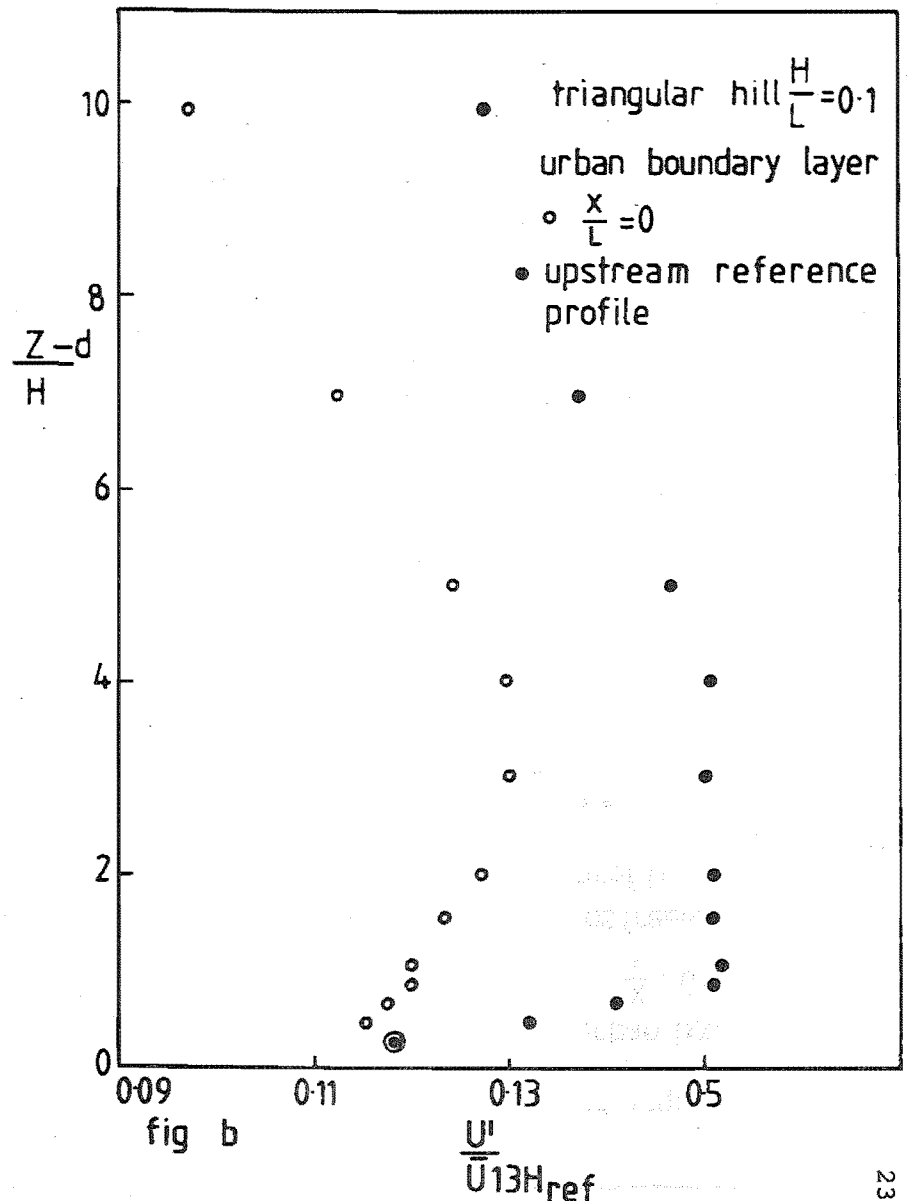

fig b

FIG. 10.4 TURBULENCE PROFILES UPSTREAM AND AT CREST FOR $\frac{H}{L}$ = 0·1

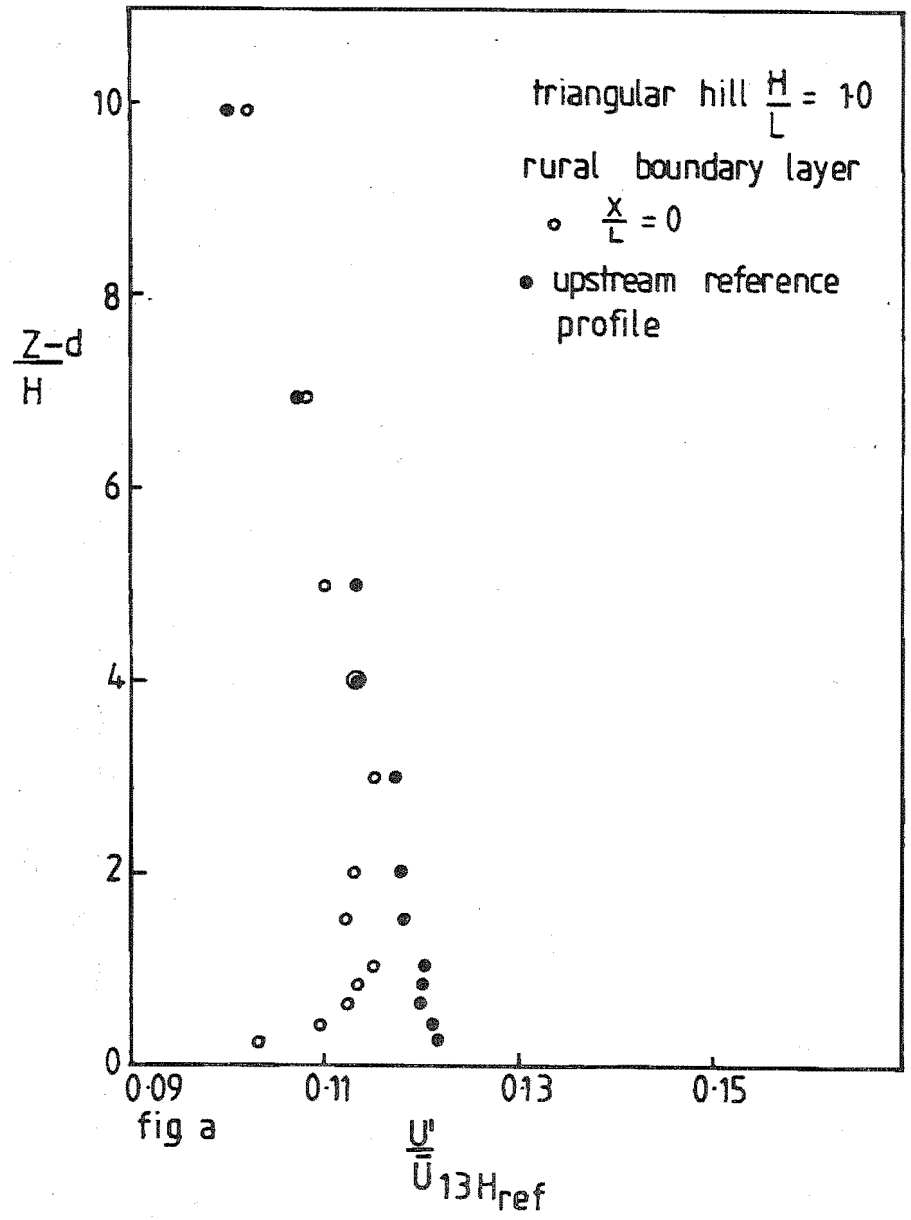

fig a

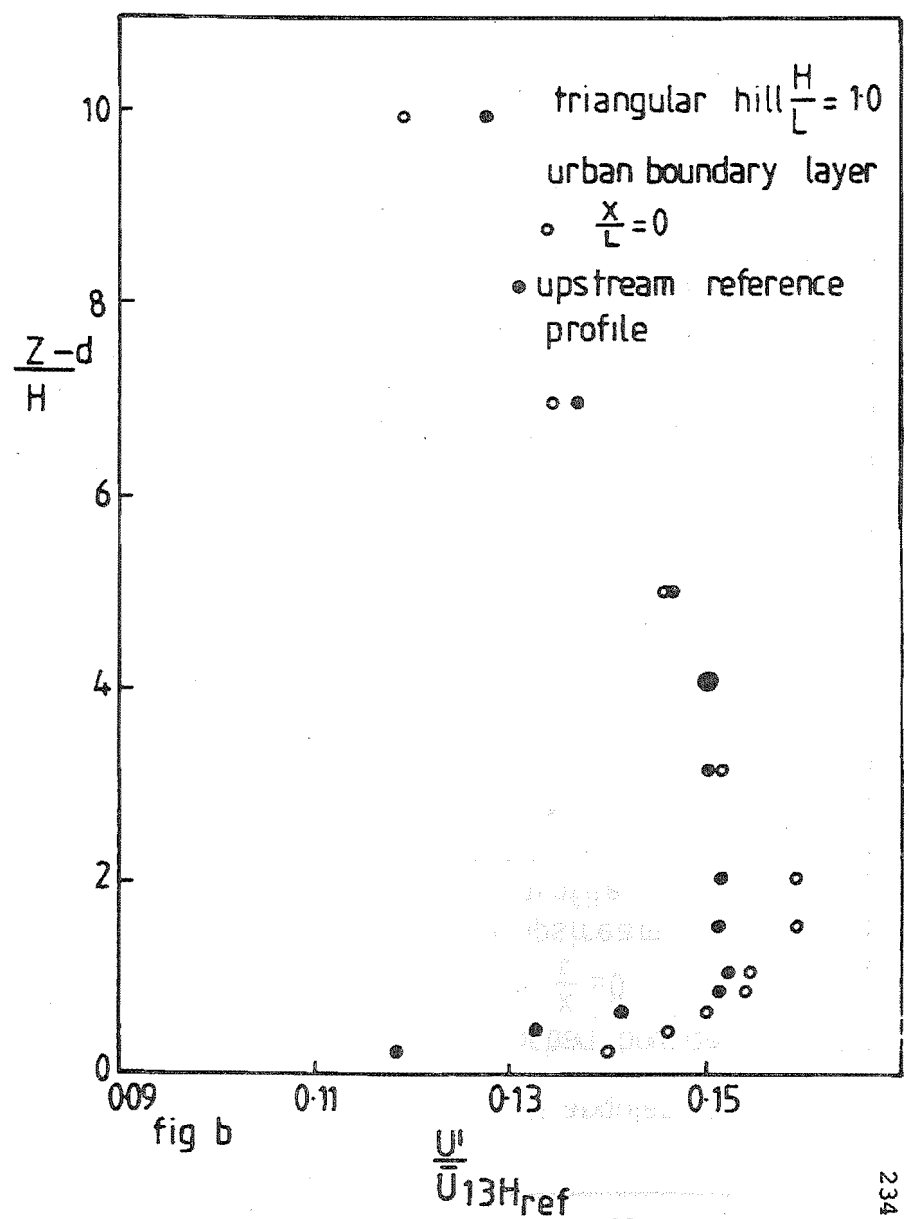

fig b

FIG. 10.5 TURBULENCE PROFILES UPSTREAM AND AT THE CREST FOR $\frac{H}{L} = 1{\cdot}0$

boundary layer scale	$\frac{z}{H}$	$\frac{z}{H}$ = 0.2									$\frac{z}{H}$ = 1.0									$\frac{z}{H}$ = 2.0								
		10H upstream of the hill			crest			10H downstream of the hill			10H upstream of the hill			crest			10H downstream of the hill			10H upstream of the hill			crest			10H downstream of the hill		
		k_p	n_p	T_E	k_p	n_p	T_E	k_p	n_p	T_E	k_p	n_p	T_E	k_p	n_p	T_E	k_p	n_p	T_E	k_p	n_p	T_E	k_p	n_p	T_E	k_p	n_p	T_E
		m^{-1}	H_z	ms	m^{-1}	H_z	ms	m^{-1}	H_z	ms	m^{-1}	H_z	ms	m^{-1}	H_z	ms	m^{-1}	H_z	ms	m^{-1}	H_z	ms	m^{-1}	H_z	ms	m^{-1}	H_z	ms
urban 1:400	0.1	1.30	6.3	20.2	0.37	4.4	36.2	0.60	6.0	37.6	0.88	6.9	33.2	0.40	4.9	39.7	0.40	4.5	49.4	0.40	4.1	47.6	0.25	3.2	40.3	0.25	3.0	38.8
	1.0	1.30	6.3	20.2	0.85	7.3	37.9	0.65	5.1	29.5	0.88	6.9	33.2	0.48	5.2	42.9	0.62	5.7	36.1	0.40	4.1	47.6	0.38	4.5	40.7	0.42	4.4	40.6
rural 1:300	0.1	0.82	6.4	17.7	0.28	3.6	29.2	0.96	7.9	22.2	0.37	4.1	27.6	0.30	4.0	34.5	0.39	4.6	32.2	0.35	4.3	28.0	0.34	4.8	34.2	0.34	4.3	32.0
	1.0	0.82	6.4	17.7	0.34	4.3	25.6	2.90	15.9	12.9	0.37	4.1	27.6	0.33	4.5	28.7	1.10	8.7	15.6	0.35	4.3	28.0	0.33	4.6	29.9	0.70	7.7	20.9

TABLE 10.1 Integral time scales and spectral peak values for the triangular hills in the model urban boundary layer.

At the hill crests in both simulated boundary layers there is a shift of the spectral peak to lower wave numbers compared to the upstream reference spectra. The shift to lower wave numbers is larger for those hills in the urban boundary layer. For example consider the spectra for the hill with $\frac{H}{L}$ of 1.0 at a height of $\frac{z-d}{H} = 1.0$. In the urban boundary layer the spectral peak is 0.45 of its upstream value whereas the corresponding value for the rural boundary layer is 0.81. This trend decreases with height above the crest. At $\frac{z-d}{H} = 2.0$ there is virtually no difference between the spectra at the crest and the upstream reference spectra in either boundary layer.

Values of the integral time scale calculated from the measured autocorrelation functions are presented in table 10.1. These values may be compared to values for the same hills in the model rural boundary layer, as presented in table 4.1. Relative to the upstream reference values the integral time scales at the crest and downstream of the model hills are considerably greater in the urban boundary layer than in the rural boundary layer. For example consider the hill with $\frac{H}{L} = 1.0$ at a height of $\frac{z-d}{H} = 0.2$. In the urban boundary layer the integral time scale is 1.9 times its upstream value at the crest and 1.5 times its upstream reference value downstream of the hill. In the rural boundary layer the integral time scale is 1.5 times its upstream value at the crest and 0.7 times its upstream reference value downstream of the hill.

10.4 Discussion of the experimental results

An increase in the surface roughness caused the amplification factors at the hill crest to increase and a larger reduction in the velocity fluctuations over the hill. The energy spectra showed a much larger shift to lower wave numbers at the hill crest following an increase in the surface roughness. This indicated a larger decrease in the average eddy size.

In this section the experimental results are discussed and compared with the literature reviewed in Chapter two.

10.4.1 Comparison with theoretical models

Alexander and Coles (1971) calculated the velocity profiles over two hill shapes subject to incident mean velocity profiles with power law exponents of 0.16 and 0.28. The speedup over the hills was found to be

slightly greater for the 0.16 mean velocity profile which corresponded to the smoother surface. Alexander and Coles suggest that this is because of the gentler slope of the approach velocity profile. This result is contrary to the conclusions of the other investigations discussed in this section and also to the experimental results presented in section 10.3. The absence of confirmation of the trends found by Alexander and Coles is probably due to their incorrect assumptions regarding the eddy viscosity as discussed in section 2.1.1.

From his theoretical study of wind flow over hills, Sacre (1974) concluded that an increase in the surface roughness and the accompanying change in the upstream mean velocity profile could increase the speedup effects by about 30%.

Bowen and Lindley (1974) applied their potential flow model to the flow over escarpments. They found that an increase in the power index of the mean velocity profile increased the amplification factors at the escarpment crest.

Jackson and Hunt (1975) tabulate the change in the fractional speedup for different values of the surface roughness Z_o. For a fixed hill shape the fractional speedup increases by a maximum of about 10% for an order of magnitude increase in Z_o. The amount of the increase decreases with height.

Astley (1977) presented results for the flow over an escarpment of slope 1:2 obtained using a finite element method in conjunction with a frozen vorticity assumption. The variation of the fractional speedup with height for uniform flow and incident mean velocity profile power law exponents of $\frac{1}{6}$ and $\frac{1}{12}$ were calculated at a number of positions over the hill surface. The results show that the speedup at the crest decreases as the mean velocity profile power law exponent of the upstream reference profile decreases, corresponding to a decrease in the surface roughness.

Bouwmeester et.al. (1978) investigated changes in the amplification factor at the hill crest with the surface roughness of the approach flow by utilising the inviscid flow model presented by Derickson and Meroney (1977). The mean velocity over a bell-shaped hill with $\frac{H}{L} = 0.1$ was calculated for values of $\frac{Z_o}{\delta}$ ranging from 4.6×10^{-4} to 2.8×10^{-8} and values

of $\frac{H}{\delta}$ of 4, 0.4 and 0.04. The values of $\frac{Z_o}{\delta}$ are generally too small to represent realistic surface conditions: E.S.D.U. (1972) quotes a value of $\frac{Z_o}{\delta} \doteq 10^{-4}$ for a rural atmospheric boundary layer. The upwind velocity distribution used by Bouwmeester et.al. for $\frac{H}{\delta} = 0.4$ and the corresponding fractional speedup profiles at the hill crest are shown in figures 10.6 and 10.7. The results show a slight decrease in the fractional speedup as the surface roughness decreases. This trend was found to be largest for small values of $\frac{H}{\delta}$.

The above theoretical studies generally support the results presented in section 10.3 of an increase in the amplification factor at the hill crest as the surface roughness of the approach flow increases.

10.4.2 Comparison with laboratory work.

de Bray (1973) made measurements over escarpments in a wind tunnel using a number of boundary layers with different mean velocity profiles. Because of the similarity of the potential flow fields around the leading parts of bodies irrespective of their downstream shape the results obtained from escarpments should be similar to those measured over the model hills used in the present work.

Mean velocity measurements were made over an escarpment with a sine ramp of $\frac{H}{L} \doteq 0.70$ for the case of uniform flow and shear flow with a mean velocity profile power law exponent of 0.14. Close to the ground the uniform flow yielded less speedup over the escarpment. For example at the crest the maximum amplification factor for the shear flow was 2.0 whereas for the uniform flow case it was 1.77.

Mean velocity measurements were also made over an escarpment with a source ramp which had an $\frac{H}{L}$ value considerably greater than 1.0. Three approach mean velocity profiles were used: uniform flow and mean velocity profiles with power law exponents of 0.11 and 0.14. The shear flows were found to yield much larger speedup over the escarpments and the higher the power law exponent the larger the speedup.

Bouwmeester et.al. (1978) report measurements made over a triangular hill of $\frac{H}{L} = 0.5$ for two approach flow surface roughnesses of $\frac{Z_o}{\delta} = 1.2 \times 10^{-4}$

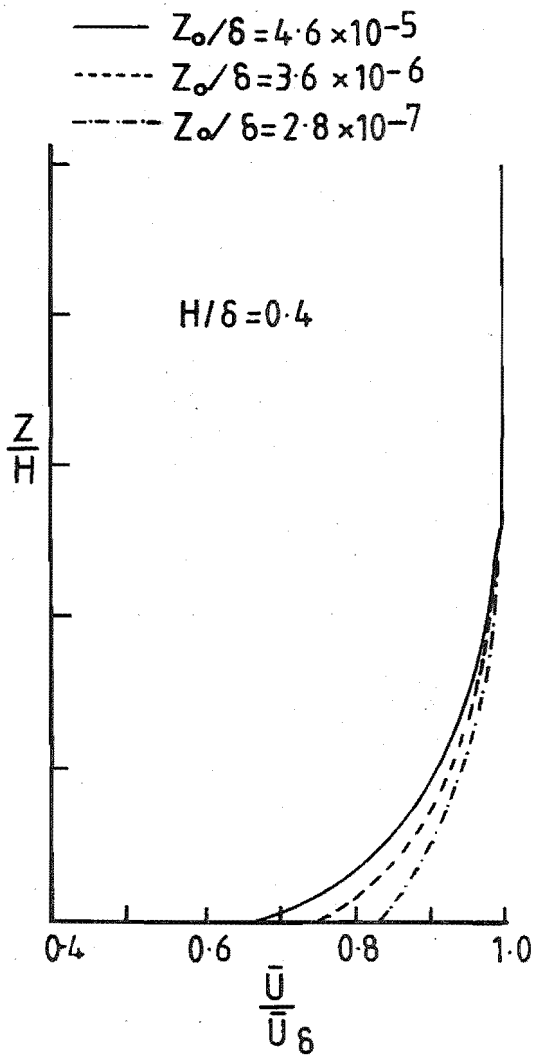

FIG. 10.6 APPROACH MEAN VELOCITY PROFILE AFTER BOUWMEESTER et. al (1978)

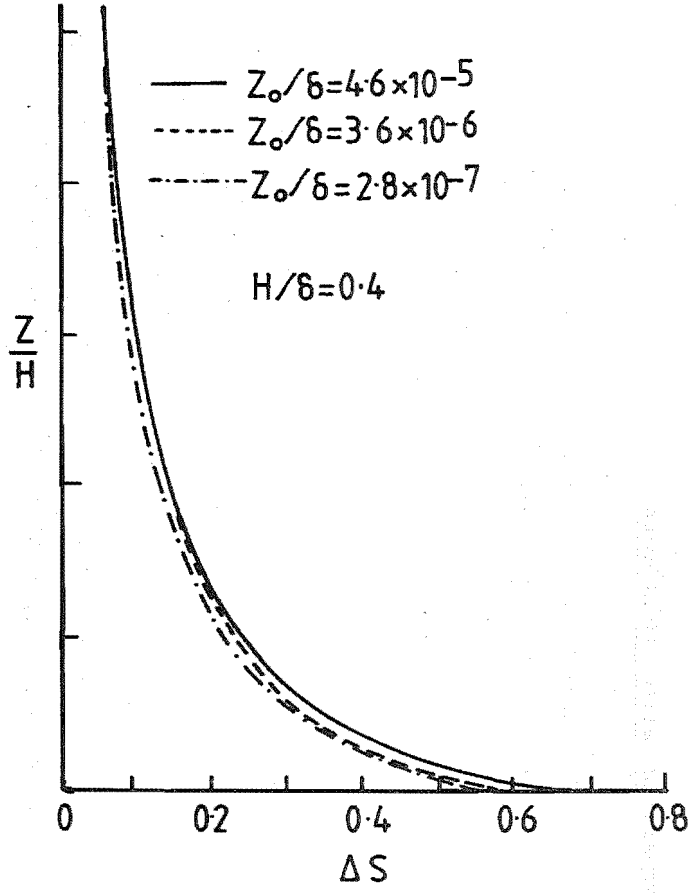

FIG. 10.7 FRACTIONAL SPEEDUP PROFILES AT THE HILL CREST AFTER BOUWMEESTER et. al. (1978)

and $\frac{z_o}{\delta} = 1.6 \times 10^{-3}$. The fractional speedup profiles at the crest are illustrated in figure 10.8 and show an increase in the speedup as the surface roughness increases. No turbulence measurements were made so a comparison with the turbulence measurements made in the present work is not possible.

10.4.3 Comparison with field work

Bowen and Lindley (1974) made measurements over a sloping escarpment and a cliff in the field. The amplification factors were found to be consistently greater for the cliff which had an upwind mean velocity profile power law exponent of 0.45 than for the sloping escarpment which had an exponent of 0.10. The field results were in contrast to wind tunnel measurements which showed that the cliff and sloping escarpments should have the same amplification factors. The results presented in section 10.3 showed that the incident mean velocity profile significantly affects the amplification factors over hills. The low incident mean velocity gradient for the sloping escarpment would cause the amplification factor to be reduced compared to those for the sloping escarpment with the higher velocity gradient. The field results therefore show much better correlation with the wind tunnel results than originally believed.

10.5 Conclusions to the study of the influence of the boundary layer characteristics on the wind flow over hills

In this chapter measurements were made over triangular hills of aspect ratio 0.1 and 1.0 in a simulated urban boundary layer. These measurements were compared with those made over the same hills in a model rural boundary layer of a similar scale.

The trends found in the flow over the model hills in the rural boundary layer were amplified in the model urban boundary layer. At the hill crests the amplification factors were larger. There was a larger decrease in the velocity fluctuations and the spectral peaks shifted to lower wave numbers compared to the upstream reference values.

The available theories and laboratory work which are concerned with the wind flow over hills showed that an increase in the surface roughness of the approach flow increased the amplification factors over the hills.

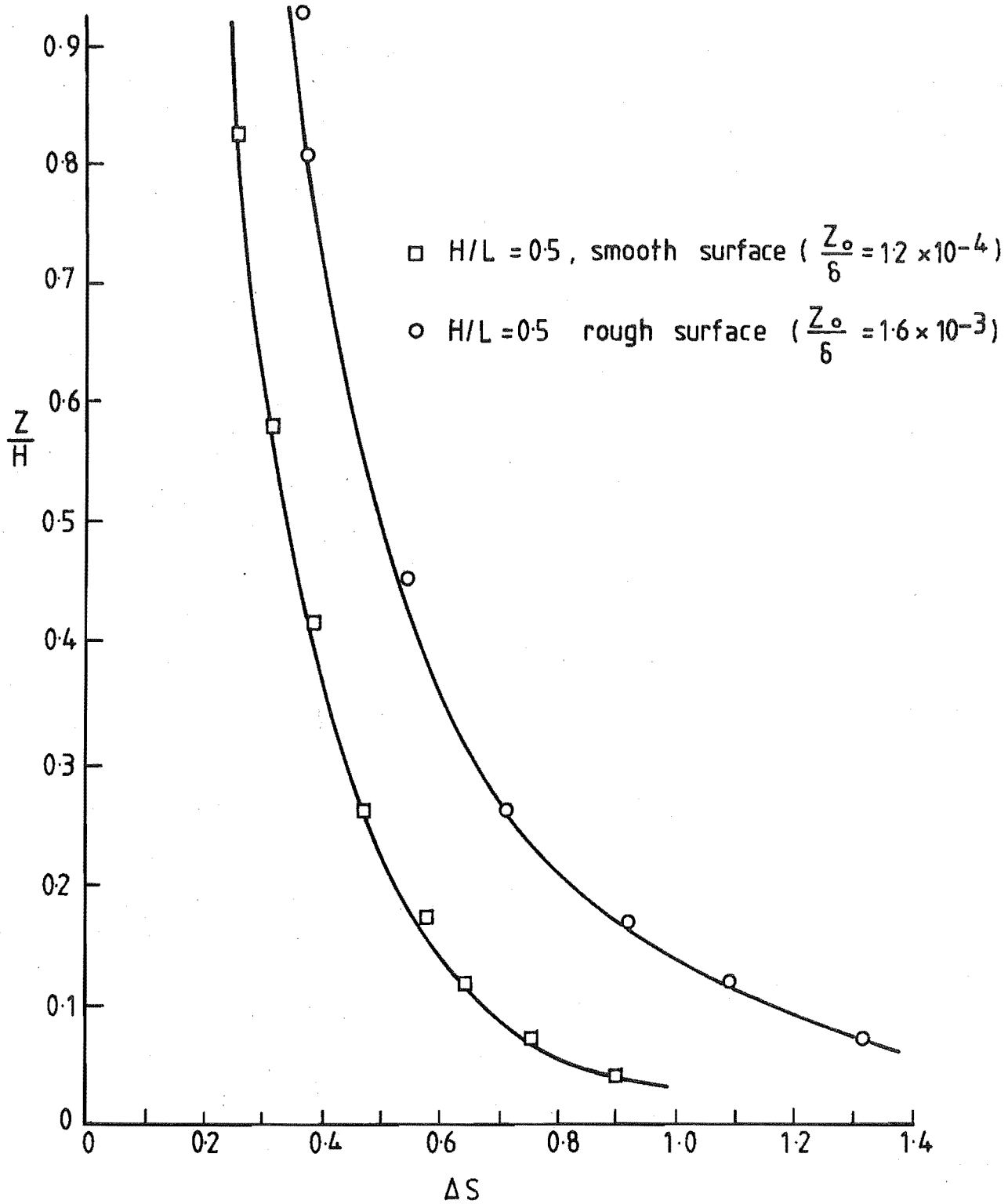

FIG. 10.8 COMPARISON OF FRACTIONAL SPEEDUP PROFILES AT THE CREST OF A TRIANGULAR HILL AFTER BOUWMEESTER et. al. (1978)

This trend was supported by measurements made in the work presented in this chapter. The author is aware of no turbulence measurements with which the present work could be compared.

CHAPTER 11

SUMMARY OF CONCLUSIONS

The major objectives of this project as recorded in Chapter one were:

(a) To review the numerical, laboratory and field work concerned with the wind flow over simple hill shapes.

(b) To recommission the atmospheric boundary layer wind tunnel in the Department of Mechanical Engineering at the University of Canterbury and develop a number of simulated atmospheric boundary layers. The model boundary layers required were a rural boundary layer of about 1:300 scale, an urban boundary layer of about 1:300 scale and a rural boundary layer of about 1:3000 scale.

(c) To develop a digital data handling system capable of accepting the output from a hot wire anemometer and analysing the data collected.

(d) To investigate the affect of the hill slope, hill height, hill shape and approach boundary layer parameters on the wind flow over hills by means of a series of tests in simulated atmospheric boundary layers.

The conclusions from the project are summarised below:

(a) The literature reviewed in Chapter two showed the need for well documented experimental work concerned with investigating the wind flow over hills. There is a particular shortage of rigorous field tests. Field tests are required which are concerned with measuring the mean velocity and turbulence components over a large number of approximately two-dimensional hill shapes in the atmosphere. It is essential that the upstream approach boundary layer characteristics are established.

(b) Following the removal of the fans from upstream of the working section the recommissioned atmospheric boundary layer wind tunnel had a much better entry flow to the working section.

A versatile boundary layer generating system consisting of a coarse grid, trip fence and uniform surface roughness was used to generate a number of simulated atmospheric boundary layers. This boundary layer generating system is widely used for modelling atmospheric shear flows.

Three model boundary layers were developed in the present work. All showed reasonable similarity to atmospheric flows and other simulations. The rate of increase of the longitudinal integral length scale with height was generally unsatisfactory. This is a common problem of simulated atmospheric boundary layers generated using a grid, trip fence and uniform surface roughness.

The three simulated atmospheric boundary layers developed provide a useful extension to the atmospheric boundary layer wind tunnel facility in the Department of Mechanical Engineering at the University of Canterbury.

(c) A digital data handling system capable of accepting the voltage output from a single hot wire anemometer was developed. The software for recording the signal on a storage device was written together with a suite of programmes which enable all the turbulence parameters of interest to be calculated.

The affect of a cosine taper, high frequency filtering, record size and signal throughput rate on the turbulence parameters were determined and a suitable sampling frequency and sample size selected.

When further hardware is available the system can be extended to handle two channels of hot wire signals.

The digital signal processing system developed has proved superior to the existing analog equipment. Greater flexibility, reliability and faster processing times were achieved with the digital equipment.

(d) Measurements over a number of triangular hills with slopes between 3^{o} and 27^{o} showed that the velocity fluctuations decreased and the mean velocity increased towards the hill crests. Once a certain slope was reached large scale separated flow occurred in the region after the crest and as the hill slope was increased further an upstream vortex formed.

For the steeper hills the upstream vortex and downstream wake region produced the equivalent of a higher potential flow ridge and an effectively more gentle slope for the main flow which was outside the separation region. Hence the largest increase in wind speed occurred for a hill of intermediate slope (14^{o}) rather than for the steepest hill (27^{o}).

The flow over round crested and sharp crested hills with the same value of $\frac{H}{L}$ were compared. The absence of a sharp edged crest led to the round crested hills having slightly higher velocities and lower velocity fluctuations for the same incident approach flow.

As the hill height was increased the amplification factors over the hills decreased but the velocity fluctuations remained at about the same level relative to the upstream values.

An increase in the surface roughness of the approach flow caused the amplification factors to increase, and a larger decrease in the velocity fluctuations to occur in the flow over the hills.

Further tests over model hills are needed to establish the importance of three-dimensional effects on the wind flow over the hills. The present work could also be usefully extended by using the fast response propellor anemometers described by Flay (1978) to investigate the wind flow over hills in the atmosphere.

LIST OF REFERENCES

ABE, M. (1941) "Mountain Clouds, Their Form and Connected Air Current. Part II", Bull. Central Met. Observatory of Japan, 3, pp.93-145, 1941.

AKINS, R. E. and PETERKA, J. A. (1975) "Computation of Power Spectral Densities and Correlations Using Digital FFT Techniques", Colorado State University Report CER75-76REA-JAP13, December 1975.

ALEXANDER, A. J. and COLES, C. F. (1971) "A Theoretical Study of Wind Flow over Hills", 3rd International Conference on Wind Effects on Buildings and Structures, pp.95-103, Tokyo, 1971.

ANTONIA, R. A. and LUXTON, R. E. (1971, 1972) "The Response of a Turbulent Boundary Layer to a Step Change in Surface Roughness. Part 1: Smooth to Rough", JFM 48, pp.721-761, 1971. "....Part 2: Rough to Smooth", JFM 53, pp.737-757, 1972.

ARCHIBALD, P. B. (1973) "An Analysis of the Winds of Site 300 as a Source of Power", Report UCLR-51469, Lawrence Livermore Laboratories, University of California, Livermore, California.

ASTLEY, R. J. (1977) "A Finite Element Frozen Vorticity Solution for Two-Dimensional Wind Flow over Hills", Proc. of 6th Australasian Hydraulics and Fluid Mechanics Conference, pp.443-446, Adelaide, Australia, December 1977.

ASTLEY, R. J., LINDLEY, D., BOWEN, A. J., AND FLAY, R. G. J. (1977) "Aspects of Wind Flow in Urban and Rural Boundary Layers", Royal Met. Soc. Summer Conf. on Urban Meteorology, McQuarrie University, Sydney, Australia, February 1977.

BARTKOWSKI, Z. (1965) "Wind Flow Over Small Hills", Swiss Aero-Revue, 1.

BEARMAN, P. W. (1968) "Digital Analysis of Hot-Wire Data", N.P.L. Aero Report 1273, June 1968.

BENDAT, J. S. and PIERSOL, A. G. (1971) "Random Data : Analysis and Measurement Procedures", Wiley.

BERGLAND, G. D. (1969) "A Guided Tour of the Fast Fourier Transform", I.E.E.E. Spectrum, 6, pp.41-52, July 1969.

BINGHAM, C., GODFREY, M. D., and TUKEY, J. W. (1967) "Modern Techniques of Power Spectrum Estimation", I.E.E.E. Transactions on Audio and Electroacoustics, AU-15, pp.56-66, June 1967.

BITTE, J. and FROST, W. (1976) "Atmospheric Flow Over Two-Dimensional Bluff Surface Obstructions", NASA Report CR-2750.

BLACKMAN, R. B. and TUKEY, J. W. (1958) "The Measurement of Power Spectra," Dover.

BOUWMEESTER, R. J. B., MERONEY, R. N., and SANDBORN, V. A. (1978) "Sites for Wind-Power Installations: Wind Characteristics Over Ridges", Draft Final Report : Part I, Colorado State University Report CER77-78RJB-RNM-VAS51, June 1978.

BOWEN, A. J. (1977) "A Review of Current Research Relevant to the Optimum Siting of Wind Power Installations in Hilly Terrain", Mechanical Engineering Dept., Univ. of Canterbury Report for the Institution of Mechanical Engineers (London) and the N.Z. Energy Research and Development Committee.

BOWEN, A. J. and LINDLEY, D. (1974) "Measurement of the Mean Wind Flow over Various Escarpment Shapes", Proc. of the 5th Australasian Conference on Hydraulics and Fluid Mechanics, pp.211-219, Univ. of Canterbury, Christchurch, N.Z., December 1974.

BOWEN, A. J. and LINDLEY, D. (1977) "A Wind-Tunnel Investigation of the Wind Speed and Turbulence Characteristics Close to the Ground Over Various Escarpment Shapes", Boundary-Layer Meteorology, 12, pp.259-271, 1977.

BRADLEY, E. F. (1968) "A Micrometeorological Study of Velocity Profiles and Surface Drag in the Region Modified by a Change in Surface Roughness", Qu. Jnl. Roy. Met. Soc., 94, p.361-379, 1968.

BRENNER, N. M. (1969) "Fast Fourier Transform of Externally Stored Data", I.E.E.E. Transactions on Audio and Electroacoustics, AU-17, pp.128-132, June, 1969.

BRIGHAM, E. O. (1974) "The Fast Fourier Transform", Prentice-Hall.

BUIJS, H. L. (1969) "Fast Fourier Transformation of Large Arrays of Data", Applied Optics, 8, pp.211-212, January 1969.

BUSCH, N. E. and PANOFSKY, H. A. (1968) "Recent Spectra of Atmospheric Turbulence", Qu. Jnl. Roy. Met. Soc., 94, pp.132-148, 1968.

CAMPBELL, G. S. and STANDEN, N. M. (1969) "Progress Report II on Simulation of Earth's Surface Winds by Artificially Thickened Wind Tunnel Boundary Layers", N.A.E. Lab. Tech. Rep. LTR-LA-37, N.R.C., Ottawa.

CHANG, S. C. (1966) "Velocity Distributions in the Separated Flow Behind a Wedge-Shaped Model Hill", Colorado State University Report CER65-SCC66, 1966.

CHEESEWRIGHT, R. (1972) "The Application of Digital Techniques to Hot-Wire Anemometry in Highly Turbulent Flows", Fluid Mechanics in the Industrial and Medical Environment, ed. D. J. Cockrell, Leicester University Press.

COOK, N. J. (1973) "On Simulating the Lower Third of the Urban Adiabatic Boundary Layer in a Wind Tunnel", Atmos. Environment, 3, pp.197-214, 1973.

COOK, N. J. (1977) "Determination of the Model Scale Factor in Wind-Tunnel Simulations of the Adiabatic Atmospheric Boundary Layer", J. Industrial Aerodynamics, 2, pp.311-321, 1977/78.

COOLEY, J. W., LEWIS, P. A. W., and WELCH, P. D. (1967) "Application of the Fast Fourier Transform to Computation of Fourier Integrals, Fourier Series and Convolution Integrals", I.E.E.E. Transactions on Audio and Electroacoustics, AU-15, pp.79-84, June 1967.

CORBY, G. A. (1954) "The Airflow Over Mountains - A Review of the State of Current Knowledge", Qu. Jnl. Roy. Met. Soc., 80, pp.491-521, 1954.

COUNIHAN, J. (1969) "An Improved Method for Simulating an Atmospheric Boundary Layer in a Wind Tunnel", Atmos. Environment, 3, pp.197-214, 1969.

COUNIHAN, J. (1971) "Wind Tunnel Determination of the Roughness Length as a Function of the Fetch and the Roughness Density of the Three-Dimensional Roughness Elements", Atmos. Environment, 6, pp.637-642, 1971.

COUNIHAN, J. (1973) "Flow Over Two-Dimensional Hills and Plateaux in Simulated Boundary Layer Flow", Central Electricity Research Laboratories Note No. RD/L/N277/73, U.K., 1973.

COUNIHAN, J. (1973) "Simulation of an Adiabatic Urban Boundary Layer in a Wind Tunnel", Atmos. Environment, 7, pp.673-689, 1973.

COUNIHAN, J. (1974) "Flow Over Concatenated Sinusoidal Hills", Central Electricity Research Laboratories Note No. RD/L/N57/73, U.K., 1974.

COUNIHAN, J. (1975) "Adiabatic Atmospheric Boundary Layers: A Review and Analysis of Data from the Period 1880-1972", Atmos. Environment, 9, pp.871-905, 1975.

DAVENPORT, A. G. (1961) "The Spectrum of Horizontal Gustiness Near the Ground in High Winds", Qu. Jnl. Roy. Met. Soc., 87, pp.194-211, 1961.

DAVENPORT, A. G. (1963) "The Relationship of Wind Structure to Wind Loading", Proc. of Conference on Wind Effects on Buildings and Structures, pp.53-102, N.P.L., June 1963.

DAVENPORT, A. G. and ISYUMOV, N. (1967) "The Application of the Boundary Layer Wind Tunnel to the Prediction of Wind Loading", Proc. of Int. Symp. on Wind Effects on Buildings and Structures, pp.201-230, N.R.C., Ottawa, 1967.

DAVIDSON, B. (Chairman) (1964) "Sites for Wind-Power Installations, W.M.O. Technical Note No. 63, 1964.

de BRAY, B. G. (1973) "Atmospheric Shear Flows Over Ramps and Escarpments", Industrial Aerodynamics Abstracts, 5, pp.1-4, 1973.

DEAVES, D. M. (1975) "Wind Over Hills : A Numerical Approach", J. Industrial Aerodynamics, 1, pp.371-391, 1975/76.

DERICKSON, R. G. and MERONEY, R. N. (1977) "A Simplified Physics Airflow Model for Evaluating Wind Power Sites in Complex Terrain", Proc. of Summer Computer Simulation Conference, Chicago, U.S.A., July 1977.

ELISEEV, V. S. (1973) "Stereophotogrammetric Investigation of the Air Flow in the Boundary Layer of the Atmosphere Above a Hill", Air Pollution and Atmospheric Diffusion, ed. M. E. Berlyand, pp.95-108, Wiley.

E.S.D.U. (1972) "Characteristics of the Wind Speed in the Lower Layers of the Atmosphere Near the Ground : Strong Winds (Neutral Atmosphere)", Engineering Sciences Data Unit, London, U.K..

E.S.D.U. (1974) "Characteristics of the Atmospheric Turbulence Near the Ground. Part II, Single Point Data for Strong Winds (Neutral Atmosphere)." Engineering Sciences Data Unit, London, U.K..

FEASEY, R. (1978) "Wind Pressure Measurements on a Multi-Storey Building", Thesis presented for degree of Ph.D. in Mechanical Engineering, University of Auckland, Auckland, N.Z., 1978.

FIELD, J. H. and WARREN, R. (1933) "A Survey of the Air Currents in the Bay of Gibraltar, 1929-30, Geophys. Mem. (London), No.59, 1933.

FLAY, R. G. J. (1978) "Structure of a Rural Atmospheric Boundary Layer near the Ground", Thesis presented for degree of Ph.D. in Mechanical Engineering, University of Canterbury, Christchurch, N.Z., 1978.

FOSBERG, M. A., MARLATT, W. E., and KRUPNAK, L. (1976) "Estimating Airflow Patterns Over Complex Terrain", U.S.D.A. Forest Service Research Paper RM-162, 1976.

FRAENKEL, L. E. (1961) "On Corner Eddies in Plane Inviscid Shear Flow", JFM, 11, pp.400-406, 1961.

FREESTON, D. H. (1974) "Atmospheric Shear Flows Over Ramps and Escarpments", Paper presented at the 5th Australasian Conference on Hydraulics and Fluid Mechanics, Univ. of Canterbury, Christchurch, N.Z., December 1974.

FRENKIEL, J. (1962) "Wind Profiles Over Hills (In Relation to Wind Power Utilisation)", Qu. Jnl. Roy. Met. Soc., 88, pp.156-169, 1962.

FRENKIEL, J. (1963) "Gusts Over Hills (In Relation to Wind Power Utilisation)", Qu. Jnl. Roy. Met. Soc., 89, pp.281-283, 1963.

FROST, W., MAUS, J. R., and FICHTL, G. H. (1974) "A Boundary-Layer Analysis of Atmospheric Motion Over a Semi-Elliptical Surface Obstruction", Boundary-Layer Meteorology, 7, pp.165-184, 1974.

GANDEMER, J. (1973) "La Soufflerie à Couche Limite Turbulente du CSTB", Cahiers du Centre Scientifique et Technique du Batiment, No. 141, 1973.

GARTSHORE, I. S. and de CROOS, K. A. (1976) "Roughness Element Geometry Required for Wind Tunnel Simulations of the Atmospheric Wind", A.S.M.E. Technical Paper 76-WA/FE-18, 1976.

GOLDING, E. W. and STODHART, A. H. (1952) "The Selection and Characteristics of Windpower Sites", E.R.A. Technical Report C/T 108, 1952.

GOLDING, E. W. (1955) "The Generation of Electricity by Wind Power", Spon, London.

HADEEN, K. D. and FRIEND, A. L. (1972) "The Air Force Global Weather Central Operational Boundary-Layer Model", Boundary-Layer Meteorology, 3, pp.98-112, 1972.

HANFF, E. S. (1973) "An Economical High Speed Data Acquisition and Processing System for Wind Tunnel Experiments", 5th Int. Congr. on Instrum. in Aerosp. Simulation Facilities, California Institute of Technology, Pasadena, Sept. 10-12, 1972, pp.252-256. Published by I.E.E.E. (73-CHO 784-9AES), New York 1973.

HARDMAN, C. E., HELLIWELL, N. C., and HOPKINS, J. S. (1973) "Extreme Winds Over the United Kingdom for Periods Ending 1971", Met. Office, Climatological Memorandum No. 50A, H.M.S.O.

HARDY, D. M. (1977) "Wind Studies in Complex Terrain", Lawrence Livermore Laboratories Report, University of California.

HARRIS, R. I. (1968) "Measurement of Wind Structure at Heights up to 598ft. Above Ground Level", Proc. Symposium on Wind Effects on Buildings and Structures, Loughborough University of Technology, U.K., 1968.

HARRIS, R. I. (1970) "The Nature of the Wind", C.I.R.I.A. Seminar, Modern Design of Wind Sensitive Structures, London, pp.29-55, 1970.

HEWLETT-PACKARD. "A Pocket Guide to the 2100 Computer", Hewlett-Packard.

HEWLETT-PACKARD. "Moving-Head Disc Operating System", 2nd ed. Hewlett-Packard, March 1971.

HEWLETT-PACKARD. (1971) "HP Assembler, Programmers Reference Manual", 3rd ed. Hewlett-Packard, June 1971.

HEWLETT-PACKARD. (1972) "Operating and Service Manual 13210A, Disc Drive Interface Kit (for the 2100 series computers)", Hewlett-Packard, March 1972.

HEWLETT-PACKARD (1973) "Operating and Service Manual 12539C, Time Base Generator Interface Kit (for the 2100 series computers)", Hewlett-Packard, January 1973.

HINZE, J. O. (1959) "Turbulence", McGraw-Hill.

HODGE, J. G. (1974) "General Purpose Data Acquisition System Employing Transponding Terminals", Final Year Project Report, Department of Electrical Engineering, University of Canterbury, N.Z..

HODGE, J. G. (1978) "Data Acquisition From a Range of Transducers Using a Mini-Computer Based System", Thesis presented for degree of M.E. in Mechanical Engineering, Univ. of Canterbury, Christchurch, N.Z., 1978.

HUNT, J. C. R. and FERNHOLZ, H. (1975) "Wind-Tunnel Simulation of the Atmospheric Boundary Layer : A Report on Euromech 50", JFM, 70, pp.543-559, 1975.

JACKSON, P. S. (1975) "A Theory for Flow Over Escarpments", Proc. Fourth International Conference on Wind Effects on Buildings and Structures, pp.33-40, London, 1975.

JACKSON, P. S. and HUNT, J. C. R. (1975) "Turbulent Wind Flow Over a Low Hill", Qu. Jnl. Roy. Met. Soc., 101, pp.929-955, 1975.

JENKINS, G. M. and WATTS, D. G. (1968) "Spectral Analysis and its Applications", Holden-Day.

JENSEN, M. (1958) "The Model-Law for Phenomena in Natural Wind", Ingeniϕren, 2, pp.121-128, Denmark, 1958.

JENSEN, N. O. and PETERSON, E. W. (1978) "On the Escarpment Wind Profile", Qu. Jnl. Roy. Met. Soc., 104, pp.719-728, 1978.

JUUL, J. (1949) "Investigation of the Possibilities of Utilisation of Wind-Power", Electroteknikeren, 45, pp.607-635, 1949.

KAIMEL, J. C., WYNGAARD, J. C. and HAUGEN, D. A. (1968) "Deriving Power Spectra from a Three-Component Sonic Anemometer", J. Appl. Meteorol., 7, pp.827-837, 1968.

KIYA, M. and ARIE, M. (1972) "A Free-Streamline Theory for Bluff Bodies Attached to a Plane Wall, JFM, 56, pp.201-219, 1972.

LANGE, K. O. (1961) "Some Aspects of Site Selection for Wind Power Plants on Mountainous Terrain", Proc. of the United Nations Conference on New Sources of Energy, Rome 1961, 7, pp.125-128.

LINDLEY, D., ASTLEY, R. J., FLAY, R. G. J., and BOWEN, A. J. (1977) "Topographical Modification to the Atmospheric Boundary Layer", Symposium on the Interaction Between Climate and Building Design, Conseil International du Batiment - Seventh Congress and General Assembly, Edinburgh, 14-21 September 1977.

LO, A. K. (1977) "Boundary Layer Flow Over Gentle Curvilinear Topography with a Sudden Change in Surface Roughness", Qu. Jnl. Roy. Soc., 103, pp.199-209, 1977.

LONG, R. R. (1953) "Some Aspects of the Flow of Stratified Fluids. I. A Theoretical Investigation", Tellus, 5, p.42-58, 1953.

MAHRER, Y. and PIELKE, R. A. (1975) "A Numerical Study of the Air Flow Over Mountains Using the Two-Dimensional Version of the University of Virginia Mesoscale Model", J. of Atmos. Sciences, 32, pp.2144-2155, 1975.

MELBOURNE, W. H. (1977) "Development of Natural Wind Models at Monash University", Proc. of 6th Australasian Hydraulics and Fluid Mechanics Conference, pp.190-194, Adelaide, Australia, December 1977.

MERONEY, R. N., SANDBORN, V. A., BOUWMEESTER, R. J. B. and RIDER, M. A. (1976) "Sites For Wind Power Installations : Wind Tunnel Simulation of the Influence of Two-Dimensional Ridges on Wind Speed and Turbulence", Colorado State University Report CER76-77-RNM-VAS-RB-MAR5, 1976.

MERONEY, R. N., BOWEN, A. J., LINDLEY, D. and PEARSE, J. R. (1978) "Wind Characteristics Over Complex Terrain : Laboratory Simulation and Field Measurements at Rakaia Gorge, New Zealand", Colorado State University Report CER77-78 RNM29, 1978.

MITSUTA, Y. (1971) "Characteristics of Air Flow Over the Barriers in the Storm", Proc. 3rd International Conference on Wind Effects on Buildings and Structures, pp.33-44, Tokyo, 1971.

MULHEARN, P. J. (1978) "A Wind-Tunnel Study of the Effects of a Surface Roughness Change : Rough to Smooth", Boundary-Layer Met., 15, pp.3-30, 1978.

NICHOLS, J. M. (1973) "The Airflow Over Mountains - Research 1958-1972", W. M. O. Technical Note No. 127, 1973.

NORTH, R. J., JEFFREY, R. W., DOLMAN, J. A. and TUCK, A. N. (1976) "Digital Computer Aspects of the Instrumentation and Control of the New R.A.E. 5 Metre Low Speed Tunnel, A.G.A.R.D. Conference Proceedings, No.210, 1976.

OPPENHEIM, A. V. and WEINSTEIN, C. J. (1972) "Effects of Finite Register Length in Digital Filtering and the Fast Fourier Transform," Proc. I.E.E.E., 60, pp.957-976, August 1972.

PANOFSKY, H. A. (1969) "The Structure of Atmospheric Shear Flows", Paper 1, Conf. Proc. No.48, "The Aerodynamics of Atmospheric Shear Flows", A.G.A.R.D. Fluid Dynamic Panel Specialists Meeting, Munich, 1969.

PANOFSKY, H. A. and PETERSEN, E. L. (1972) "Wind Profiles and Change of Terrain Roughness at Risφ", Qu. Jnl. Roy. Met. Soc., 98, pp.845-854, 1972.

PAPESCH, A. J. G. (1971) "The Problem of Wind Damage in Canterbury Forests", N.Z. Engineering, 26, pp.293-297, 1971.

PETERSON, E. W. (1969) "Modification of Mean Flow and Turbulent Energy by a Change in Surface Roughness Under Conditions of Neutral Stability", Qu. Jnl. Roy. Met. Soc., 95, pp.561-575, 1969.

PETERSON, E. W., KRISTENSEN, L. and SU, C. C. (1976) "Some Observations and Analysis of Wind Over Nonuniform Terrain, Qu. Jnl. Roy. Met. Soc., 102, pp.857-869, 1976.

PETTERSSEN, S. (1961) "Some Aspects of Wind Profiles", Proc. of the United Nations Conference on New Sources of Energy, Rome 1961, 7, pp.133-136.

PLATE, E. J. (1971) "Aerodynamic Characteristics of Atmospheric Boundary Layers", U.S. Atomic Energy Commission.

PLATE, E. J. and LIN, C. W. (1965) "The Velocity Field Downstream From a Two-Dimensional Model Hill - Part 2", Colorado State University Report, CER65EJP-CWL41, 1965.

PUTNAM, P. C. (1948) "Power from the Wind", van Nostrand Reinhold Co., New York.

QUENEY, P. (1947) "Theory of Perturbations in Stratified Currents with Application to Airflow Over Mountain Barriers", Chicago Univ. D., Misc. Report, No.23, 1947.

QUENEY, P., CORBY, G. A., GERBIER, N., KOSCHMIEDER, H., and ZIEREP, J. (1960) "The Airflow Over Mountains", W. M. O. Technical Note No. 34, 1960.

RAINE, J. K. (1974) "Modelling the Natural Wind : Wind Protection by Fences", Thesis presented for degree of Ph.D. in Mechanical Engineering, Univ. of Canterbury, Christchurch, N.Z., 1974.

RAJASOORIA, G. P. D., HAINES, D. F. and POO, A. N. (1977) "Digital Data Evaluation of Turbulence Parameters Using a Mini-Computer", Proc. of 6th Australasian Hydraulics and Fluid Mechanics Conference, pp.524-527, Adelaide, Australia, December 1977.

RAO, K. S., WYNGAARD, J. C. and COTÉ, O. R. (1974) "The Structure of the Two-Dimensional Internal Boundary Layer Over a Sudden Change of Surface Roughness", J. of Atmos. Sciences, 31, pp.738-746, 1974.

RAYMOND, D. J. (1972) "Calculation of Airflow Over an Arbitrary Ridge Including Diabatic Heating and Cooling", J. of Atmos. Sciences, 29, pp.837-843, 1972.

RIDER, N. E., PHILIP, J. R. and BRADLEY, E. F. (1963) "The Horizontal Transport of Heat and Moisture - a Micrometeorological Study", Qu. Jnl. Roy. Met. Soc., 89, pp.507-531, 1963.

RIDER, M. A. and SANDBORN, V. A. (1977) "Measurements of the Mean and Longitudinal Turbulent Velocities Over Varying Hill Shapes", Colorado State University Research Memorandum No.28 CER77-78 MAR-VAS28.

RIDER, M. A. and SANDBORN, V. A. (1977a) "Boundary Layer Turbulence Over Two-Dimensional Hills", Colorado State University Report CER77-78 MAR-VAS4, 1977.

SACRE, C. (1974) "Estimation Theorique des Proprietes de l'Ecoulement de l'Air sur une Colline Bi-Dimensionelle", Centre Scientifique et Technique du Batiment, Nantes, France.

SACRE, C. (1978) "An Experimental Study of the Airflow Over a Hill in the Atmospheric Boundary Layer", Submitted for Publication to Boundary-Layer Meteorology.

SCHLICHTING, H. (1960) "Boundary-Layer Theory", McGraw-Hill.

SCORER, R. S. (1949) "Theory of Waves in the Lee of Mountains", Qu. Jnl. Roy. Met. Soc., 75, pp.41-56, 1949.

SHELLARD, H. C. (1963) "The Estimation of Design Wind Speeds", Proc. of Conference on Wind Effects on Buildings and Structures, pp.30-51, N.P.L., U.K., June 1963.

SHIR, C. C. (1972) "A Numerical Computation of Air Flow Over a Sudden Change of Surface Roughness", J. of Atmos. Sciences, 29, pp.304-310, 1972.

SINGLETON, R. C. (1967) "A Method for Computing the Fast Fourier Transform with Auxiliary Memory and Limited High-Speed Storage", I.E.E.E. Transactions on Audio and Electroacoustics, AU-15, pp.91-98, June 1967.

STONE, H. S. (1972) "Introduction to Computer Organisation and Data Structures", McGraw-Hill.

SUNDARAM, T. R., LUDWIG, G. R. and SKINNER, G. T. (1972) "Modelling of the Turbulence Structure of the Atmospheric Surface Layer", A.I.A.A. Journal, 10, pp.743-750, June 1972.

TAGG, J. R. (1957) "Wind Data Related to the Generation of Electricity by Wind Power", E.R.A. Technical Report C/T 115, 1957.

TAYLOR, P. A. (1969) "The Planetary Boundary Layer Above a Change in Surface Roughness", J. of Atmos. Sciences, 26, pp.432-440, 1969.

TAYLOR, P. A. (1977a) "Some Numerical Studies of Surface Boundary-Layer Flow Above Gentle Topography", Boundary-Layer Meteorology, 11, pp.439-465, 1977.

TAYLOR, P. A. (1977b) "Numerical Studies of Neutrally Stratified Planetary Boundary-Layer Flow Above Gentle Topography. I. Two Dimensional Cases", Boundary-Layer Meteorology, 12, pp.37-60, 1977.

TAYLOR, P. A. and GENT, P. R. (1974) "A Model of Atmospheric Boundary-Layer Flow Above an Isolated Two-Dimensional 'Hill'; An Example of Flow Above 'Gentle Topography'," Boundary-Layer Meteorology, 7, pp.349-362, 1974.

TEMPLIN, R. J. (1969) "Interim Progress Note on Simulation of Earth's Surface Winds by Artificially Thickened Wind Tunnel Boundary Layers", N.R.C., Ottawa, Canada, N.A.E. Lab. Tech. Rep. LTR-LA-22, February 1969.

TEUNISSEN, H. W. (1970) "Characteristics of the Mean Wind and Turbulence in the Planetary Boundary-Layer", U.T.I.A.S. Review No. 32.

TEUNISSEN, H. W. (1972) "Simulation of the Planetary Boundary Layer in a Multiple Jet Wind Tunnel", U.T.I.A.S. Report No. 182, June 1972.

TOWNSEND, A. A. (1965) "The Response of a Turbulent Boundary Layer to Abrupt Changes in Surface Conditions", JFM, 22, pp.799-882, 1965.

TIELEMAN, H. W., REINHOLD, T. A. and MARSHALL, R. D. (1978) "On the Wind Tunnel Simulation of the Atmospheric Surface Layer for the Study of Wind Loads on Low-Rise Buildings", J. Industrial Aerodynamics, 3, pp.21-38, 1978.

WAX, M. P. (1954) "An Experimental Study of Wind Structure", E.R.A. Technical Report C/T 114, 1954.

WEIDNER, G. A. and STEARNS, C. R. (1978) "Topographic Influence on Surface Winds", Boundary-Layer Meteorology, 14, pp.167-182, 1978.

WOOD, D. H. (1977) "The Growth of the Internal Layer Following a Step Change in Surface Roughness", Dept. of Aeronautics, Imperial College of Science and Technology, Report I.C. Aero TN 77-101, 1977.

YUEN, C. K. and FRASER, D. (1976) "Digital Spectral Analysis", Report 76-1, Dept. of Information Service, Hobart University, Australia.

APPENDIX 1

THE FLOW MEASURING EQUIPMENT

A1.1 Description of the flow measuring equipment

The flow measuring equipment consisted of two DISA 55D00 hot wire anemometer sets and a DISA correlator unit as shown in figure 3.3. Each DISA 55D00 anemometer set was comprised of:-

DISA 55D01 constant temperature anemometer,
DISA 55D10 linearizer,
DISA 55D25 auxiliary unit,
DISA 55D27 constant temperature anemometer power booster,
DISA 55D30 DC voltmeter
DISA 55D35 RMS voltmeter.

The DISA correlator unit consisted of:

DISA 55D70 correlator,
DISA 55D75 time delay unit,
DISA 55B01 sweep drive unit.

The hot wire anemometer equipment was used in the constant temperature mode and the signal was linearised. The instructions in the DISA operating manuals were followed for the flow conditions encountered in the tunnel.

Raine (1974) describes the important features of the operating procedure for this anemometer equipment. The probe calibration procedure described by Raine was not used in the present work as a hot wire calibrator unit was available.

A1.2 Probe calibration procedure

The hot wire probe was cleaned daily prior to calibration. The method of cleaning the probes was to wash the probes in acetone and then rinse them in ethyl alcohol.

After cleaning, the probe operating resistance was set and the probe was linearised using a Thermosystems (T.S.I.) Model 1125 calibrator unit shown in figure A1.1. The calibrator unit was used with a 1.65 cm diameter nozzle. This calibrator gives a uniform, swirl free flow over the range of velocities encountered in the wind tunnel. The calibrator pressure drop was measured using a Schiltknect micromanometer.

The daily linearisation procedure involved setting two velocities such that the higher velocity corresponding approximately to the maximum speed in the wind tunnel was exactly twice the lower velocity. The lineariser exponent was adjusted so the voltage output from the lineariser was halved when the air velocity was halved. The linearised output was also suitably zeroed.

The hot wire anemometer calibration constant was set so that the entire 10V range of the linearised anemometer output was used when the probe was mounted in the wind tunnel. Care was taken to ensure that the signal would not be clipped by exceeding the 10V range. This was done by checking the signal on a Hewlett Packard 141B oscilloscope.

A1.3 Thermal drift

The hot wire anemometer output voltage drifted as the ambient temperature changed. The hot wire probe was therefore regularly traversed back to a reference position. The small voltage changes between returns to the reference position were noted and intermediate anemometer voltage readings adjusted using a linear interpolation procedure.

A1.4 Effect of large velocity fluctuations and flow inclination on the velocity readings

The effect of large velocity fluctuations on the hot wire anemometer response has been discussed by a number of authors. It is generally recognised that hot wire anemometers rapidly lose their accuracy at ratios of $\frac{u'}{U}$ greater than about 0.25.

This limitation of the hot wire anemometer was important in the present work in the measurements made over the steeper hills and in the model urban boundary layer close to the ground.

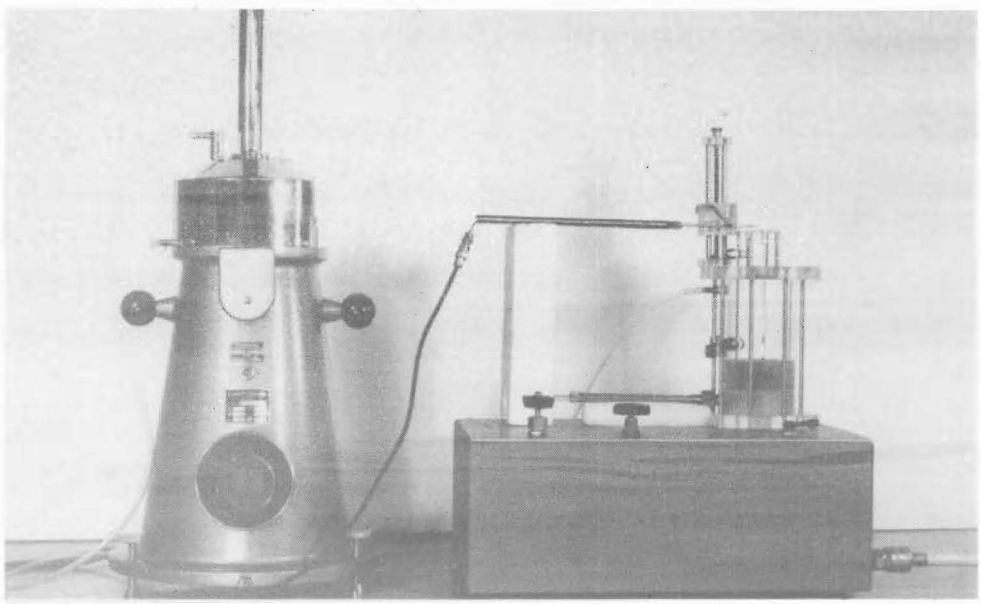

Fig. A1.1 The hot wire calibrator unit

The inclination of the flow to the hot wire also affects the accuracy of the anemometer. The steepest model hills had a slope of about 26°. It is likely that the flow inclination was never more than 26° and it was probably less than this at the measuring position closest to the hill surface. The actual flow direction in the separated flow after the hill crest is uncertain.

Information on the accuracy of hot wire anemometers at intensities of turbulence greater than 0.25 is scarce. After a review of the available literature Raine (1974) examined the signal from a hot wire anemometer. His findings are presented in table A1.1 and show that the effect of flow inclination and high turbulence intensity readings on the mean velocity should be less than 5%.

Raine concluded on the basis of his analysis that the error in $\frac{u'}{\overline{U}}$ as measured at the anemometer output would be approximately as follows:

$\frac{u'}{\overline{U}} = 0.2$ error less than 1%

$\frac{u'}{\overline{U}} = 0.4$ error less than 4%

$\frac{u'}{\overline{U}} = 0.7$ error about 15%

It was decided to record and plot all the velocity values as read from the voltmeters connected to the anemometer output and accept that the values of u' are rather uncertain at high turbulence intensities.

A1.5 Use of the X probe

The DISA 55A32 X probe was used to measure the U, V and W velocity components, $-\overline{uw}$ Reynolds stress and the v and w velocity component energy spectra.

Close agreement was always obtained between the U velocity component measured using the X probe and the measurements made with the single wire probes. This provided a useful check on the operation of the X probe.

Ratio $\frac{\bar{U}_{\theta_{eff}}}{\bar{U}_\theta}$		Flow inclination θ			
		0^o	5^o	10^o	25^o
$\frac{u'}{\bar{U}_\theta}$	0.05	1.00003	1.0004	1.0005	1.0008
	0.1	1.001	1.0015	1.0019	1.003
	0.2	1.005	1.006	1.0075	1.012
	0.4	1.02	1.025	1.03	1.049
	0.7	1.06	1.075	1.09	1.15

TABLE A1.1 Hot wire anemometer errors after Raine (1974)

Notation:

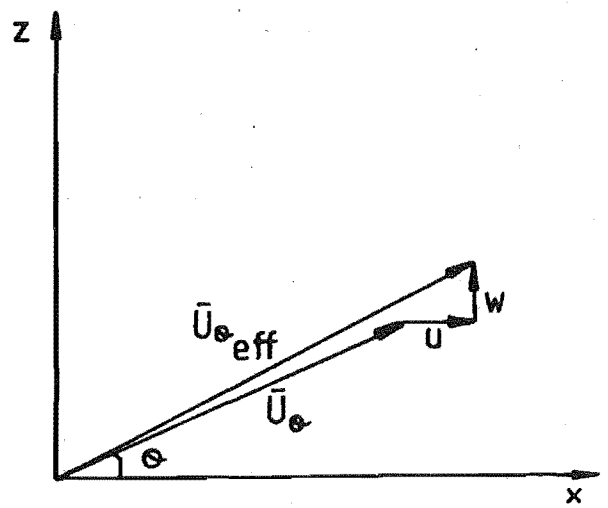

Fig. A1.2 Effective cooling velocity $\bar{U}_{\theta_{eff}}$ after Raine (1974)

The X probe was connected to the hot wire equipment as shown in figure A1.3. Calibration of the probe was performed using the T.S.I. Model 1125 calibrator unit in the same way as for the single wire probes as described in section A1.2. Care was always taken to ensure that the linearisor output voltage was less than 4V. This is the maximum voltage which can be handled by the inverter of the DISA 55D25 auxiliary unit.

The signal from the X probe was examined by Raine (1974). Assuming an angle of 45^{o} between the wires and for the probe in a vertical plane the outputs from the dual summing unit and correlator are given by Raine as:

$$E_{D.S.U.\ (e_1-e_2)} = 2k_3Gw \qquad (A1.1)$$

$$E_{D.S.U.\ (e_1+e_2)} = 2k_3Gu \qquad (A1.2)$$

$$E_{correlator\ \overline{(e_1+e_2)(e_1-e_2)}} = 4k_3^2\,G^2\,\overline{uw} \qquad (A1.3)$$

Raine also investigated the effect of the inclination of the flow to the probe axis and the inclination of the probe wires to the probe axis by angles of other than 45^{o}. The result of Raine's investigation are presented in tables A1.2 and A1.3.

The relatively poor resolution obtainable with a maximum voltage range of 4V and the errors associated with adjusting both hot wire channels to have the same output for the same flow conditions limited the accuracy of the X probe measurements. The readings from the X probe were judged accurate to:

u' : $\pm$ 5%

v' : $\pm$ 5%

w' : $\pm$ 5%

$\overline{uw}$: $\pm$10%

In retrospect it was considered more accurate to calibrate the X probe by performing velocity and yaw calibrations with the probe mounted on suitable traversing gear. This could be performed in a uniform flow with low turbulence intensity such as well above the wind tunnel floor. Such a

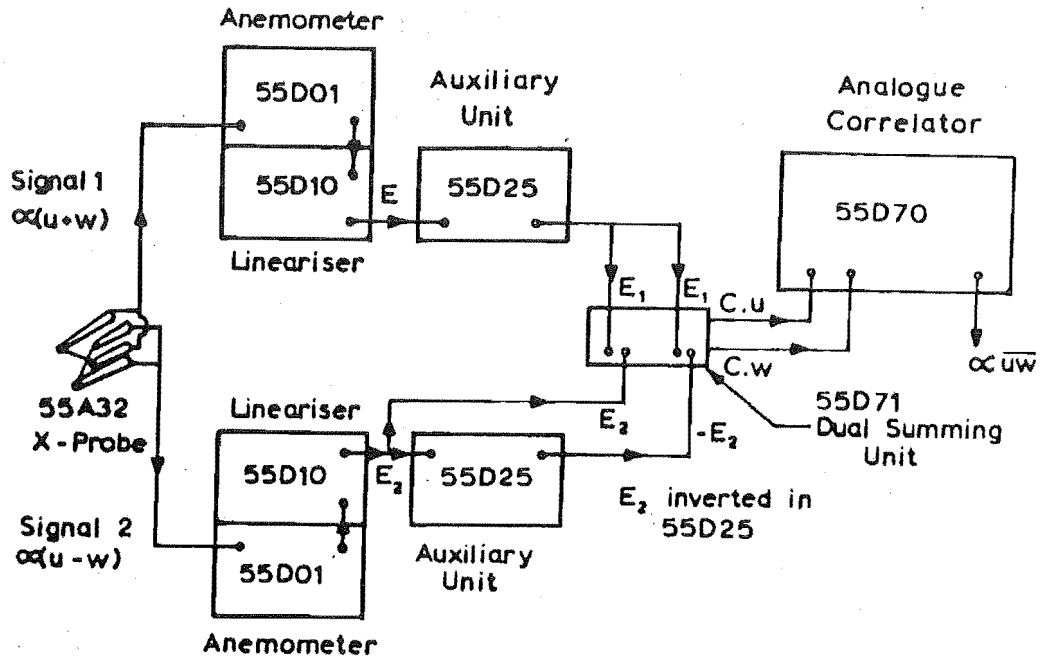

FIG A1·3 EQUIPMENT CONNECTION FOR MEASUREMENT OF REYNOLDS STRESS AFTER RAINE (1974)

Angle of flow inclination to probe axis (γ)	Fractional errors in u', w', $\overline{uw}$ %		
	$\frac{\Delta u'}{U'}$	$\frac{\Delta w'}{w'}$	$\frac{\Delta \overline{uw}}{\overline{uw}}$
+ 10	- 18.2	+ 6.42	- 59.0
+ 7	- 12.5	+ 3.06	- 40.4
+ 5	- 8.8	+ 1.54	- 28.7
+ 4	- 7.0	+ 0.98	- 23.0
+ 2	- 3.5	+ 0.24	- 11.6
- 0.5	+ 0.9	+ 0.02	+ 3.0
- 2	+ 3.5	+ 0.24	+ 12.1
- 4	+ 7.0	+ 0.98	+ 25.0
- 5	+ 8.8	+ 1.54	+ 31.8
- 7	+ 12.5	+ 3.06	+ 46.5
- 10	+ 18.2	+ 6.42	+ 71.9

TABLE A1.2 Errors in X probe signal through inclination of the flow to the probe axis after Raine (1974).

Notation:

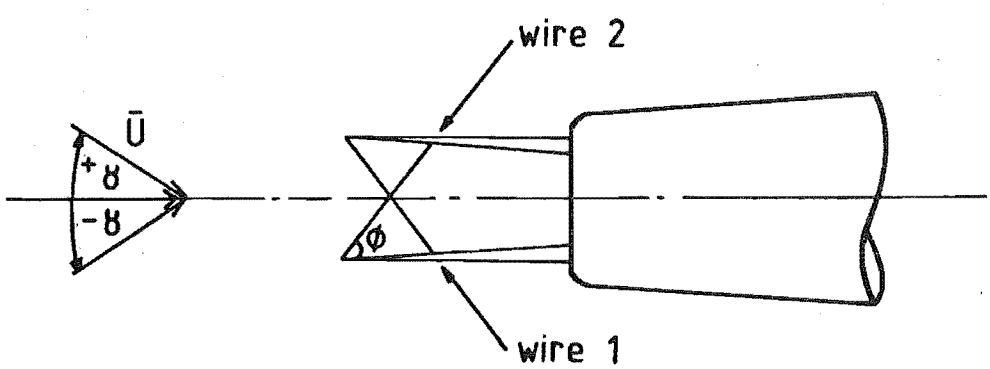

FIG. A1.4 Flow inclination to the X probe

Actual probe wire angle	Fractional errors in u', w', $\overline{uw}$ % for an assumed probe wire angle of 45°		
	$\frac{\Delta u'}{U'}$	$\frac{\Delta w'}{w'}$	$\frac{\Delta \overline{uw}}{\overline{uw}}$
40	0	+19.2	+19.2
41	0	+15.0	+15.0
42	0	+11.1	+11.1
43	0	+ 7.2	+ 7.2
44	0	+ 3.6	+ 3.6
45	0	0	0
46	0	- 3.4	- 3.4
47	0	- 6.8	- 6.8
48	0	-10.0	-10.0
49	0	-13.1	-13.1
50	0	-16.1	-16.1

TABLE A1.3 Errors in X probe signal through inclination of the probe wires by angles other than 45° after Raine (1974).

calibration procedure would enable the actual X probe wire angles to be determined rather than assuming they are 45°. Table A1.3 shows that the wire angle is a critical parameter in the measurement of turbulence parameters with the X probe.

A1.6 Accuracy of the measurements

Mean velocity measurements

The largest available meter damping was used on the DISA 55D30 DC voltmeter but even so the meter reading fluctuated considerably. The mean velocity readings were judged accurate to ±2%.

Velocity fluctuation measurements

The DISA 55D35 RMS voltmeter was operated with a 30s time constant. Because of meter fluctuations caused by the turbulent flow the meter readings were probably accurate to ±2%.

Energy spectra

When using the Bruel and Kjaer 2114 $\frac{1}{3}$ octave bandwidth spectrometer and 2307 level recorder the following averaging times were used:-

2 - 10 Hz	T = 30s	paper speed = 0.01 mm/s
10 - 50 Hz	T = 10s	paper speed = 0.03 mm/s
50 - 200 Hz	T = 3s	paper speed = 0.1 mm/s
200 - 10,000 Hz	T = 1s	paper speed = 0.1 mm/s

These were considerably larger than the values used by Raine but closely follow his recommended values.

Because of the drift in the hot wire signal over the 90 minute period required to record each spectrum and considering the fluctuating record produced, the accuracy on $\frac{\Delta nS(n)}{nS(n)}$ was judged to be ±7.5%.

The sources of error in the digitally calculated spectra are discussed in section 11.6 of Appendix two. A useful estimate of the scatter about the true spectral density function can be perceived from the figures in section 11.4.3 of Appendix two. The digitally calculated spectra were

considered more accurate than those measured using the analog equipment.

Correlation measurements

From repeatability checks on the Reynolds stress measurements, the Reynolds stress measurements were judged accurate to ±10%.

Auto and cross-correlations were measured by recording the correlator output on a HP7035B X-Y recorder. The error in the measured correlation functions was probably about ±5%. This error was considerably reduced for the correlations measured using the digital system. Sources of error in the digitally calculated correlations are discussed in section 11.6 of Appendix two.

E R R A T A - VOL. I

P. 50 Raine (1976) should read Raine (1974)

P.70 Equation 3.8 should read equation 3.7

Equation 3.9 should read equation 3.8

Equation 3.10 should read equation 3.9

P.72 Last line: $\frac{\lambda_e}{k}$ should read $\frac{\lambda_e}{k_r}$

P.135) x and o symbols should be interchanged.
P.136)

P.212 Should be $L_{ux}k$ not L_{ux}

P.235 Last line, 4th column from end - should be 29.9

E R R A T A - VOL. II

P.22 Line 3: electric → electrical

P.24 In Section 5.3 it is not clear that the data word must be complemented after being returned from the analogue to digital converter.

P.58 4th paragraph: sebments → segments